Investigating the phosphatidylinositol 3' kinase signalling pathway in transgenic mouse models of breast cancer

Trisha Rao

Department of Biochemistry

McGill University, Montreal

August 2014

A thesis submitted to McGill University in partial fulfillment of the requirements of the degree of Doctor of Philosophy in Biochemistry

This thesis is dedicated to the memory of Joyce Hoffman

June 7, 1924 ~ August 11, 2014

Abstract

The phosphatidylinositol 3' kinase (PI3K)/Akt signalling pathway is activated in several human cancers. PI3K signalling is enhanced by mutations in the p110α isoform of PI3K or through loss of negative regulators such as the tumour suppressor phosphatase and tensin homologue deleted on chromosome 10 (PTEN). This proto-oncogenic pathway can also be induced in cancer downstream of activated receptor tyrosine kinases such as HER2/ErbB2, which is overexpressed in 30% of breast cancers. In fact, PI3K pathway activation in breast cancer has been associated with resistance to HER2-targeted therapies. In this thesis, we have used transgenic mouse models to investigate the importance of PI3K signalling in ErbB2-mediated mammary tumourigenesis.

Our laboratory has previously shown that mammary-specific deletion of Pten can accelerate mammary tumour initiation and metastasis driven by endogenous expression of activated ErbB2. Here, we have validated these findings by demonstrating that Pten loss can cooperate with transgenic overexpression of activated ErbB2 during mammary tumour progression. We have also showed that expression of a constitutively activated p110α transgene in the mammary epithelium can enhance the metastatic potential of ErbB2-induced tumours. Conversely, it seems that disruption of PI3K signalling can impair transformation in the mammary gland. We have demonstrated that genetic ablation of p110α dramatically delays mammary tumour onset and impairs pulmonary metastasis in mammary tumour models induced by either activated ErbB2 or by the viral oncogene polyomavirus middle T antigen (PyV mT). In order to carry out the latter studies, we generated and characterized a new mouse model of PyV mT-driven mammary tumourigenesis that incorporates temporal and spatial regulation of PyV mT and Cre recombinase expression. Importantly, mammary tumours lacking p110α eventually

developed after long latencies in both the ErbB2 and PyV mT strains. We have preliminary evidence to suggest that the emergence of some p110α-deficient tumours is associated with an upregulation of osteopontin (OPN), a secreted extracellular matrix-associated protein with relevance in breast cancer. We believe that increased OPN expression could be due to enhanced PI3K signalling through non-α p110 isoforms, which in turn may be a result of Pten loss.

The results from these studies suggest that activation of the PI3K/Akt pathway might collaborate with HER2/ErbB2 signalling in breast cancer progression and malignancy. Although we can conclude from our work that transformation downstream of activated ErbB2 is initially dependent on the α isoform of p110, it is likely that patients with HER2-positive breast cancer will eventually encounter resistance to p110α-specific inhibitors used as single agents. In these cases, pan PI3K inhibitors may help in preventing the potential reactivation of PI3K signalling through non-targeted p110 isoforms.

Résumé

La voie de signalisation de la kinase en 3' phosphatidylinositol (PI3K)/Akt est activée dans plusieurs cancers humains. Des mutations de l'isoforme p110α de la kinase PI3K ainsi que la perte de régulateurs négatifs tel que le suppresseur de tumeur "phosphatase and tensin homologue on chromosome 10" PTEN sont à l'origine de l'augmentation de la signalisation de la voie de PI3K. L'activation des récepteurs tyrosines kinases tels HER2/ErbB2, qui sont surexprimés dans 30% des cancers du sein, peuvent aussi induire cette voie proto-oncogénique. En fait, l'activation de la voie PI3K dans les cancers du sein a été associée à une résistance aux thérapies ciblées contre HER2. Dans cette thèse, nous avons utilisé un modèle de souris transgénique pour étudier l'importance de la signalisation de la kinase PI3K dans la tumorigenèse mammaire associée à ErbB2.

Notre laboratoire a récemment démontré que la suppression de Pten peut accélérer l'initiation des tumeurs mammaires et les métastases causées par l'expression endogène d'une forme active d'ErbB2. Dans la présente étude, nous avons validé ces résultats en démontrant que lors de la progression de la tumeur mammaire, la perte de Pten peut coopérer avec la surexpression de la forme active d'ErbB2. Nous avons aussi montré que l'expression constitutive d'une forme active du transgene p110α dans l'épitélium mammaire augmente le potentiel métastatique des tumeurs induites par ErbB2. Inversement, il semble que le blocage de la signalisation de la kinase PI3K empêche la transformation des glandes mammaires. Notre étude démontre que l'ablation génétique de l'isoforme p110α ralentit dramatiquement le temps d'apparition des tumeurs et entrave la formation de métastases pulmonaires dans les modèles de tumeurs mammaires induites par la forme active d'ErbB2 ainsi que l'oncogène viral "polyomavirus middle T antigen" (PyV mT). De plus, en préparation d'études ultérieures, nous

avons généré et caractérisé un nouveau modèle de souris développant des tumeurs mammaires induites par le PyV mT incorporant une régulation temporelle et spatiale de l'expresssion PyV mT et la "Cre recombinase". De façon importante, les tumeurs mammaires privées de p110α se développent éventuellement après un long temps de latence dans les deux modèles de souris, soit ErbB2 et PyV mT. Des évidences préliminaires de nos recherchent suggèrent que l'émergence de tumeurs déficientes en p110α est associée avec la régulation positive de l'ostéopontine, une protéine associée et sécrétée de la matrice extracellulaire, souvent impliquée dans les cancers du sein. Nous croyons que l'augmentation de l'expression de l'osteopontine pourrait être due à l'augmentation de la signalisation de PI3K par des isoformes autres que p110α, ce qui pourrait être une conséquence de la perte de Pten.

Les résultats de cette étude suggèrent que l'activation de la voie de signalisation PI3K/Akt pourrait collaborer avec HER2/ErbB2 dans la progression et la malignité du cancer du sein. Même si notre travail conclut que la transformation en aval de l'activation d'ErbB2 est initialement dépendante de l'isoforme α de p110, il est probable que les patientes atteintes d'un cancer du sein HER-2 positifs vont éventuellement développer une résistance aux inhibiteurs spécifiques pour l'isoforme α de p110, si ceux-ci sont administrés seuls. Alternativement, des inhibiteurs à large spectre pour PI3K pourraient aider à prévenir la réactivation potentielle de PI3K en ciblant tous les isoformes.

Acknowledgements

This work would not have been possible without the guidance and support of my supervisor, Dr. Bill Muller. Thank you for accepting me into your lab seven years ago and giving me the opportunity to learn and grow as a scientist while working on such interesting projects. I truly appreciate all of the time and energy you put into making my graduate experience worthwhile.

I would also like to acknowledge my Research Advisory Committee: Dr. Peter Siegel, Dr. Maxime Bouchard, and Dr. David Dankort. Throughout my time here you have always been supportive of my development as a graduate student. Thank you for your advice and thoughtful discussions during our meetings. A special thanks to Dr. David Dankort for his extra time spent teaching me about the trials and tribulations of gene targeting.

Many of the reagents, animal strains, and some experiments were provided by collaborators in other laboratories and at other institutions. Thank you to Dr. Amancio Carnero, Dr. Lewis Chodosh, Dr. Wayne Phillips, Dr. Jean Zhao, Dr. Tamera Utermark, Dr. Michael Hallet, Dr. Robert LeSurf, and Sean Cory.

So much appreciation goes to all past and present members of the Muller lab. I want to acknowledge all of the assistance and support from our technicians and research assistants: Vasilios Papavasiliou, Cynthia Lavoie, Virginie Sanguin-Gendreau, Dongmei Zuo, Sonya Lam, Elitza Germanov, Celine Champigny, Julie-Émilie Huot Marchand. Special thanks to Virginie Sanguin-Gendreau for translating my abstract into French for this thesis. Many postdocs, research associates, and fellow students have been so helpful to me. In particular, I would like to thank Dr. Babette Schade, Dr. Rachelle Dillon, Dr. Richard Marcotte, Dr. Hicham Lahlou, Dr. Harvey Smith, Dr. Chen Ling, and Dr. Jill Ranger for training me on so many different protocols

but also for giving continuous guidance and mentorship. Grad school would not have been as much fun without the lasting friendships I have made. Thanks to Dr. Jill Ranger, Dr. Chen Ling, Vi-Minh-Tri Su, Jason Turpin, Laura Jones, Nelly Abdel-Malak, Ian Swanson, and Elitza Germanov for always being there for me no matter what. I am lucky to have made such a wonderful friend in Jill, who has continued to encourage and support me even after leaving the lab. Thank you especially for your editorial assistance, advice and support with this thesis.

A big thank you goes to Alexandra Simond who has helped me so much since she started in the lab this past year. I appreciate everything you have done and know you will do an excellent job with the continuation of these projects.

To my far away friends, you are always there for me even if you don't understand everything when I explain what I've been doing all of these years. Amanda Moore, it has been awesome sharing the grad school experience with you.

To my Canadian Aunt and Uncle, April and Murray James: thank you for your support through the years. To my Canadian grandparents, Terry and Joyce Hoffman: thank you for taking a genuine interest in my studies and always encouraging me to do my best. This thesis is dedicated to the memory of my Grandma Joyce who was an inspiring woman that I was lucky to have had in my life.

Mom and Dad, you have been so supportive since the beginning and I am very lucky to be so loved. It means so much to know how proud of me you are. I can't thank you enough.

Lastly, thank you to my husband, Tom. I have leaned on you the most throughout this degree, and especially while writing this thesis. You have been an unwavering support, as always. I could not have done this without you.

Preface & contribution of authors

Mouse strains and reagents from collaborators:

Dr. Amancio Carnero provided the MMTV-myr-p110α strain (Chapter 3).

Dr. Jean J. Zhao provided the conditional p110α strain (Chapters 4 and 6).

Dr. Lewis Chodosh provided the MMTV-rtTA strain (Chapters 5 and 6).

Dr. Wayne Phillips provided the conditional $p110\alpha^{HR}$ knock-in strain (Chapter 4).

Dr. C. Ormandy contributed the pTE vector used to generate the TetOMIC vector (Chapter 5).

Dr. S. Dilworth contributed antibodies for PyV mT (Chapters 5 and 6).

Technical services

Paraffin-embedding, sectioning and hematoxylin and eosin (H&E) staining was performed in Histology Core Facilities at the Royal Victoria Hospital and at the Goodman Cancer Research Centre by Myriam Barielles, Marcin Bakinowski, Sonya Lam, Vi-Minh-Tri Su, Elitza Germanov, Jo-Ann Bader, and Julie-Émilie Huot-Marchand. Sectioning of OCT-embedded samples was performed by Dr. Dongmei Zuo. Slides were scanned by Dr. Babette Schade, Dr. Dongmei Zuo, Dr. Laurent Huck, and Julie-Émilie Huot-Marchand.

Vasilios Papavasiliou and Cynthia Lavoie performed orthotopic tumour transplants and tumour cell injections for all studies.

Chapter 3 contributions

Dr. Nathalie Dourdin contributed to the initial characterization of the transgenic mice and performed the Southern blot shown in Figure 3-5C.

Dr. Babette Schade contributed 50% of the work in characterizing the transgenic mice including necropsies, processing of samples, data collection and the preparation of some figures.

Cynthia Lavoie assisted with monitoring and necropsies of transgenic mice.

Sonya Lam contributed to the initial characterization of biochemical signalling in tumours by immunoblot.

Chapter 4 contributions

Sean Cory performed bioinformatic analysis of microarrays under the supervision of Dr. Michael Hallet (Figure 4-16, 4-17A).

Alexandra Simond assisted with necropsies for Figures 4-2A and 4-20; performed immunoblots for Figures 4-8B, 4-13B, and 4-22; performed the short-term GDC-0941 experiment for Figure 4-13B; assisted with necropsies, prepared protein lysates and generated immunoblots for Figure 4-22B.

Cynthia Lavoie and McGill Animal Care technicians administered GDC-0941 and vehicle gavage treatments to NCr mice (Figures 4-13B and 4-14).

Virginie Sanguin-Gendreau assisted with tissue chopping and epithelial cell isolation (Figure 4-2A and 4-20).

Chapter 5 contributions

Sonya Lam generated the cloning construct for the TetOMIC strain with assistance from Dr. Chen Ling.

The Goodman Cancer Research Centre Transgenic Core Facility performed pronuclear injections to generate the MIC strain.

Dr. Harvey W. Smith screened the founder lines for the TetOMIC strain and assisted with sample preparation and analysis of recurrent rtTA/MIC tumours.

Dr. Jill J. Ranger contributed 50% of the work in generating and characterizing the MMTV-rtTA/TetOMIC mice including monitoring/palpations, necropsies, processing of samples, data collection, and the preparation of most figures.

Laura Jones and Dr. Frédéric Ancot provided additional rtTA/MIC wholemounts for the 2 week induction timepoint (Figure 5-3).

Cynthia Lavoie performed resection surgeries for de-induced rtTA/MIC mice (Figures 5-10 and 5-11).

Dr. Pierre LePage and Dr. Sébastien Brunet at Génome Quebec performed DNA sequencing of recurrent rtTA/MIC tumours.

Chapter 6 contributions

Alexandra Simond assisted with necropsies (Figure 6-4).

Publications arising from this thesis:

Schade B*, **Rao T***, Dourdin N, Lesurf R, Hallet M, Cardiff RD, Muller WJ. PTEN-deficiency in a luminal ErbB-2 mouse model results in dramatic acceleration of mammary tumorigenesis and metastasis. 2009. *J. Biol. Chem*. **284**.

co-first authors

Utermark T*, **Rao T***, Cheng H, Wang Q, Lee SH, Wang ZC, Iglehart JD, Roberts TM, Muller WJ, Zhao JJ. The p110α and p110β isoforms of PI3K play divergent roles in mammary gland development and tumorigenesis. 2012. Genes Dev. **26**.

co-first authors

(Contributed data for Figure 3 A-D and Supplemental Figure 3 B-C)

Rao T*, Ranger JJ*, Smith HW, Lam SH, Chodosh L, Muller WJ. Inducible and coupled expression of polyomavirus middle T antigen and Cre recombinase: an *in vivo* model of synthetic viability for mammary tumour progression. 2014. *Breast Cancer Res*. **16**.

co-first authors

Table of Contents

List of Figures

List of Tables

List of Abbreviations

4EBP - eukaryotic initiation factor 4E binding protein

Akt - v-akt thymoma viral oncogene homolog

amg - adjacent mammary gland

AMPK - adenosine monophosphate-activated kinase

APC - anaphase-promoting complex

AREG - amphiregulin

BAD - BCL-2 associated death promoter

BCR - breakpoint cluster region

BH - BCR homology

BIM - BCL-interacting mediator of cell death

BRCA - breast cancer-associated

Cdc42 - Cell Division Cycle 42

CDH1- cadherin 1

CDK - cyclin-dependent kinase

CEF - chicken embryonic fibroblast

DCIS - ductal carcinoma *in situ*

dox - doxycycline

EGF - epidermal growth factor

EGFR - EGF receptor

EMT - epithelial-mesenchymal transition

ErbB2 - v-erb-b2 avian erythroblastic leukemia viral oncogene homolog 2

$ErbB2^{KI}$ - ErbB2 knock-in

ER - estrogen receptor

FAK - focal adhesion kinase

FKHRL/FOXO - forkhead transcription factor

Gab - Grb2-associated binding protein

GAP - GTPase-activating protein

GATA3 - GATA binding protein 3

GEF - guanine nucleotide exchange factor

GFP - green fluorescent protein

GPCR - G-protein-coupled receptors

Grb - growth factor receptor bound protein

GSK3β - glycogen synthase kinase 3 β

GTRosa - gene trap ROSA 26

H&E - haematoxylin and eosin

HER - human epidermal growth factor receptor

HRas - Harvey rat sarcoma viral oncogene homologue

HRP - horse radish peroxidase

IGF1 - insulin-like growth factor 1

IGF1R - IGF1 receptor

INPP4 - Inositol Polyphosphate-4-Phosphatase

IRES - internal ribosome entry site

IRS - insulin receptor substrate

IκB - inhibitor of κ B

IκKα - inhibitor of κ kinase α

KRas - Kirsten rat sarcoma viral oncogene homologue

LA - lobular-alveolar

LKB1 - liver kinase B1

MAPK - mitogen-activated protein kinase

MDM2 - mouse double minute 2

MEF - mouse embryonic fibroblast

MEK - MAPK/extracellular signal-related kinase kinase

mg - mammary gland

MIC - PyV mT-IRES-Cre recombinase; TetO-MIC

MIN - mammary epithelial neoplasia

MMP - matrix metalloproteinase

MMTV-LTR - mouse mammary tumour virus long terminal repeat

mTOR - mammalian target of rapamycin

mTORC - mTOR complex

Myc - v-myc avian myelocytomatosis viral oncogene homologue

myr - myristoylated

NDL - Neu deletion 2-5

NEDD4 - neural precursor cell expressed, developmentally down-regulated 4, E3 ubiquitin protein ligase

Neu - neuro/glioblastoma derived oncogene homologue

NFκB - nuclear factor κ light chain enhancer of activated B cells

NIC - NDL-IRES-Cre recombinase

NRas - neuroblastoma Ras viral (v-ras) oncogene homologue

OPN - osteopontin

PDGFR- platelet-derived growth factor receptor

PDK1 - phosphoinositide-dependent kinase 1

PH - pleckstrin homology

PHTS - PTEN hamartoma tumour syndromes

PI - phosphatidylinositol

PI(3,4,5)P2 - phosphatidylinositol (3,4,5) bisphosphate

PI(3,4,5)P3 - phosphatidylinositol (3,4,5) trisphosphate

PI3K - PI 3' kinase

PR - progesterone receptor

PRas40 - proline-rich Akt substrate of 40 kilodaltons

PTEN - phosphatase and tensin homologue on chromosome 10

PyV mT - polyomavirus middle T antigen

RANKL - receptor NFκB ligand

RB - retinoblastoma protein

Rheb - Ras Homolog Enriched In Brain

RTK - receptor tyrosine kinase

RT-qPCR - reverse transcription-quantitative polymerase chain reaction

rtTA - reverse tetracycline transactivator

SGK - serum and glucocorticoid-inducible kinase

SH - Src homology

SHC - Src homology 2 domain containing

SHIP2 - SH2 Domain-Containing Inositol 5'-Phosphatase

Src - v-src sarcoma viral oncogene homolog

STARD3 - star-related lipid transfer domain containing 3

Stat - signal transducer and activator of transcription

TDLU - terminal ductal-lobular unit

TEB - terminal end bud

TetO - tetracycline operon

TIMP - tissue inhibitor of metalloproteinase

TNBC - triple-negative breast cancer

TP53 or p53 - tumour protein 53

TSC - tuberin sclerosis complex

tum - mammary tumour

VEGF - vascular endothelial growth factor

WAP - whey acidic protein

XBP1 - X-box binding protein 1

1 General introduction and literature review

1.1 Breast cancer: a prevalent and heterogeneous disease

1.1.1 Epidemiology of breast cancer

The most common cancer in Canadian women is breast cancer, representing 24% of all new cancer cases and 14% of all cancer deaths estimated for 2014 [1]. In more tangible terms, 1 in 9 Canadian women will develop breast cancer in her lifetime while 1 in 30 will die from it. The implementation of breast cancer screening programs has led to an increase in incidence statistics up until the early 2000s after which it decreased and then stabilized [1]. Concurrent improvements in treatment opportunities in addition to early diagnosis have helped to steadily reduce breast cancer-related deaths [1].

There are several non-modifiable risk factors of breast cancer, with the highest relative risk in women attributable to age, family history, and inherited genetic mutations [2]. About 10% of breast cancers are hereditary and caused by loss-of-function mutations in one or both alleles of tumour suppressor genes, such as the breast cancer associated (BRCA) genes (*BRCA1* and *BRCA2*), p53 (*TP53*), and phosphatase and tensin homologue deleted on chromosome ten (*PTEN*) [3, 4]. These germline mutations manifest as cancer susceptibility syndromes and can increase the risk of breast cancer [5-8].

The remainder of breast cancers, and thus the majority, of breast cancers are caused by somatic gene alterations. Indeed, some of these genes are also familial cancer predisposition genes like *TP53*, which is the most frequently mutated gene in sporadic breast cancers (37%) [4]. Another tumour suppressor with relevance in both hereditary and spontaneous cancers is PTEN, which antagonizes the proto-oncogenic phosphatidylinositol 3' kinase (PI3K)/Akt pathway (described in more detail in sections 1.3 and 1.4). Interestingly, this signalling pathway can also

become activated through somatic point mutations in the PI3K catalytic subunit, p110α (*PIK3CA* gene), which happens to be the second most frequently mutated gene in breast cancers after *TP53* (36%) [4].

In addition to somatic mutations, breast cancers may exhibit increased DNA copy number and increased expression of particular proto-oncogenes. For example, about 20-30% of cases exhibit gene amplification of human epidermal growth factor receptor 2 (*HER2*), a member of the epidermal growth factor receptor (EGFR) family of receptor tyrosine kinases (RTKs), and this feature is correlated with poor patient outcome (described in more detail in section 1.2.1) [9, 10]. The *HER2* gene is part of a core amplicon on chromosome 17 that includes other genes such as growth factor receptor bound 7 (*GRB7*) and star-related lipid transfer domain containing 3 (*STARD3*) that are co-amplified with *HER2* in breast cancer [11]. The value of HER2 expression as a prognostic factor, as well as its capacity for identifying candidates for HER2-targeted therapies, has established it as an important clinical marker in breast cancer diagnosis (see section 1.1.3) [12].

1.1.2 Anatomical and histological features of the breast

The adult breast is comprised of glandular and stromal tissue which together experience dramatic architectural changes to allow for the production of milk. The mammary ducts are arranged in a radial fashion and organized into distinct lobes, each of which contains a cluster of several terminal ductal-lobular units (TDLUs) [13]. The TDLUs, the sites of milk production, drain into ducts that open to the nipple.

The anatomy and histology of the human breast is very similar to that of the murine mammary gland and so the development and function of this dynamic organ has been mainly studied in mice [13]. Mammary ducts are hollow lumens lined by an inner luminal epithelial layer and an outer myoepithelial layer. The duct is enclosed and supported by a basement membrane made up of extracellular matrix (ECM) components, such as collagen IV and laminin [14]. In addition to structural support for the ductal cells, this membrane maintains the shape and polarity of the ductal epithelial cells [15]. The basement membrane separates the ducts from the stromal component of the gland which includes cells such as adipocytes, fibroblasts, endothelium, and immune cells [16]. The integrity of the basement membrane is influenced the activities of proteases and protease inhibitors which are secreted by the ductal epithelium [17]. This process allows for the remodelling of the ductal network during all phases of mammary gland development.

The postnatal stages of murine mammary gland development include pubertal growth, pregnancy-lactation, and involution. At birth, the immature mammary gland consists of a rudimentary network of ductal epithelium surrounded by mesenchyme/stroma [18]. The release of hormones, such as estrogen, at the onset of puberty promotes the elongation and lateral secondary and tertiary branching of the ductal network through the proliferation of mammary stem cells [19, 20]. At the end of puberty, the virgin mammary gland consists of a predominantly adipose-rich stroma that surrounds a fully developed system of ductal epithelium.

During pregnancy, estrogen and progesterone cause induce secondary and tertiary side-branching of the ductal network so that it fills the fat pad [21, 22]. The ductal termini differentiate into alveoli which produce milk in response to the hormone prolactin [23]. Milk secretion from the ducts is regulated by contraction of the myoepithelium in combination with

regulation from stromal components [24, 25]. Forced weaning of pups leads to the cessation of milk production and initiates involution [26]. This stage comprises the apoptosis of alveolar cells and regression of the ductal network to a pre-pregnancy state [27]. The initial phase of involution is reversible, however past this point (2 days post-weaning) the gland is committed to extensive remodelling of the epithelium and stroma to revert back to the virgin-like anatomy [28, 29]. After the completion of this process, the mammary gland returns to a resting state until the next entry into the reproductive phase.

Several hormones and growth factors (and their respective receptors) have been implicated in murine mammary gland development [20-22, 30]. Thus, the dysregulation of the molecular signalling which dictates the normal function of the mammary gland has the potential to initiate transformation. Indeed, these same key signalling proteins can be associated with breast cancer in humans. For example, the receptors for the hormones estrogen and progesterone (which are primarily involved in pubertal and pregnancy stages of development, respectively) are overexpressed in many breast cancers and major prognostic and predictive factors (see next section) [31].

The majority of breast cancers in women originate in the mammary ducts (ductal carcinoma) although some types occur in TLDUs (lobular carcinoma) [2]. Transformation in the mammary gland becomes histologically evident when ductal lumens begin to fill with hyperproliferating luminal cells, eventually producing a completely filled structure that is contained by the basement membrane and clinically designated as ductal carcinoma *in situ* (DCIS). These early lesions become invasive when the proliferating tumour cells break through the basement membrane and invade into the surrounding mammary stroma. If the tumour cells can enter the vasculature or lymphatic system, they can undergo metastatic dissemination and

colonize distant sites in the body. Indeed, the majority of breast cancers diagnosed are invasive or infiltrating [2].

The development of breast cancer and its progression to malignancy depend on the well-established hallmarks of cancer: sustaining proliferation, evading of growth suppressors, resisting cell death, enabling replicative potential, inducing angiogenesis, and activating of invasion and metastasis [32]. More recently, additional qualities have been recognized as emerging cancer hallmarks: avoiding immune destruction, tumour-promoting inflammation, genome instability and mutation, and deregulating cellular energetics [32]. Understanding the genes and signaling pathways involved in driving these hallmarks will be critical for developing better diagnostic tools and treatments for breast cancer patients.

1.1.3 Diagnosis, classification, and treatment of breast cancers

Breast cancer is currently diagnosed by the size of the tumour, involvement of regional lymph nodes, and the presence of distant metastases which are all considered for breast cancer staging [2]. The spreading of breast cancer to other organs in the body confers the most advanced stage, IV, which is associated with the worst prognosis. Breast cancers are also classified on the basis of immunohistochemical staining of cell-surface receptors. The three major receptors identified to be of significant prognostic importance are estrogen and progesterone receptors (ER/PR- or hormone receptor-positive) and HER2 (HER2-positive) [12, 31]. The relative expression of these markers dictates treatment regimens due to their predictive nature with regard to response to specific therapies. While ER-positive tumours are dependent on estrogen and are treated using endocrine or hormone therapy, there is no benefit for ER-negative tumours [31]. Likewise,

tumours that are positive for HER2 expression are candidates for HER2-targeted therapies [12]. Therapeutic options are extremely limited for triple-negative breast cancers (TNBCs), an aggressive subset of breast cancers that do not express any of these markers ($ER^-/PR^-/HER2^-$), and mainly consists of chemotherapy [33]. In general, resistance to the therapy (both *de novo* and acquired) is a common problem and often reflects the receptor status or treatment (see section 1.4.3). This has emphasized the need for a deeper understanding of breast tumours on a molecular level.

Although not yet used as a standardized diagnostic tool, researchers currently classify breast cancers by gene expression profiling. Microarray analysis of breast tumours demonstrated that they cluster into approximately four major subtypes based on an "intrinsic" gene set: luminal (comprised of subgroups A, B, and C), HER2-enriched, basal-like, and normal-like [34, 35]. Expression of ER and a number of genes typical of luminal cells make up the ER-positive/luminal subtypes. Luminal A tumours express relative higher ER levels than luminal B and C tumours; luminal C tumours share features with the HER2-enriched and basal-like subtypes [35]. Tumours that are negative for ER expression are subdivided into two groups: the HER2-positive subtype which exhibits overexpression of HER2 and the HER2 amplicon (also called the HER2-enriched subtype to avoid confusion with tumours clinically defined by immunohistochemical overexpression of HER2 protein) and the basal-like subtype that is characterized by expression of basal cell markers (e.g. keratin 5, keratin 17, laminin). A fourth subtype called normal-like was shown to be enriched in adipose- and basal-specific genes.

Importantly, these different subtypes correlate with clinical outcome, with the best overall or relapse-free survival observed for the luminal A subtype and the worst associated with HER2-enriched and basal-like subtypes [35]. The assignment of molecular subtypes and their

associations with prognosis and sometimes therapeutic response has been shown to be reproducible using several data sets by numerous independent groups [36-39]. Furthermore, these types of analyses have also led to the identification of additional subtypes, such as claudin-low which exhibits stem-cell like features [40, 41]. Many studies have extended gene expression profiling to the stromal compartments of developing tumours, recognizing the relevance of non-cell-autonomous pathways in breast cancer [42-44]. Substantial efforts have been put toward linking microarrays of breast tumours with other platforms that analyze somatic mutation, DNA copy number, and protein expression [4, 45-47]. This has revealed limitations of immunohistochemical classification by ER/PR/HER2 status due to a lack of absolute concordance with the correspondingly named intrinsic subtype, but has also identified significant associations with particular molecular features [4]. For example, while activating mutations in the *PIK3CA* gene are most often associated with the luminal subtypes, loss-of-function mutations in the *BRCA1* and *TP53* tumour suppressors occur most frequently in basal-like cancers [4].

Although global profiling of breast cancers has confirmed the presence of heterogeneity between individual samples on a molecular level, it has also revealed that there are classes of tumours that share distinct features which correlate with response to treatment. The development of successful therapies relies not only on the identification of these inherent similarities and differences in human tumours but also on comprehensive data acquired from preclinical breast cancer models, the most relevant source being transgenic mice.

1.2 Mouse models of breast cancer

Technological advances in mouse model design have been made which allow for conditional regulation of genetic alterations, including both spatial and temporal control. While germline

knockout strains are useful for identifying genes essential for viability or development, further analysis of adult animals could be impeded by postnatal death or abnormalities. Germline models can be useful for studying cancers caused by hereditary mutations however tumour development may occur in several organs and is likely influenced by an altered tumour microenvironment. Modelling sporadic cancer is best accomplished with conditional gene targeting where genetic alterations can be introduced in a particular tissue.

Studying the role of a gene in the development and/or transformation of a specific cell compartment requires the use of tissue-specific promoters. This approach often involves exploiting the natural expression patterning in the organism and takes advantage of gene promoters that are active in a particular tissue or during a particular developmental stage. A mammary-specific example of this is the WAP promoter, which normally drives expression of this milk protein during pregnancy and lactation [48, 49]. WAP promoter activity is stimulated by insulin, hydrocortisone, and prolactin. Although activity from WAP is detectable in virgin mice, it increases dramatically during pregnancy and transgenic expression in mice is best observed in parous animals. Tissue-specific promoters can also be derived from exogenous sources, as is the case for the mouse mammary tumour virus long terminal repeat promoter (MMTV-LTR or MMTV). Early studies of inbred mouse strains revealed that particular lines were susceptible to spontaneous mammary tumours; the transmissible agent or "milk factor" was passed from nursing mothers to their pups and was later identified as the mouse mammary tumour virus [50]. The MMTV promoter is regulated by glucocorticoids and can be used to drive the expression of transgenes to the both virgin and reproductive mammary glands [51-53]. Indeed, the MMTV promoter was used in early mouse models of mammary tumourigenesis

validating the oncogenic capabilities of HRas, c-Myc, or c-Neu (activated rat isoform of HER2) [53-55].

The WAP and MMTV promoters are not only useful in overexpressing genes of interest; they can be coupled to Cre recombinase to produce mammary-specific gene knockouts. A Cre recombinase-inducible conditional mouse strain is generated by inserting 34-base pair palindromic sequences denoted as LoxP sites on either side of one or multiple exons of a gene of interest (creating a LoxP-flanked or "floxed" allele) [56]. In the presence of Cre recombinase, the LoxP sites are recombined and the floxed region is excised which in the case of a gene knockout strategy results in a null phenotype. The tissue-specificity of Cre recombinase determines the tissue-specificity of the gene knockout; thus the use of the WAP-Cre or MMTV-Cre transgenes directs conditional ablation to the mammary epithelium [57, 58]. This approach continues to be employed in studying the function of genes in mammary gland development and tumourigenesis. Furthermore, multiple genes can be ablated to investigate cooperative effects between oncogenes and/or tumour suppressors. For example, mammary-specific loss of either the *Brca1* or *Brca2* tumour suppressor genes leads to mammary tumour formation after a long latency [59, 60]. For both of these models, concurrent deletion of the p53 tumour suppressor accelerated mammary tumour onset. The collaboration between these two genetic alterations is reflective of the fact that *BRCA1* mutations are often coincident with *TP53* mutations in human cancer [61].

Cre recombinase/LoxP systems can be expanded to other genetic alterations, such as the removal of a floxed transcriptional "stop" cassette upstream of a transgene or the introduction of latent point mutations in an endogenous gene. The former strategy was used in conjunction with the MMTV-Cre transgene in a mouse model of ErbB2-driven breast cancer [62], while the latter

has been used with tissue-specific Cre recombinase expression or retroviral delivery to the organ of interest [63-66]. Floxed "stop" cassettes have also been used to regulate the expression of reporter genes, such as β-galactosidase or green fluorescent protein (GFP), providing a visual indication of Cre expression and function in a given strain [67, 68].

An additional level of regulation that is becoming increasingly more common is the use of inducible promoters such as the TetON/TetOFF systems [69, 70]. Inducible systems offer the most control over transgene expression by allowing the researcher to choose when to turn expression on or off. This is critical if transgene expression is detrimental to normal development, but also allows one to induce expression at the most physiologically appropriate age. Tissue-specificity is rendered at the level of the tetracycline transactivator (tTA) transgene. In the TetOFF system, a transgene is expressed downstream of a tetracycline operon (TetO) which is bound by the tTA; doxycycline, a tetracycline derivative, can bind the tTA and displace it from the TetO thereby turning off transgene expression. The TetON system differs by using a reverse tTA (rtTA) which binds to the TetO in response to doxycycline to turn on transgene expression. Doxycycline is easily administered to mice in their water or food, making this a relatively simple approach to temporal control of transgene expression. In fact, the generation of an MMTV-driven rtTA strain has transformed the way oncogenes are introduced to the mammary epithelium, as seen with c-Myc, activated Neu (NeuNT), and KRas [71-73]. Inducible models provide the means to generate tumours and then effectively turn off the oncogenic signal that initiated transformation to mimic clinical inhibition. In doing so, researchers can address whether a tumour is dependent on this genetic alteration and also whether recurrent tumours emerge.

1.2.1 HER2/Neu models

The discovery that HER2 was overexpressed in breast and ovarian cancers launched efforts to investigate the *in vivo* transforming abilities of this proto-oncogene, specifically in the mammary gland. Transgenic mouse models have been extremely valuable for studying the functions of HER2 during mammary development and tumourigenesis.

HER2 was originally identified as a viral transforming gene, Neu, in rat neuroblastoma which was found to be related to EGFR [74, 75]. EGFR, HER2, HER3 and HER4 comprise the EGFR family of RTKs (Egfr, ErbB2, ErbB3, and ErbB4 in mice, respectively). A variety of ligands, including epidermal growth factor (EGF), amphiregulin (AREG), neuregulins, heregulins, and tumour necrosis factor α, induce receptor dimerization and phosphorylation of cytoplasmic tails. Phosphorylated residues act as docking sites for intracellular proteins, including kinases and adaptor molecules, leading to activation of numerous downstream signalling events. All EGFR family members have the capacity to recruit Src homology 2 domain containing (SHC) and Grb2 adaptor molecules to specific phosphotyrosine residues [76]. Grb2 can associate with the guanine nucleotide exchange factor (GEF) son of sevenless homolog 1 (SOS) which in turn activates Ras/mitogen-activated protein kinase (MAPK) signalling. This pathway is also induced downstream of SHC which can interact directly with Grb2. Another important scaffold is created upon binding of Grb2 to Grb2-associated binding protein 1 (Gab1), which recruits the p85 regulatory subunit of PI3Ks [77]. Direct recruitment of PI3Ks to HER3 is possible due to the presence of six p85 docking sites [76].

HER2 is considered an orphan receptor since no ligands have been identified for it however crystal structures indicate that it is in a constitutively "open" conformation making it ready for pairing with other family members [78]. Thus overexpression of HER2 in cancer is

thought to promote increased receptor heterodimerization and activation of proto-oncogenic signalling. The HER2/HER3 heterodimer, which together engage the Ras/MAPK and PI3K/Akt signalling pathways, is thought to be a potent oncogenic unit in breast cancer cells [79]. This coupling may be evolutionarily determined since HER3 uniquely lacks kinase activity and so it can only function in a heterodimer [80].

HER2, as well as other members of the EGFR family and their ligands, are active participants in the normal development of the mammary gland. Analysis of murine mammary glands indicates that EGFR family receptors are differentially expressed at various stages of mammary development [81]. EGFR family ligands are also widely expressed, although genetic studies have identified AREG as the major ligand involved in development [82, 83]. While EGFR and ErbB2 are expressed at all stages, ErbB3 and ErbB4 expression is upregulated during puberty and reproductive stages. Due to embryonic lethality of germline knockouts, most studies on the role of individual EGFR family members were carried out using other genetic techniques [84-87]. Transplantation experiments indicated a role for AREG/EGFR signalling in mammary stroma which may also involve heterodimerization with ErbB2 [88, 89]. Epithelial-specific expression of a dominant negative mutant of EGFR also led to ductal defects [90]. Furthermore, expression of an EGFR hypomorphic allele, waved-2, caused a lactational defect in some mice due to a reduction in both epithelial content and milk production in postpartum glands [91]. Conditional ablation of ErbB2 in the mammary epithelium causes defective ductal outgrowth and branching but does not impact on reproductive stages of development [92]. In contrast, loss of ErbB4 in the mammary epithelium impaired LA development and is required for Stat5 activation during lactation [93, 94]. Transplantation of ErbB3-deficient mammary buds blunts ductal outgrowth, a phenotype also observed with mammary-specific expression of an ErbB3 mutant

that is uncoupled from PI3K [95, 96]. The latter model also exhibited accelerated involution due to increased apoptosis. The importance of EGFR family signalling in the mammary gland during development provides support for the implication of these pathways, particularly downstream of HER2, in mammary tumourigenesis as demonstrated by *in vivo* studies.

Conditional mouse models have been especially important in experimentally validating HER2 as a proto-oncogene in breast cancer (Table 1-1). Transgenic mice expressing an activated mutant of Neu, the rat orthologue of HER2, in the mammary epithelium developed mammary tumours that were metastatic to the lung (MMTV-c-Neu or MMTV-NeuNT) [55, 97, 98]. However, HER2 is rarely mutated in breast tumours and so it was important to determine if wildtype ErbB2 had transforming potential [99]. Mice were engineered to express the wildtype version of Neu (MMTV-Neu) and tumours eventually developed but after a much longer latency, suggesting the requirement for additional genetic changes [100]. In fact, mutations were discovered in the Neu transgene itself, the majority of which were in-frame deletions in the extracellular domain of the receptor [101]. Molecular analysis of these Neu deletion mutants revealed that the loss of cysteine residues disrupted intramolecular disulphide bonds while promoting intermolecular bridges [102]. Transgenic expression of the Neu deletion mutants (MMTV-NDL) resulted in metastatic mammary tumours arising earlier than the parental wildtype Neu strain [103]. Interestingly, an analogous alteration was identified in human cancers as a splice isoform of HER2 that homodimerizes via a similar mechanism [102, 104].

Table 1-1: HER2/Neu transgenic mouse models of breast cancer

Model	Penetrance	Tumour onset	Tumour multiplicity	Lung metastasis
MMTV-NeuNT [55] *activated point mutant of Neu*	100%	89 d (T_{50})	multifocal	yes
MMTV-Neu [100] *wildtype Neu*	~70%	205 d (T_{50})	focal	72% (8 m)
MMTV-NDL [103] *Neu deletion mutant (NDL2-5)*	100%	161 ± 10 d (average)	multifocal	67% (4-9 w pp)
MMTV-NDL-IRES-Cre (NIC) [105, 106] *Neu deletion mutant (NDL2-5) coupled to Cre recombinase*	100%	146 d (average)	multifocal	56% (6 w pp)
MMTV-rtTA/ TetO-NeuNT [71] *inducible point activated Neu*	100%	42 d (T_{50})	focal	92%
NeuNT/MMTV-Cre (ErbB2 "knock-in"; ErbB2^{KI}) [62] *Knock-in of Cre recombinase-inducible NeuNT at* erbb2 *locus*	~80%	15.8 m (average)	focal	2%

d: days; w: weeks; m: months; pp: post-palpation

The Neu-driven mouse models described so far had the potential to be extremely useful for studying the function of other genes in the context of a developing tumour. Early attempts to study the mammary-specific role of a particular gene in the MMTV-driven oncogene model involved crossing in LoxP-flanked alleles of this gene as well as an MMTV-driven Cre recombinase transgene. However, the MMTV promoter is only active in approximately 70% of the mammary epithelium, resulting in stochastic Cre recombinase expression in oncogenic tumour tissue; a selection for oncogene-positive/Cre recombinase-negative cells arises in the developing tumour, precluding excision of the conditional allele of interest. This phenomenon has occurred in several strains where the oncogene and Cre recombinase are on separate MMTV-driven transgenes indicating that in each case the conditional gene was most likely essential to tumourigenesis [107-110] (unpublished observations; Ranger JJ, Muller WJ). To circumvent this selection process, the MMTV-NDL transgene was redesigned to couple expression with Cre recombinase through use of an internal ribosome entry site (IRES) thereby creating the MMTV-NIC (Neu-IRES-Cre recombinase) strain [105]. In mice carrying this transgene every mammary tumour cell expresses both Neu and Cre recombinase and thus any conditional loci present in the genome of this cell should be recombined and completely ablated. The MMTV-NIC model has been successfully used to define the roles of several genes in ErbB2-mediated mammary tumourigenesis, including members of the PI3K/PTEN pathway [105-107, 111-114].

Although the transgenic Neu models continue to be very practical for studying ErbB2-mediated mammary tumourigenesis, the transgene is overexpressed beyond physiological levels by a strong viral promoter. With this in mind, a gene targeting approach was used to knock in a Cre recombinase-inducible NeuNT transgene downstream of the endogenous *erbb2* promoter [62]. This design would ensure that the mutant transgene would be under normal transcriptional

control and expressed comparably to the wildtype *erbb2* gene. Mice carrying this targeted allele along with the MMTV-Cre transgene (NeuNT/MMTV-Cre or ErbB2^{KI}) develop focal, poorly metastatic mammary tumours after a long latency. The ErbB2^{KI} tumours showed selective amplification of the NeuNT transgene as well as a number of chromosomal aberrations associated with human breast cancer [115-117]. These included amplifications of regions in chromosome 11 and deletions in chromosome 4; the former maps to the recombinant NeuNT transgene and is syntenic with the human HER2 amplicon on chromosome 17. Indeed, mammary tumours from ErbB2^{KI} mice also exhibited evidence of amplified expression of genes in their *erbb2* amplicon, such as *grb7* and *stard3*. Thus the ErbB2^{KI} mouse model encompasses physiological expression of activated ErbB2 and tumour development progresses as a result of genetic alterations that are correlative with features of human breast cancer.

Regardless of the model, mammary tumours induced by activated ErbB2 exhibit a characteristic solid comedo-adenocarcinoma histology which resembles DCIS in human breast cancer [13, 115]. These tumours are also positive for luminal cytokeratins, which is likely because the MMTV promoter targets the luminal cell compartment. Interestingly, gene expression profiles of murine mammary tumours from the MMTV-Neu strain do not cluster with those of human breast cancers of the HER2-enriched subtype [118]. Although in general murine mammary tumours express relatively low levels of ER, and thus ER-regulated genes, they do exhibit increased expression of luminal-specific genes Gata3 and Xbp1 and so they are considered to be luminal-like.

An interesting feature of MMTV-NDL tumours is that they overexpress ErbB3 and this is also observed in HER2-expressing breast cancers suggesting a co-dependence of these two related RTKs [103, 119]. Conditional ablation of ErbB3 delays mammary tumourigenesis

induced by activated Neu [120]. Despite the fact that the majority of phosphotyrosine docking sites in ErbB3 are specific for PI3K p85, this interaction may not be absolutely necessary for tumour initiation in Neu-driven models as expression of an ErbB3 mutant that is uncoupled from PI3K does not affect tumour development in the MMTV-NDL model [96]. Mouse models have also been used to demonstrate the importance of signalling by EGFR, but not ErbB4, in ErbB2 mammary tumourigenesis [121, 122]. The EGFR family ligand, transforming growth factor α, can also cooperate with overexpression of Neu enhance mammary tumourigenesis [123].

HER2/Neu mammary tumour mouse models are useful tools for studying the signalling pathways that are likely initiated by this proto-oncogene in breast cancer. Furthermore, mammary tumours from these mouse strains share many features with HER2-expressing patient tumours, making them excellent systems for modelling this disease experimentally.

1.2.2 Polyomavirus middle T antigen (PyV mT) models

Although several mouse models manipulating human genes or their orthologues have been invaluable for breast cancer research, a widely used mouse strain that more accurately models the phenotypic progression of the human disease happens to be driven by a viral oncogene called polyomavirus middle T antigen (PyV mT). The growing number of PyV mT mammary tumour models collectively emphasizes the relevance of this non-physiological oncogene to the field of breast cancer (Table 1-2).

Polyomavirus (PyV) was originally identified as tumour-inducing in newborn mice [124-126]. PyV is alternatively spliced to produce a large, middle and small T antigen although transformation requires only the middle T antigen (mT) [127-130]. The PyV mT protein is

membrane-anchored with most of its length protruding into the cytoplasm [131, 132]. The cytoplasmic portion of PyV mT is without kinase activity as it lacks the ability to bind ATP [132]. Instead, PyV mT is complexed with the protein phosphatase 2A scaffold which is required to recruit c-Src family kinases [133]. Phosphorylation of specific residues on PyV mT by c-Src in turn allows the binding of adaptors and kinases. This feature allows PyV mT to mimic the signal transduction abilities of RTKs. Two major tyrosine phosphorylated sites are Y250 and Y315 which recruit the SHCA adaptor and the p85 regulatory subunit of PI3K, respectively [134-137]. Transformation downstream of PyV mT is dependent on the recruitment of these proteins and the signalling pathways they induce (described in more detail below) [138, 139]. Indeed, transgenic expression of PyV mT in the mouse can lead to tumour formation in many epithelial tissues [140].

The MMTV promoter was used to drive PyV mT to the mammary epithelium and in some founder lines mammary tumours were detected in mice as early as 3-4 weeks of age and developed in multiple glands [141]. Histological analysis of the inguinal mammary glands from young MMTV-PyV mT mice reveals a gradient of transformation, with the older and more advanced lesions proximal to the nipple, and newer lesions at earlier stages of tumourigenesis towards the terminal end buds of the epithelial network [142]. Mammary tumour development in this strain closely mimics breasts cancer progression observed in humans, evolving through four distinct stages: hyperplasia, mammary intraepithelial neoplasia (MIN)/adenoma, early carcinoma and late carcinoma [143]. Invasiveness was characterized histologically by disruption of the basement membrane, loss of myoepithelial cells, and infiltration of leukocytes. Molecularly, PyV mT mammary tumours also resemble human breast cancers as they show

Table 1-2: PyV mT transgenic mouse models of breast cancer

Model	Penetrance	Tumour onset	Tumour multiplicity	Lung metastasis
MMTV-PyV mT [141] *polyomavirus middle T antigen*	100%	40 d (T_{50})	multifocal	93.3% (8 w pp)
MMTV-rtTA/TetO-PyV mT-IRES-Luc [73] *inducible polyoma virus middle T antigen coupled to firefly luciferase*	100%	3-4 w (average)	multifocal	yes (6 w pp)
MMTV-rtTA/TetO-PyV mT-IRES-Cre (MIC) [144] *inducible polyoma virus middle T antigen coupled to Cre recombinase*	87.1%	7 d (T_{50})	multifocal	100% (>4 cm^3 burden)

d: days; w: weeks; m: months; pp: post-palpation

upregulation of ErbB2 and cyclin D1. Although ER and PR are upregulated during earlier stages of progression, tumours are negative for these receptors, similar to other mammary models like MMTV-Neu [143]. MMTV-PyV mT tumours are also transcriptionally comparable to the luminal-like profile of MMTV-Neu tumours as both models express luminal genes and

cytokeratins [118]. Another clinically relevant feature of this model is that PyV mT-induced mammary tumours are capable of metastasizing to the lungs with close to 100% incidence [141]. The MMTV-PyV mT strain has since become an established tool in studying breast tumourigenesis and metastasis *in vivo*.

The desire to investigate other genes in the context of PyV mT tumourigenesis initiated studies that incorporated conditional strains and the MMTV-Cre transgene. However these experiments led to the same issues encountered with MMTV-NDL/MMTV-Cre systems, where Cre expression was selectively turned off in the developing tumour in order to retain expression of the conditional genes that were presumably essential for tumourigenesis. This prompted the development of a Cre-coupled transgene analogous to the MMTV-NIC strain, specifically PyV mT-IRES-Cre or "MIC" [105]. Our laboratory has recently generated a doxycycline-inducible MIC strain for this purpose (TetOMIC) [144] (described in Chapter 5).

Although PyV mT is not oncogenic in humans, its use as an experimental tool has advanced the field of mammary tumourigenesis and provided insight into the progression of breast cancer in humans. Importantly, research using PyV mT models have helped to identify key proto-oncogenes in human cancer, such as c-Src and PI3K, in addition to the downstream signalling pathways that they initiate during transformation.

1.3 The PI3K signalling pathway

The PI3K pathway is generally considered to be one of the most frequently activated signalling pathways in human malignancies. This can occur through activation of upstream inputs (e.g. growth factor receptors or Ras), loss of negative regulators (e.g. PTEN), or activating mutations

in the p110α isoform of PI3K (*PIK3CA* gene). *PIK3CA* mutations occur in over 30% of breast cancers — making it the second most commonly mutated gene in breast cancer after *TP53* — and loss of PTEN expression has been reported in close to half of all cases [4]. PI3K pathway activation leads to several biological processes that encompass the hallmarks of cancer. Biochemical, structural, and *in vivo* studies on the many isoforms of the PI3K family have helped to elucidate this pathway which is as integral to normal development and function as it is to facilitating transformation.

PI3Ks are a family of lipid kinases that phosphorylate the 3' hydroxyl group on the inositol ring of phosphoinositides (PI) in cell membranes. In order for these reactions to occur, PI3Ks must be recruited to membrane-associated proteins including RTKs, G-protein-coupled receptors (GPCRs), and Ras. The mechanism of PI3K activation has been proposed through examining the relationship between the regulatory and catalytic subunits using conventional structure-function studies as well as crystal structure analysis. An important effector of PI3K signalling is Akt, which phosphorylates several downstream substrates to initiate cell proliferation, survival, and migration. Akt indirectly activates mammalian target of rapamycin (mTOR), a major regulator of translation as well as other metabolic processes. The PI3K/Akt/mTOR axis has come to be regarded as a key pathway associated with breast cancer.

1.3.1 Class I PI3K isoforms

Several isoforms of PI3K exist in mammals and they are categorized into three classes based on their lipid substrates. Class I PI3Ks phosphorylate PI(4,5)P2 to produce the key second messenger, PI(3,4,5)P3, while class II and III are believed to only catalyze the phosphorylation

of PI [145]. Little is known about the functions of the three members of class II (PIK3C2-α, -β, and -γ) [146]. The single class III PI3K, vacuole protein sorting 34 (VPS34), is involved in autophagy, endosomal trafficking, and phagocytosis [147]. While it is not clear if class II and III are relevant in disease, it has become well-established that class I isoforms have significance in human cancer.

Further subdivision of class I PI3Ks into subgroups A and B reflects primarily differences in regulatory subunits. Class IA includes the p110α, -β, and -δ catalytic subunits (encoded by *PIK3CA*, *PIK3CB*, and *PIK3CD*, respectively) which can interact with one of five regulatory subunits collectively referred to as p85 [148-151]. p85 regulatory subunits are encoded by three genes: *PIK3R1* encodes for p85α and two variants, p55α and p50α; *PIK3R2* generates p85β; and *PIK3R3* produces p55γ [152, 153]. While p110α and -β are ubiquitously expressed, p110δ is mainly found in leukocytes of the immune system [154]. The domain organization of the catalytic and regulatory subunits combined with structural data has revealed how the subunits interact and provide insight into mechanisms of activation (Figure 1-1). All of the class IA catalytic subunits have an N-terminal p85-binding domain, followed by a Ras-binding domain, a C2 domain, a helical domain, and the C-terminal kinase domain. The N-termini of the p85α/β regulatory subunits contain a Src homology 3 (SH3) domain and a breakpoint cluster region (BCR) BCR homology (BH) domain flanked by proline-rich regions; at the C-termini is the p110-binding domain, also referred to as the inter-Src homology 2 (iSH2) domain as it is in between two Src homology 2 (SH2) domains (termed nSH2 and cSH2 for N-terminal SH2 and C-terminal SH2, respectively). The remaining p85 isoforms share the C-terminal regions however they lack most of the N-terminus (Figure 1-1).

Crystal structures of p110α complexed with truncated versions of p85 show several

Figure 1-1: Class I PI3Ks

The α, β, δ isoforms of p110 are the class IA catalytic subunits. They have similar domain structures including a p85-binding domain (p85-BD), Ras-binding domain (RBD), C2 domain, helical, and kinase domain. The location of the three cancer-associated hotspot mutations in p110α are indicated (E542K, E545K, H1047R). The p85-binding domain of p110 interacts with the inter-SH2 (iSH2) domain of class IA regulatory subunits. p85α and β are comprised of an SH3 domain, a BCR homology domain (BH), and the iSH2 which is flanked by SH2 domains (nSH2 and cSH2). The N-terminal domains of p85 are absent in p55α/γ and p50α. The only class IB catalytic subunit is p110γ which lacks a p85-binding domain and interacts by an unknown mechanism with its regulatory subunits, p101 and p84. Solid arrows indicate interactions between subunits.

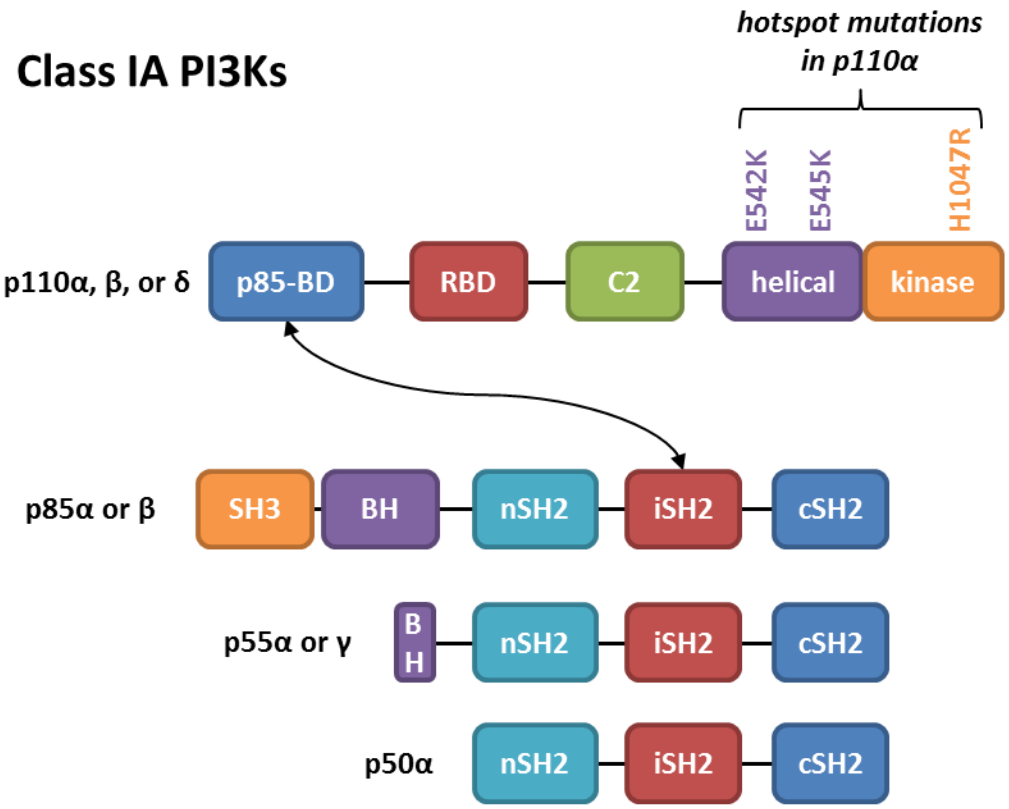
Class IA PI3Ks
hotspot mutations in p110α
E542K
E545K
H1047R
p110α, β, or δ
p85-BD
RBD
C2
helical
kinase
p85α or β
SH3
BH
nSH2
iSH2
cSH2
p55α or γ
B H
nSH2
iSH2
cSH2
p50α
nSH2
iSH2
cSH2

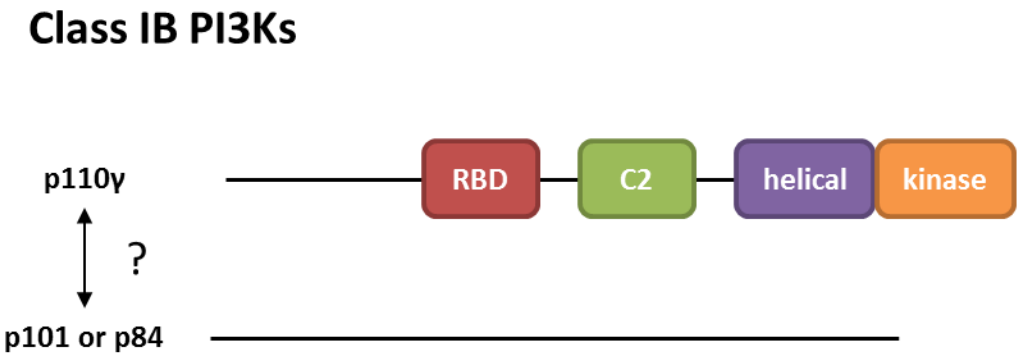
Class IB PI3Ks
p110γ
RBD
C2
helical
kinase
?
p101 or p84

contacts between the two subunits (Figure 1-1) [155-157]. The main binding interaction is mediated by the p85-binding domain in p110α and the iSH2 domain in p85. The nSH2, iSH2, and cSH2 domains of p85 also contact other regions of p110α, specifically the C2, helical, and kinase domains, which keep p110α in an inhibited state. This structural evidence confirmed earlier biochemical studies which had designated both inhibitory and stabilizing functions for p85 towards p110α [158, 159]. Similar interactions have been identified in complexes of p110β or p110δ with regions of p85, albeit with some variances [160, 161]. Binding of the SH2 domains in p85 to phosphorylated tyrosine residues (pYXXM motifs) precludes contact with p110 thereby releasing it from inhibition [156, 162, 163]. Membrane localization can be inherent to this SH2-phosphotyrosine interaction (when binding to RTKs) or it may require recruitment by membrane-associated proteins such as Ras (when binding to adaptors). Proximity to the membrane allows the activated p110 to engage the inositol head group of PI(4,5)P2 in the kinase domain and catalyze phosphorylation of the 3' hydroxyl group.

Class IA PI3Ks can be directly activated by RTKs that contain the p85-SH2 consensus motif (pYXXM) [162, 163]. Many RTKs have been reported to stimulate PI3K activity, including platelet-derived growth factor receptor (PDGFR), insulin receptor, IGFR, and members of the EGFR and fibroblast growth factor receptor families [164-166]. However the p85-SH2 consensus motif is not universal to these receptors and some must utilize adaptor molecules to act as intermediates, such as insulin receptor substrates 1 and 2 (IRS1/2) and Gab1/2 (via a Shc/Grb2 scaffold) [167-169]. In the case of the EGFR family, heterodimerization with HER3, which contains several p85 docking sites, can also provide an indirect mechanism of PI3K activation for the other family members lacking the motif [166]. RTKs that induce Ras can use this as an alternate route to activate p110α and -δ isoforms, but not p110β, which instead

interacts with Rac1 and Cdc42 GTPases [150, 170, 171]. p85 prevents activation by Ras until it becomes engaged by phosphotyrosine thereby dictating a sequential activation of p110 by RTKs and then Ras [172]. Class IA PI3Ks also signal downstream of integrins through p85-SH3 domain interactions with Src family kinases as well as phosphorylation of p85 by focal adhesion kinase (FAK), leading to activation of p110 subunits [173-176].

p110γ (*PIK3CG*), the single catalytic subunit in class IB, was considered to be the only PI3K isoform mediating signalling downstream of Gβγ subunits of GPCRs until p110β was also found to have this capability [151, 177-179]. p110γ has the same domain structure as class IA p110s, apart from the p85-binding domain, and interacts with one of two regulatory subunits, p101 or p87 [180-182]. While p110γ is directly activated exclusively by GPCRs, it may also respond to Ras via its Ras-binding domain [183]. Like p110δ, normal expression of p110γ is mainly leukocytic [154].

The coordination of signalling through the various members of the PI3K family allow for the activation of many downstream signalling pathways. In addition to isoform specificities with regard to activation, cellular localization and tissue distribution likely play a major role in determining how PI3Ks are activated and which signalling pathways are induced.

1.3.2 Signalling through the PI3K/Akt/mTOR axis

All class I PI3Ks contribute to the activation of Akt and mTOR which is important during both normal and tumourigenic circumstances (Figure 1-2). Class I PI3Ks catalyze the production of PI(3,4,5)P3, an important second messenger that recruits proteins to the membrane that contain specific lipid-binding domains. The best characterized of these is the pleckstrin homology (PH)

Figure 1-2: The PI3K/Akt/mTOR signalling axis

Class IA PI3Ks can be recruited to activated growth factor receptors either through direct interaction with the p85 regulatory subunit of PI3K as shown in the figure or through adaptor molecules (not shown). Membrane localization of PI3K allows the p110 catalytic subunit to phosphorylate PI(4,5)P2 which generates PI(3,4,5)P3 which in turn recruits PH-domain containing proteins such as Akt and PDK1. Akt is phosphorylated by PDK1 as well as mTORC2 to become activated after which it can phosphorylate many substrates leading to pathways that induce cellular survival, proliferation, growth, and migration. A major downstream effector of Akt is mTORC1 which becomes activated via the TSC1/2/Rheb axis. mTORC1 induces translation through the phosphorylation of S6 kinase and 4EBP1. S6 kinase can initiate a negative feedback loop to attenuate PI3K signalling. PI(3,4,5)P3 can be dephosphorylated by the PTEN tumour suppressor to antagonize the activation of proteins such as Akt. Activating and inactivating interactions/modifications are represented by arrows and blunt ends, respectively. Direct and indirect interactions/modifications are represented by solid and dashed lines, respectively.

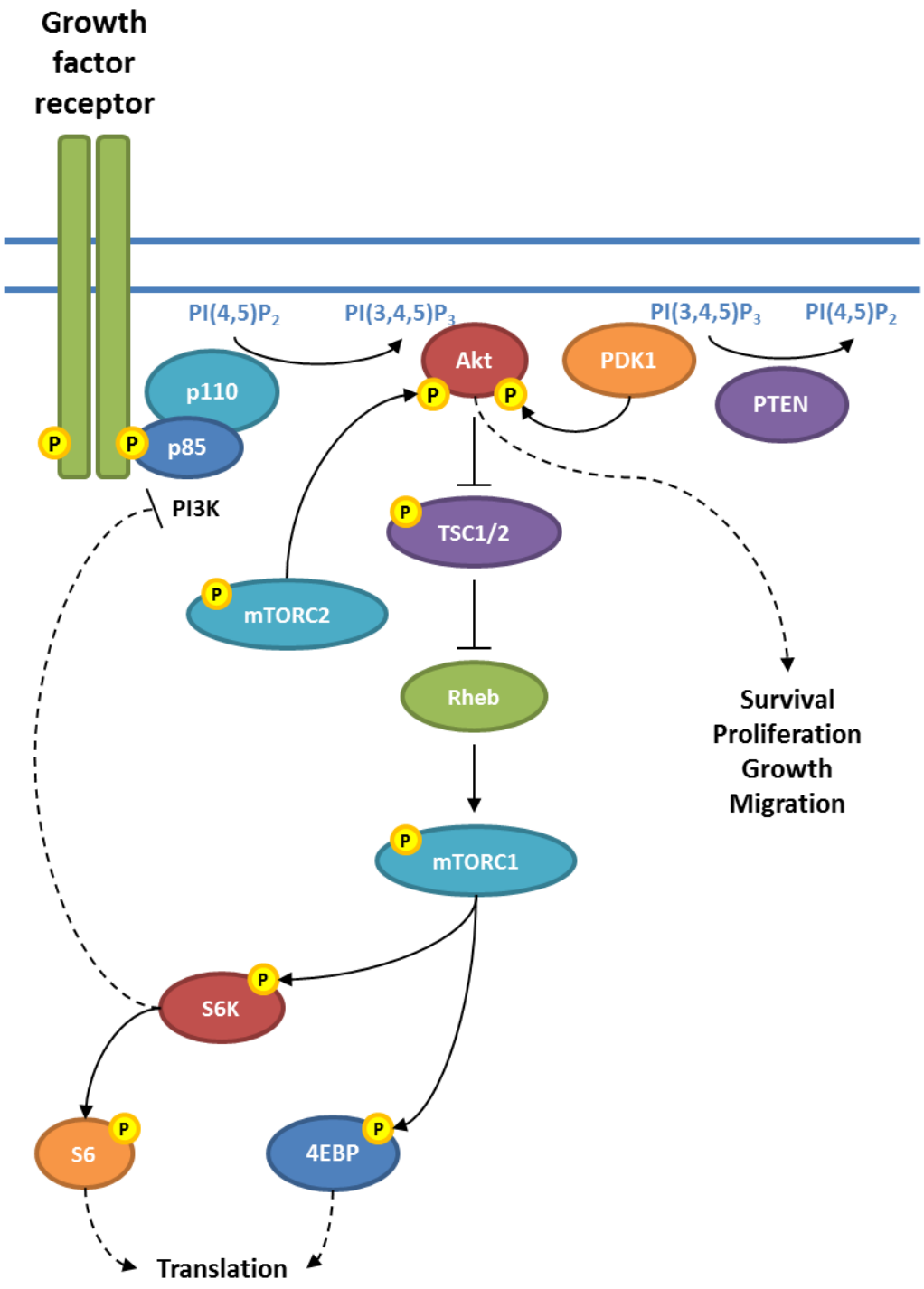
Growth factor receptor
PI(4,5)P2
PI(3,4,5)P3
PI(3,4,5)P3
PI(4,5)P2
Akt
PDK1
PTEN
p110
p85
P
PI3K
TSC1/2
mTORC2
Rheb
Survival
Proliferation
Growth
Migration
mTORC1
S6K
S6
4EBP
Translation

domain which is present in a large group of effector molecules that include kinases and regulators of small GTPases. The first and most extensively studied class I PI3K effector is Akt, which binds to PI(3,4,5)P3 through its PH domain [184, 185]. Akt is a serine-threonine kinase that requires activation by another PH domain-containing protein, phosphoinositide-dependent kinase 1 (PDK1), and the mammalian target of rapamycin (mTOR) complex 2 (mTORC2). PDK1 also requires membrane recruitment via a PI(3,4,5)P3-PH domain interaction before it can phosphorylate Akt on threonine 308 by PDK1, thus activation of Akt requires membrane localization [177, 186-189]. Full activation of Akt requires phosphorylation on serine 473 by mTORC2 [190]. Activated Akt can phosphorylate several substrates that participate in a broad range of cellular effects including survival, cell cycle progression, and motility (discussed in 1.3.4). It is important to note that there are three isoforms of Akt (Akt1, -2, and -3) that exhibit distinct biological functions; for example, Akt1 inhibits while Akt2 promotes breast cancer cell migration and invasiveness in both *in vitro* and *in vivo* contexts [191-194].

A central node in signalling downstream of Akt is mTOR complex 1 (mTORC1) which is involved in several metabolic processes, such as enhanced synthesis of proteins and lipids as well as suppression of autophagy. Akt activates mTORC1 by phosphorylating tuberin sclerosis complex 2 (TSC2) which disrupts its association with TSC1 leading to inactivation of the TSC1/2 complex [195-197]. TSC2 is a GTPase-activating protein (GAP) for the small GTPase Ras homologue enriched in brain (Rheb) and its inhibition by Akt leads to Rheb-mediated activation of mTORC1 [198-200]. mTORC1 is best known for its role in initiating translation and it does so by phosphorylating eukaryotic initiation factor 4E binding protein 1 (4EBP1) and S6 kinase, which in turn leads to the activation of proteins involved in translation [201]. Akt can

also activate mTORC1 by directly phosphorylating proline-rich Akt substrate of 40 kilodaltons (PRas40), a subunit of the complex which negatively regulates mTOR [202].

mTORC1 is also important for initiating negative feedback loops that downregulate Akt signalling. S6 kinase can phosphorylate the adaptor molecule IRS-1 which prevents recruitment of p85 and IRS-1-dependent activation of Akt [203]. This mechanism prevents tumourigenesis in Tsc2-deficient mice and impairs the clinical response of tumours to mTOR inhibition in patients [204, 205]. As discussed later, targeting multiple nodes of the PI3K pathway, especially those upstream of mTOR, appears to rectify this. In addition, S6 kinase-mediated phosphorylation of IRS-1 may also lead to MAPK activation. This alternative feedback loop was identified as a mechanism for MAPK activation in cancer patients after treatment with an mTOR inhibitor [206].

1.3.3 The PTEN tumour suppressor

In addition to negative feedback mechanisms, the pool of PI(3,4,5)P3 at the membrane, and thus the activation of Akt, is controlled by the lipid phosphatases SH2 domain-containing inositol 5'-phosphatase (SHIP2), PTEN, and inositol polyphosphate-4-phosphatase (INPP4). SHIP2 and PTEN act directly on PI(3,4,5)P3 by removing the phosphate group from the 5' and 3' positions, respectively [207-210]. The product of SHIP2, PI(3,4)P2, can be further dephosphorylated by INPP4 to produce PI3P [211]. Of these phosphatases, PTEN has been the most extensively characterized with regard to PI3K signalling since its identification as a tumour suppressor in many human cancers (Figure 1-2) [212, 213]. The tumour suppressive role for PTEN was originally attributed to its lipid phosphatase activity, which was found to be critical in controlling

Akt signalling [208, 209, 214-216]. As a result, several biological processes associated with the PI3K/Akt signalling were uncovered through studying PTEN function and vice versa.

The PTEN gene is encoded by 9 exons which give rise to an N-terminal PI(4,5)P2-binding domain, followed by the phosphatase domain, C2 domain, C-tail containing region, and PDZ-binding domain. The phosphatase domain of PTEN has activity towards both lipid and protein substrates. The idea that the lipid phosphatase activity of PTEN is responsible for its tumour suppressive function has been challenged by recent studies investigating protein phosphatase-dependent roles of PTEN, some of which may impact on cellular transformation. PTEN mutants lacking protein phosphatase activity, including some which are found in Cowden's syndrome patients, have been used *in vitro* to identify potential substrates and the consequences of their dephosphorylation. Inhibition of cell spreading and migration has been shown to involve PTEN-mediated dephosphorylation of the c-Src family kinase Fyn and FAK [217, 218]. Furthermore, loss of either lipid or protein phosphatase activities inhibits cell invasion [219, 220]. PTEN can also upregulate cyclin D1 in a protein phosphatase-dependent manner to cause cell cycle arrest [221, 222]. The dephosphorylation of the proto-oncogene c-Src by PTEN has also been reported, which may have important clinical implications in PTEN-deficient cancers [223].

PTEN may also exert some of its effects in the nucleus, as it has been found to localize to centromeres and can promote upregulation of the DNA repair enzyme, Rad51 [224]. Nuclear import of PTEN is dependent on mono-ubiquitination by the E3 ligase NEDD4-1 on a single lysine residue which is mutated in patients with Cowden syndrome; intestinal polyps from these patients show exclusion of PTEN from the nucleus [225]. More recently, mechanistic details into the nuclear functions of PTEN have been uncovered, including activation of the anaphase

promoting complex (APC)-cadherin 1 (CDH1) complex which regulates the degradation of cell cycle machinery [226]. Interestingly, PTEN regulation of APC-CDH1 occurs independently of its phosphatase activity. It is possible that additional nuclear functions of PTEN are distinct from PI3K signalling given that PTEN does not dephosphorylate PI(3,4,5)P3 on nuclear membranes [227].

Given that loss of PTEN is a common phenomenon in human cancer, many research efforts have been put towards understanding PTEN expression, stability, and function. In addition to mutations throughout the gene and in the promoter, PTEN is subject to a complex network of regulators including epigenetic silencers, transcriptional activators and repressors, non-coding RNAs, and post-translational modifiers. PTEN has also been found to interact with several proteins that affect its phosphatase activity and/or stability.

1.3.4 Biological outputs of PI3K signalling

PI3K can induce several cellular processes, including survival, proliferation, and migration, many of which are mediated by Akt and its diverse range of effectors. While these biological outputs are necessary for normal cellular function, they are prime candidates for co-option during transformation as a result of dysregulation of PI3K pathway components.

Cell survival

Early studies identified a role for PI3K/Akt in mediating cell survival downstream of IGF1 in neuronal cells [228]. Akt appears to promote survival through several mechanisms that prevent

the activation of apoptosis, such as the direct phosphorylation of BCL-associated death promoter (BAD) [229, 230]. The phosphorylation of BAD on serine 136 by Akt results in the sequestration of BAD by the 14-3-3 adaptor protein so that it cannot antagonize pro-survival BCL-2 family members such as BCL-XL and BCL-2 [231, 232]. Inhibition of BAD prevents activation of the mitochondrial apoptotic pathway, which leads to the activation of caspases. Akt has been reported to phosphorylate the pro-apoptotic caspase 9 to inhibit its protease activity, thereby further halting induction of the intrinsic cell death machinery [233].

Another important subset of Akt targets are the forkhead transcription factor (FKHRL or FOXO) family which are prevented from nuclear localization by Akt-dependent phosphorylation. When phosphorylated, FKHRL1/FOXO3 is held in the cytoplasm by 14-3-3 which precludes expression of pro-apoptotic genes such as Fas ligand and BCL-interacting mediator of cell death (BIM) [234, 235]. PI3K activates this pathway through a second mechanism that is independent of Akt, specifically through serum and glucocorticoid-inducible kinase (SGK) which also phosphorylates FKHRL1 leading to its inhibition [236]. SGK belongs to the same kinase family as Akt and is recruited to membrane PI(3,4,5)P3 through its PH domain [237].

Regulation of MDM2 by Akt allows PI3K signalling to regulate levels of the p53 tumour suppressor. Akt phosphorylation of MDM2 enhances its nuclear translocation and thereby promotes its ability to ubiquitinate p53; conversely, overexpression of PTEN in glioblastoma cells leads to stabilization of p53 [238, 239]. So while PI3K/Akt prevents p53-mediated transcription of pro-apoptotic genes, PTEN is required for p53-mediated apoptosis. Interestingly, PTEN expression is dependent on p53-mediated transcription of the PTEN gene [240]. Additional studies have demonstrated that overexpression of PTEN induces apoptosis by

downregulating Akt activation in breast cancer cell lines [208, 216, 241, 242]. On the other hand, Pten-deficient mouse embryonic fibroblasts (MEFs) are resistant to apoptotic stimuli due to enhanced activation of Akt; this can be reversed by re-expression of PTEN [209].

Akt also influences survival signalling downstream of the NFκB transcription factor. Phosphorylation of inhibitor of κ kinase α (IκKα) by Akt allows it to phosphorylate inhibitor of κ B (IκB) which targets it for proteosomal degradation and relieves inhibition of NFκB [243, 244]. It has also been reported that Akt-activated IKKα can directly phosphorylate and activate NFκB [245].

Cell cycle progression

PI3K/Akt signalling promotes cell cycle progression by controlling the expression, stability and activity of cell cycle regulators. The cyclin-dependent kinase (CDK) inhibitors p27 and p21 bind to and inactivate cyclin-CDK complexes during the G1 phase of the cell cycle, causing growth arrest. Akt activation causes downregulation of p27 through inhibition of FOXO-mediated transcription [246]. p27 is also phosphorylated directly by Akt leading to cytoplasmic retention, which is thought to prevent the inhibition of the cyclin E/CDK2 complex [247-249]. These findings were demonstrated in breast cancer cell lines and these studies also showed correlations between activated Akt and cytoplasmic p27 in human breast tumours with poor prognosis. Reduced p27 expression has also been observed in PTEN-deficient cancer cell lines [250, 251]. The involvement of PI3K/Akt signalling in this pathway was first noted by studying PTEN expression in glioblastoma cells [215] .

Phosphorylation of p21 by Akt has been shown to promote cytoplasmic sequestration in some cellular contexts and can also prevent interactions with other proteins that drive cell cycle progression, such as proliferating cell nuclear antigen (PCNA) and CDK2 [252, 253]. Interestingly, p21 phosphorylation and cytoplasmic localization was demonstrated in HER2-expressing human breast tumours and was found to correlate with poor prognosis [252, 254]. An additional level of regulation is imparted by p53, which induces expression of p21 [255]. As discussed earlier, p53 can be degraded in response to Akt activation thus counteracting the tumour suppressive role of p53 in favour of the proto-oncogenic function of Akt resulting in cell cycle progression [238, 239].

Within cell cycle control, Akt can also act stabilize nuclear cyclin D1, allowing for the G1-S phase transition. Cyclin D1 can be phosphorylated by glycogen synthase kinase 3 β (GSK3β) which promotes its relocalization to the cytoplasm and degradation by the proteasome [256]. Akt can phosphorylate GSK3β to inhibit its activity, leading to nuclear retention and stabilization of cyclin D1 levels [257].

Cell metabolism

The PI3K/Akt pathway is an important mediator of insulin signalling and the systemic relevance of this became clear from genetic inactivation studies in mice. Akt can enhance glucose uptake in part by the direct inhibitory phosphorylation of AS160, a Rab GAP, leading to membrane localization of the glucose transporter GLUT4 [258-260]. Akt is also involved in promoting glycogen synthesis through inhibition of GSK3β [257]. Phosphorylation by Akt can inhibit FOXO and PGC-1α transcription factors which induce expression of gluconeogenic enzymes in

the liver, such as phosphoenolpyruvate carboxykinase and glucose-6-phosphatase [261, 262] . Additional changes in tumours can alter other metabolic products; indeed, Akt activates ATP-citrate lyase which is a key enzyme in fatty acid synthesis [263].

In addition to insulin signalling, PI3Ks promote cell growth *in vivo* and this is likely mediated by mTORC1 which activates key pathways involved in cellular metabolism including the translation of proteins [264]. mTORC1 can also respond to low energy levels in the cell through the liver kinase B1 (LKB1)/adenosine monophosphate-activated kinase (AMPK) pathway. LKB1 phosphorylates and activates AMPK, which in turn phosphorylates TSC2, allowing for activation of mTORC1 [265].

Cell polarity and motility

PI3K can induce cell motility through the activation of Rho family GTPases which modulate cytoskeletal dynamics to induce lamelipodia formation, membrane ruffling, and migration. Several GEFs for Rho GTPases contain PH domains and can be recruited and activated through PI(3,4,5)P3 binding. The GEF Vav can induce Rac-dependent lamelipodia formation and membrane ruffling [266, 267]. A second GEF for Rac, P-Rex1, was found to be activated by PI(3,4,5)P3 [268]. Studies in PTEN-deficient cells uncovered a similar role for the regulation of another GTPase involved in maintaining cell polarity and actin remodelling, Cdc42 [269, 270]. Both RhoA and Arf appear to be activated by the GEF ARAP3 which is also recruited to PI(3,4,5)P3 [271].

1.4 Insights from mouse models propel PI3K pathway inhibitors into the clinic

1.4.1 *In vivo* models define isoform-specific functions of PI3K pathway members

Mouse models of PI3Ks have not only confirmed the biological functions delineated *in vitro*, they have provided insight into the systemic consequences of genetic ablation and assigned specific roles for individual isoforms. A variety of approaches were taken including the use of catalytically inactive mutants and tissue-specific promoters. The discrepancies between germline knockouts and inactive mutants highlight stoichiometric equilibrium within the cell, while comparisons between germline and conditional knockouts stress the significance of cellular context.

Initial germline knockouts of the p110α catalytic subunit resulted in embryonic lethality at day E10.5 due to impaired proliferation [272]. Homozygous expression of a catalytically inactive mutant of p110α also caused growth retardation and embryos died at the same stage as what was observed in the germline knockout [273, 274]. Embryonic lethality in this case, and in mice with endothelial-cell specific deletion of p110α, was attributed to vascular abnormalities [274]. This study established p110α as a key regulator of angiogenesis during development, and mechanistically this was linked to RhoA-mediated migration of endothelial cells. p110α is also important during development specifically downstream of Ras since disruption of Ras binding significantly reduces viability of pups and those that survive have defective lymphatic vasculature [275]. MEFs from these animals exhibited impaired growth factor-induced Akt activation and proliferation. Furthermore, MEFs from mice expressing conditional p110α alleles treated with Cre recombinase *in vitro* show reduced activation of Akt in the presence of growth factors [276].

Characterization of heterozygous kinase-dead p110α mutants, which survive to adulthood, revealed a metabolic growth defect associated with impaired insulin signalling. Insulin resistance had also been observed in mice heterozygous for both p110α and p110β [277]. Identification of p110α as the major PI3K involved in the insulin response *in vivo* was also supported by *in vitro* studies using isoform-specific inhibitors [278]. Given the involvement of p110α in metabolic signaling, it was not surprising that this isoform also had a role in controlling cell size. Cardiac-specific expression of a dominant negative p110α transgene, a truncation mutant lacking the kinase domain, led to decreased heart size [279].

Non-redundancy between the α and β isoforms of p110 became clear when it was found that germline knockout of p110β was lethal at an earlier stage than with ablation of p110α [280]. *In vitro* studies at the time also indicated specific roles for the two isoforms in cancer cells, with p110α mediating cell survival and p110β promoting DNA synthesis [281]. Unexpectedly, mice expressing a kinase-dead mutant of p110β were viable but grew slowly and exhibited insulin resistance with age, uncovering a kinase-independent role for p110β in development and metabolism [282]. A more prominent role for p110β in insulin signalling was found upon liver-specific deletion of p110β [283]. *In vitro* ablation of p110β in MEFs from the conditional p110β mice confirmed a proliferative function for the isoform which could be rescued by expression of both wildtype p110β and the kinase-dead mutant. Both studies validated the recruitment of p110β to both RTKs and GPCRs *in vivo* and independently identified novel kinase-independent roles for p110β in cell proliferation and endosomal trafficking.

Disruption of p110δ or -γ by germline knockout or inactivation of the kinase domain in mice produces viable pups with severe defects in lymphocyte development and function [284-288]. These phenotypes reflect the immune-specific expression of these two isoforms. Mice

lacking p85α or -β also exhibit dysregulation of some leukocytic components [289, 290]. In addition to immune defects, p110$\gamma^{-/-}$ animals have impaired insulin sensitivity [291].

The dual role of p85 regulatory subunits in controlling the inhibition and activation of p110 subunits was further emphasized by knocking out single and multiple p85 isoforms. Germline deletion of one or more (but not all) isoforms of p85 unexpectedly led to enhanced insulin sensitivity [292-295]. Complete loss of p85 genes, on the other hand, impairs insulin signalling which was observed in liver- and muscle-specific knockouts of *PIK3R1/2* and in MEFS isolated from germline double knockouts [277, 296, 297]. Loss of p85 in the heart also affected organ size due to reduced cell size [298].

The PTEN tumour suppressor has also been studied extensively *in vivo*. Homozygous ablation of Pten resulted in early embryonic lethality [299, 300]. Although the major phenotype of Pten$^{+/-}$ animals is the development of tumours (discussed in the next section), Pten mouse models have underscored the importance of PI3K signalling in several *in vivo* processes. In addition to tumours, Pten$^{+/-}$ mice develop an autoimmune disorder due to impaired Fas-mediated apoptosis of T lymphocytes and T-cell specific ablation of Pten confirmed an *in vivo* role for Pten in regulating proliferative and apoptotic signals [301, 302]. Deletion of Pten in adipose tissue or the liver resulted in increased insulin sensitivity [303, 304]. Loss of PTEN also appears to confer hypertrophy in certain organs due to increased cell growth [305-308].

1.4.2 PI3K-mediated transformation *in vitro* and mammary tumourigenesis *in vivo*

Although there is considerable data demonstrating the myriad of functions of PI3K pathway members, major roles have also been identified in the normal and transformed mammary gland.

Indeed, some components of the PI3K pathway have been shown to function in normal mammary gland development. Mammary-specific ablation of p110α causes impaired ductal outgrowth in pubertal mice while expression of activated transgenes of p110α, Akt1 or Akt2 delay the involution process [114, 193, 194, 309-312]. Interestingly, mice overexpressing PTEN in the mammary gland exhibit defective lactation [313]. These collective findings, combined with the discovery that several PI3K pathway members are altered in human cancer, prompted studies of these factors in the context of breast cancer.

Loss of PTEN

Germline mutations in the PTEN gene cause a variety of cancer predisposition disorders collectively called PTEN hamartoma tumour syndromes (PHTS). One of the most studied PHTS is Cowden's disease, in which the majority of cases are associated with loss-of-function mutations in PTEN [8, 314]. Individuals with Cowden's have increased susceptibility for breast, thyroid, and uterine cancer. Hereditary PTEN mutations in Cowden's occur at many loci in the gene. In sporadic cancers, PTEN can suffer mutations as well as insertions and deletions along the length of gene. Mapping of the PTEN gene was accomplished by analysing a putative tumour suppressor locus on chromosome 10 that was deleted in human cancers [212, 213]. Allelic deletion of PTEN is a common event in breast cancer, prostate cancer, melanoma and glioma and is often a cause of loss of heterozygosity (LOH) [315]. Although allelic deletion at the PTEN locus is observed in many cancers, there are a variety of mechanisms which designate it as a haploinsufficient tumour suppressor. In addition to genomic aberrations, loss of PTEN function can also be due to reduced expression as a result of promoter methylation, regulation by

non-coding RNAs, and inhibitory post-translational modifications [316, 317]. This "continuum" model of PTEN tumour suppression is prevalent in breast cancers where about half of cases exhibit PTEN deficiency by mechanisms other than gene mutation [315-317]. Indeed mutation of PTEN is relatively rare in sporadic breast cancers (3%) [4]. PTEN loss has been found to be associated with BRCA1-deficient breast cancers and sensitivity to poly-ADP-ribose polymerase (PARP) inhibitors [318, 319]. It is therefore not surprising that PTEN mutation or loss occurs in 35% of basal-like cancers which tend to harbour *BRCA1* mutations [4]. There is also correlations between PTEN loss and HER2-enriched subtype (19%) as well as HER2 amplification; breast cancers harbouring both of these alterations may be more resistant to HER2-targeted therapies [4, 320-322].

PTEN-deficient cancer cell lines have provided an ideal model system for highlighting how PI3K/Akt signalling could contribute to cellular transformation [215, 242]. Since germline deletion of Pten is embryonic lethal, the generation of Pten knockout cells *in vitro* was accomplished using MEFs from $Pten^{-/-}$ mice; these cells exhibited increased activation of Akt and resistance to apoptosis [209, 300]. However this was soon overshadowed by the phenotype of animals heterozygous for the Pten conditional allele which validated the tumour suppressive role of Pten in an *in vivo* context.

Several $Pten^{+/-}$ strains were published and all presented with characteristics of Cowden's syndrome, developing neoplasia or tumours in several tissues, the most frequently affected being the mammary gland, endometrium, thyroid and prostate [299, 300, 323, 324]. Mammary gland tumours were detected in approximately half of the female cohort for one particular strain of $Pten^{+/-}$ mice [324]. Single-copy knock-in of a hypomorphic Pten allele also resulted in tumours in multiple organs including the mammary gland, and brought forth the concept that reducing

PTEN expression in the absence of allelic loss could also influence tumour susceptibility and penetrance in a dosage-dependent manner [325]. This was further supported by similar phenotypes in mice where Pten expression was decreased by germline expression of short hairpin RNAs [308]. Interestingly, the acute loss of both PTEN alleles induces p53-mediated cellular senescence which causes irreversible growth arrest and has been shown to suppress prostate tumourigenesis *in vivo*. This was originally thought to occur via $p19^{Arf}$-mediated inhibition of MDM2 but recently it was shown to be more dependent on upregulation of p53 via mTORC1 [326, 327]. These findings provide a potential rationale for why partial decreases in PTEN expression may be more conducive to tumourigenesis than complete deletion and may explain the major contribution of non-genetic means of PTEN loss in human cancer. Ablation or hypomorphic expression of other pathway members (specifically Akt1, PDK1, and components of mTORC1/2) suppresses tumourigenesis in $Pten^{+/-}$ mice [328-330]. This evidence suggests that tumourigenesis in Pten-deficient models is due to enhanced PI3K signalling.

To address the effect of homozygous ablation of Pten in specific tissues, conditional knockouts were subsequently generated; of these, tumours developed most rapidly with Pten deficiency in the mammary gland, prostate, and T cells [331-333]. Mammary epithelial-specific deletion of Pten led to increased ductal outgrowth and branching as compared to controls, as well as evidence of lobular-alveolar budding which does not normally occur until pregnancy [331]. Enhanced lobular-alveolar development persisted during pregnancy and caused a delay in involution. These phenotypes were accompanied by increased proliferation of mammary epithelial cells during puberty and pregnancy, while reduced apoptosis was observed during involution. Tumour formation was detected in mice as young as 2 months and presented with a variety of histopathologies including fibroadenoma and pleiomorphic adenocarcinoma.

The conditional Pten mouse model has been used to study whether loss of Pten can cooperate with other oncogenic events during mammary tumourigenesis, including activation of HER2/ErbB2. Pten deficiency accelerated tumourigenesis and increased metastasis to the lungs in the ErbB2^{KI} model (NeuNT/MMTV-Cre), in which endogenous expression of an ErbB2 point mutant is coupled to Pten ablation in the mammary epithelium [334]. Mammary tumours arising in Pten-deficient/ErbB2^{KI} mice exhibited a variety of histopathologies, including some reminiscent of tumours from single mutants (adenomyoepithelioma typical of Pten knockout and solid ErbB2-type comedo-adenocarcinoma) as well as a Wnt1 signature phenotype and a previously uncharacterized morphology. These tumours expressed high levels of ErbB2 protein although the ErbB2 transgene was not amplified; this in contrast to the amplification of the ErbB2 transgene in the ErbB2^{KI} strain [62]. Approximately half of the Pten$^{+/-}$/ErbB2^{KI} tumours had undergone loss of heterozygosity at the Pten locus. Positive staining for both luminal and basal cytokeratins combined with gene expression profiling suggested that Pten-deficient/ErbB2^{KI} tumours were similar to tumours from basal-type mouse models. When compared to human data sets, these tumours clustered with the HER2- and basal-like molecular subtypes. Interestingly, mammary tumours from mice with germline heterozygous loss of Pten also display basal characteristics and cluster with the basal-like subtype of breast cancers including BRCA1-deficient tumours [318]. Pten$^{-/-}$/MMTV-Cre animals were also characterized in this study and interestingly did not develop tumours, possibly due to the p53-mediated senescence program that can be induced upon acute loss of Pten [326, 327]. This phenotype was contrasted by the complete penetrance of mammary tumours observed previously by Li *et al* and might be explained by differences in the genetic background of the mice [331]. Enhancement of

mammary tumourigenesis and metastasis by Pten loss was also shown in a mouse model with transgenic expression of activated ErbB2 (discussed in more detail in Chapter 3) [106].

Activation of PI3K

In addition to PTEN, activating mutations in other components of the PI3K signalling pathway can be detected in breast cancer. The most prevalent of these mutations occurs in the *PIK3CA* gene, which encodes the p110α isoform of PI3K [320, 335-339]. *PIK3CA* mutations are observed in 36% of breast cancer cases, making it one of the most frequently mutated genes in breast cancer along with TP53 [4]. Mutations in *PIK3CA* are single nucleotide substitutions, the majority of which cluster in exons 9 and 20 which correspond to the helical and kinase domains of the protein, respectively. The most frequent mutations are at three "hotspots", including two glutamic acid to lysine substitutions at residues 542 and 545 (helical domain) and conversion of a histidine at position 1074 to arginine (kinase domain) (Figure 1-1). There is a strong correlation between *PIK3CA* mutations and luminal A and B subtypes (45% and 29%, respectively) as well as hormone receptor-positivity in general [4, 320, 340]. Like ER-positive/luminal cancers, *PIK3CA*-mutant cancers have also been associated with better prognosis [341-344]. However, these findings contradict data from other studies which conclude that *PIK3CA* mutations correlate with poor outcome or had no correlation with outcome [345-348]. Interestingly mutations can be detected at early stages of breast cancer (i.e. DCIS) as well as in invasive breast cancer [348-350]. This suggests that these mutations may have more influence on tumour initiation than during later stages of progression and malignancy.

Many studies have investigated whether PTEN deletion and *PIK3CA* mutation are mutually exclusive events in breast cancer. Although some studies have reported co-existence of these alterations in the same tumour, the current view is that this is relatively rare and for the most part they are considered to be mutually exclusive [4, 317, 320, 351, 352]. This may be reflective of the fact that PTEN loss occurs at the highest frequency in the basal-like subtype while *PIK3CA* mutations are more prevalent in the ER-positive/luminal subtype. However, almost half of basal-like tumours display focal amplification of the wildtype *PIK3CA* gene [4]. Furthermore, basal-like cancers are more associated with PI3K pathway activation than luminal cancers. Activation of Akt and its downstream effectors is more often associated with loss of PTEN and amplification of *PIK3CA* than with *PIK3CA* mutation, a phenomenon that has been previously documented [4, 351]. In support of this, another study demonstrated that Akt is not significantly activated in *PIK3CA*-mutated cancer cells and breast tumours and proposed that transformation could be driven by Akt-independent mechanisms downstream of mutant *PIK3CA* [353]. This suggests that endogenous expression of *PIK3CA* mutants may not be as effective in activating Akt in the presence of functional PTEN.

The ultimate relevance of *PIK3CA* mutation in human breast cancers is still under intense investigation however it has become clear that activation of the PI3K pathway has an important role in *de novo* and acquired therapeutic resistance. There are conflicting conclusions regarding the prognostic value of *PIK3CA* mutations in hormone treatment [342, 344, 351]. However, inhibitors against mammalian target of rapamycin (mTOR), a downstream effector of the pathway, seem to have more clinical promise in combating resistance to endocrine therapies (see section 1.4.3). *PIK3CA* mutations appear to have more influence with regard to resistance to HER2-targeted therapies such as trastuzumab [321]. In fact, mutations in *PIK3CA* are also

associated with HER2 overexpression and occur in 39% of tumours of the HER2-enriched subtype [4, 320].

Like many other cellular proto-oncogenes, the transforming potential of PI3K was first investigated using viral PI3K. The PI3K gene from avian sarcoma virus (v-p3k) transformed chicken embryonic fibroblasts (CEFs) and could also induce angiogenesis in the chorioallantoic membrane of the chicken embryo [354-356]. Interestingly, c-p3k, the cellular counterpart of v-p3k, which encodes p110α, could only transform CEFs when localized to the membrane by fusion with Gag or myristoylation sequences [355]. The lipid kinase activity of these membrane-targeted c-p3ks were increased and allowed for constitutive activation of Akt, a requirement for oncogenicity in this system.

These studies, in addition to the known prevalence of *PTEN* deletion in cancers at the time, prompted the sequencing of PI3K genes in human tumours which revealed the existence of activating mutations in *PIK3CA* (p110α) [335]. Since this first report, it is now known that many cancers harbour these mutations, often with high frequency as is the case in breast cancer [320, 335-339]. The three hotspot mutants (E542K, E545K and H1047R) were subsequently characterized extensively *in vitro* to determine if they were truly oncogenic (Figure 1-1). Initial experiments revealed an increased lipid kinase activity for all mutants [335, 357]. These mutants were able to recapitulate the effects of the viral PI3K gene in the embryonic chicken system, and could induce tumour formation *in vivo* by injection into chick wings [357, 358]. In human colorectal cancer cells, *PIK3CA* hotpot mutants caused enhanced Akt activation and downstream signalling, growth factor-independent proliferation, resistance to apoptosis, increased migration and invasion, and anchorage-independent growth [359]. More importantly, subcutaneous injection of mutant cells in mice resulted in tumour growth *in vivo*.

Studies using immortalized human mammary epithelial cell culture systems identified these same oncogenic phenotypes upon expression of the *PIK3CA* mutants, including orthotopic tumour growth in mice [360, 361]. When cultured in three dimensional systems, mutant mammary epithelial cells exhibited abnormal acinar development [360]. Interestingly, some non-hotspot mutations in *PIK3CA* also show transforming potential *in vitro* [362]. In general, mutational activation of *PIK3CA* was more effective at transformation than membrane anchoring by myristoylation [358, 361]. Mutation of p110β at a residue analogous to the E545K in p110α (E552K) did not confer oncogenicity in human mammary epithelial cells, which could only be achieved for this isoform upon myristoylation [361]. These observations provide a possible explanation for the selective mutation of p110α in human cancer.

The structure of p110α was critical in predicting the mechanisms of action for cancer-associated mutations [155, 156]. The two helical domain hotspot mutants, E542K and E545K, are located at the interface of the nSH2 domain of the p85 regulatory subunit. Substitution of the negatively charged glutamic acid with a positively charged lysine causes a charge reversal that is thought to disrupt the inhibitory interactions with p85. This hypothesis was supported by *in vitro* experiments in which mutation of basic residues in the p85 nSH2 domain to glutamate abrogated inhibition of wildtype p110α; furthermore, these p85 mutants could effectively inhibit p110α E545K through restoration of the electrostatic interaction [156]. Crystallization of the H1047R mutant revealed conformational changes when compared to the wildtype structure which are thought to enhance interaction with membrane phospholipids [157]. In agreement with these structure-based conclusions, biochemical assays in CEFs demonstrated differential requirement for p85 and Ras binding by the different mutants. Interaction with p85 is necessary for transformation by H1047R but not by helical domain mutants [363]. It is likely that the relief of

p85 inhibition conferred by E542K and E545K precludes the requirement for p85. On the other hand, transformation by helical domain mutants requires binding of Ras, while the H1047R mutant does not [363]. Presumably the increased membrane localization predicted by the H1047R mutant structure circumvents the need for membrane recruitment by Ras. These mechanistic differences may manifest in distinct biological consequences in the context of transformation. For example, E545K was superior to H1047R in promoting orthotopic growth and lung colonization of breast cancer cells in mice [364]. A recent study has also suggested the E545K, and not H1047R, can directly interact with IRS-1 for membrane localization[365]. However, these studies contrast with an *in vivo* model of mammary tumourigenesis, where E545K expression initiated tumours later than with expression of H1047R [311].

Although Akt activation is generally considered a robust readout for PI3K pathway activation, clinical data as well as studies in breast cancer cell lines suggest that this may not be the case downstream of *PIK3CA* mutations specifically. As discussed earlier, PTEN-deficient breast cancers exhibit higher activation of Akt than those with *PIK3CA* mutations [4, 351]. An *in vitro* study reported reduced Akt activation in *PIK3CA* mutant cancer cells and went on to identify SGK3 as the dominant mediator of mutated p110α [353]. These findings suggest that clinical targeting of PI3K or upstream activators will hopefully attenuate both Akt-dependent and -independent arms of tumourigenic signalling.

Several mouse models have been generated to study activating p110α mutations *in vivo*, the majority of which are specific to the mammary gland. One of the first strains expressed a myristoylated *PIK3CA* transgene under the control of the MMTV promoter (MMTV-myr-p110α) [309]. Membrane-anchoring of p110α increased the propensity for abnormal ductal structures however complete tumour formation was only apparent upon histological analysis of mammary

glands in 12% of virgin mice; this proportion doubled in multiparous animals. In contrast to the low penetrance of tumours in the MMTV-myr-p110α model, the p110α H1047R mutant was more potently oncogenic in a variety of mammary-specific transgenic models that have very recently been characterized [310, 366, 367]. This likely reflects the relatively weaker *in vitro* transforming potential of myristoylated p110α in comparison to that of the hotspot mutants [361]. The first *in vivo* model demonstrating the oncogenicity of the H1047R mutant utilized a Tet-inducible transgene that when expressed in the lung caused adenocarcinoma [368]. A similarly designed Tet-inducible H1047R mutant transgene was used in combination with the MMTV-rtTA strain to investigate its potential in mammary tumour initiation [367]. Mammary tumours developed in bigenic mice after 7 months of doxycycline induction. At the same time, two additional H1047R transgenic strains were published in which a Cre-inducible transgene was knocked in at the Rosa26 locus [310, 366]. Expression of the knock-in transgenes in the mammary epithelium was achieved by crossing to either the MMTV-Cre or WAP-Cre strains. Mammary tumours developed in all MMTV-Cre virgin mice (with the average onsets at approximately 6 months of age) and all WAP-Cre mice after pregnancy.

Although the p110α H1047R transgene could induce mammary tumours *in vivo*, the aforementioned models lack physiological relevance since expression is not driven by the *PIK3CA* gene promoter. To attain endogenous levels of the H1047R mutant, constructs targeting the murine *PIK3CA* allele were designed to include a Cre-inducible exon containing the H1047R substitution [65, 66]. The targeted allele produces wildtype p110α in the absence of Cre and expresses the H1047R mutant in the presence of Cre; both gene products are under the control of the endogenous *PIK3CA* promoter and can undergo normal splicing events. Heterozygous expression of the H1047R mutant in the mammary gland was achieved using the MMTV-Cre

strain and resulted in mammary tumours after about 1.5 years although all mice were affected; tumour onset could be accelerated by pregnancy. The much longer latency in these strains when compared to the transgenic models are likely due to differences in expression levels and indicate that endogenous p110α H1047R requires additional genetic aberrations for tumour initiation. Indeed, in some models of p110α activation mammary tumours showed evidence of p53 mutation, with one study identifying two tumours with mutations in p53 that are analogous to mutations found in some cancers [66, 309].

Despite the differences in strain design, mammary-specific expression of p110α H1047R resulted in enhanced branching and dilation of ducts as well as premature lobular-alveolar development during puberty. In general, mammary tumours were heterogeneous in their histopathology, with adenomyoepithelioma and adenosquamous carcinoma being the major types in transgenic mice and fibroadenomas and carcinomsarcoma/sarcoma in the endogenous knock-in animals. H1047R-driven tumours expressed both luminal and basal cytokeratins, with evidence of double-positive cells in some instances suggestive of a bipotent cell of origin. Lastly, these tumours were ER-positive, a common feature of human breast cancer that often overlaps with the presence of *PIK3CA* mutations. Metastasis data was reported for only one of these H1047R transgenic models, where lung lesions were detected only rarely in tumour-bearing mice [366]. Interestingly, a recent study characterized WAP-Cre/E545K mutant mice which develop tumours later than the WAP-Cre/H1047R strain [311]. The heterogeneous E545K tumours were most often adenosquamous carcinoma and stained positively for luminal/basal cytokeratins and ERα.

Studies have investigated whether p110α mutants can cooperate with other oncogenic events. Transgenic H1047R expression can cooperate with p53 loss in the mammary gland

leading to accelerated tumour onset and a wider range of tumour histopathologies [366]. Interestingly, despite the overexpression of nuclear p53 (reflective of inactivating mutations) in tumours induced by myr-p110α, no synergistic effects were observed between myr-p110α expression and loss of one p53 allele in the germline; instead, dysregulation of the retinoblastoma tumour suppressor pathway enhanced tumourigenesis in these mice [309]. More recently, the inducible H1047R transgene was crossed to the MMTV-HER2 strain leading to enhanced tumourigenesis and metastasis in double mutants compared to single mutants [369]. This model is representative of the fact that *PIK3CA* mutations often associate with HER2 overexpression in breast cancer [4, 320]. It is interesting to note that ovarian-specific expression of the H0147R mutant causes hyperplasia that requires concurrent deletion of Pten in order to progress to adenocarcinoma [64]. This may have relevance in breast cancer for the possible subset of tumours with both genetic alterations [317, 351, 352].

Cancer-associated mutants of p85α, as well as analogous truncations generated experimentally, maintain their abilities to bind and stabilize class IA p110 subunits however they lack inhibitory function leading to enhanced Akt signalling and transformation [370, 371]. Although infrequent in human cancer, mutation of p85 regulatory subunits may represent an alternative mechanism for activating wildtype p110 enzymes to initiate transformation.

Loss of PI3K

Determining if PI3K isoforms are essential for mammary epithelial transformation involves removal of PI3K in systems driven by oncogenes such as HER2 and PyV mT. The development of knock-in strains carrying kinase-dead p110 genes or conditional p110 alleles has allowed us to

study the impact of p110 function on *in vivo* tumourigenesis in these established mouse models of cancer. These studies also shed light on the relative contributions of the different p110 isoforms as well as the compensatory abilities of non-targeted isoforms in a given oncogenic context.

Isoform selectivity may also play a role downstream of specific oncogenic signals. MEFs from a conditional p110α strain can be treated with Cre recombinase *in vitro* to ablate p110α expression, resulting in impaired Akt activation downstream of a variety of growth factors [276]. In contrast to wildtype MEFs, p110α-deficient cells could not undergo transformation in the presence of IGFIR/IGF or activated mutants of either Neu or EGFR. This suggested that the p110α isoform may be critical for cellular transformation downstream of these growth factor receptors, and possibly others, *in vivo*. In fact, mutation of the Ras-binding domain in p110α impairs *in vivo* lung tumourigenesis mediated by oncogenic Ras and this interaction may have a partial requirement in lung tumour maintenance [275, 368, 372].

The p110α isoform also appears to be critical for mammary tumourigenesis mediated by activated ErbB2/Neu. We recently demonstrated that conditional deletion of p110α severely impairs tumourigenesis in a mouse model driven by activated ErbB2 (MMTV-NIC), while our collaborators observed the opposite effect in p110β-deficient/NIC mice (described in more detail in Chapter 4) [114]. Even in the absence of oncogene expression, conditional ablation of p110β in the mammary gland induced hyperplasia. The p110β phenotype was unexpected and also contrasted with a separate study in which expression of a kinase-dead p110β mutant delayed mammary tumourigenesis in a similar model of activated ErbB2 (NeuT) [282]. This is most likely explained by differences in the stoichiometry of p110 subunits when comparing a conditional knockout versus conditional knockin of an inactive mutant. *In vitro* assays suggested

that in the NIC model loss of p110β frees up RTKs for binding of p110α leading to enhanced tumourigenesis. The converse situation in p110α knockouts does not cause increased oncogenicity due to the lower intrinsic kinase activity of p110β (and other p110s) relative to p110α [276, 278, 373]. By contrast, in mice expressing catalytically inactive p110β in the NeuNT model receptor occupancy is maintained by the mutant protein which acts as a dominant negative in this context. The conditional strains also allowed for investigation of each isoform in the maintenance of ErbB2-driven tumour cells. *In vitro* ablation of either isoform in NeuT cells followed by orthotopic injection in nude mice revealed that p110α impaired, while p110β enhanced, *in vivo* tumour outgrowth [114].

PI3K signalling is also important for PyV mT-driven mammary tumourigenesis. Mice with mammary-specific expression of an Y315/322F mutant, which abrogates both direct and indirect recruitment of PI3K, have impaired mammary tumourigenesis and metastasis when compared to wildtype PyV mT animals [193, 194, 374]. The development of tumours expressing the Y315/322F mutant may occur through upregulation of ErbB2 and ErbB3, an ideal way to reactivate PI3K signalling [374]. Transfection of the Y315F mutant in immortalized mammary epithelial cells from both mice and humans also impairs transformation *in vitro* [375]. This study went on to suggest that PyV mT may be dependent on the recruitment of the p110α isoform specifically. Using p110α-ablated MEFs they demonstrated that this isoform was required for PyV mT-mediated transformation both *in vitro* and in orthotopic injections in nude mice. These findings were validated *in vivo* where heterozygous loss of p110α in the mammary epithelium delayed tumour onset in the MMTV-PyV mT model while p110β ablation enhanced tumour burden [114]. These phenotypes, as well as effects on tumour maintenance in PyV mT cells, were similar to those observed in the activated ErbB2 model and again are likely due to the

relative occupancy of receptors by each isoform. Whether a catalytically inactive p110β produces a delay in PyV mT mammary tumourigenesis remains to be seen. The fact that loss of only one p110α allele could increase tumour latency suggests that p110α is likely an essential mediator of tumourigenesis downstream of PyV mT. Thus it may not be surprising that homozygous deletion of p110α could not be achieved in the PyV mT due to potential selection for Cre recombinase-negative cells [108, 114]. However, the recent generation of a Cre recombinase-coupled PyV mT model (TetOMIC) circumvents this issue so that the impact of complete p110α loss on PyV mT mammary tumourigenesis can be addressed (elaborated on in Chapters 5 and 6) [144].

Although one study shows that p110β kinase activity is important for ErbB2-driven mammary tumour initiation, the compensation by p110α in the complete absence of p110β protein in both the ErbB2 and PyV mT models is suggestive of a dominant role for p110α in mammary tumourigenesis [114, 282]. Indeed, both ErbB2- and PyV mT-driven mammary tumours are more sensitive to p110α-specific pharmacological inhibitors than those specific for p110β *in vitro* and orthotopically *in vivo* [114]. However, transformation in other tissues or tumours driven by different oncogenic events may exhibit differential dependence on p110 isoforms. This may be especially true considering genetic alterations in the PI3K pathway itself. Knockdown of p110α impaired growth of colon cancer cell lines with *PIK3CA* mutation but not in cancer cells lacking PTEN [376]. Instead, these PTEN-deficient lines exhibited a dependence on p110β. This is in line with the fact that breast cancer cells lacking PTEN have increased sensitivity to p110β-specific inhibitors [377]. A requirement for p110β, but not p110α, was also observed in an *in vivo* model of prostate cancer induced by conditional Pten loss [283]. Prostate tumour development was also reduced in germline $Pten^{+/-}$ mice lacking p110β function but was

not affected by inactivation of p110α [378]. Interestingly, loss of p110α activity appeared to have some effect in impairing transformation of other tissues in these mice. Other Pten-deficient tumour models seem to depend on both isoforms [379]. Recent work suggests that isoform selectivity might be based on yet other oncogenic events. Murine ovarian tumours driven by Pten-deletion and KRas exhibit a requirement for p110α and not p110β, while the opposite is true for Pten-null tumours also lacking p53 [380]. A very recently published report might reconcile whether tissue context or mode of activation defines p110 isoform choice during tumourigenesis: in contrast to the Pten-deficient prostate models which were dependent on p110β and not p110α, prostate-specific expression of PyV mT is not affected by loss of p110β and instead requires p110α [283, 378, 381]. This observation recapitulates the selective dependence of PyV mT on p110α for tumourigenesis in the mammary gland [114].

The inducible p110α H1047R transgenic mouse was used to determine if mammary tumours generated in this strain were dependent on the initiating oncogenic signal itself [367]. Upon doxycycline withdrawal, some tumours regressed completely but the majority only partially regressed before resuming growth indicating that mutant p110α was already dispensable. Recurrence was shown to be mediated by reactivation of PI3K signalling in some cases, while other recurrent tumours evolved via a PI3K-independent mechanism, specifically amplification of the c-Myc proto-oncogene. This study provided an elegant approach to predicting *de novo* and acquired resistance to inhibition of mutant p110α *in vivo*. The applicability of these "loss-of-function" models is evident considering the many therapies targeting the PI3K pathway that are currently undergoing preclinical and clinical trials.

1.4.3 Clinical targeting of PI3K pathway members in breast cancer

While many of the current efforts in PI3K research are directed at improving the efficacy of PI3K inhibitors in cancer patients, first generation compounds were instrumental in uncovering the biological outputs of PI3K signalling. The first inhibitors against PI3K activity were the naturally occurring antifungal wortmannin (non-competitive, irreversible) and the chemically synthesized LY294002 (ATP competitive) [382, 383]. These compounds lack class I p110 isoform selectivity and are thus called "pan" inhibitors. Many studies have used these compounds to define functions attributable to PI3K signalling and to link these functions to PTEN regulation [188, 215, 228, 230, 237, 301, 384, 385]. While wortmannin and LY294002 are potent inhibitors of PI3K they exhibited high toxicities at low doses *in vivo* which have prevented their transition to the clinic so they have remained as key experimental tools for *in vitro* research. The second generation of pan PI3K inhibitors exhibit improved pharmacodynamics and tolerance *in vivo*. The reversible ATP-competitive pan PI3K inhibitor GDC-0941 (Pictilisib, Genentech) is currently in clinical trials for the treatment of several cancer types, including breast, and has been characterized extensively in *in vitro* and *in vivo* preclinical models [66, 386]. Another pan PI3K inhibitor, BKM120 (Buparlisib, Novartis) is also being tested in cancer patients.

In addition to pan PI3K inhibitors, a new class of compounds have been generated which exhibit enhanced selectivity for particular p110 isoforms. The many overlapping functions between the different p110 isoforms might suggest that targeting all isoforms might be more efficacious. However, the choice to target a single isoform is supported by experiments using chemical and genetic approaches that have identified isoform-specific functions. These arguments may resolve themselves when considering certain contexts where particular isoforms

are more prevalent. As discussed earlier, p110β-specific inhibitors may be most useful in Pten-deficient breast and prostate cancers [283, 376, 377]. The use of p110α-specific inhibitors may circumvent the issue that current PI3K inhibitors are generally not selective for *PIK3CA* hotspot mutants. Indeed, a p110α-specific compound, A66, was found to have better sensitivity in cancer cells with *PIK3CA* mutation [387]. The p110α-specific inhibitor BYL719 (Novartis) is entering clinical trials in breast cancer treatment. Furthermore, the restricted expression of p110δ to leukocytes may explain the clinical success of the p110δ-specific inhibitor GS-1101 (Idelalisib, Gilead) in combination with other therapies in blood cancers.

Rapamycin and other inhibitors of mTOR represent another widely studied group of compounds that have been valuable not only in elucidating mechanistic details of PI3K pathway activation but also in the treatment of cancers. Less toxic analogues of rapamycin ("rapalogues"), such as everolimus (RAD001), have been used extensively in preclinical models and are currently being tested in a variety of settings in the clinic. mTOR inhibitors can effectively dampen hyperactive PI3K/Akt signalling induced by PTEN loss and impair tumour growth in xenografts and in mouse models of Pten-deficiency [388-391]. However in circumstances where the PI3K pathway is not already activated, mTOR inhibition can enhance Akt activation by preventing S6K-mediated negative feedback; this has been observed in RAD001-treated human tumours [205]. Targeting mTOR in combination with upstream components of the pathway may circumvent this issue. In fact several dual PI3K/mTOR inhibitors have been developed for this reason. These inhibitors exploit the fact that PI3K and mTOR belong to the same superfamily.

The problem of resistance has emerged for inhibitors targeting PI3K, mTOR, and those that inhibit both proteins. Several mechanisms have been identified which appear to confer

resistance to PI3K pathway inhibition. In some cases this is due to compensation by other components of the pathway. Consistent with the rationale for developing dual PI3K/mTOR inhibitors, breast cancer cell resistance to a p110α-specific inhibitor was found to be caused by enhanced mTORC1 activation and could be reversed with RAD001 treatment [392]. In other cases, insensitivity evolves as a result of other oncogenic events. In breast cancer cells, PI3K pathway inhibitors have been shown to lead to upregulation and increased signalling of HER/ErbB RTKs [393, 394]. These cells also exhibited increased activation of MAPK in response to PI3K/mTOR inhibition, which fits with earlier findings that the sensitivity of breast cancer cells to PI3K inhibitors may depend on the activation of Ras [377, 394, 395]. This is also true in a mouse model of lung cancer driven by KRas, where treatment with the dual PI3K/mTOR inhibitor NVP-BEZ235 (Novartis) does not result in antitumour activity [368]. In line with this, mTOR inhibition has been associated with MAPK activation in several *in vitro* and *in vivo* models as well as in human breast tumours [206, 396]. In many of these systems, resensitization or synergistic efficacy could be accomplished by combining PI3K pathway inhibition with inhibitors targeting the compensatory mechanism (e.g. HER2 and/or MEK inhibitors) [206, 368, 377, 394, 396]. Targeting both PI3K and MAPK pathways may have some clinical benefit for a variety of cancers despite increased side-effects [397]. Another candidate involved in resistance to PI3K pathway inhibition is the proto-oncogenic c-Myc signalling axis which is enhanced either through amplification/overexpression or increased activation of upstream inputs [367, 398, 399].

These studies suggest that PI3K pathway inhibition in the clinic may be more valuable when combined with other therapies, especially in reversing *de novo* and/or acquired resistance. Activation of PI3K/Akt signalling, most often through *PIK3CA* mutation or PTEN loss, can

further exacerbate insensitivity to standard treatments, which in breast cancer include chemotherapies, endocrine therapy (ER-positive tumours), and HER2-targeted therapies (HER2-positive tumours). This may not be surprising given the high prevalence of *PIK3CA* mutations in ER-positive/luminal and HER2-positive breast cancers, the latter of which also exhibit frequent loss of PTEN expression [4, 320]. One of the first studies on the *PIK3CA* hotspot mutants demonstrated their ability to turn breast cancer cells resistant to the chemotherapeutic agent paclitaxel [360]. In breast cancer cells that are resistant to endocrine therapy, increased activation of HER/ErbB receptors is observed which may in turn enhance PI3K signalling [400]. The use of mTOR inhibitors has been found to restore sensitivity to endocrine therapy in resistant breast cancer cells [401, 402]. Despite these findings, there is conflicting clinical data regarding whether PI3K pathway activation is predictive of outcome in endocrine-treated breast cancers [342, 351, 403, 404]. The aforementioned rapalogues have shown success in improving the efficacy of endocrine therapies in patients that had progressed on these treatments (e.g. the ongoing BOLERO-2 and TAMRAD clinical trials) [405, 406]. Upcoming trials will be assessing the effects of combining endocrine treatment with a pan PI3K inhibitor (such as BMK120 or GDC-0941) in resistant patients (BELLE-2 clinical trial) [407].

An even larger body of preclinical and clinical evidence demonstrates PI3K pathway-mediated resistance against HER2-targeted therapies in breast cancer. These therapies include the widely used monoclonal antibody targeting HER2, trastuzumab (Herceptin, Genentech), as well as the dual EGFR/HER2 tyrosine kinase inhibitor, lapatinib (Tykerb, GlaxoSmithKline). *PIK3CA* mutation or knockdown of PTEN can render breast cancer cells resistant to trastuzumab or lapatinib *in vitro* and in xenografts [321, 408-410]. PTEN-deficient breast cancers are also insensitive to trastuzumab treatment which has been suggested to be due loss of PTEN protein

phosphatase activity against c-Src [223, 409]. In fact, using RNA interference screening in breast cancer cells, PTEN was identified as a molecular determinant of resistance to trastuzumab or lapatinib [321, 411]. This analysis was extended to patient data which identified that activation of the PI3K pathway predicts poor outcome after trastuzumab treatment [321, 412-415]. There may be a greater effect observed with PTEN loss alone, as a recent study found that *PIK3CA* mutations were not statistically significant with trastuzumab benefit [416]. Similarly, some studies associate either *PIK3CA* mutations or PTEN loss with lapatinib resistance while another identifies only PTEN as a determinant of response [352, 415].

As seen with PI3K inhibition, lapatinib treatment leads to upregulation of HER3 expression which can directly activate PI3K [417]. Furthermore, PI3K pathway inhibition appears to restore sensitivity to HER2-targeted agents in preclinical models [408-411, 418-420]. In trastuzumab-resistant breast cancer patients, combined inhibition of mTOR improved response [421, 422]. A newly designed clinical trial (NeoPHOEBE) plans to combine trastuzumab treatment with the pan PI3K inhibitor BMK120 in HER2-positive breast cancer patients that have been stratified for *PIK3CA* mutation.

Our understanding of the PI3K pathway in normal functions and in diseases such as breast cancer will continue to evolve with the development and characterization of new mouse strains. The ongoing drug trials for cancer treatment and the ones yet to come will continue to depend on *in vivo* models to serve as important preclinical models for testing the efficacy of therapies as well as predicting potential mechanisms of resistance. Genetically modified mouse models in particular will remain critical research tools for investigating new targets for therapeutic intervention in breast cancer.

1.5 Thesis rationale and objectives

Although it is well established that components of the PI3K pathway are frequently altered in human cancer, the contribution of specific molecular events can be difficult to assess without the insight from genetically modified mouse models. Given that *PIK3CA* mutations and PTEN loss are prevalent aberrations in HER2 -positive breast cancers and have been associated with resistance to therapy, we chose to investigate whether PI3K signalling can cooperate with activated ErbB2 during mammary tumourigenesis. Using mouse strains with mammary-specific loss of Pten or transgenic expression of activated p110α, we have been able to determine their effects on mammary tumour development and progression in a model driven by activated ErbB2. We took the opposite approach to explore the *in vivo* requirement for p110α in murine mammary tumourigenesis, which had not been addressed in the field up to this point. A conditional p110α strain was used in conjunction with our activated ErbB2 model as well as a newly characterized inducible PyV mT model. The characterization of p110α-deficient mammary tumours has provided insight into molecular mechanisms that may have relevance in patients with resistance to PI3K inhibitors. Collectively, these studies have allowed us to study the *in vivo* consequences of modulating PI3K signalling in mouse models of breast cancer development, progression, and metastasis.

2 Materials and methods

2.1 Animal work

2.1.1 General animal husbandry

All mice were housed in the animal facility at the Goodman Cancer Research Centre. Ethical approval was obtained for the use of animals and all experiments were done in accordance with the animal care guidelines at the Animal Resource Centre of McGill University. All strains described in this study were on an FVB/N genetic background, except for the Flox-Pten/NIC and $p110\alpha^{HR}$/NeuNT/Cre strains which were on a mixed genetic background (Chapters 3 and 4, respectively). Several previously characterized strains were used in this study:

Conditional strains: Pten knockout ($Pten^{flx}$) [423]; conditional p110α knockout ($p110\alpha^{flx}$) [276]; conditional $p110\alpha^{HR}$ knockin (p110α H1047R mutant) [64]

Transgenic p110α strain: MMTV-myr-p110α [309]

Activated Neu strains: MMTV-NDL (Neu deletion 2-5 transgene) [103]; MMTV-NIC (Neu deletion 2-5-IRES-Cre recombinase transgene) [105]; $ErbB2^{KI}$ (conditional NeuNT knockin strain crossed with the MMTV-Cre strain) [58, 62]

PyV mT strains: MMTV-PyV mT [141]; MMTV-rtTA/TetOMIC (see below for more details) [144, 424].

Cre recombinase reporter strains: GTRosa (ROSA26 β-galactosidase reporter) [67]; GFP reporter [68]

Generation of the MIC construct and characterization of the rtTA/MIC bigenic strain

The MIC construct was created using the pTE-mElf5-IRES-eGFP vector (a generous gift from Dr. C. Ormandy). Briefly, after removal of the mElf5 and eGFP transgenes, PyV mT cDNA was

subcloned between the Tet operon (TetO) and internal ribosome entry site (IRES), followed by subcloning of Cre recombinase cDNA downstream of the IRES (TetO-PyV mT-IRES-Cre recombinase; abbreviated as "MIC"). Derivation of the MIC strain was conducted in the Transgenic Core Facility in the Goodman Cancer Research Centre using standard pronuclear injection of FVB/N single cell embryos [55]. Progeny were screened for germline transmission of the MIC transgene by PCR genotyping. MIC mice were crossed to the MMTV-rtTA strain to drive expression of the transgene to the mammary epithelium [424]. Experimental and control rtTA/MIC animals of at least 8 weeks of age were given drinking water containing 2 mg/mL doxycycline (Sigma Aldrich) in light-blocking bottles each week. De-induction experiments involved the withdrawal of doxycycline from animals at endstage tumour burden followed by monitoring for tumour regression. For resection surgeries, mice were anesthetised prior to excising a small piece of tumour for embedding and flash freezing; the incision was sutured and painkillers administered for one week.

2.1.2 Mammary tumour development and monitoring

Mice were monitored for mammary tumour formation by biweekly physical palpation. Tumour growth was measured using callipers and volumes calculated using the following formula: (4/3 x (3.14159) x (length/2) x (width/2)^2). Unless otherwise indicated, transgenic animals were sacrificed either 6 or 8 weeks after detection of the first mass (all NIC and NDL strains, respectively) or when total tumour volume reached 4-6 cm^3 (all rtTA/MIC strains). For all studies, animals were sacrificed when a single tumour reached 2.5 cm^3 as per animal care guidelines. Athymic nude mice (NCr) were utilized for orthotopic transplantation and injection

assays. Mice were sacrificed at the tumour burden limit (2.5 cm^3) or at a defined timepoint as indicated.

2.1.3 Necropsy and sample processing

Material from necropsied mice was flash frozen in liquid nitrogen (in some cases, tissues were set in an OCT medium before freezing) or fixed in 10% neutral buffered formalin and embedded in paraffin wax. Fixed and embedded mammary tissues were sectioned at 4 μm and either stained by hematoxylin and eosin (H&E) or processed further as indicated. Inguinal mammary glands were wholemounted on glass slides, incubated in acetone, and stained with hematoxylin overnight. Wholemounted glands were destained (70% EtOH, 1% HCl), dehydrated (70%, 100% EtOH, and xylenes) and mounted using Permount mounting media (Fisher). For ductal outgrowth measurements, images of H&E-stained wholemounts were analyzed using Aperio Imagescope software to measure the distance between the centre of the lymph node and the terminal end bud of the longest duct. Quantification of lesions in mammary glands and lungs was accomplished by scanning H&E-stained slides with a Scanscope XT Digital Slide Scanner. Aperio Imagescope software was then used to calculate the area of lesions relative to the total area of the section or to quantify the number of different types of ductal lesions (10 fields per sample). For NIC transgenic strains, lung metastases were manually counted in 5 x 50 μm step-sections.

2.1.4 Epithelial cell isolation from mammary glands and tumours

For the isolation of mammary epithelial cells, all (or as many as possible) mammary glands were excised from the animal and all purified epithelial cells were used for downstream applications. Due to low yields, samples from mice of the same genotype were often pooled as indicated. Excised mammary glands were finely chopped using a mechanical McIlwain tissue chopper and dissociated at 37°C for 1.5-2 hours in at least 10 mL of digestion media (DMEM, 1% penicillin-streptomycin, 24 mg/mL collagenase B, 24 mg/mL dispase II). Mammary gland samples were centrifuged at 800 RPM for 3 minutes and pellets were resuspended in 1 mL Ack lysis buffer (0.15 M NH_4Cl, 10 mM $KHCO_3$, 0.1 mM EDTA) to eliminate red blood cells. An additional 10 mL of PBS containing 2 mM EDTA and 2% BSA was added to the sample before centrifuging at 800 RPM for 3 minutes. Cell pellets were resuspended in PBS/EDTA/BSA, passed through a 70 μm cell strainer, and pelleted by centrifuging at 800 RPM for 3 minutes. Cell pellets were incubated with a cocktail containing biotinylated antibodies against lineage antigens (CD5, CD45R (B220), CD11b, Anti-Gr-1 (Ly-6G/C), 7-4, and Ter-119 antibodies) followed by anti-biotin beads to isolate lineage-negative cells (Magnetic Cell Sorting [MACS] kit from Milteny Biotec). Samples were also incubated with antibodies against CD31 and CD90 to remove endothelial cells and fibroblasts, respectively. Samples were then passed through the MACS separating columns inside the MACS magnetic field as per the manufacturer's instructions. Columns were washed three times with PBS/EDTA/BSA buffer and the effluent containing the epithelial-enriched cell population was collected and processed for RNA extraction (see section 2.3.1).

Mammary tumours were chopped and digested in the same manner as mammary glands. Dissociated tumour samples were pelleted by centrifuging at 800 RPM for 3 minutes and treated

with Ack lysis buffer. Pelleted cells were incubated in PBS containing 1 mM EDTA for 10 minutes. Cells were washed once in PBS and then resuspended in PBS. Cells were counted using an automated cell counter (Cellometer) and the appropriate number of cells either plated for primary cell culture or prepared for mammary fat pad or tail vein injections into NCr mice (see 2.1.5 for additional details).

Primary tumour cells were maintained in primary cell culture media (DMEM, 1% penicillin-streptomycin, 50 μg/mL gentamycin, 5% fetal bovine serum, 5 μg/mL insulin, 5 ng/mL EGF, 1 μg/mL hydrocortisone, 35 μg/mL bovine pituitary extract) and incubated at 37°C, 5% CO_2. For drug treatments in the NDL cell line, GDC-0941 (LC Labs) was prepared in DMSO and added to cells at final concentrations of 50 nM and 250 nM (final DMSO concentration of 0.1%) for 2 or 6 hours prior to harvesting for protein extraction.

2.1.5 Transplants and injections in athymic nude mice

Transgenic mammary tumours were maintained by serial transplantation in athymic nude mice (NCr strain). A small tumour piece was excised and kept in PBS on ice until orthotopic implantation into the fat pad of the inguinal mammary gland of the recipient. When tumours reached 2.5 cm^3 they were transplanted again in the same manner.

For orthotopic tumour outgrowth assays, 2.5 x 10^5 cells in 30 μL of PBS were injected into the fat pad of the inguinal mammary gland of NCr mice. Tumours were measured biweekly using calipers and animals were sacrificed when masses reached 2.5 cm^3 or at a defined timepoint as indicated. For drug treatments, GDC-0941 (LC Labs) was prepared in a vehicle solution (50% OraPlus, 50% dH_2O) so that administration of a 100 μL volume to animals would result in a final

dosage of 125 mg/kg. For short-term GDC-0941 experiments testing drug efficacy, mice were treated by gavage with 125 mg/kg of drug or vehicle and sacrificed at 2, 6 and 12 hours post-treatment. For long-term GDC-0941 experiments testing tumour outgrowth inhibition, mice were treated daily by gavage with 125 mg/kg of drug or vehicle; mice were sacrificed when tumours reached 2.5 cm^3 or after a maximum of 6 weeks of treatment.

For lung colonization assays, 5.0 x 10^5 cells in 100 µL of PBS were injected into the lateral tail vein of NCr mice. Mice were sacrificed 4 weeks post-injection and lungs harvested for paraffin-embedding.

2.2 DNA analyses

2.2.1 DNA extraction

Tail pieces or flash frozen mammary gland/tumour tissue were digested in 500 µL of tail buffer (10 mM Tris, 100 mM NaCl, 10 mM EDTA,0.5% SDS) containing 10 µL of 20 mg/mL proteinase K and incubated at 55°C overnight. Tail DNA was extracted by adding 200 µL of 5 M NaCl to the digestion, mixing, and centrifuging at 13 000 RPM for 5 minutes. Supernatant was transferred to a new tube and DNA was precipitated by adding two volumes of 100% EtOH, mixing, and centrifuging at 13 000 RPM for 10 minutes at 4°C. Supernatant was discarded and DNA pellets were air-dried before resuspending in 200-400 µL of Tris-EDTA buffer (10 mM Tris, 0.5 mM EDTA, pH 7.8).

Mammary gland/tumour DNA was extracted by adding 500 µL of phenol/chloroform solution to the digestion, mixing, and centrifuging at 13,000 RPM for 5 minutes. Supernatant (aqueous phase) was transferred to a new tube and extracted again using 500 µL of chloroform.

Supernatant was transferred to a new tube and DNA was precipitated in the same manner as tail DNA. To prepare DNA from mammary tumour and lung lesions for sequencing (see 2.2.4 for additional details), extractions were performed using the Qiagen AllPrep DNA/RNA Mini Kit.

2.2.2 PCR genotyping and excision of conditional alleles

PCR genotyping was performed on 1 μL of tail DNA using Qiagen Taq DNA polymerase, 10X buffer, $MgCl_2$, 5 mM dNTPs, and 10 μM of the primers listed below in a total volume of 25 μL. The following loci/transgenes were genotyped using the listed primers:

Gene	**Primer**	**Primer Sequence (5' to 3')**
Cre	Forward	GCTTCTGTCCGTTTGCCG
	Reverse	ACTGTGTCCAGACCAGGC
GFP	Forward	AAGTTCATCTGCACCACCG
	Reverse	TGCTCAGGTAGTGGTTGTCG
GTRosa	1	GCGAAGAGTTTGTCCTCAACC
	2	GGAGCGGGAGAAATGGATATG
	3	AAAGTCGCTCTGAGTTGTTAT
PyV mT	Forward	GGAAGCAAGTACTTCACAAGGG
	Reverse	GGAAAGTCACTAGGAGCAGGG
rtTA	Forward	ACCGTACTCGTCAATTCCAAGGG

	Reverse	TGCCGCCATTATTACGACAAGC
Neu	Forward	TTCCGGAACCCACATCAGGCC
	Reverse	GTTTCCTGCAGCAGCCTACGC
Pten	Forward	ACTCAAGGCAGGGATGAG C
	Reverse	GCCCCGATGCAATAAATATG
myr-p110α	Forward	TGAATTGGCCGCTCGCGAATC
	Reverse	CACTGGCATGCCAATAAC
$p110\alpha^{flx}$ (genotyping)	Forward	CTGTGTAGCCTAGTTTAGAGCAACCATCTA
	Reverse	CCTCTCTGAACAGTTCATGTTTGATGGTGA
$p110\alpha^{flx}$ (excision)	Forward	GCACTTCTCAGTGCTGTCG
	Reverse	AAAGGAGTTGGCCTCAAGC

Genotyping PCRs for GTRosa, Cre, GFP, rtTA, PyV mT, and Neu were run on the following program: (1) 94°C - 2 minutes, (2) 94°C - 30 seconds, (3) 58°C - 45 seconds, (4) 72°C - 1 minute, (5) repeat steps 2-4 for an additional 29 cycles, (6) 72°C - 4 minutes, (7) 4°C.

Genotyping PCRs for Pten were run on the following program: (1) 94°C - 5 minutes, (2) 94°C - 30 seconds, (3) 60°C - 1 minute, (4) 72°C - 1 minute, (5) repeat steps 2-4 for an additional 34 cycles, (6) 72°C - 2 minutes, (7) 4°C.

Excision PCRs for p110α^{flx} were run on the following program: (1) 94°C - 1 minute, (2) 94°C - 30 seconds, (3) 57°C - 30 seconds, (4) 72°C - 1 minute, (5) repeat steps 2-4 for an additional 34 cycles, (6) 72°C - 5 minutes, (7) 4°C.

2.2.3 Southern blot

To determine Pten LOH status, mammary tumour DNA was digested overnight with *SacI* and separated on a 0.5% agarose gel. The gel was then washed (250 mM HCl for 10 minutes; 1.5 M NaCl/0.5 M NaOH for 2 x 15 minutes) and transferred overnight onto a positively charged nylon membrane in 10X SSC buffer (0.3 M NaCl, 30 mM sodium citrate-2H2O). After transfer, the membrane is cross-linked in a UV oven and then incubated in prehybridization buffer (5X SSC, 5X Denhardt's solution, 0.5% SDS, 10% dextran sulfate, 10 μg/ml denatured salmon sperm DNA) at 42°C with rotation for 3-4 hours. The Pten-specific probe was generated by PCR on mouse genomic DNA with the following primers: sense 5'-CGTAGCCACAGGGACTCCTA-3' and antisense 5'-ATTCGTGACGGTGTCAATCA-3'. The probe was denatured, radioactively labelled with 50 μCi ^{32}P-dCTP using Klenow enzyme at 37°C for 45 minutes, and column-purified. The membrane was incubated overnight at 42°C with rotation in hybridization solution (prehybridization buffer containing 1 million cpm/mL of the denatured radioactive probe and salmon sperm DNA). The membrane was washed at 65°C with rotation in low stringency wash buffer (2X SSC) 2 x 15 minutes at room temperature and then with a high stringency wash buffer (0.1X SSC, 0.1% SDS) 2 x 15 minutes before developing.

2.2.4 DNA sequencing

Total DNA was extracted from flash frozen mammary tumours and lung lesions using a Qiagen AllPrep DNA/RNA Mini Kit. Genomic DNA was analysed by Sanger sequencing (Applied Biosystems 3730 DNA Analyser) using the following primers to detect single nucleotide polymorphisms in known mutational "hotspots" of HRas, KRas1, NRas and Trp53:

Genomic region	**Primer**	**Primer Sequence (5' to 3')**
HRas exon2/exon3	Forward	CCTTGGGTCAGGCATCTATT
	Reverse	AAAGACATAAAGCCTCAGTGTGC
KRas exon 2	Forward	GAAGATGAAAGTACTGGTTTCCA
	Reverse	TGCACCTATGGTTCCCTAACA
KRas exon 3	Forward	TCACCTTGTAAAAGATGCACTG
	Reverse	AAAACAGGAATTCTGCATACTTGA
NRas exon 2	Forward	AGTGGAAGGCCACGTGTATC
	Reverse	GGAAATCCTCAGTAAGCACGA
NRas exon 3	Forward	TGCATGCGTGTGATTATGTATG
	Reverse	AAAAGTTGTATGTTTCCTAAGTCCA
Trp53 exon 2	Forward	ACGTGGTTGGTTACCTCTGC
	Reverse	GATACAGGTATGGCGGGATG
Trp53 exons ¾	Forward	CCAGCCTGGGATAAGTGAGA

	Reverse	GCTAAAAAGGTTCAGGGCAAA
Trp53 exons 5/6	Forward	TGGTGCTTGGACAATGTGTT
	Reverse	CCCTTCTCCCAGAGACTGCT
Trp53 exons 7/8/9	Forward	GTAGGGAGCGACTTCACCTG
	Reverse	AAGACCTGGCAACCTGCTAA
Trp53 exon 10	Forward	GTTGGGAACCAACTTTCAGA
	Reverse	TGTCCCTCATACCCCTTAACA
Trp53 exon 11	Forward	CAGAAGTATTCCAGTGTGTTCTGTG
	Reverse	CTACTCAGAGAGGGGGCTGA

2.3 RNA analyses

2.3.1 RNA extraction

Total RNA was extracted from flash frozen mammary tumours or lung lesions using Qiagen RNEasy Mini/Midi Kits or Qiagen AllPrep DNA/RNA Mini Kits. RNA concentrations were calculated using a NanoDrop spectrophotometer.

2.3.2 Microarray

Extracted RNA was labeled using an Amino Allyl MessageAmp II aRNA Amplification Kit (Applied Biosystems) and Cy3 and Cy5 dyes (Amersham Biosciences) in preparation for

microarray hybridization. Dye-labeled RNA was hybridized onto a Whole Mouse Genome Oligo 4 × 44 K Microarray platform (Agilent) against a universal mouse reference RNA (Stratagene). The resulting arrays were scanned using a Microarray Scanner (model G2565BA; Agilent Technologies) and processed using Feature Extraction software (Agilent). Raw probe intensities were background normalized using median in R/Bioconductor. Differential expression was evaluated using LIMMA. The heatmap is based on the 500 most variable genes. Hierarchical clustering was performed using a person correlation distance metric and Ward's algorithm.

2.3.3 Reverse transcription and quantitative PCR (RT-qPCR)

cDNA was prepared by reverse transcribing 1 μg of RNA using M-Mulv Reverse Transcriptase (#M0253S) or Protoscript II Reverse Transcriptase, Oligo-dT(23VN) and a murine RNase inhibitor (New England Biolabs). Real-time quantitative PCR was performed on the cDNA using Roche LightCycler 480 SYBR Green I Mastermix and run on a Roche LightCycler 480 instrument. All samples were run in triplicate and normalized to Gapdh to generate relative transcript levels using the formula: 2^(average GAPDH crossing point - average target X crossing point). Primer sequences were as follows:

Transcript	**Primer**	**Primer sequence (5' to 3')**
Gapdh	Forward	CATCAAGAAGGTGGTGAAGC
	Reverse	GGGAGTTGCTGTTGAAGTCG
PyV mT	Forward	CCCGATGACAGCATATCCCC
	Reverse	CTTGTTCCCCCGGTAGGATC

Pik3ca	Forward	TCCATCAGCTTCTGCAAGAC
	Reverse	CTTCCCTTTCTGCTTCTTGG
Spp1	Forward	CAGCCTGCACCCAGATCCTA
	Reverse	GCGCAAGGAGATTCTGCTTCT
Itgav	Forward	TTGGGGACGACAACCCTCTGACAC
	Reverse	TGCGGAGGGATAGAAACGATGAG
Itgb3	Forward	GCTTTGGGGCCTTCGTGGACAA
	Reverse	CATGGGCAAGCAGGCATTCTTCAT
Pten	Forward	CATTGCCTGTGTGTGGTGATA
	Reverse	AGGTTTCCTCTGGTCCTGGTA

2.4 Protein analyses

2.4.1 Protein extraction

Flash frozen mammary gland or tumour pieces were crushed finely with a mortar and pestle under liquid nitrogen and lysed in PLCγ lysis buffer (50 mM HEPES, 150 mM NaCl, 10% glycerol, 1% Triton X-100, 1 mM EGTA, 1.5 mM $MgCl_2$, 10 mM NaF, 10 mM sodium pyrophosphate) containing 1 µg/mL leupeptin, 1 µg/mL aprotinin, and 1 mM Na_3VO_4. Samples were incubated on ice for 1 hour and then centrifuged at 13 000 RPM for 10 minutes at 4°C. Supernatants were transferred to a new tube and protein concentration was determined using a Bradford assay.

2.4.2 Immunoblot

Protein lysates were diluted in 6X SDS-PAGE loading buffer (0.375M Tris pH 6.8, 12% SDS, 60% glycerol, 0.6M DTT, 0.06% bromophenol blue) and boiled for 5 minutes. 20 μg of denatured samples were separated using SDS-PAGE and then transferred to PVDF membranes. Membranes were blocked in TBST (150 mM NaCl, 20 mM Tris-HCl [pH 7.5], 0.05% Tween-20) containing 5% BSA for 1 hour at room temperature and then incubated with primary antibodies (diluted in TBST/2% BSA) overnight at 4°C. After washing 3 x 5 minutes in TBST, membranes were incubated with horseradish peroxidase (HRP)-conjugated secondary antibodies (diluted 1:10 000 in TBST/2% BSA) for 1 hour at room temperature. Membranes were washed 3 x 5 minutes in TBST, incubated in enhanced chemiluminescence (ECL) detection reagent solution for 5 minutes at room temperature. Membranes were then exposed to Hyperfilm ECL film for times ranging from 5 seconds to 10 minutes depending on the antibody and the levels of protein expression. The following primary antibodies were used for immunoblotting:

Antibody	**Supplier/Catalog #**	**Dilution**
Akt (pan)	Cell Signalling 9272	1:1000
Akt (Akt1/2)	Santa Cruz sc-1619	1:1000
Akt (pan, phospho; S473)	Cell Signalling 9271	1:1000
Bad	BD Transduction 610391	1:1000
Bad (phospho; S136)	Cell Signalling 5286	1:1000
c-Myc	Santa Cruz sc-764	1:500
Cre recombinase	Novagen/EMD Millipore 69050	1:1000
E-cadherin	BD Biosciences 610182	1:5000

Egfr	Cell Signalling 2322	1:1000
Egfr (phospho; Y1068)	Cell Signalling 3777	1:1000
ErbB2	Santa Cruz sc-284	1:1000
ErbB2 (phospho; Y1248)	Santa Cruz Biotechnology 12352	1:500
ErbB3	Santa Cruz sc-283	1:1000
ERα	Santa Cruz sc-542	1:1000
Gsk3α/β (phospho; S21/9)	Cell Signalling 9331	1:1000
Gsk3β	Cell Signalling 9315	1:1000
Hsp90	Cell Signalling 4874	1:1000
OPN	Santa Cruz sc-21742	1:1000
Pdgfrβ	Cell Signalling 3175	1:1000
Pdgfrβ (phospho; Y1021)	Cell Signalling 2227	1:1000
PI3K p110γ	Cell Signalling 5405	1:1000
PI3K p110α	Cell Signalling 4255	1:1000
PI3K p110β	Santa Cruz sc-602	1:1000
PI3K p85	Upstate 05-217	1:1000
Pten	Cell Signalling 9559	1:1000
PyV mT	Dr. S. Dilworth (Ab750)	1:1000
PyV mT	Dr. S. Dilworth (Ab762)	1:1000
S6	Cell Signalling 2317	1:1000
S6 (phospho; S235/236)	Cell Signalling 4858	1:1000

Tsc2	Cell Signalling 3612	1:1000
Tsc2 (phospho; T1462)	Cell Signalling 3611	1:1000
α/β-tubulin	Cell Signalling 2148	1:5000
α-tubulin	Cell Signalling 2125	1:5000
αv integrin	Santa Cruz sc-6617	1:500
β3 integrin	Abcam ab119992	1:1000
β-actin	Sigma A9718	1:10 000

2.4.3 Immunoprecipitation

Protein lysates (500 μg) were incubated with 5 μL of p85 antibody (Upstate 05-217) overnight at 4°C with rotation. 25 μL of protein G beads were added to each sample before incubating for 2 hours at 4°C with rotation. Samples were washed three times in lysis buffer and then boiled for 5 minutes in 25 μL of 2X SDS gel loading buffer (0.125 M Tris pH 6.8, 4% SDS, 20% glycerol, 0.2 M DTT, 0.02% bromophenol blue). Denatured samples were loaded on SDS-PAGE gels and immunoblotted as described in the previous section.

2.4.4 Immunohistochemistry

Sections of paraffin-embedded samples were deparaffinized and dehydrated in xylenes and 100% EtOH. Sections were rehydrated prior to antigen retrieval in 10 mM sodium citrate in a pressure cooker for 10 minutes. Slides were cooled for 1 hour and then blocked in Power Block (Biogenex) for 10 minutes at room temperature. Primary antibodies were added to slides and incubated for either 1 hour at room temperature or overnight at 4°C. Endogenous peroxidases

were quenched in PBS containing 3% hydrogen peroxide for 30 minutes. Biotinylated secondary antibodies and avidin (Vector Elite) were added for 1 hour and 30 minutes at room temperature, respectively. Sections were exposed to DAB reagent (Vectastain) for 5 seconds to 5 minutes depending on the antibody used. Slides were rinsed in dH_2O, tap water, and then counterstained with 20% Harris Modified Haematoxylin (Fisher) for 30 seconds. Sections were then dehydrated, cleared in xylenes, and mounted using Clearmount (America Master Tech). Terminal deoxynucleotidyl transferase dUTP nick end labeling (TUNEL) assays were performed using an Apoptag Peroxidase *in situ* Kit (Millipore) on paraffin-embedded sections. Counterstaining with 20% Harris Modified Haematoxylin and mounting was performed as usual. Aperio Imagescope software was use to quantify positive staining in 10 fields per section (nuclei for Ki67 and TUNEL; pixels for CD31). The following primary antibodies were used for immunohistochemistry:

Antibody	**Supplier/Catalog #**	**Dilution**
PyV mT	Dr. S. Dilworth (Ab762)	1:100
Cre recombinase	Covance PRB106C	1:600
Ki67	Abcam ab15580	1:1000
CD31	BD Biosciences 550274	1:100
OPN	Santa Cruz sc-21742	1:100
Pten	Cell Signalling 9559	1:100

2.4.5 β-galactosidase assay

OCT-embedded mammary tumours were cryosectioned at 7-10 μm. After fixing in PBS containing 0.2% glutaraldehyde for 10 minutes, slides were rinsed 3 x 5 minutes in base staining

buffer (2 mM $MgCl_2$, 0.01% sodium deoxycholate, 0.02% NP-40 in PBS). X-gal staining was performed by incubating slides in the dark overnight at 37°C in staining buffer (base staining buffer containing 5 mM $K_4Fe(CN)_6$, 5 mM $K_3Fe(CN)_6$, and 1 mg/mL x-galactosidase in DMF). Stained slides were rinsed 3 x 5 minutes in PBS, fixed again in PBS/glutaraldehyde, rinsed 3 x 5 minutes in PBS and then counterstained with nuclear fast red for 5-10 minutes. After rinsing in dH_2O for 2 x 3 minutes, slides were dehydrated and mounted.

2.4.6 Phospho-RTK array

The Proteome Profiler Mouse Phospho-RTK Array Kit from R&D Systems was used according to the manufacturer's instructions. Arrays spotted with RTK probes were incubated with 200 μg of protein lysate followed by biotin-conjugated phospho-tyrosine antibody (EMD Millipore #16-103, 1:1,000) and fluorescently-conjugated streptavidin (Mandel Scientific #LIC-926-32230, 1:1,000) to allow for visualization on the Odyssey Imaging System (LI-COR Biosciences). Fluorescence intensities for each probe were normalized to a PBS probe (negative control).

3 PI3K pathway activation in mouse models of ErbB2 mammary tumourigenesis

3.1 Introduction

Loss of the PTEN tumour suppressor, which negatively regulates the proto-oncogenic PI3K/Akt pathway, is frequently observed in breast cancer through multiple mechanisms including genomic aberrations and downregulated expression. It is estimated that PTEN deficiency occurs in approximately one fifth of HER2-overexpressing breast cancers [4]. Furthermore, PTEN has been shown to be a significant determinant in predicting patient response to HER2-targeted therapies such as trastuzumab [320, 321]. These associations suggest that HER2 overexpression and PTEN deficiency may cooperate in breast cancer and so we chose to investigate this in a mouse model of mammary tumourigenesis. Our laboratory previously studied Pten deficiency in the ErbB2^{KI} mouse model (NeuNT/MMTV-Cre), where Cre-inducible expression of activated ErbB2 is driven by the endogenous *erbb2* promoter [62, 334]. Consistent with our hypothesis, Pten loss accelerated tumour initiation and metastasis in ErbB2^{KI} mice. To further validate these findings in a second model of ErbB2-mediated tumourigenesis, we turned to the MMTV-NIC strain [105]. In this context, activated ErbB2 expression is strongly induced by a viral promoter in contrast to the physiological levels of expression in the ErbB2^{KI} model; tumours develop far more quickly and with multifocal penetrance in NIC mice making it a practical model to work with. In addition, the coupling of Cre recombinase to the ErbB2 transgene in the NIC also allows for simultaneous overexpression of activated ErbB2 and Cre-mediated excision of conditional alleles. This is not the case in the ErbB2^{KI} strain, where Cre-mediated excision likely occurs before amplification of the NeuNT transgene. Studying the genetic ablation of Pten in the NIC model would allow us to rapidly confirm our previous findings while ensuring that Pten loss more closely coincided with activated ErbB2 overexpression.

Activation of PI3K signalling in breast cancer can also be enhanced by activating mutations in the *PIK3CA* gene. Like PTEN loss, *PIK3CA* mutations are associated with HER2 overexpression and resistance to treatments targeting HER2 [4, 320, 321]. To determine whether these two genetic alterations would synergize during mammary tumourigenesis in mice we crossed our MMTV-NDL model to a strain with mammary-specific expression of a myristoylated p110α transgene (myr-p110α), which anchors the protein to the membrane as an artificial means of constitutive activation [103, 309].

Characterization of the Pten-deficient/NIC model and the myr-p110α/NDL model allowed us to compare and contrast phenotypes induced by different mechanisms of PI3K pathway activation in the context of ErbB2-driven mammary tumourigenesis. Interestingly, while loss of Pten dramatically accelerated tumour initiation in the NIC model, metastasis of ErbB2 mammary tumours was enhanced by either Pten deficiency or myristoylation of p110α (unpublished observations, T. Rao and W.J. Muller) [106].

3.2 Results

Dramatic reduction in tumour latency in NIC mice lacking one or both Pten alleles

To coordinate the simultaneous overexpression of activated ErbB2 with genetic ablation of Pten in the mammary epithelium, we bred our MMTV-NIC mice with a conditional Pten strain (Figure 3-1). Cohorts of NIC mice that were wildtype, heterozygous and homozygous for the conditional Pten allele were generated and monitored for mammary tumour formation. While wildtype NIC animals developed tumours at approximately 5 months of age (consistent with

Figure 3-1: Conditional loss of Pten in the NIC model

Breeding strategy to generate mice with mammary epithelial-specific expression of activated ErbB2/Neu and ablation of Pten. The conditional Pten strain ("Flox-Pten") carries a Pten allele in which exon 5 is flanked by LoxP sites (schematic modified from [423]). When crossed with the MMTV-NIC strain ("NIC")[105], the conditional Pten allele(s) will undergo Cre-mediated recombination specifically in the mammary epithelium.

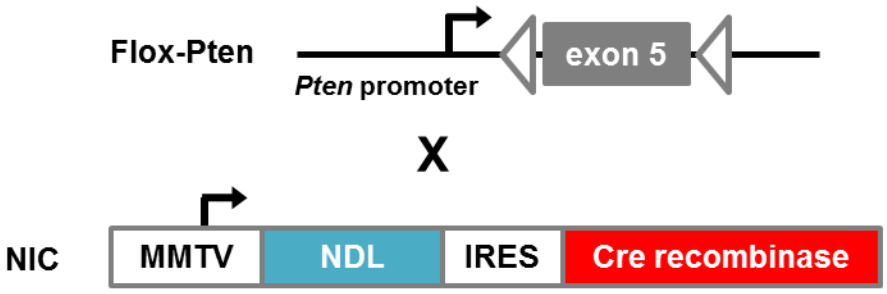
Flox-Pten
exon 5
Pten promoter
X
NIC
MMTV
NDL
IRES
Cre recombinase

previous studies), tumours occurred significantly earlier in Pten$^{flx/wt}$/NIC mice; tumour latency was even further reduced in the Pten$^{flx/flx}$/NIC group (Figure 3-2) [105].

It was clear that Pten loss could cooperate with ErbB2 activation to accelerate tumour initiation and it followed next to determine if tumour burden was correspondingly affected. The total tumour volume was not significantly different between Pten-deficient/NIC mice and wildtype counterparts however the estimated volume per tumour was significantly smaller in Pten-null/NIC animals (Figure 3-3A). The tumours in all cohorts were solid adenocarcinoma which is typical of the NIC model (Figure 3-3B) [105].

Pten-deficient/NIC tumours have greater metastatic potential which may be due to increased angiogenesis

After observing the relatively early development of tumours in Pten-null/NIC mice we were interested in determining if these tumours were also more invasive. Lungs from tumour-bearing mice from each of the genetic cohorts were analyzed for the presence of metastases and both the incidence and number of lesions were increased by complete Pten ablation (Figure 3-4A). Both the size of individual tumours and the fact that the mice were tumour-bearing for approximately the same length of time suggests that neither of these factors influenced the metastasis data; however the results would need to be validated by lung colonization experiments to prove this assumption (Figure 3-3A).

A greater metastatic burden could be due to many factors including the accessibility of cells in the primary tumour to the vasculature. Indeed, blood vessel density was significantly increased in Pten-null/NIC tumours relative to wildtype samples as assessed by immunohistochemical

staining with the endothelial cell marker CD31 (Figure 3-4B). This angiogenic advantage conferred by Pten-deficiency may therefore allow NIC tumour cells to more readily metastasize to the lung.

Pten$^{flx/wt}$/NIC tumours undergo loss of heterozygosity at the *Pten* locus

We began the molecular characterization of the Pten-deficient/NIC tumours by first assessing Pten protein expression. Both the homozygous and heterozygous samples showed reduced Pten protein as compared to wildtype NIC controls as shown by immunoblot and immunohistochemical analyses (Figure 3-5A and B). Immunohistochemical staining further revealed that residual Pten protein in the immunoblot is likely originating from contaminating stromal cells which should retain wildtype Pten alleles in this conditional model.

We hypothesized that the absence of Pten protein in the tumour sections from Pten$^{flx/wt}$/NIC mice was potentially due to loss of heterozygosity (LOH), a common occurrence in tumour suppressor genes (including PTEN) in human cancers. Southern blot analysis was performed on tumour DNA to probe for the existence of the wildtype and excised Pten alleles in the different genetic cohorts. Four out of five Pten$^{flx/wt}$/NIC samples had undergone LOH as only the excised Pten allele was detected (Figure 3-5C), providing evidence that this clinical phenomenon had emerged in our mouse model.

Figure 3-2: Accelerated tumour onset in NIC animals that have lost one or both Pten alleles

Kaplan-Meier tumour onset curve for NIC mice that are wildtype, heterozygous, or homozygous for the conditional Pten allele. The table indicates for each genotype the penetrance (percentage of animals that develop tumours), T_{50} (age when 50% of the animals have tumours), and average tumour onset with standard deviation. P values were calculated using a two-tailed t-test.

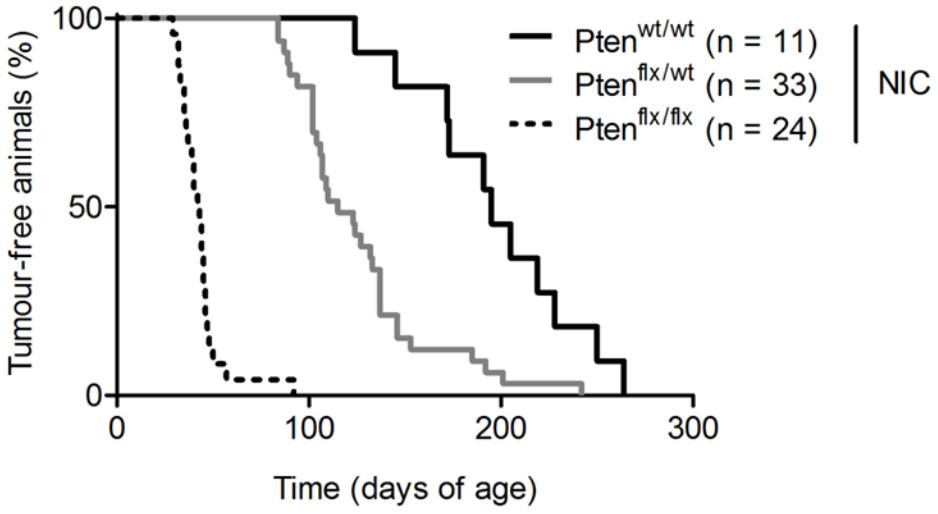

NIC	Penetrance	T_{50} (days of age)	Average onset (days of age)
$Pten^{wt/wt}$	100% (11/11)	195	197 ± 42.5
$Pten^{flx/wt}$	100% (33/33)	115	126 ± 36.4 (*p < 0.0001*)
$Pten^{flx/flx}$	100% (24/24)	42	43 ± 12.3 (*p < 0.0001*)

Figure 3-3: Pten-null/NIC mice exhibit comparable total tumour volume and tumour histology to wildtype animals

(**A**) Tumour burden for the indicated genotypes is represented as the average total tumour volume (top) and average total tumour volume relative to the number of tumours (bottom). Error bars are standard error of mean. P values were calculated using a two-tailed t-test.

(**B**) H&E-stained sections of tumours from wildtype NIC and Pten-deficient/NIC mice. Scale bar is 100 μm.

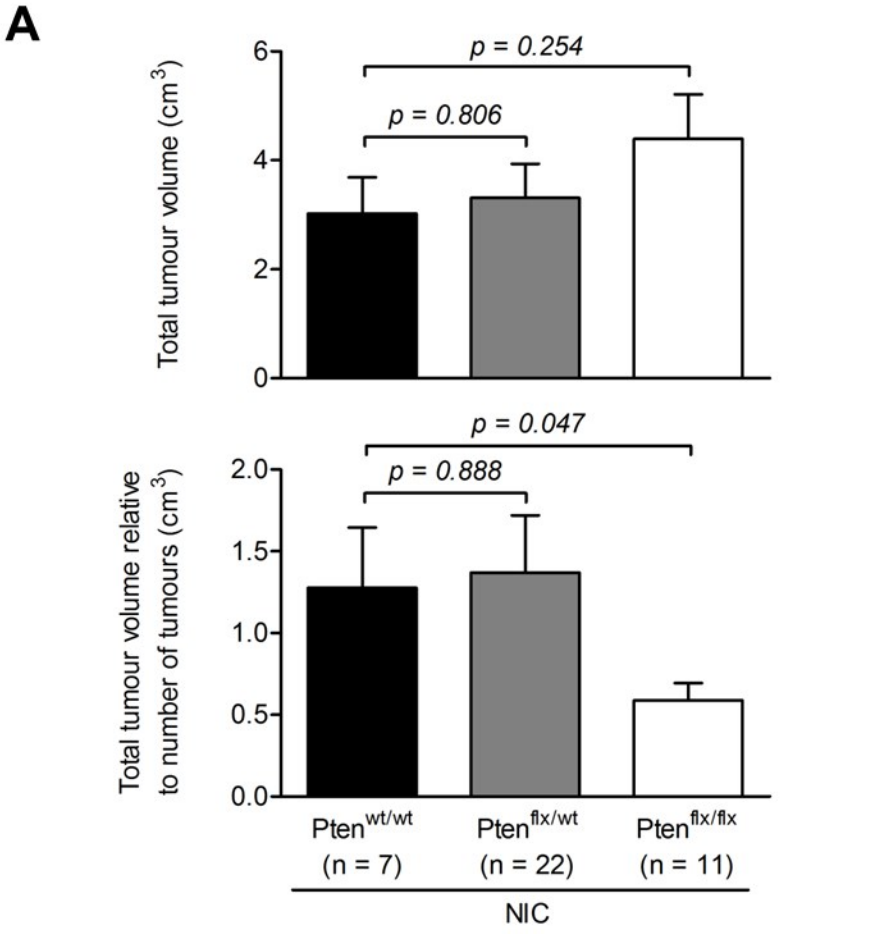
A
p = 0.254
p = 0.806
Total tumour volume (cm3)
6
4
2
0
p = 0.047
p = 0.888
Total tumour volume relative to number of tumours (cm3)
2.0
1.5
1.0
0.5
0.0
Ptenwt/wt (n = 7)
Ptenflx/wt (n = 22)
Ptenflx/flx (n = 11)
NIC

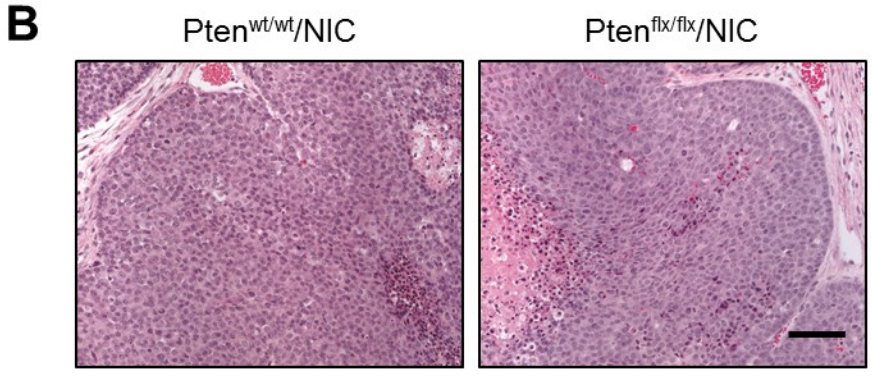
B
Ptenwt/wt/NIC
Ptenflx/flx/NIC

Figure 3-4: Enhanced lung metastasis in Pten-null versus -wildtype NIC mice correlates with differential blood vessel density in the primary tumours

(**A**) Incidence of lung metastasis in tumour-bearing mice expressed as a percentage (left) as well as the average number of lesions per lung lobe in metastasis-positive ("met+") animals (right) for the indicated genotypes. Error bars are standard error of mean. P values were calculated using a two-tailed t-test.

(**B**) Representative images of tumour sections from wildtype NIC and Pten-null/NIC mice stained with the endothelial cell marker CD31 (left). Scale bar is 100 μm. Quantification of CD31 staining is shown by the average percentage of positive pixels (right). Error bars are standard error of mean. P values were calculated using a two-tailed t-test.

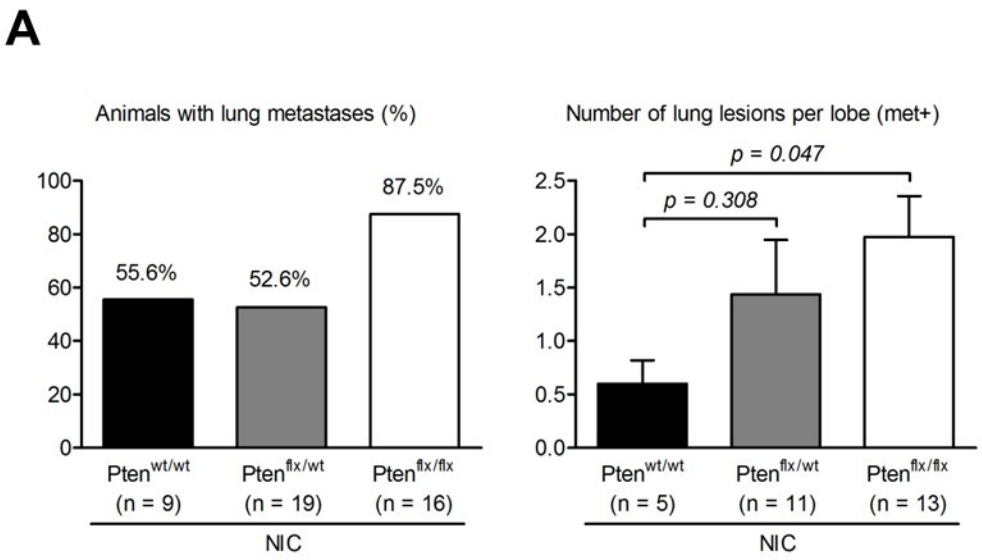
A
Animals with lung metastases (%)
100
80
60
40
20
0
55.6%
52.6%
87.5%
Pten^wt/wt (n = 9)
Pten^flx/wt (n = 19)
Pten^flx/flx (n = 16)
NIC
Number of lung lesions per lobe (met+)
p = 0.047
p = 0.308
2.5
2.0
1.5
1.0
0.5
0.0
Pten^wt/wt (n = 5)
Pten^flx/wt (n = 11)
Pten^flx/flx (n = 13)
NIC

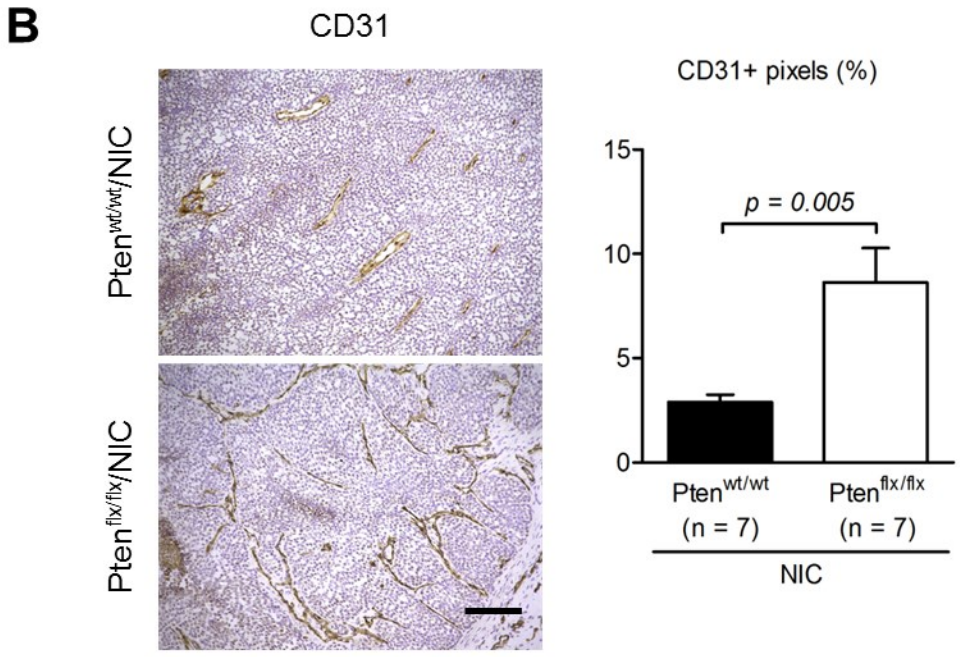
B
CD31
Pten^wt/wt/NIC
Pten^flx/flx/NIC
CD31+ pixels (%)
p = 0.005
15
10
5
0
Pten^wt/wt (n = 7)
Pten^flx/flx (n = 7)
NIC

Figure 3-5: Reduced Pten expression in Pten-deficient/NIC tumours is accompanied by loss of the wildtype Pten allele in heterozygous tumours

(**A**) Immunoblot of tumour lysates from the indicated genotypes using a Pten-specific antibody. β-actin was used as a loading control. Numbers correspond to the mouse ID for each sample.

(**B**) Pten staining by immunohistochemistry in tumour sections from the indicated genotypes. The bottom row images are higher magnifications of the top row images. Scale bars are 100 μm.

(**C**) Southern blot of tumour DNA from the indicated genotypes using a probe specific to the *Pten* locus. Wildtype and excised alleles are indicated by arrows. Numbers correspond to the mouse ID for each sample.

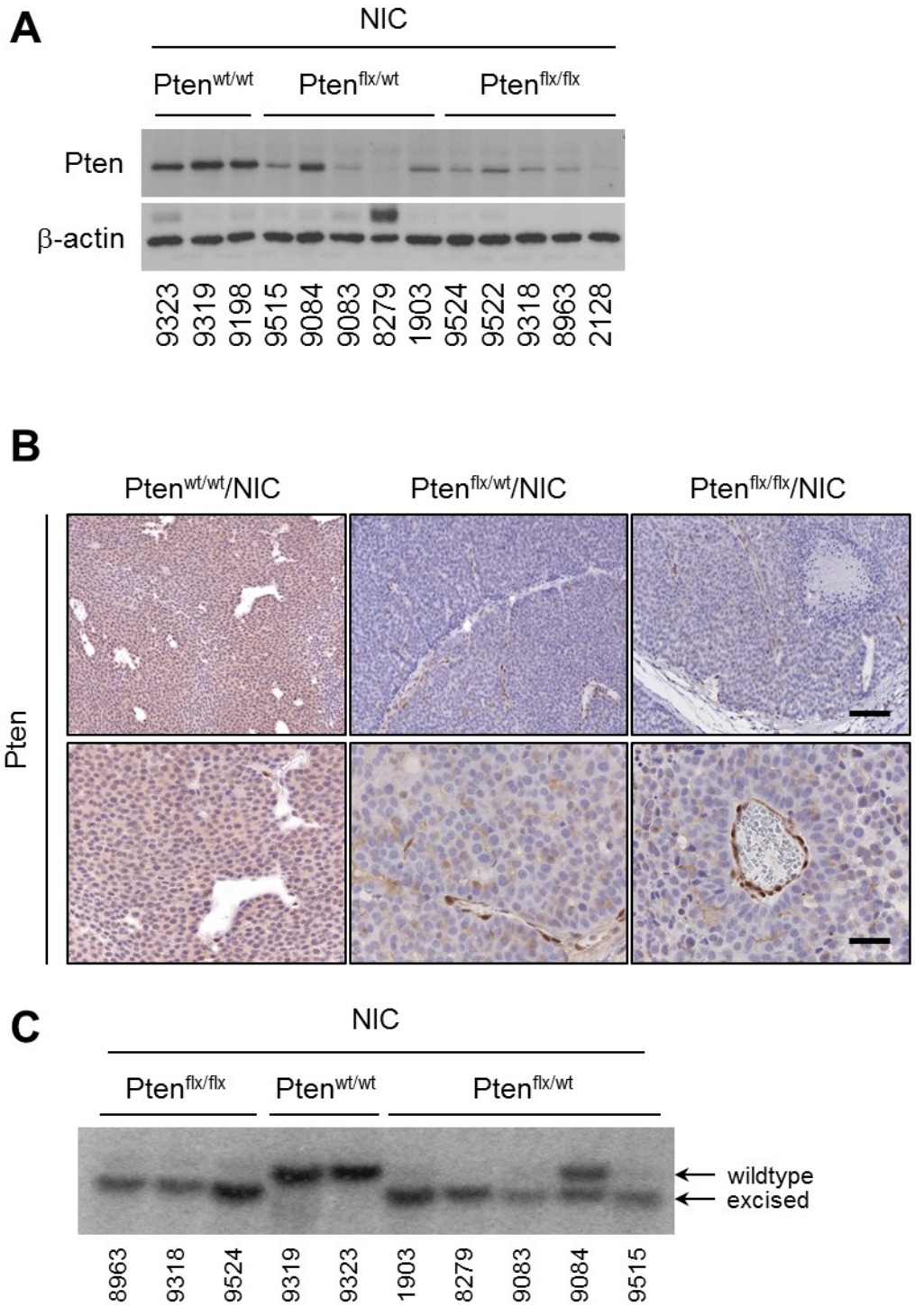
A
NIC
Pten^wt/wt
Pten^flx/wt
Pten^flx/flx
Pten
β-actin
9323
9319
9198
9515
9084
9083
8279
1903
9524
9522
9318
8963
2128
B
Pten^wt/wt/NIC
Pten^flx/wt/NIC
Pten^flx/flx/NIC
Pten
C
NIC
Pten^flx/flx
Pten^wt/wt
Pten^flx/wt
wildtype
excised
8963
9318
9524
9319
9323
1903
8279
9083
9084
9515

Hyperactivation of Akt signalling in Pten-deficient/NIC tumours

PTEN is a well-established suppressor of PI3K/Akt signalling and its absence can lead to dysregulated activation of this pathway and subsequent cellular transformation. Akt phosphorylation was assessed in Pten-wildtype and -null/NIC tumours by immunoblot and strong activation was observed in the latter (Figure 3-6A). Interestingly, the phosphorylation of the Akt substrates Tsc2, Bad, and Gsk3β, was also increased in Pten-deficient/NIC samples relative to wildtype counterparts (Figure 3-6B).

Myristoylation of p110α does not accelerate mammary tumour onset in NDL mice

To generate mice with mammary epithelial-specific expression of activated ErbB2 and myristoylated p110α, MMTV-NDL mice were crossed to a strain in which p110α cDNA is expressed downstream of a human Src myristoylation sequence under the control of the MMTV promoter (myr-p110α/NDL) (Figure 3-7). We monitored cohorts of mice carrying the NDL or myr-p110α transgene alone in parallel with bigenic mice for mammary tumour formation. Similar to the NIC model (which uses the same oncogenic ErbB2 mutant), tumours arise in NDL females at approximately 5-6 months of age, whereas myr-p110α alone is not a potent oncogene in the mammary gland and tumour incidence is relatively low [103, 309]. These phenotypes were observed as expected however myr-p110α did not accelerate tumour initiation in NDL mice and actually caused a slight but significant delay in average tumour onset (Figure 3-8). One possible explanation for this unanticipated result was that co-expression of the two transgenes had caused developmental defects which interfered with tumourigenesis. To investigate this hypothesis, we prepared H&E-stained wholemounts of mammary glands from NDL, myr-

p110α/NDL, and myr-p110α mice at 10 weeks of age. All genotypes were comparable to each other and to an FVB control gland in terms of overall ductal structure and outgrowth measurements (Figure 3-9).

Despite the delayed tumour onset in myr-p110α/NDL mice relative to the NDL cohort, tumour burden was similar in terms of the number and collective volume of tumours (Figure 3-10). Histologically, masses from both groups were solid adenocarcinoma (Figure 3-11A, top row). Examination of adjacent mammary glands from tumour-bearing NDL and myr-p110α/NDL mice revealed the presence of lesions in both histological sections and wholemounted glands for both genotypes (Figure 3-12A, middle and bottom rows). Quantification of lesion area in the wholemounts was not significantly different between the two genotypes (Figure 3-11B).

Myr-p110α/NDL tumours have increased metastatic potential as compared to NDL tumours

We next proceeded to analyze lungs from tumour-bearing mice to look for differential metastatic capacities between myr-p110α/NDL and NDL tumours. Animals had been sacrificed 6-8 weeks after initial palpation of tumours and the equivalent tumour burdens allowed us to compare the two cohorts directly. The incidence of lung metastasis in tumour-bearing animals was similar in both groups, occurring in 80-90% of mice (Figure 3-12, left). However counting of lung lesions in metastasis-positive samples revealed a significant increase in lesion number for bigenic mice as compared to NDL alone (Figure 3-12, right).

Figure 3-6: Pten-null/NIC tumours have increased phosphorylation of Akt and downstream targets in contrast to wildtype NIC samples

(**A**) Immunoblot of tumour lysates from the indicated genotypes using antibodies against phosphorylated Akt (S473) and Akt. β-actin was used as a loading control. Numbers correspond to the mouse ID for each sample.

(**B**) Tumour lysates from the indicated genotypes were immunoblotted for phosphorylated and total forms of Tsc2 (T1462), Bad (S136), and Gsk3α/β (S21/9) (isoforms distinguished by arrowheads; total protein blot is for Gsk3β). β-actin was used as a loading control. Numbers correspond to the mouse ID for each sample.

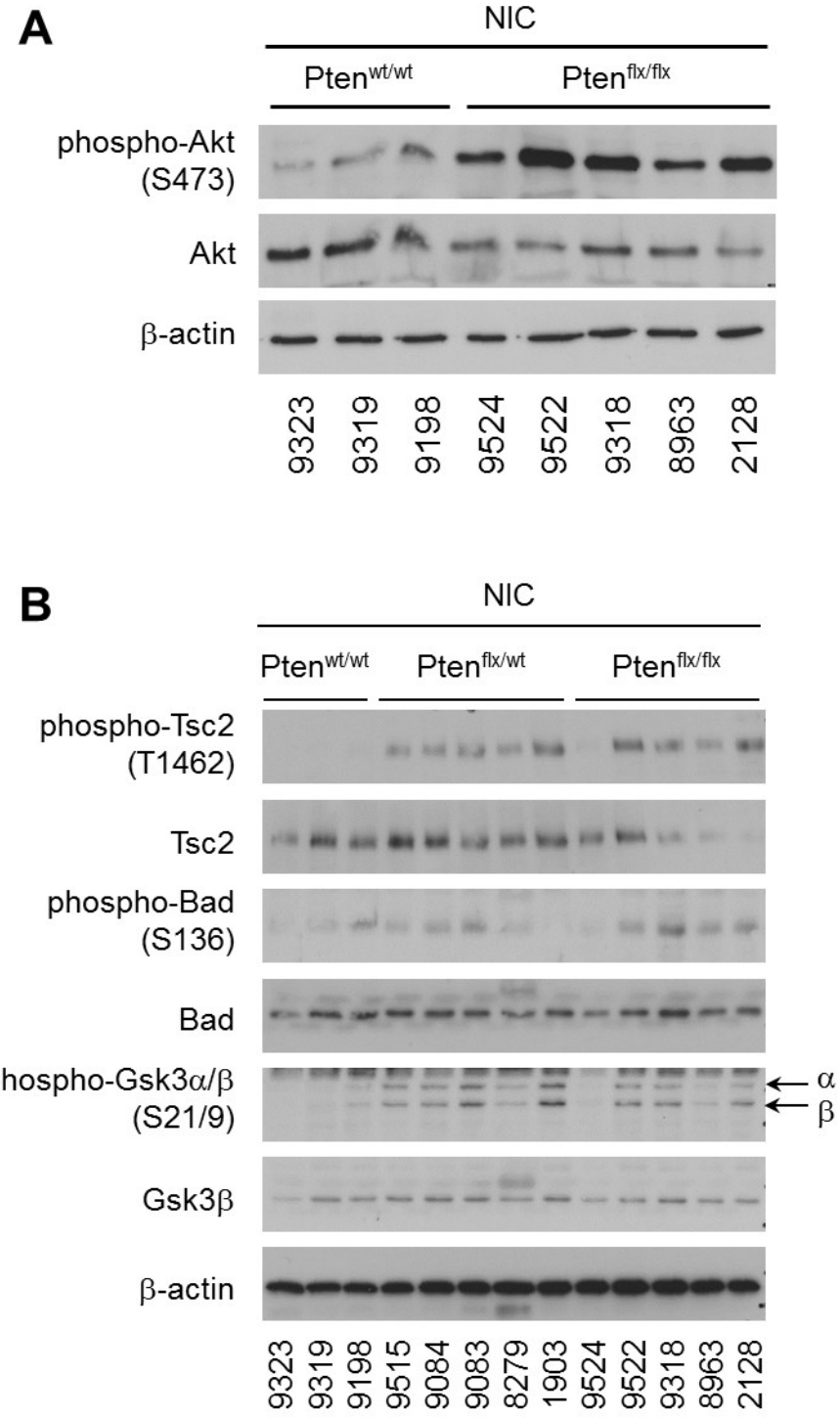
A
NIC
Pten^wt/wt
Pten^flx/flx
phospho-Akt (S473)
Akt
β-actin
9323
9319
9198
9524
9522
9318
8963
2128
B
NIC
Pten^wt/wt
Pten^flx/wt
Pten^flx/flx
phospho-Tsc2 (T1462)
Tsc2
phospho-Bad (S136)
Bad
phospho-Gsk3α/β (S21/9)
α
β
Gsk3β
β-actin
9323
9319
9198
9515
9084
9083
8279
1903
9524
9522
9318
8963
2128

Figure 3-7: Overexpression of myristoylated p110α in the NDL model

Breeding strategy to generate mice with mammary epithelial-specific expression of activated ErbB2/Neu and myristoylated PI3K p110α (*Pi3kca*). A human Src myristoylation sequence ("SRC myr") followed by mouse *PIK3CA* cDNA is driven by the MMTV promoter resulting in expression of myristoylated p110α in the mammary epithelium ("myr-p110α") (schematic based on [309]). This strain is crossed to the MMTV-NDL2-5 ("NDL") strain to generate bigenic mice [103]).

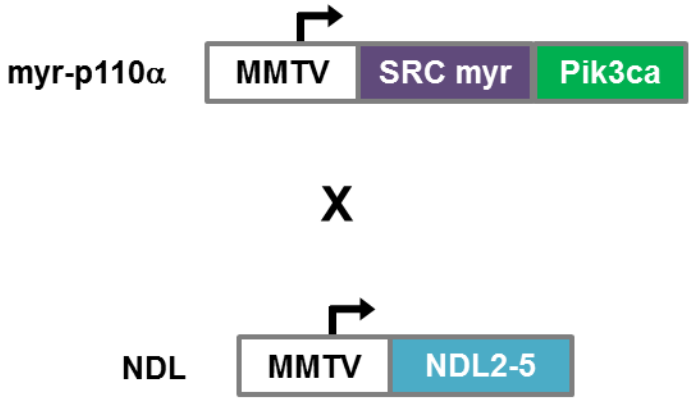
myr-p110α
MMTV
SRC myr
Pik3ca
X
NDL
MMTV
NDL2-5

Figure 3-9: Myristoylated p110α and activated ErbB2 fail to cooperate in tumour initiation

Kaplan-Meier tumour onset curve for myr-p110α/NDL mice and single transgene controls. The table indicates for each genotype the penetrance (percentage of animals that develop tumours), T_{50} (age when 50% of the animals have tumours), and average tumour onset with standard deviation. P values were calculated using a two-tailed t-test.

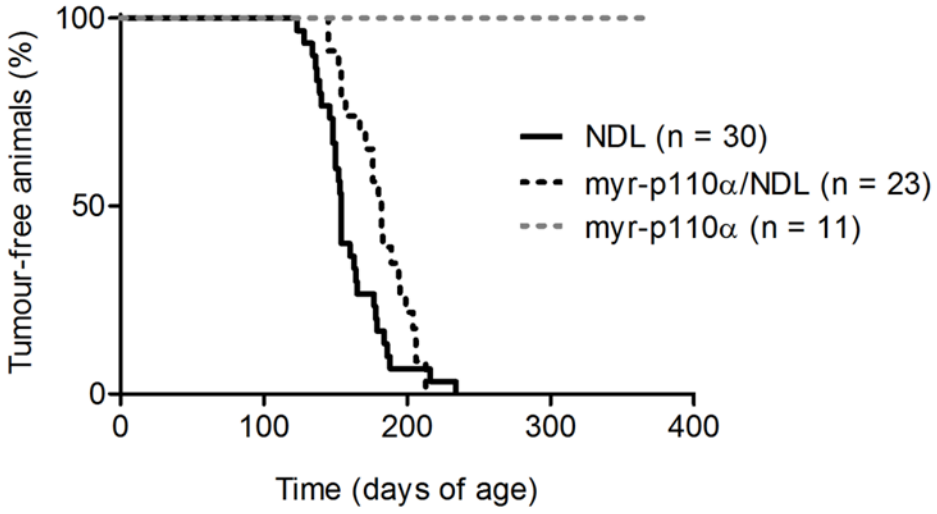

Genotype	Penetrance	T_{50} (days of age)	Average onset (days of age)
NDL	100% (30/30)	154	160 ± 24.7
myr-p110α/NDL	100% (23/23)	182	180 ± 21.7 (*p = 0.0029*)
myr-p110α	0% (0/11)	n/a	n/a

Figure 3-9: Co-expression of the myr-p110α and NDL transgenes does not disrupt normal ductal outgrowth

Representative H&E-stained mammary gland wholemounts from 10-week-old wildtype NDL and myr-p110α/NDL mice (left) and corresponding average ductal outgrowth (right) for each group as indicated. Age-matched myr-p110α and FVB mice are shown as controls. Scale bar is 100 μm. Error bars are standard error of mean. P values were calculated using a two-tailed t-test.

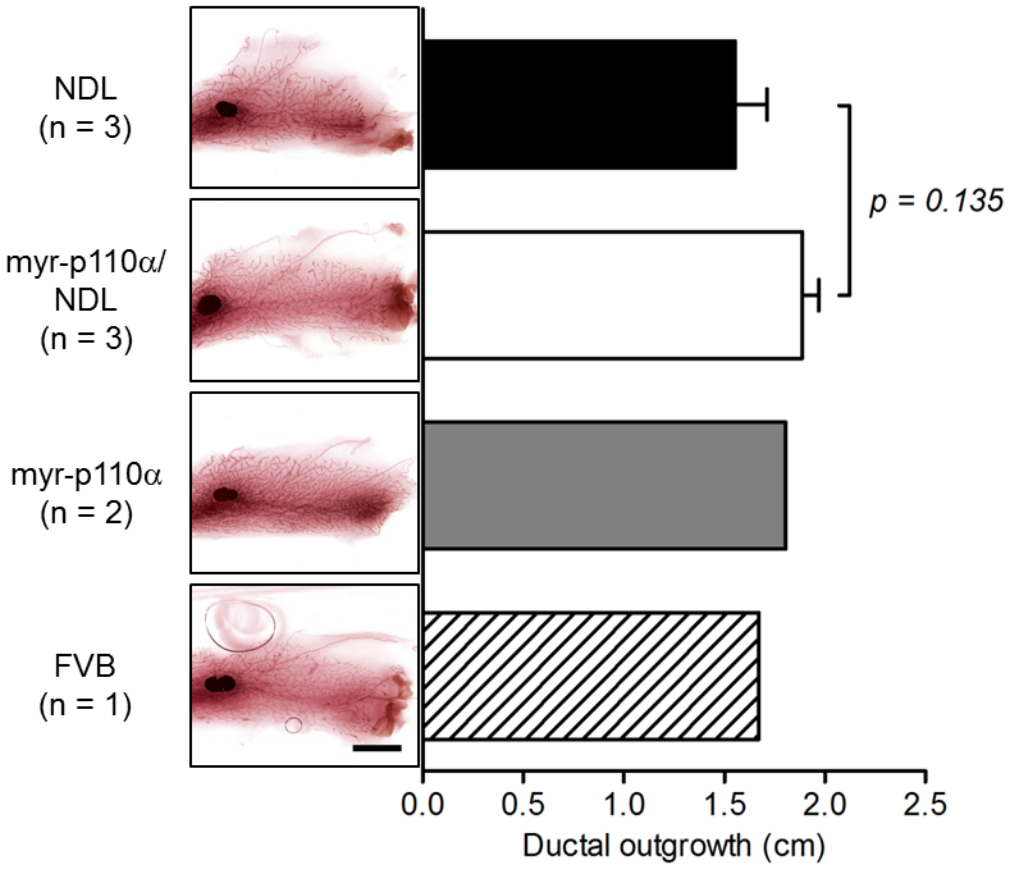
NDL
(n = 3)
myr-p110α/
NDL
(n = 3)
myr-p110α
(n = 2)
FVB
(n = 1)
p = 0.135
0.0
0.5
1.0
1.5
2.0
2.5
Ductal outgrowth (cm)

Figure 3-10: Myr-p110α/NDL tumours develop and grow to similar extent to NDL tumours

Tumour burden for the indicated genotypes is represented as the average total number of tumours (top) and average total tumour volume (bottom) at weekly time-points after palpation of the first mass. Error bars are standard error of mean. P values at 8 weeks post-palpation were calculated using a two-tailed t-test.

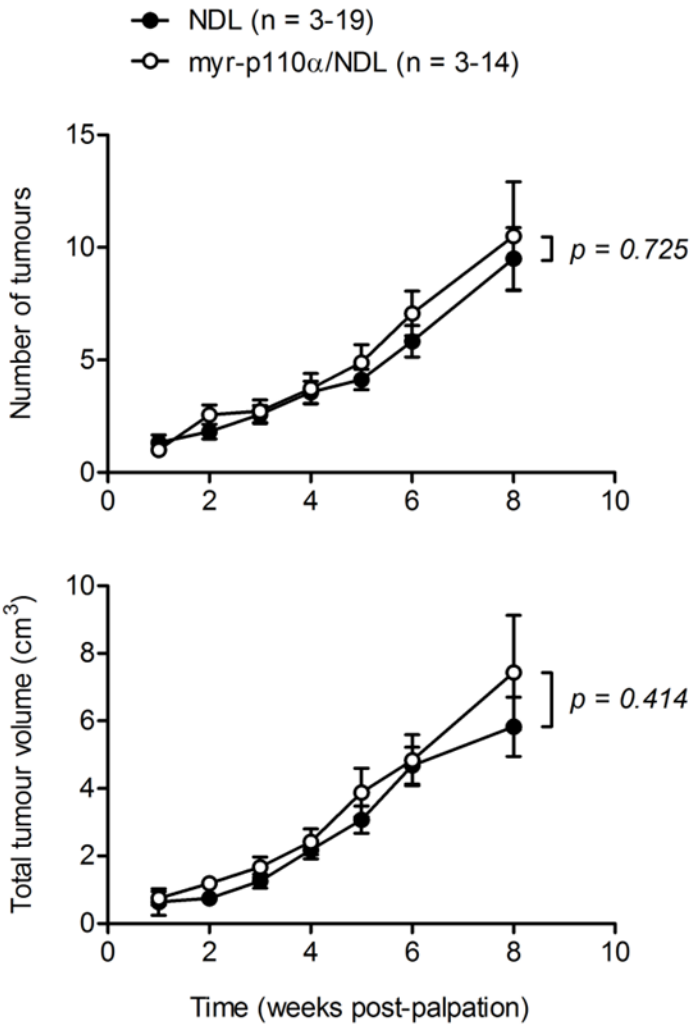
NDL (n = 3-19)
myr-p110α/NDL (n = 3-14)
Number of tumours
p = 0.725
Total tumour volume (cm3)
p = 0.414
Time (weeks post-palpation)

Figure 3-11: NDL and myr-p110α/NDL mice exhibit comparable tumour histology and degree of transformation in adjacent mammary glands

(**A**) Histological sections of tumours (top) stained with H&E from the indicated genotypes as compared to H&E-stained histological sections (middle) and wholemounts (bottom) of adjacent mammary glands. Scale bar is 100 μm for the histological sections (top and middle rows) and 5 mm for the wholemounts (bottom row).

(**B**) The size of the lesions in the wholemounts shown in (A, bottom row) was quantified as the percentage of lesion area relative to total gland area and averaged for the indicated groups. Error bars are standard error of mean. P values were calculated using a two-tailed t-test.

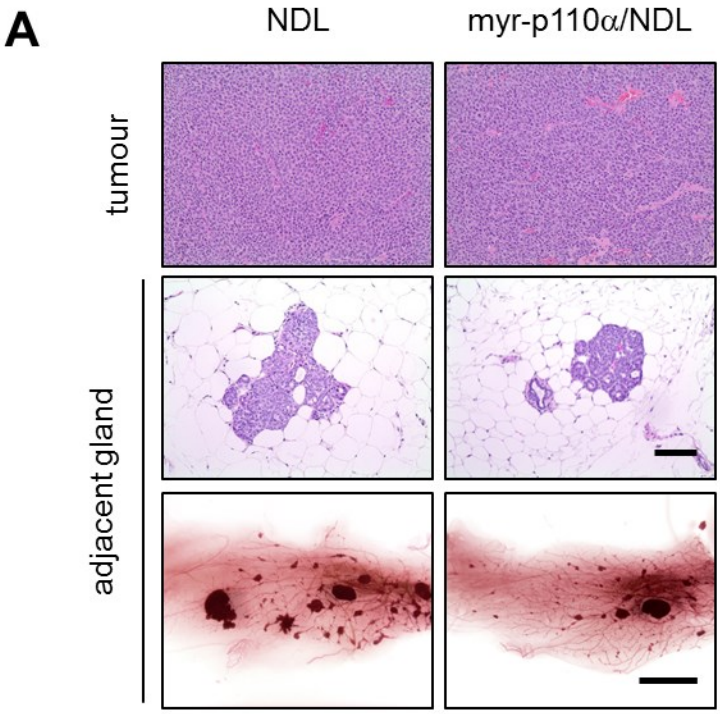
A
NDL
myr-p110α/NDL
tumour
adjacent gland

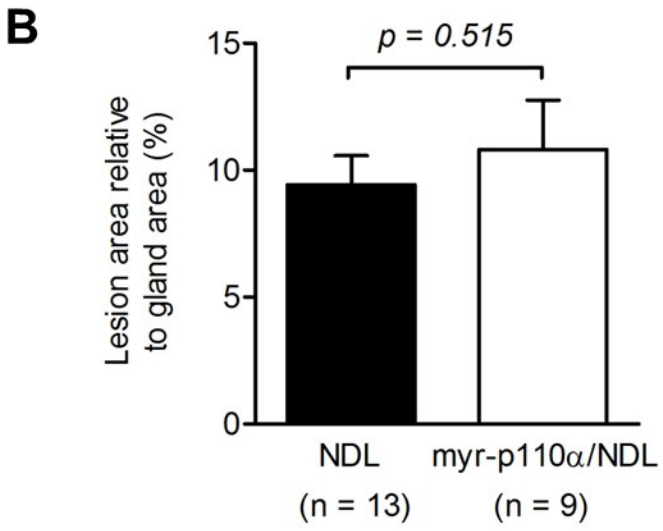
B
p = 0.515
Lesion area relative to gland area (%)
15
10
5
0
NDL
(n = 13)
myr-p110α/NDL
(n = 9)

Figure 3-12: Myristoylated p110α in NDL tumours leads to an increase in pulmonary metastases

The percentage of tumour-bearing mice with lung metastases (left) as well as the number of lung lesions in metastasis-positive ("met+") animals (right) for the indicated genotypes. Error bars are standard error of mean. P values were calculated using a two-tailed t-test.

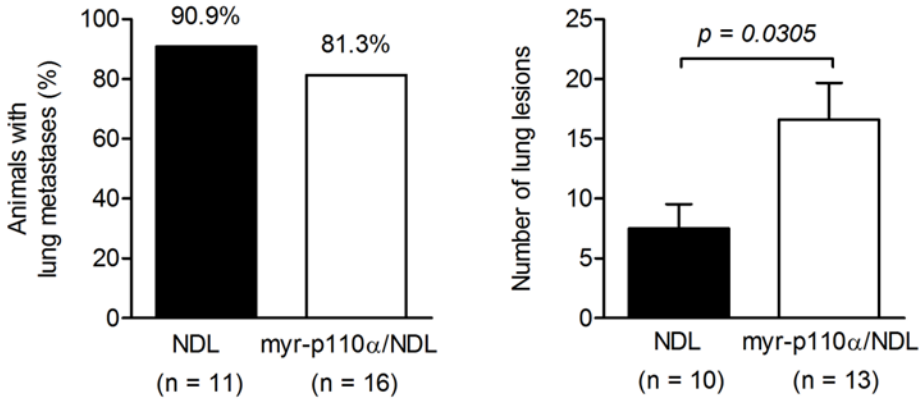
Animals with lung metastases (%)
100
80
60
40
20
0
90.9%
81.3%
NDL
(n = 11)
myr-p110α/NDL
(n = 16)
Number of lung lesions
25
20
15
10
5
0
p = 0.0305
NDL
(n = 10)
myr-p110α/NDL
(n = 13)

Signalling in NDL tumours does not appear to be altered by expression of myr-p110α

To see if we could identify a molecular determinant in primary tumours that might confer a more invasive phenotype, we assayed NDL and myr-p110α/NDL tumour lysates by immunoblot. Expression of p110α and ErbB2 was constant for all samples (Figure 3-13). We did not observe any remarkable variations in Akt phosphorylation, aside from slight elevation in two myr-p110α/NDL samples. The increased activation of Akt in these two tumours did not correlate with malignancy since one was metastatic to the lung while the other was not. Since ERα expression is a common feature in mammary tumour mouse models driven by activated p110α mutants, we blotted for this marker as well [65, 309, 310]. A few bigenic tumour samples showed slightly higher levels of ERα however there was no dominant trend among the groups.

Figure 3-13: Akt activation and ERα expression are not dramatically changed between NDL and myr-p110α/NDL tumours

Tumour lysates of the indicated genotypes were immunoblotted with the following antibodies: p110α, ErbB2, phospho-Akt (S473), Akt, ERα, and α/β-tubulin (loading control). Numbers correspond to the mouse ID for each sample.

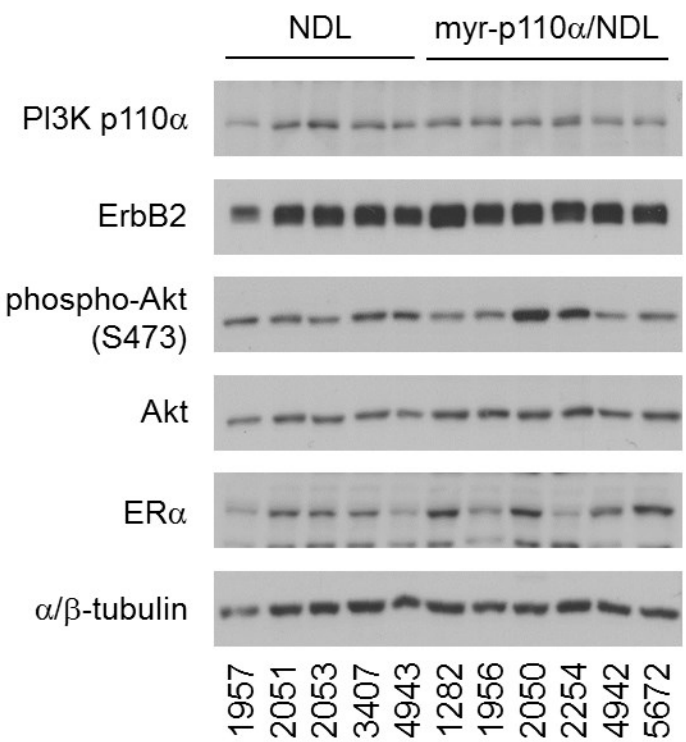
NDL
myr-p110α/NDL
PI3K p110α
ErbB2
phospho-Akt (S473)
Akt
ERα
α/β-tubulin
1957
2051
2053
3407
4943
1282
1956
2050
2254
4942
5672

3.3 Discussion

Loss of PTEN enhances tumour initiation and metastasis in the NIC model

A proportion of HER2-overexpressing breast cancers also exhibit loss of PTEN, prompting us to investigate whether these two oncogenic events can cooperate in an experimental mouse model of mammary tumourigenesis [106]. Using a conditional Pten strain in conjunction with the MMTV-NIC model, we have shown that mammary-specific ablation of Pten accelerates tumour onset induced by activated ErbB2 (Figure 3-2). Tumours arising in Pten-deficient/NIC mice grew to the same overall volume as wildtype counterparts although an estimation of individual tumour size suggested that masses were smaller in $Pten^{flx/flx}$/NIC animals (Figure 3-3). Taken another way, wildtype NIC mice presented with fewer tumours than mice lacking Pten which may indicate that Pten loss has a greater impact on initiating transformation in the mammary epithelium than in driving the growth of masses after they have developed.

We observed an increase in metastatic burden in the lungs from tumour-bearing $Pten^{flx/flx}$/NIC animals as compared to wildtype NIC mice which we attributed to an associated enhancement in blood vessel density (Figure 3-4). Angiogenesis can assist primary tumour growth and can also allow invasive tumour cells to enter the bloodstream and metastasize. Since the increased vasculature in Pten-null/NIC tumours compared to wildtype NIC tumours was not correlated with increased tumour size, it is possible that angiogenesis in this model might have less importance in promoting growth at the primary site and be more purposed toward enabling metastasis (Figure 3-3A and 3-4). Nevertheless, the angiogenic phenotype is reflective of communication between the Pten-deleted epithelial cells and the Pten-proficient stromal cells. Pten in non-epithelial cells of the tumour microenvironment has also been shown to influence tumour-stroma interactions as demonstrated by a study in which fibroblast-specific knockout of

Pten enhanced the growth of ErbB2-induced tumours in mice [425]. Further analysis of this system revealed that Pten-deficient fibroblasts secrete factors that promote tumour cell and endothelial cell proliferation; the identified factors were used to generate a secretome gene signature that was predictive of outcome in breast cancer patients [426]. Pten may therefore elicit tumour suppressive functions from many cell compartments in the mammary gland. Our data show that in ErbB2-expressing mammary epithelium Pten is an important negative regulator of transformation as well as later stages of malignancy.

PTEN-deficient/NIC tumours exhibit increased Akt signalling which may be driven by PTEN LOH in heterozygous samples

Relative to wildtype NIC tumours, both $Pten^{flx/wt}$ and $Pten^{flx/flx}$/NIC tumours showed reduced protein levels of Pten by immunoblot but more importantly lacked Pten expression specifically in the tumour epithelium as shown by immunohistochemistry (Figure 3-5A and B). The absence of Pten expression in NIC tumours heterozygous for Pten is likely due to LOH of the wildtype Pten allele which was observed in the majority of tumours analyzed (Figure 3-5C). Pten LOH was also detected in tumours of some germline $Pten^{+/-}$ mouse strains and as well as tumours from the the Pten-deficient/$ErbB2^{KI}$ cross [323, 324, 334]. These models all recapture a mechanism that can drive both hereditary and sporadic tumours in humans. The fact that Pten LOH occurs in two different murine models of ErbB2-induced mammary tumourigenesis further supports the cooperation of these two oncogenic events when they overlap in human breast cancer [322].

Pten-null/NIC tumours exhibited increased phosphorylation of Akt and a subset of its targets as compared to Pten-proficient/NIC samples indicating that in the absence of Pten, PI3K

signalling is amplified (Figure 3-6). Phosphorylation of Tsc2, Bad, and Gsk3β by Akt inhibits these proteins and, by mechanisms discussed earlier, induces processes including translation, cell survival, and proliferation [198-200, 231, 232, 257]. Activation of these and other Akt-mediated signalling pathways likely promotes tumour initiation and progression of Pten-null/NIC tumours. It should be noted that we did not investigate the identity of the Akt isoform(s) involved which would be an interesting to determine given their differential roles in mammary tumourigenesis specifically [194]. Taken together, Pten LOH and enhanced PI3K/Akt signalling occur with Pten deficiency in our ErbB2-driven mouse model, both of which are clinically relevant features of breast cancer.

PTEN deficiency exerts differential effects on ErbB2-driven tumour histopathology in the ErbB2^{KI} and NIC models

Loss of Pten in the NIC model recapitulated the accelerated tumour onset and enhanced lung metastasis observed in the Pten-deficient/ErbB2^{KI} model, including Pten LOH in heterozygous animals [334]. One marked difference between these models was the effect of Pten loss on tumour morphology. The homogenous solid adenocarcinoma that is typical of both the ErbB2^{KI} and NIC models was altered by Pten ablation in the former but not the latter. Pten-deficient/ErbB2^{KI} tumours emerged with heterogeneous histopathologies. In contrast, NIC tumours maintain an adenocarcinoma phenotype regardless of Pten status (Figure 3-3B). The discrepancies in histology may reflect differences in the timing of ErbB2 overexpression that are inherent to each tumour model. Tumour initiation and progression in the ErbB2^{KI} strain is dependent on amplification of the NeuNT transgene and so overexpression of activated ErbB2 in

this model likely occurs much later than in mice carrying the MMTV-driven NIC transgene. The stronger expression of the NIC transgene at very early stages of tumourigenesis probably confers a more dominant ErbB2 phenotype that masks effects of concurrent Pten deletion in selecting a cell type for tumour initiation. In the ErbB2^{KI} model, Pten deletion probably occurs well before overexpression of ErbB2, perhaps leading to a mixed tumour pathology and cytokeratin profile. Taken together, these studies demonstrate that Pten deficiency can synergize with ErbB2 activation in two different mouse models to accelerate tumour onset and promote pulmonary metastasis.

Selective effect of myristoylated p110α on metastasis, but not initiation, of NDL tumours

We next investigated whether a similar effect on ErbB2-driven mammary tumourigenesis could be potentiated by constitutive membrane localization of p110α. Mice expressing this transgene in the mammary epithelium develop neoplastic lesions that in a few rare cases progress to adenocarcinoma [309]. Unexpectedly, mammary-specific expression of myristoylated p110α delayed tumour onset in the MMTV-NDL model (Figure 3-9). Examination of wholemounted mammary glands prior to tumour initiation showed that no differences in mammary gland development as a result of transgene expression (Figure 3-10). However, defects may not be detectable on such a gross scale and more detailed histological and molecular analyses of mammary epithelial cells from young mice may reveal reasons for the observed delay in tumour initiation. One conceivable outcome might be the upregulation of p53 in premalignant mammary epithelium, which can induce senescence in response to PI3K pathway activation [326, 427]. Because tumours do develop in myr-p110α/NDL mice, the potential induction of p53-mediated

senescence may be a transitory condition that is eventually overcome by overexpression of activated ErbB2. Another possibility could be mosaic expression of NDL and myr-p110α in bigenic mice since they are on separate transgenes and the MMTV promoter is known to be active in only 70% of mammary epithelial cells [108]. We were unable to test this hypothesis since the myr-p110α transgene lacks any exogenous tag that can be detected by a readily available antibody. Ultimately the slight delay in tumour onset in myr-p110α/NDL mice proved to be the only characteristic that directly opposed our original hypothesis. ErbB2-type adenocarcinoma developed similarly between bigenic and NDL mice, with no differences in burden for both measurable tumours or lesions in adjacent mammary glands (Figure 3-11 and 3-12).

Although myristoylation of p110α did not reduce tumour latency in the NDL model, it did lead to increased numbers of lung metastases (Figure 3-11 and 3-13). This suggests that tumour cells in bigenic animals may possess an advantage over NDL cells at any point during the metastatic cascade. Preliminary immunoblots of tumours from both genotypes did not identify any signalling phenotypes that associated with increased numbers of lung lesions (Figure 3-14). Further molecular analyses will be necessary to uncover differential expression of metastasis-promoting features in the primary tumour but also in the lung lesions themselves; these may involve invasive and migratory signatures as well as markers of tumour cell survival and proliferation. Given the established role of the microenvironment at both the primary and secondary tumour sites, additional experiments can be performed to investigate stromal cells and factors that may be permissive to metastasis such as immunohistochemical staining of vasculature and immune infiltrates. In doing so we may be able to determine why signalling

through myristoylated p110α enhances the metastatic dissemination of ErbB2-expressing tumour cells but has no apparent effect on the initial development of these tumours.

Consistent activation of Akt is lacking in myr-p110α/NDL tumours

The immunoblot analyses also revealed that only two of the myr-p110α/NDL samples assayed had relatively higher expression of phosphorylated Akt (Figure 3-14). Previous studies with myr-p110α have demonstrated that it is only weakly transforming both *in vitro* and *in vivo* [309, 361]. The modest activation of Akt by myr-p110α shown in other systems, including in the mammary epithelium of the MMTV-myr-p110α strain, may be masked by relatively stronger oncogenic signalling from the NDL transgene in our model. These findings contrast with the robust Akt signalling detected in Pten-deficient/NIC tumours and support the idea that the PI3K pathway is not equivalently activated downstream of Pten ablation and myr-p110α expression (Figure 3-6). These data coincide with clinical data demonstrating that activation of PI3K signalling in breast cancer correlates better with PTEN loss than with mutation of *PIK3CA* [4, 351]. However an important caveat to this is the fact that myr-p110α does not fully mimic point mutation of p110α as it is considered to be comparatively less active *in vitro* and in mouse models [309, 310, 361, 366, 367]. This conclusion may explain why Pten loss but not myristoylation of p110α accelerated ErbB2-driven tumour initiation. Another possibility for both the preclinical and clinical scenarios is the assumption that signalling initiated by p110α activation is restricted by the presence of a functional Pten.

Myr-p110α/NDL tumours exhibited expression of ERα by immunoblot, a characteristic of other mammary tumour mouse models driven by mutant *PIK3CA* as well as human breast

cancers that have *PIK3CA* mutations (Figure 3-14) [4, 65, 309, 310, 320, 340, 366]. A few samples expressed somewhat more ERα than others and it would be interesting to investigate this further by performing *in situ* staining of tumours as well as investigating the expression of other luminal markers. ErbB2-driven murine mammary tumours are generally ER-negative and so even subtle increases in ERα in our myr-p110α/NDL strain would establish clinical relevance for this model to some extent. Moreover, this would further support the preceding discussion on the degree of PI3K pathway activation which is lower in ER-positive breast cancers relative to other subtypes [4]. Taken together, co-expression of activated ErbB2 and myristoylated p110α in the mammary epithelium induces some but not all of the molecular phenotypes typically associated with activated PI3K signalling in breast cancer.

The PI3K pathway is important for metastasis of ErbB2-driven tumours

An interesting feature of both the Pten-deficient/NIC and myr-p110α/NDL tumours was their enhanced ability to metastasize to the lung. Despite other obvious differences between the two models, this concurrent finding demonstrates that PI3K signalling is a critical mediator of metastasis in cells derived from ErbB2-induced tumours. As discussed earlier, the PI3K pathway can influence several cellular functions that are required for tumour invasiveness. Although one must consider that Pten has functions that are independent of PI3K signalling, our findings suggest that the Pten-deficient/NIC model is likely driven by increased Akt activation. The lack of robust Akt activation in myr-p110α/NDL tumours relative to NDL tumours suggests that even basal PI3K signalling may be able to promote metastasis of tumours induced by ErbB2, however at this point we cannot exclude the contribution from other molecular alterations in

these tumours. Future studies on this particular aspect in both models could involve more detailed analyses of lung colonization by tail vein injection of tumour cells as well as *in vitro* assays examining their migratory and invasive capabilities. The results from these experiments can be used to further compare and contrast these two different mechanisms of PI3K pathway activation during the metastatic phase of ErbB2 tumour progression.

4 Genetic ablation of PI3K p110α in a mouse model of ErbB2 mammary tumourigenesis

4.1 Introduction

In the previous chapter, we showed that signalling through the PI3K/Akt pathway could collaborate with overexpression of activated HER2/Neu in murine mammary tumourigenesis and metastasis. Given the overlap of PI3K pathway activation and HER2 overexpression in breast cancers, we hypothesized that p110α would be an essential signal downstream of activated HER2/Neu during mammary tumourigenesis [4, 320]. This appears to be the case *in vitro*, where MEFs from conditional p110α mice failed to transform when retrovirally infected with activated ErbB2 (NeuT) [276]. In addition, work from the last fifteen years has identified *in vivo* roles for p110α in developmental processes such as proliferation and angiogenesis which have the potential to be co-opted during tumourigenesis [272, 274]. Although many mammary tumour mouse models driven by activating mutations in p110α have been characterized, the requirement for p110α in breast cancer initiation and progression had not been addressed until now. In order to genetically ablate p110α in mammary epithelium expressing activated ErbB2/Neu we crossed the conditional p110α mice to our MMTV-NIC model. Preliminary results revealed that loss of both p110α alleles dramatically delayed tumour onset in this model [114]. Further evidence for the importance of p110α in tumour initiation came from the finding that in the absence of the β isoform of p110, Neu-induced tumourigenesis is accelerated due to increased signalling by p110α [114]. Despite the delay in tumour initiation in the $p110\alpha^{flx/flx/}$NIC model, tumours eventually developed in all animals indicating that p110α is not absolutely required for tumourigenesis in the NIC model (unpublished observations, T. Rao and W.J. Muller). Our characterization of these ErbB2-induced tumours that have evolved without a functional p110α may be useful in predicting possible resistance mechanisms to both pan- and isoform-specific inhibitors in patients with HER2-expressing breast cancer.

4.2 Results

Mammary gland ductal structure is intact in mice with mammary epithelial-specific ablation of p110α and overexpression of activated ErbB2

Genetic ablation of p110α in the mammary epithelium was achieved by crossing a conditional p110α strain to MMTV-NIC mice (Figure 4-1) [105, 276]. While it would have been ideal to verify loss of p110α protein expression in young animals, we encountered two limitations: (1) p110α expression in non-epithelial mammary stroma (i.e. adipocytes, fibroblasts, endothelial cells, immune cells, etc.) precludes the ability to observe a clear decrease in expression in immunoblots of bulk mammary gland lysates (data not shown); and (2) we lack a suitable antibody for immunohistochemical detection of p110α in mouse tissue. However, by enriching the epithelial cell population in mammary glands we obtained a quantitative reduction in *PIK3CA* expression at the mRNA level in $p110\alpha^{flx/flx}$/NIC mice as compared to FVB and wildtype NIC mice (Figure 4-2A).

It has been previously shown that the deletion of p110α in the mouse mammary epithelium impairs ductal outgrowth; if this defect appeared in p110α-deficient/NIC mammary glands it would compromise interpretation of future studies of tumourigenesis in this model [114]. For this reason, we examined wholemounted mammary glands from $p110\alpha^{flx/wt}$ and $p110\alpha^{flx/flx}$/NIC mice at an age when ductal outgrowth is nearing completion (10 weeks). In both cases the mammary glands exhibited normal ductal outgrowth and branching comparable to glands from a normal 10-week-old FVB mouse (Figure 4-2B, left). We suspect that overexpression of activated ErbB2 rescues the ductal outgrowth defect caused by p110α ablation.

Figure 4-1: Conditional loss of PI3K p110α in the NIC model

Breeding strategy to generate mice with mammary epithelial-specific expression of activated ErbB2 and ablation of PI3K p110α (*PIK3CA*). The conditional p110α strain ("Flox- p110α") carries a p110α allele in which exon 1 is flanked by LoxP sites [276]. When crossed with the MMTV-NIC strain ("NIC") [105], the conditional p110α allele(s) will undergo Cre-mediated recombination specifically in the mammary epithelium.

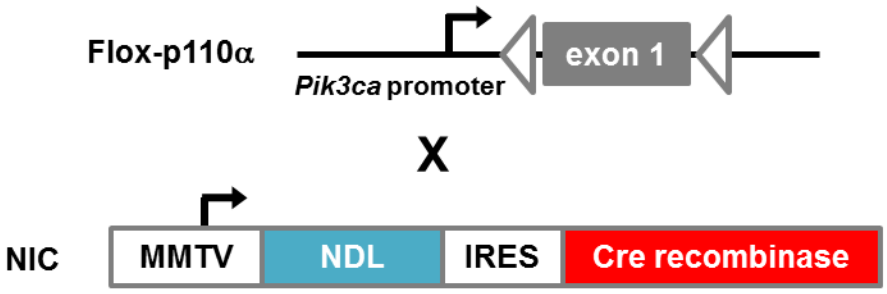
Flox-p110α
exon 1
Pik3ca promoter
X
NIC
MMTV
NDL
IRES
Cre recombinase

Figure 4-2: Normal mammary gland development in p110α-deficient/NIC animals

(**A**) Quantitative PCR for p110α (*PIK3CA*) transcript (normalized to *Gapdh* transcript) in cDNA from pre-malignant epithelium of the indicated genotypes. Samples from 1-3 animals were pooled and multiple pools were averaged for the analysis (n values indicate the total number of mice). Error bars are standard error of mean. P values were calculated using a two-tailed t-test.

(**B**) H&E-stained (left) mammary gland wholemounts from 10-week-old NIC mice carrying one or both conditional p110α alleles exhibit normal ductal structures, which are comparable to a mammary gland from an FVB animal of the same age. GFP fluorescence in the ducts of the mammary glands demonstrates expression of the Cre-inducible reporter (right; transgene schematic shown in (B)). Scale bars from left to right are 5 mm, 0.2 mm, 1 mm.

(**C**) Simplified schematic of the Cre recombinase-activated GFP reporter strain designated as "GFP" (adapted from [68]). The presence of Cre recombinase allows for removal of the floxed STOP cassette and expression of the *EGFP* transgene which encodes for the enhanced green fluorescent protein.

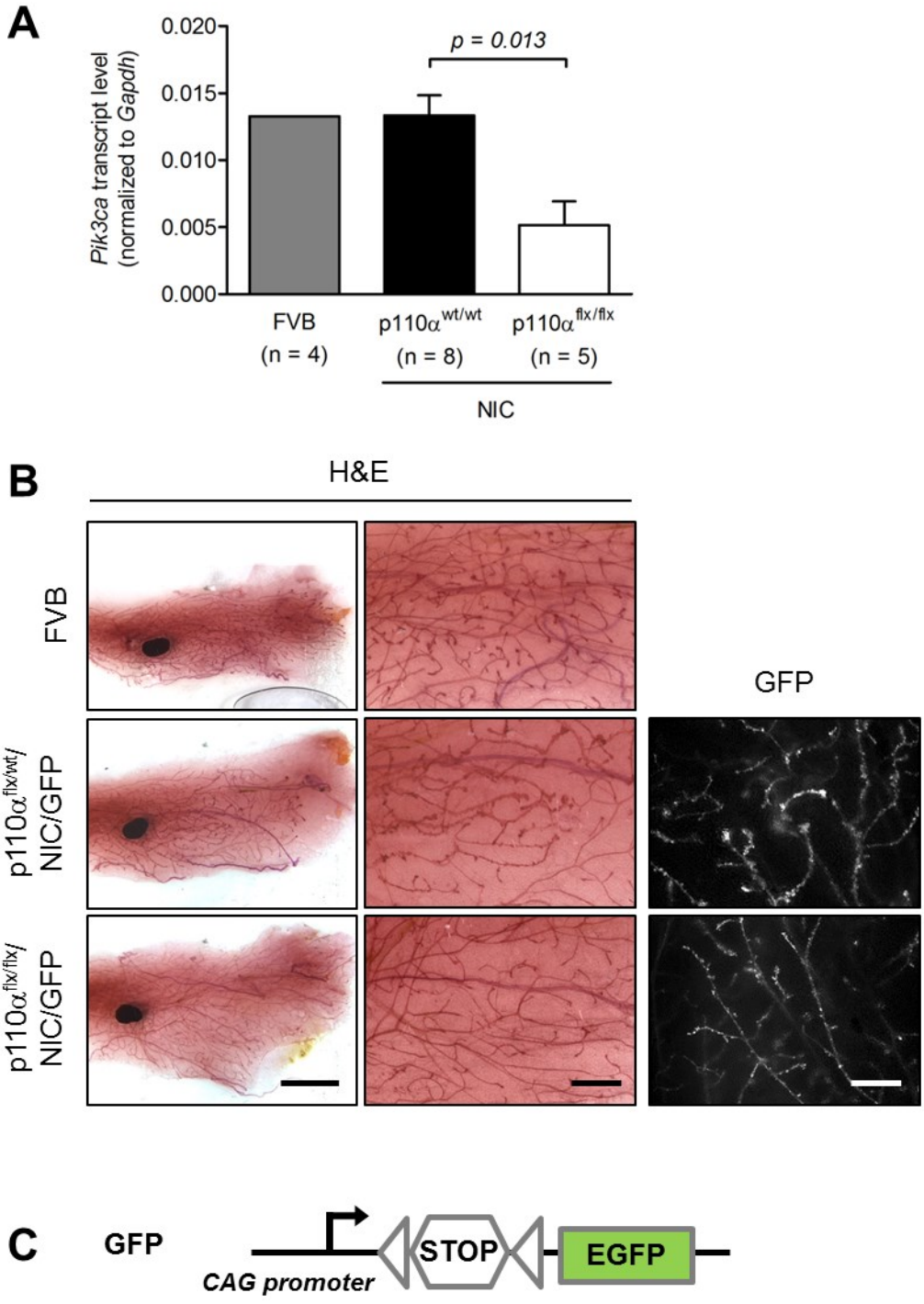
A
Pik3ca transcript level (normalized to Gapdh)
0.020
0.015
0.010
0.005
0.000
p = 0.013
FVB (n = 4)
p110α wt/wt (n = 8)
p110α flx/flx (n = 5)
NIC
B
H&E
GFP
FVB
p110α flx/wt/ NIC/GFP
p110α flx/flx/ NIC/GFP
C
GFP
CAG promoter
STOP
EGFP

In lieu of assessing p110α expression, we used an indirect method of confirming Cre recombinase function by incorporating a Cre-inducible GFP reporter transgene (Figure 4-2C) [68]. Prior to H&E staining, the wholemounted mammary glands from p110α-deficient/NIC mice were analyzed for GFP expression. Indeed, fluorescence was observed in the ductal epithelium from both heterozygous and homozygous glands (Figure 4-2B, right). The presence of a functional Cre recombinase indicates that the conditional p110α alleles present in these cells are likely being excised as well. Having confirmed normal ductal outgrowth and the presence of an active Cre recombinase in the conditional p110α/NIC strains, we were confident in proceeding with aging these mice in parallel with wildtype counterparts to study mammary tumour development.

p110α$^{flx/flx}$/NIC mice develop mammary tumours after a long latency

Animals expressing the NIC transgene and carrying one or both of the floxed p110α alleles were monitored for tumour formation alongside wildtype NIC controls. As observed previously, p110α$^{wt/wt}$/NIC mice developed tumours at approximately 4-5 months of age (Figure 4-3). Heterozygous loss of p110α significantly but only modestly delayed tumour onset. This effect was exacerbated in the homozygous cohort; animals developed tumours much later than wildtype NIC mice and with more variability in the age of onset. It should be emphasized that tumours occurred in 100% of the cohort which suggests that p110α is not absolutely essential in this context.

To demonstrate that p110α-deficient/NIC mammary epithelium had undergone Cre-mediated excision of the conditional allele, PCR of the *PIK3CA* locus was carried out which can

amplify the wildtype, floxed, and excised genomic products (Figure 4-4A, top) [276]. Indeed, the excised p110α allele was detectable in heterozygous and homozygous NIC tumour DNA while no bands were visible for floxed alleles (Figure 4-4A, bottom). This evidence for genetic ablation of p110α translated to the protein level as immunoblotting of tumour lysates revealed a clear decrease in expression in $p110\alpha^{flx/flx}$/NIC samples in contrast to wildtype and heterozygous lysates (Figure 4-4B). As these lysates were prepared from whole tumour they likely possess some degree of stromal content which provides residual p110α signal on the immunoblot. Expression of the NIC transgene was confirmed in these samples using antibodies against ErbB2 and Cre recombinase (Figure 4-4B).

Although tumours eventually developed in p110α-null/NIC mice, penetrance was limited to one or two glands unlike the multifocal nature of wildtype NIC tumours. While there was a signification reduction when compared to wildtype NIC animals in the number and total volume of tumours at 6 weeks post-palpation for $p110\alpha^{flx/wt}$/NIC mice, the effect was greater in the homozygous cohort due to the focality of masses (Figure 4-5A). Interestingly, when total tumour volume was normalized to the number of tumours for each animal, there is no difference between the genetic groups (Figure 4-5B). This estimation suggests that individual tumour size may be similar in NIC mice regardless of p110α status.

The cellular morphology of tumours from all genotypes confirmed the development of solid adenocarcinoma typical of ErbB2-driven models (Figure 4-6A, top row). However, the differential tumour multiplicity that we had observed in these mice prompted us to also examine the adjacent mammary glands from tumour-bearing animals (i.e. glands lacking palpable masses) for the incidence of early lesions. Histological analysis of these adjacent mammary glands revealed the presence of lesions in only wildtype and heterozygous NIC samples, while

Figure 4-3: Dramatically delayed tumour initiation in p110α-null/NIC animals as compared to wildtype and heterozygous counterparts

Kaplan-Meier tumour onset curve for NIC mice that are wildtype, heterozygous, or homozygous for the p110α conditional allele. The table indicates for each genotype the penetrance (percentage of animals that developed tumours), T_{50} (age when 50% of the animals have tumours), and average tumour onset with standard deviation for each of the curves shown on the graph. P values were calculated using a two-tailed t-test.

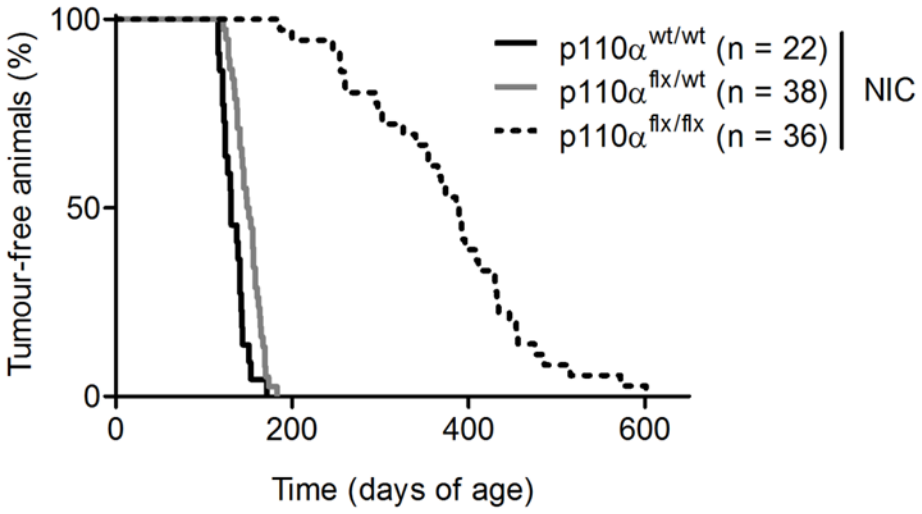

NIC	Penetrance	T_{50} (days of age)	Average onset (days of age)
$p110\alpha^{wt/wt}$	100% (22/22)	131	134 ± 13.9
$p110\alpha^{flx/wt}$	100% (38/38)	149	150 ± 15.2 (*p = 0.0002*)
$p110\alpha^{flx/flx}$	100% (36/36)	386	376 ± 96.7 (*p < 0.0001*)

Figure 4-4: Evidence of p110α ablation in tumours arising from p110α-null/NIC mice

(**A**) Schematic illustrating the wildtype and floxed *PIK3CA* alleles and the expected PCR product size when amplified using the primers shown (red arrows) (top; adapted from [276]. Cre recombination of the floxed *PIK3CA* allele results in amplification of the excised product; this is detectable in tumour DNA from NIC mice heterozygous and homozygous for the conditional p110α allele (bottom).

(**B**) Immunoblots for p110α, Cre recombinase, and ErbB2 in tumour lysates from the indicated genotypes. α-tubulin was used as a loading control. Numbers correspond to the mouse ID for each sample.

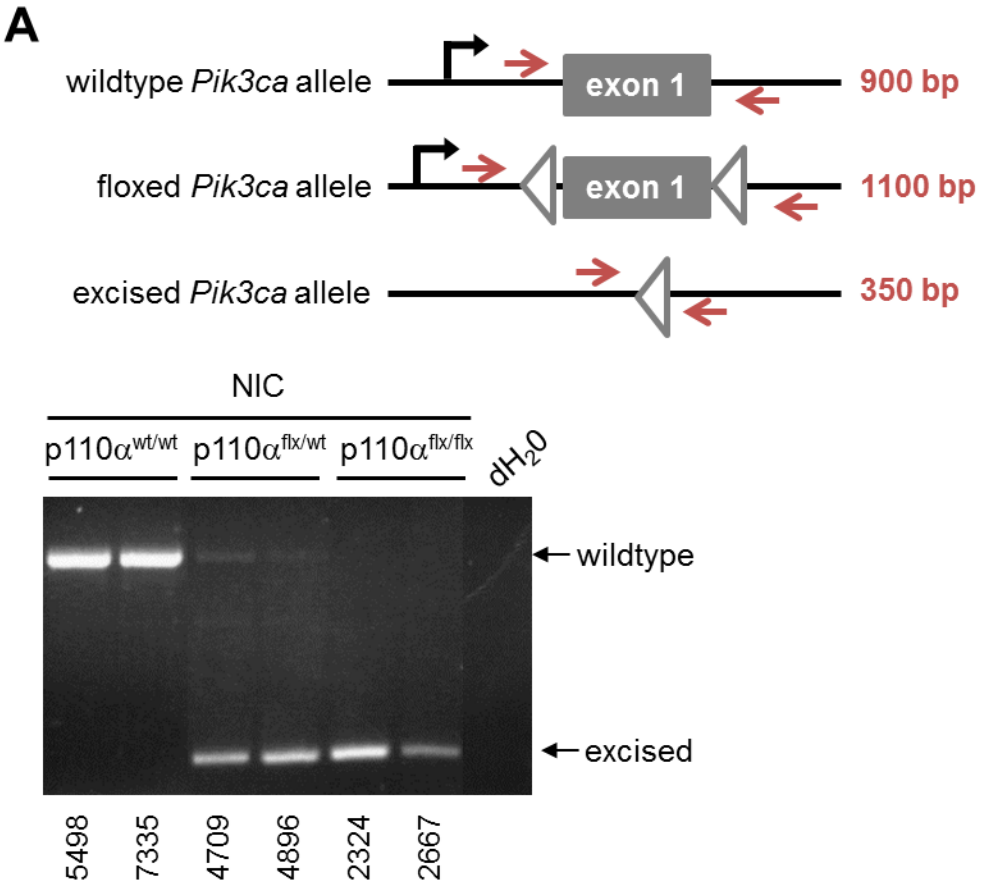
A
wildtype Pik3ca allele
exon 1
900 bp
floxed Pik3ca allele
exon 1
1100 bp
excised Pik3ca allele
350 bp
NIC
p110α^wt/wt
p110α^flx/wt
p110α^flx/flx
dH2O
wildtype
excised
5498
7335
4709
4896
2324
2667

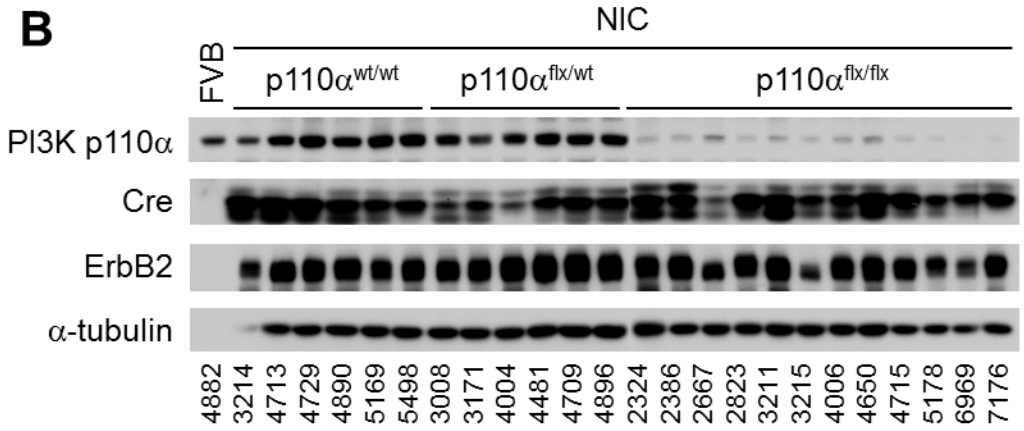
B
NIC
FVB
p110α^wt/wt
p110α^flx/wt
p110α^flx/flx
PI3K p110α
Cre
ErbB2
α-tubulin
4882
3214
4713
4729
4890
5169
5498
3008
3171
4004
4481
4709
4896
2324
2386
2667
2823
3211
3215
4006
4650
4715
5178
6969
7176

Figure 4-5: p110α-null/NIC mice develop fewer tumours than the wildtype and heterozygous cohorts

(**A**) Tumour burden for the indicated genotypes is represented as the average total number of tumours (top) and average total tumour volume (bottom) at weekly time-points after palpation of the first mass. Error bars are standard error of mean. P values at 6 weeks post-palpation were calculated using a two-tailed t-test.

(**B**) Average individual tumour volume estimated by calculating the total tumour volume relative to the total number of tumours for each animal. Error bars are standard error of mean. P values were calculated using a two-tailed t-test.

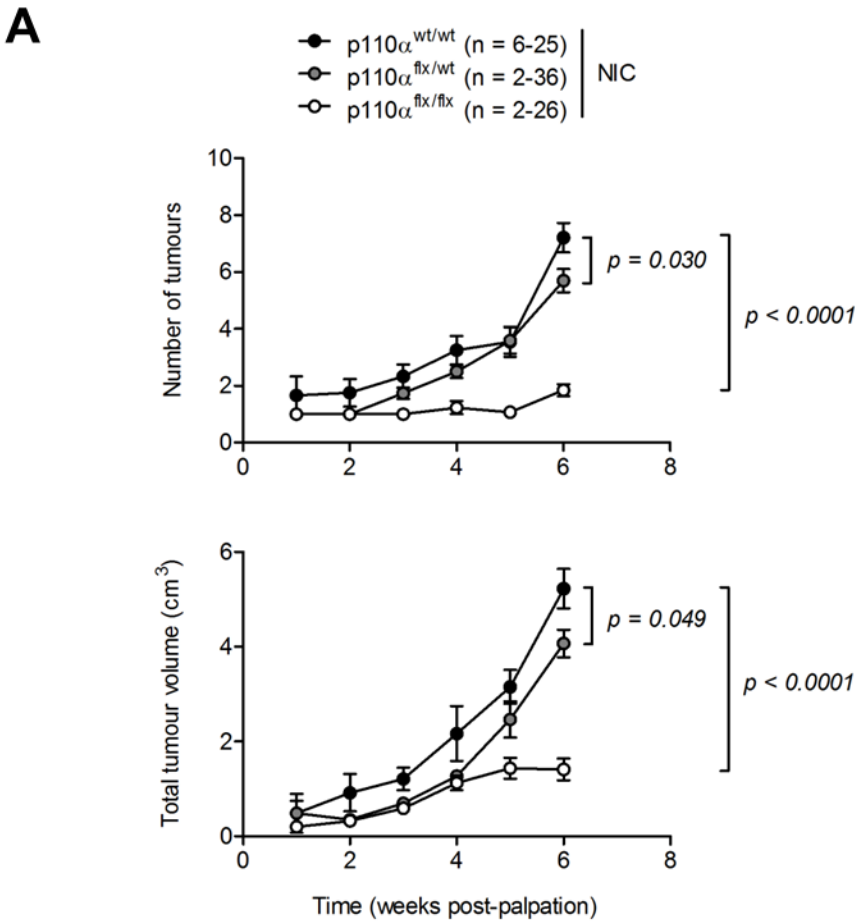
A
p110α wt/wt (n = 6-25)
p110α flx/wt (n = 2-36)
p110α flx/flx (n = 2-26)
NIC
Number of tumours
p = 0.030
p < 0.0001
Total tumour volume (cm3)
p = 0.049
p < 0.0001
Time (weeks post-palpation)

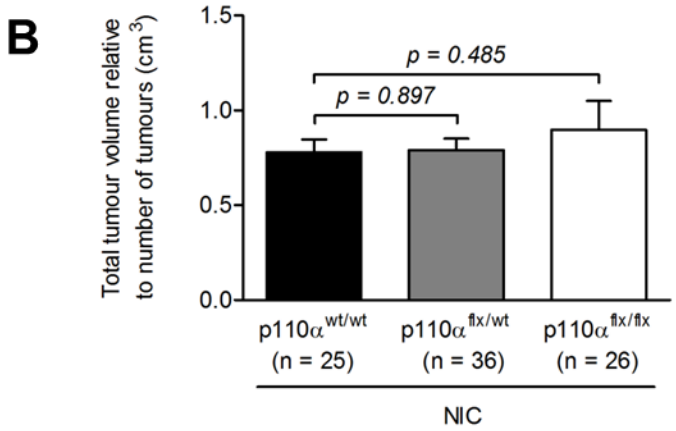
B
Total tumour volume relative to number of tumours (cm3)
p = 0.485
p = 0.897
p110α wt/wt (n = 25)
p110α flx/wt (n = 36)
p110α flx/flx (n = 26)
NIC

Figure 4-6: Tumours from all genetic groups are solid adenocarcinoma while adjacent mammary gland histology confirms the focal penetrance of p110α-null/NIC masses

(**A**) Histological sections of tumours (top) stained with H&E from the indicated genotypes as compared to H&E-stained histological sections (middle) and wholemounts (bottom) of adjacent mammary glands. Scale bar is 100 μm for the histological sections (top and middle rows) and 5 mm for the wholemounts (bottom row).

(**B**) The size of the lesions in the wholemounts shown in (A, bottom row) was quantified as the percentage of lesion area relative to total gland area and averaged for the indicated groups. Error bars are standard error of mean. P values were calculated using a two-tailed t-test.

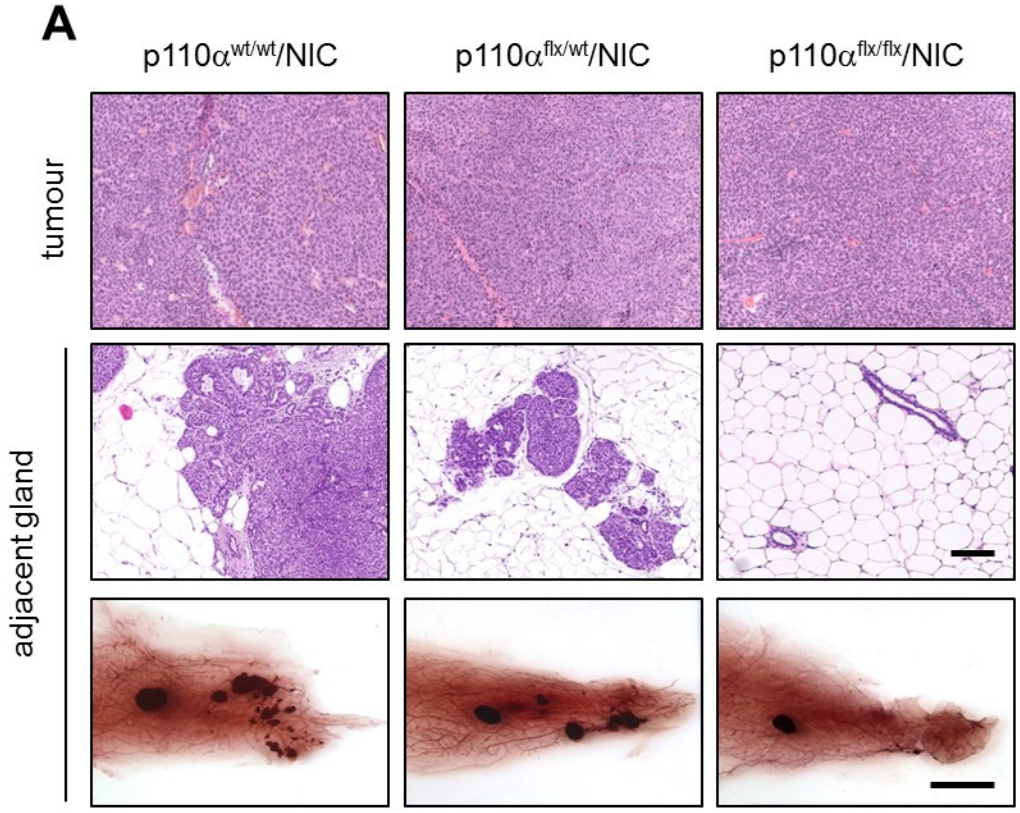
A
p110α^wt/wt/NIC
p110α^flx/wt/NIC
p110α^flx/flx/NIC
tumour
adjacent gland

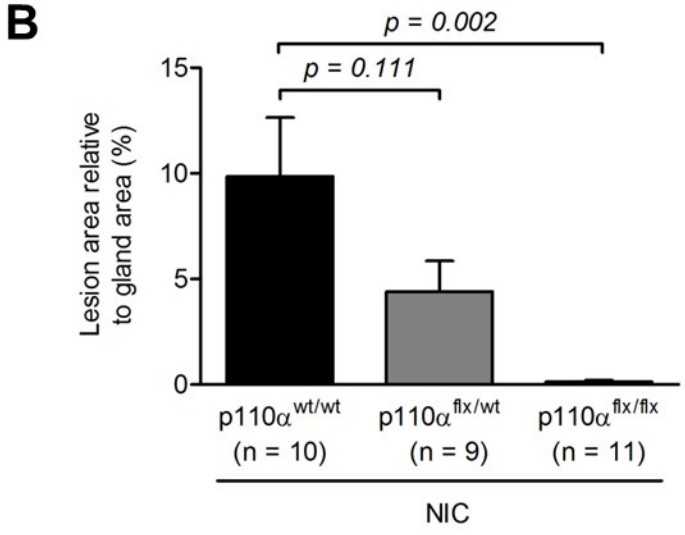
B
p = 0.002
p = 0.111
Lesion area relative to gland area (%)
15
10
5
0
p110α^wt/wt (n = 10)
p110α^flx/wt (n = 9)
p110α^flx/flx (n = 11)
NIC

homozygous glands were almost devoid of any abnormalities (Figure 4-6A, middle row). This phenotype correlated to a decrease in lesion density quantified in wholemounted adjacent mammary glands from p110α-deficient/NIC samples as compared to wildtype (Figure 4-6A, bottom row; Figure 4-6B).

Tumours from p110α-wildtype and -null/NIC mice do not differ greatly in growth rate

Our tumour burden data indicated that single masses in mice from each genetic group were about the same size at sacrifice (Figure 4-5B). This might suggest that individual tumours grew at the same rate once they had initiated, regardless of p110α status. To test this hypothesis, we first analyzed endstage primary tumours to determine if there were changes in proliferation or apoptosis between the three cohorts. Quantifications of Ki67 (proliferative marker) and TUNEL (apoptotic marker) immunostaining were similar in wildtype samples to what has been seen previously in the NIC model (Figure 4-7, top and middle) [105, 111]. These parameters were not significantly different in heterozygous or homozygous samples (data not shown; Figure 4-7, top and middle). Tumour growth can also be influenced by the recruitment of vasculature and so we also assessed blood vessel density by staining for the endothelial cell marker CD31. This factor was also unchanged between all genotypes (data not shown; Figure 4-7, bottom).

While these immunohistochemical analyses showed that proliferation, apoptosis and angiogenesis were equivalent in $p110\alpha^{wt/wt}$ and $p110\alpha^{flx/flx}$/NIC tumours, a more controlled experiment would be to test the growth rate of tumour cells in an orthotopic assay. Tumour cells from p110α-wildtype and -null/NIC mice were injected into the mammary fat pad of athymic nude mice and allowed to grow over time. All of the mice injected with the wildtype NIC

tumour cell lines developed palpable masses at approximately the same time post-injection and grew to at the same rate (Figure 4-8A). There was some variability in the time post-injection for masses to become detectable for the p110α-deficient/NIC tumour lines, with one line developing in recipients at the same time as the wildtype lines and the other two arising later (Figure 4-8A). Note that the variability was between the different lines tested and latencies for individual replicates for a single line were generally consistent. We confirmed that all p110α-deficient/NIC tumour outgrowths had maintained loss of p110α protein (Figure 4-8B).

NIC tumours lacking p110α are impaired in their ability to establish pulmonary metastases

We had now established that p110α is involved in ErbB2-mediated tumour initiation but we were also interested in whether the absence of p110α would affect the invasive potential of NIC tumours. The lungs from mice that were tumour-bearing for 6 weeks were analyzed for the presence of lesions. In NIC mice that were heterozygous p110α loss, 45% of tumour-bearing animals had lung metastases, almost half of the proportion observed in wildtype NIC mice; loss of both p110α alleles resulted in metastases in only 31.6% of tumour-bearing animals (Figure 4-9A, left). In addition to the decreased incidence of pulmonary metastases, the number of lesions in metastasis-positive animals was also significantly lower in the absence of p110α (Figure 4-9A, right).

Although these findings were striking, it could be argued that this metastatic defect was due to the smaller tumour burden in p110α-deficient/NIC mice as compared to wildtype NIC counterparts (Figure 4-5). To address this issue, we assessed lung colonization by injecting an equivalent number of cells from p110α-wildtype/NIC and -null/NIC mice into the tail veins of

Figure 4-7: Proliferation, apoptosis, and blood vessel density are unchanged between p110α-null and -wildtype/NIC tumours

Representative images of tumour sections from wildtype NIC and p110α-null/NIC mice (left) stained with a proliferative marker Ki67 (top), an apoptotic marker TUNEL (middle) and an endothelial cell marker CD31 (bottom). Arrowheads indicate TUNEL-positive nuclei. Scale bar is 100 μm. Staining quantification to the right of the corresponding images is shown by the average percentage of positive nuclei (Ki67 and TUNEL) or pixels (CD31). Error bars are standard error of mean. P values were calculated using a two-tailed t-test.

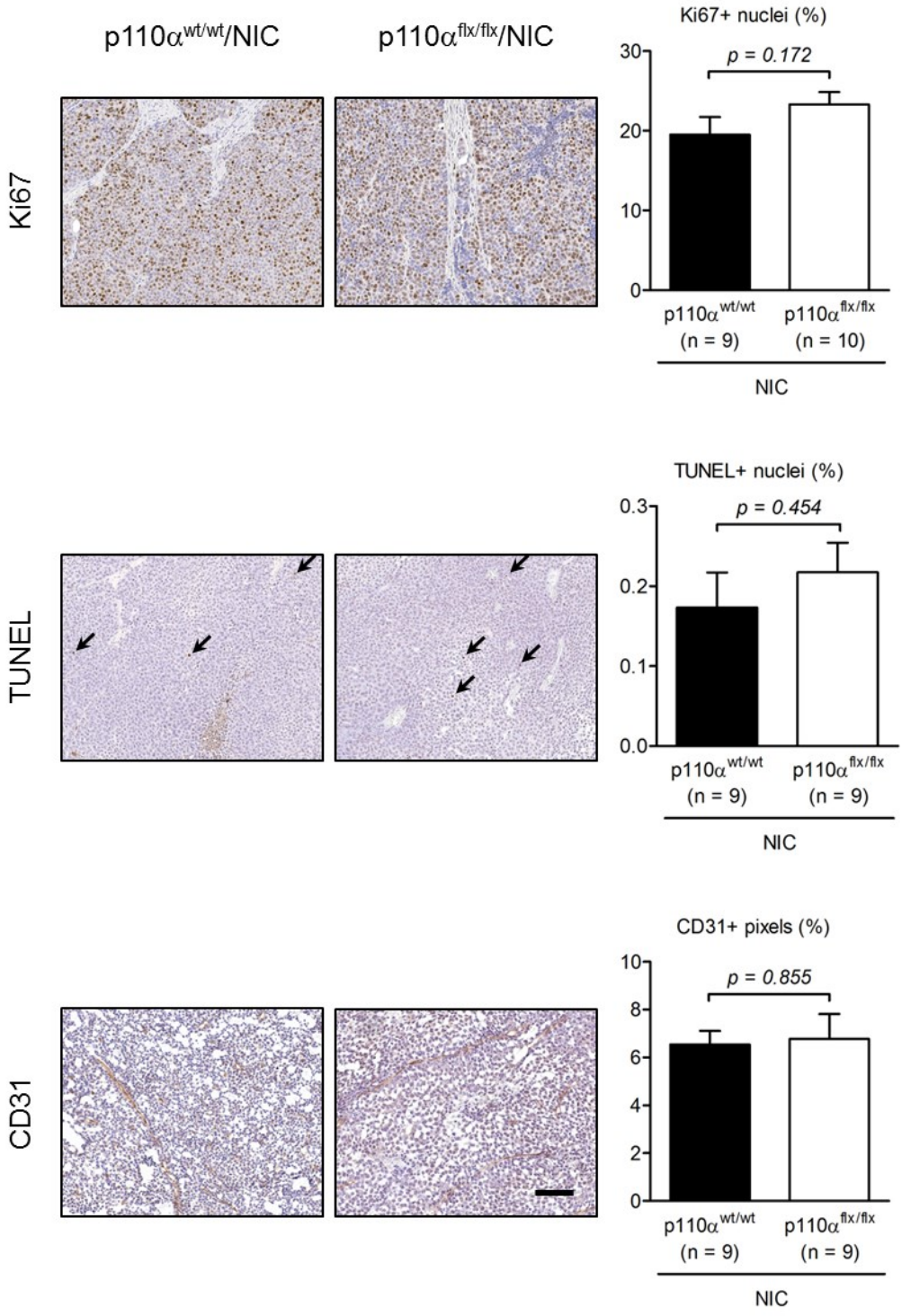
p110α^wt/wt/NIC
p110α^flx/flx/NIC
Ki67
Ki67+ nuclei (%)
p = 0.172
30
20
10
0
p110α^wt/wt (n = 9)
p110α^flx/flx (n = 10)
NIC
TUNEL
TUNEL+ nuclei (%)
p = 0.454
0.3
0.2
0.1
0.0
p110α^wt/wt (n = 9)
p110α^flx/flx (n = 9)
NIC
CD31
CD31+ pixels (%)
p = 0.855
10
8
6
4
2
0
p110α^wt/wt (n = 9)
p110α^flx/flx (n = 9)
NIC

Figure 4-8: p110α-null/NIC tumour cell outgrowths exhibit variable latencies but similar growth rates when compared to wildtype NIC cells

(**A**) Tumour outgrowth over time in NCr mice injected orthotopically with tumour cells from transgenic tumours of the indicated genotypes (250 000 cells/injection). Data is shown for 3 separate experiments (designated by different colours); for each experiment 1 p110α-wildtype/NIC line (solid circles) and 1 p110α-null/NIC line (white circles) were assayed. The graph shows individual replicates.

(**B**) Tumour lysates were prepared from 1 NCr recipient from each of the indicated lines used in the outgrowth assay shown in (A) and immunoblotted for p110α, ErbB2, and α-tubulin (loading control). Numbers correspond to the transgenic mouse ID for each sample. #79, 3888, 2552, 7083, 7582, and 1199 were used in the outgrowth assay in (A). #3888, 2552, 8905, 7582, 1199, and 7668 were used in the tail vein assay shown in Figure 5-9. Samples #8905 and 7668 are tumour transplant outgrowths from NCr mice.

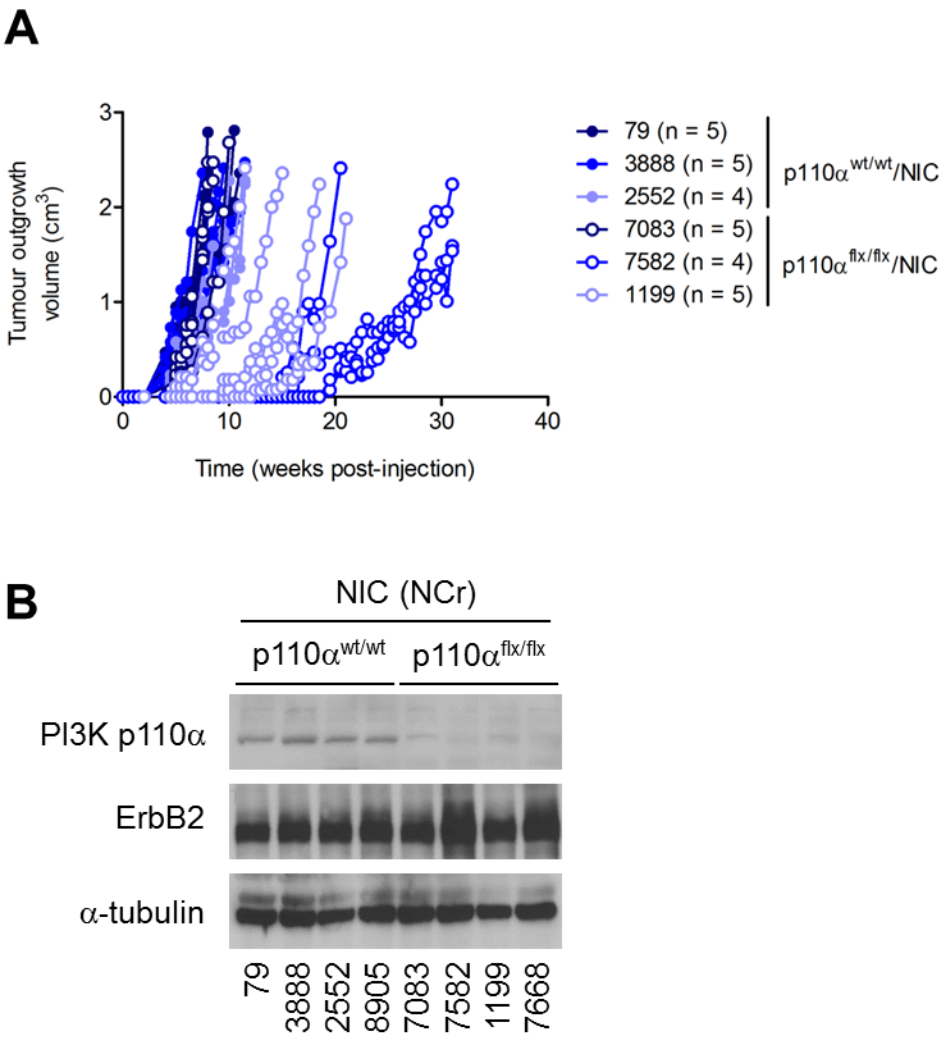
A
Tumour outgrowth volume (cm3)
Time (weeks post-injection)
79 (n = 5)
3888 (n = 5)
2552 (n = 4)
7083 (n = 5)
7582 (n = 4)
1199 (n = 5)
p110α wt/wt/NIC
p110α flx/flx/NIC
B
NIC (NCr)
p110α wt/wt
p110α flx/flx
PI3K p110α
ErbB2
α-tubulin
79
3888
2552
8905
7083
7582
1199
7668

Figure 4-9: p110α-deficiency reduces lung metastasis in tumour-bearing NIC mice and impairs lung colonization of NIC tumour cells in a tail vein assay

(**A**) The percentage of tumour-bearing mice with lung metastases (left) as well as the number of lung lesions in metastasis-positive ("met+") animals (right) for the indicated genotypes. Error bars are standard error of mean. P values were calculated using a two-tailed t-test.

(**B**) Lung colonization in NCr mice four weeks after tail-vain injections of tumour cells from transgenic tumours of the indicated genotypes (500 000 cells/injection). Representative images of H&E-stained lung sections are shown for the indicated genotypes at two magnifications (left). The arrowhead indicates the lesion that is shown below at the higher magnification. Scale bars are 500 μm (top row) and 100 μm (bottom row). Quantification of the number of lung lesions (top right) and size of lesions relative to the total lung area (bottom right) is shown for 3 separate experiments (designated by paired bars); for each experiment 1 p110α-wildtype/NIC line (black bar) and 1 p110α-null/NIC line (white bar) were assayed. Error bars are standard error of mean. P values were calculated using a two-tailed t-test. Confirmation of genotype at the protein level is shown in tumour transplant outgrowths from NCr mice in Figure 4-8 (B).

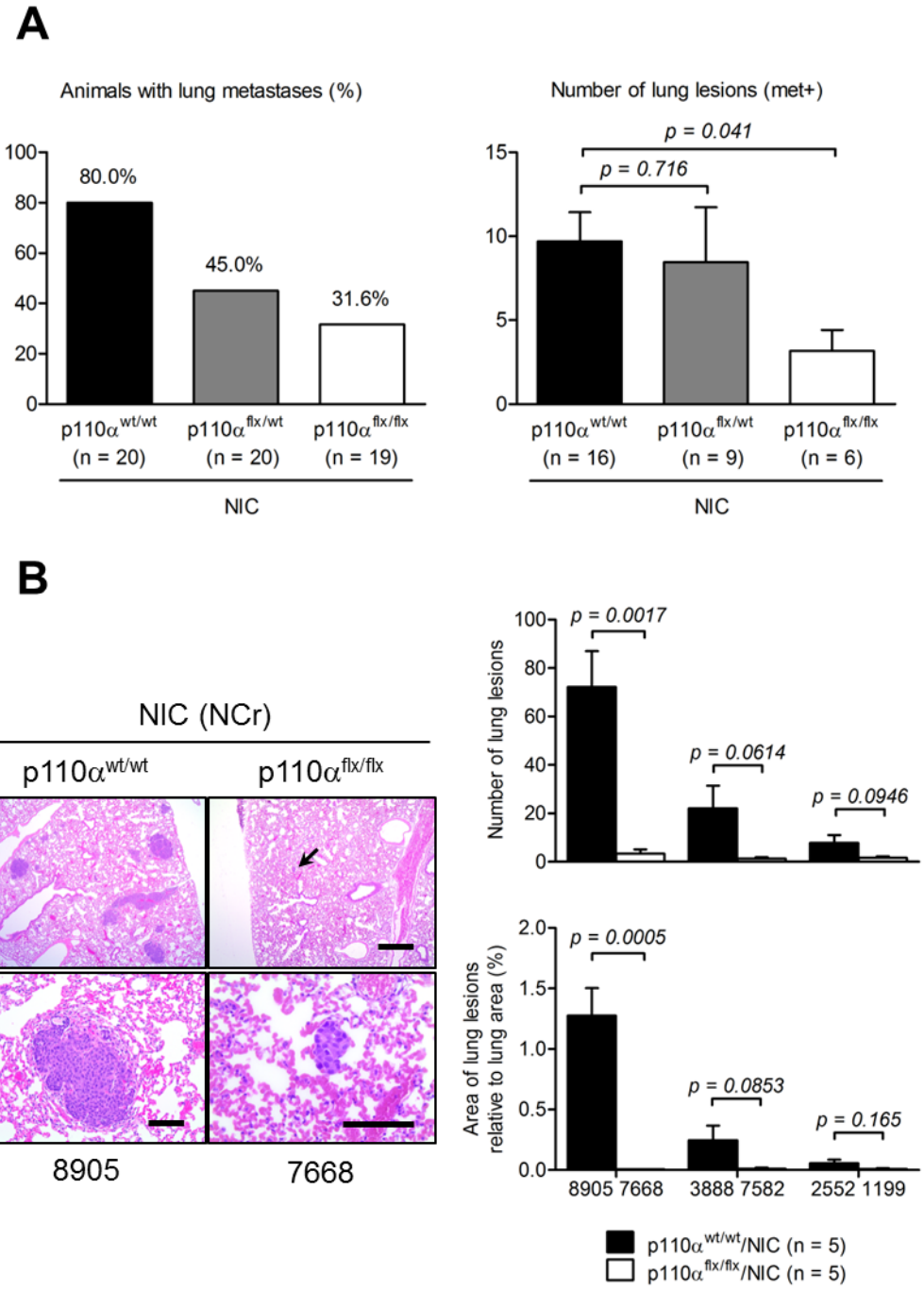
A
Animals with lung metastases (%)
100
80
60
40
20
0
80.0%
45.0%
31.6%
p110α wt/wt (n = 20)
p110α flx/wt (n = 20)
p110α flx/flx (n = 19)
NIC
Number of lung lesions (met+)
p = 0.041
p = 0.716
15
10
5
0
p110α wt/wt (n = 16)
p110α flx/wt (n = 9)
p110α flx/flx (n = 6)
NIC
B
NIC (NCr)
p110α wt/wt
p110α flx/flx
8905
7668
Number of lung lesions
p = 0.0017
p = 0.0614
p = 0.0946
Area of lung lesions relative to lung area (%)
p = 0.0005
p = 0.0853
p = 0.165
8905 7668
3888 7582
2552 1199
p110α wt/wt/NIC (n = 5)
p110α flx/flx/NIC (n = 5)

athymic nude mice. The p110α-deficient/NIC tumour lines showed a trend towards fewer and smaller lesions as compared to wildtype/NIC tumour lines, with one of three experiments reaching statistical significance (Figure 4-9B). p110α status in the tumour lines used in this assay was confirmed by immunoblotting mammary fat pad transplant outgrowths (Figure 4-8B). These results suggest that the differential metastasis in the transgenic FVB mice is true and not influenced by overall tumour burden.

p110α-deficient/NIC tumours are dependent on other p110 isoforms to maintain Akt signalling

The fact that tumours could eventually develop in p110α$^{flx/flx}$/NIC mice implies that the mammary epithelial cells had found an alternate method to drive tumour initiation. We first investigated activation of one of the major effectors of PI3K signalling, Akt. Immunoblotting of tumour lysates revealed that, although variable across samples, there were no obvious trends in Akt phosphorylation in NIC tumours wildtype or null for p110α (Figure 4-10). This maintenance of Akt activation was also evident in the sustained phosphorylation of the ribosomal protein S6, which is indirectly activated by Akt via the Tsc2/Rheb/mTORC1 pathway (Figure 4-10) [198-200]. Interestingly, some p110α-deficient/NIC tumours showed reduced Pten expression which may represent a mechanism for continued Akt signalling (Figure 4-10). In addition to loss of Pten, retention of Akt signalling could also be attributable to other p110 isoforms in the cell, such as other class I enzymes. When we analyzed p110β and -γ levels by immunoblot we found that their expression was constant across all samples; this was also the case for the p85 regulatory subunit (Figure 4-11). Furthermore, immunoprecipitation of p85

from NIC tumour lysates shows it is complexed with p110β in the absence of p110α (Figure 4-12). This analysis also revealed a consistent interaction between p85 and ErbB3, a major receptor for direct recruitment of p85-p110 heterodimers. However these results do not reveal if p110α-deficient/NIC tumours actually depend on non-p110α isoforms to sustain themselves. To test this hypothesis, we took advantage of a pan PI3K p110 inhibitor that is in clinical trials for treatment of solid tumours including breast cancers [386]. We chose to use a pan inhibitor to provide insight into whether our p110α-null/NIC tumours were dependent on any of the non-α isoforms. GDC-0941 is a competitive inhibitor of p110 which targets the ATP-binding pocket of the enzyme [386]. It has potent activity against p110α and -δ, with slightly less activity against the β and γ isoforms. In contrast to vehicle-treated controls, GDC-0941 could inhibit Akt phosphorylation at a concentration of 250 nM in a cell line derived from an ErbB2-driven murine mammary tumour (Figure 4-13A). Furthermore, mice bearing transplanted NIC tumours also exhibit decreased phosphorylation of Akt at various timepoints post-treatment with 125 mg/kg of GDC-0941 but not after treatment with vehicle (Figure 4-13B). Note that the drug did not affect expression of the ErbB2 oncogene in orthotopic tumours.

Having confirmed target inhibition in both *in vitro* and *in vivo* in our tumour model, we proceeded with testing the effects of GDC-0941 on orthotopic tumour growth of wildtype/NIC and p110α-deficient/NIC tumour cells Two lines per genotype were injected into the fat pad of athymic mice. As soon as masses were detected, the mice were started on daily treatment of GDC-0941 (125 mg/kg) or vehicle and monitored for tumour regression or growth. Drug treatment slowed the growth of masses in all tumour lines tested as compared to vehicle treated controls (Figure 4-14A). After just three weeks of treatment, the average tumour volume across replicates was significantly lower in drug-treated animals than in vehicle controls for all of the

Figure 4-10: Akt signalling remains active in p110α-null/NIC tumours

Immunoblot analysis of p110α, phosphorylated and total forms of Akt (S473) and ribosomal protein S6 (S235/236), and Pten in tumour lysates of the indicated genotypes. β-actin was used as a loading control. Numbers correspond to the mouse ID for each sample.

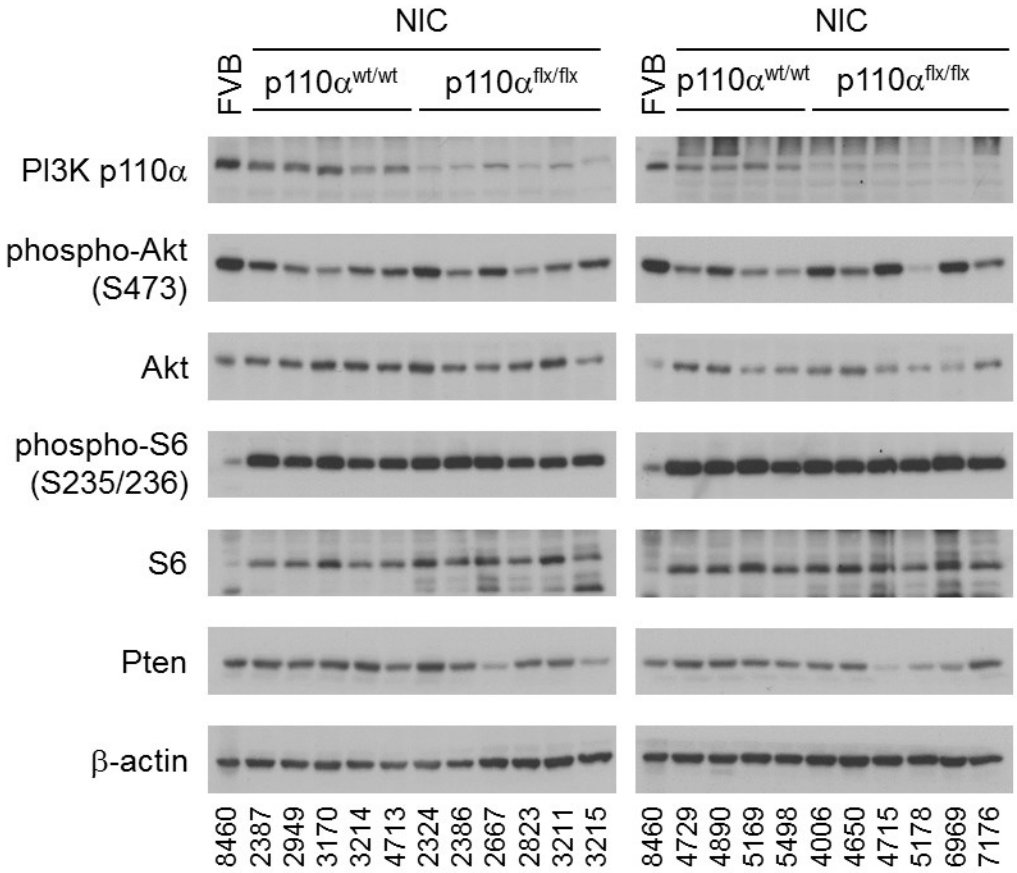
NIC
NIC
FVB
p110α^wt/wt
p110α^flx/flx
FVB
p110α^wt/wt
p110α^flx/flx
PI3K p110α
phospho-Akt (S473)
Akt
phospho-S6 (S235/236)
S6
Pten
β-actin
8460
2387
2949
3170
3214
4713
2324
2386
2667
2823
3211
3215
8460
4729
4890
5169
5498
4006
4650
4715
5178
6969
7176

Figure 4-11: PI3K isoform expression is constant in p110α-wildtype and -null/NIC tumours

Tumour lysates of the indicated genotypes were immunoblotted with antibodies against p110α, p110β, and p110γ, p85 and β-actin (loading control). Numbers correspond to the mouse ID for each sample.

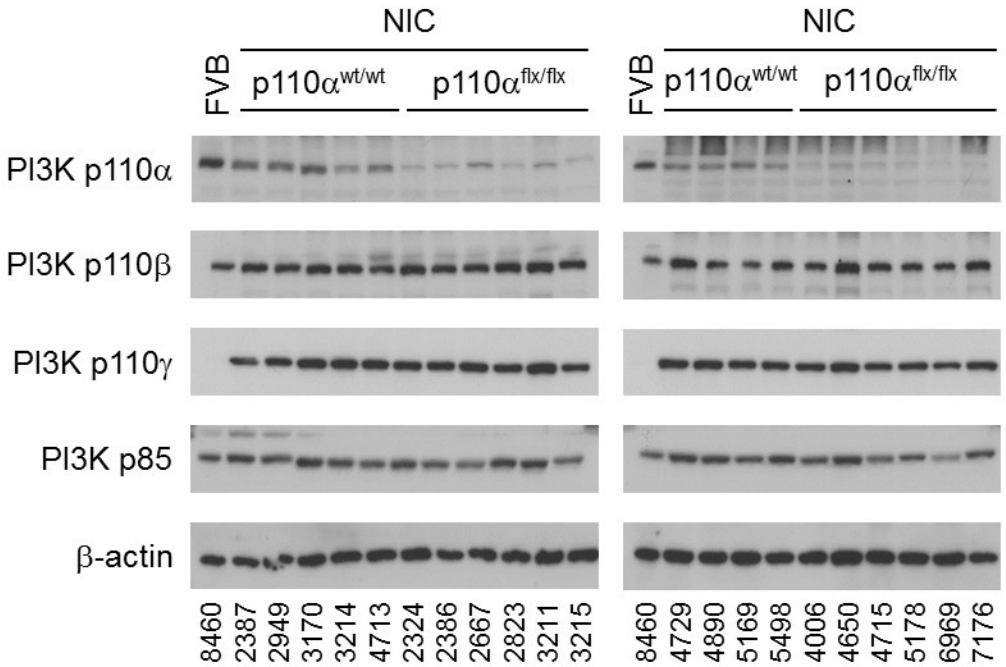
NIC
NIC
FVB
p110α^wt/wt
p110α^flx/flx
FVB
p110α^wt/wt
p110α^flx/flx
PI3K p110α
PI3K p110β
PI3K p110γ
PI3K p85
β-actin
8460
2387
2949
3170
3214
4713
2324
2386
2667
2823
3211
3215
8460
4729
4890
5169
5498
4006
4650
4715
5178
6969
7176

Figure 4-12: p85-p110β complexes may contribute to the maintenance of PI3K signalling in NIC tumours lacking p110α

p85 protein was immunoprecipitated from tumour lysates of the indicated genotypes and then probed for p110α, p110β, p85, and ErbB3 by immunoblot (top). "No Ab" refers to a control for which the p85 immunoprecipitation antibody was excluded. The lysates were immunoblotted for the same proteins in parallel (bottom). Numbers correspond to the mouse ID for each sample.

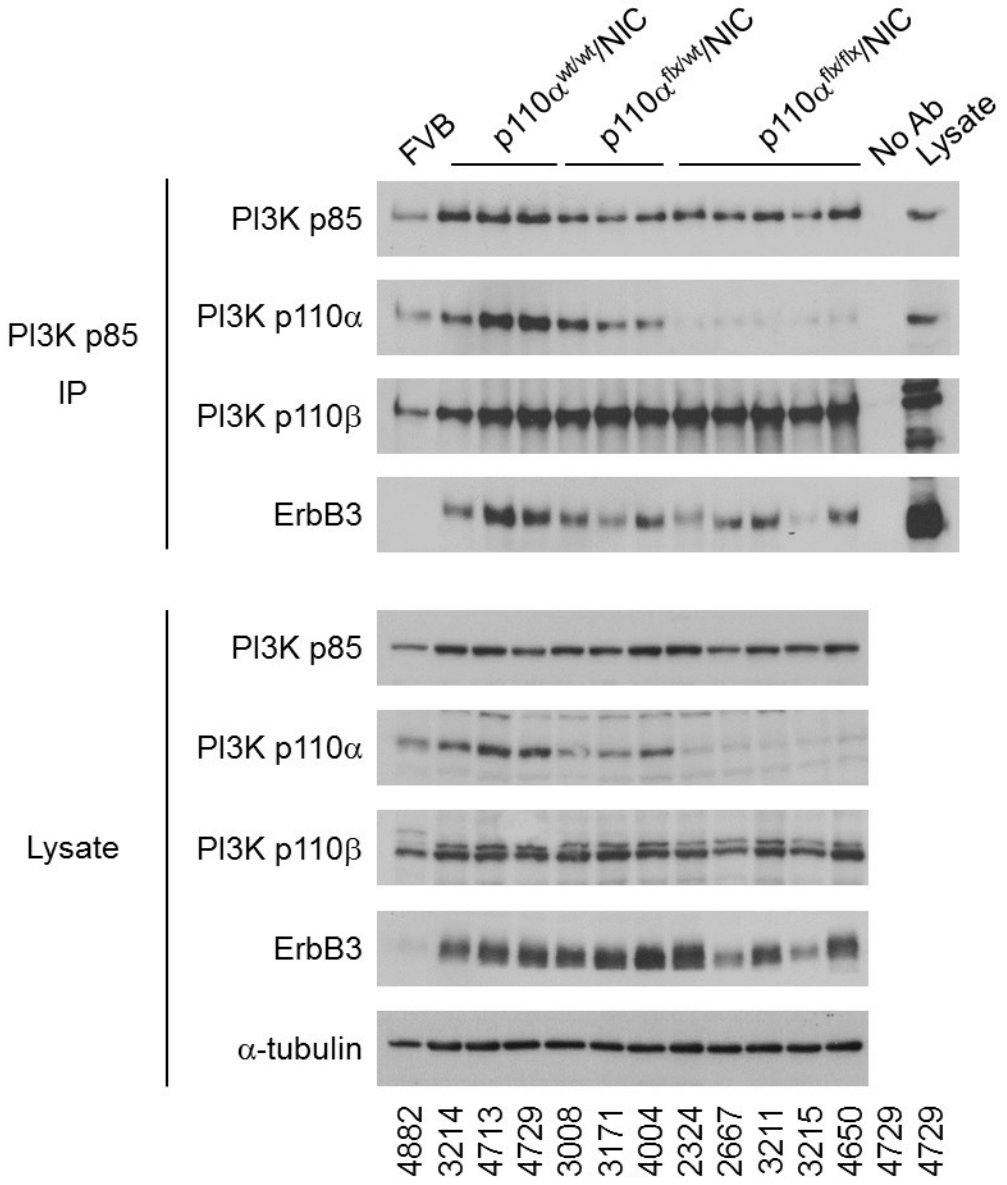
FVB
p110α^wt/wt/NIC
p110α^flx/wt/NIC
p110α^flx/flx/NIC
No Ab
Lysate
PI3K p85
IP
PI3K p85
PI3K p110α
PI3K p110β
ErbB3
Lysate
PI3K p85
PI3K p110α
PI3K p110β
ErbB3
α-tubulin
4882
3214
4713
4729
3008
3171
4004
2324
2667
3211
3215
4650
4729
4729

Figure 4-13: The pan class I PI3K p110 inhibitor GDC-0941 reduces Akt phosphorylation in ErbB2 tumour cells *in vitro* and *in vivo*

(A) Immunoblot of lysates from an NDL cell line treated for 2 hours or 6 hours with GDC-0941 at the indicated concentrations as compared to untreated and vehicle (DMSO) controls. Antibodies were directed against ErbB2, phospho-Akt (Ser473), Akt, and α-tubulin (loading control).

(B) Lysates of transplanted NIC tumours from mice sacrificed at 2, 6 and 12 hours after treatment with 125 mg/kg of GDC-0941 ("GDC") or vehicle ("veh") were immunoblotted for ErbB2, phospho-Akt (Ser473), Akt, and α/β-tubulin (loading control). The same tumour line was used for all conditions (#8665, p110$\alpha^{wt/wt}$/NIC).

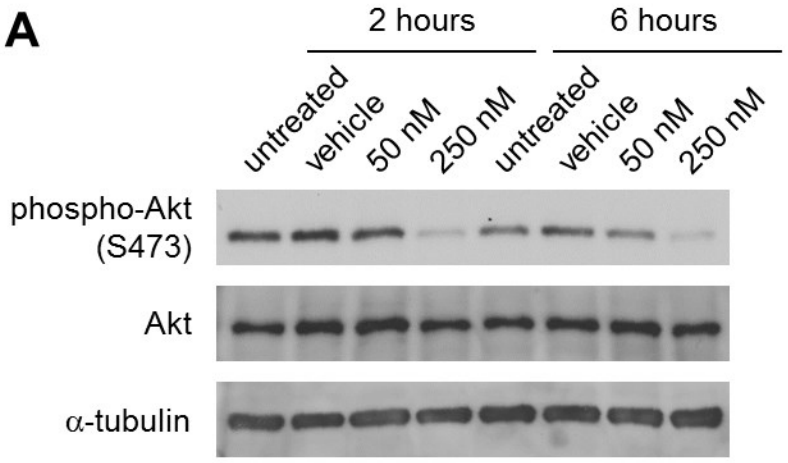
A
2 hours
6 hours
untreated
vehicle
50 nM
250 nM
untreated
vehicle
50 nM
250 nM
phospho-Akt (S473)
Akt
α-tubulin

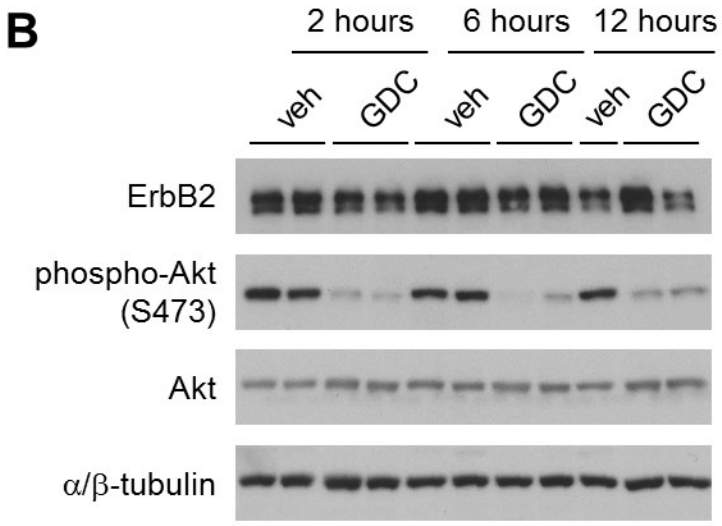
B
2 hours
6 hours
12 hours
veh
GDC
veh
GDC
veh
GDC
ErbB2
phospho-Akt (S473)
Akt
α/β-tubulin

Figure 4-14: GDC-0941 impairs outgrowth of NIC tumour cells regardless of p110α status

(**A**) Tumour outgrowth in NCr mice injected orthotopically with tumour cells from NCr transplant tumours of the indicated genotypes (500 000 cells/injection) after treatment with 125 mg/kg GDC-0941 (black) or vehicle (grey). 2 $p110\alpha^{wt/wt}$/NIC tumour lines (left; solid circles) and 2 $p110\alpha^{flx/flx}$/NIC tumour lines (right; white circles) were tested in parallel. The graph shows individual replicates.

(**B**) Average tumour outgrowth volume from the experiment shown in (A) after 3 weeks of treatment with either vehicle (grey) or GDC-0941 (black). Error bars are standard error of mean. P values were calculated using a two-tailed t-test.

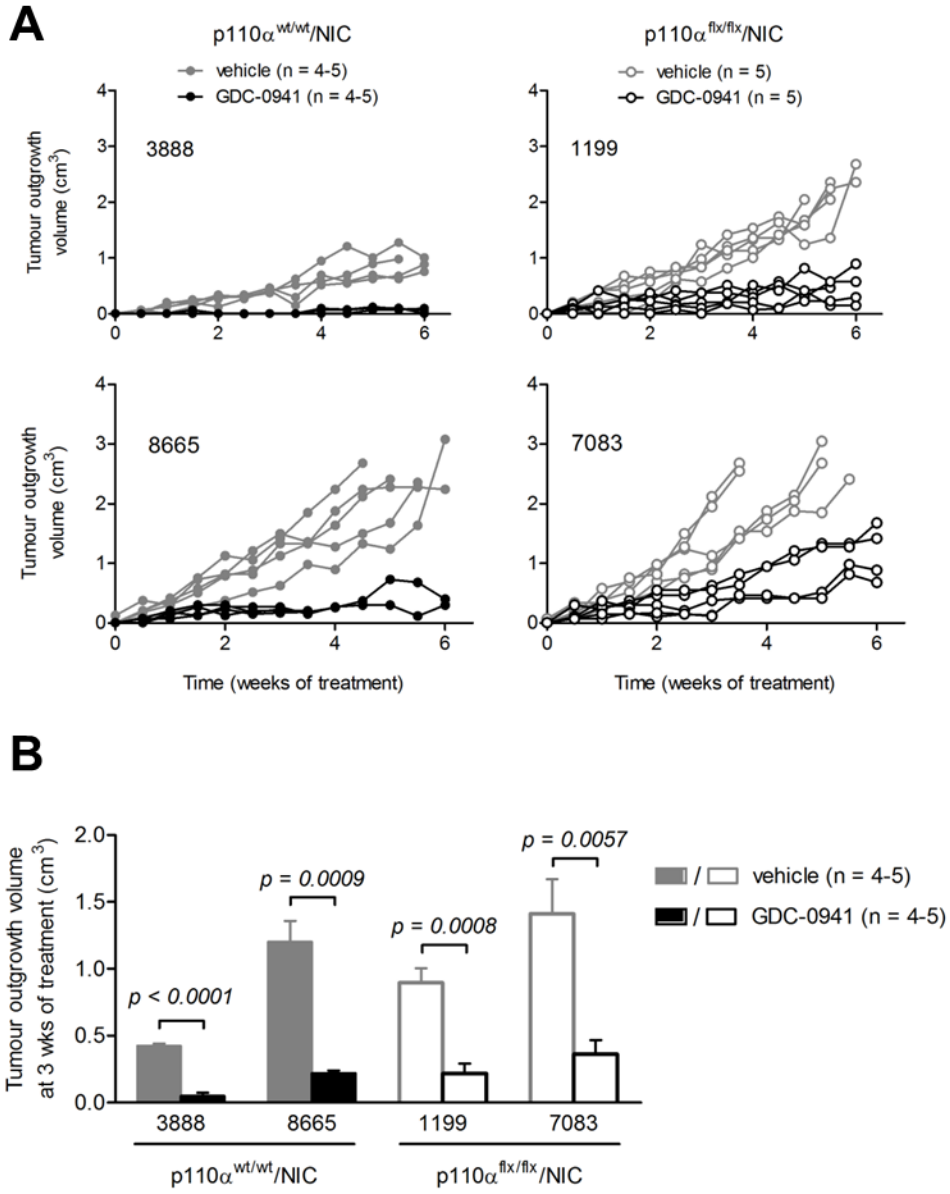
A
p110α wt/wt/NIC
vehicle (n = 4-5)
GDC-0941 (n = 4-5)
p110α flx/flx/NIC
vehicle (n = 5)
GDC-0941 (n = 5)
3888
1199
8665
7083
Tumour outgrowth volume (cm3)
Time (weeks of treatment)
B
Tumour outgrowth volume at 3 wks of treatment (cm3)
p < 0.0001
p = 0.0009
p = 0.0008
p = 0.0057
vehicle (n = 4-5)
GDC-0941 (n = 4-5)
3888
8665
1199
7083
p110α wt/wt/NIC
p110α flx/flx/NIC

tumour lines (Figure 4-14B). This indicated that p110α-null/NIC tumours were still dependent on the activity of non-α p110 isoforms to some extent.

Development of p110α-null/NIC tumours may result from dysregulated osteopontin (OPN)/αvβ3 integrin expression

To further investigate differences in molecular signalling between p110α-proficient and -deficient/NIC tumours, we turned to gene expression profiling. Individual samples were chosen for the microarray so that a range of tumour onset age and metastatic potential were represented (Figure 4-15A). Tumour mRNA isolated for the microarray was verified for p110α expression by reverse transcription-quantitative PCR (RT-qPCR) (Figure 4-15B).

Initial analysis of the microarray data by unsupervised hierarchical clustering showed that while wildtype NIC tumours were similar to each other, the $p110\alpha^{flx/flx}$/NIC tumours segregated into three unique groups (Figure 4-16). Given the heterogeneity within the p110α-deficient/NIC group we did not pursue pathway analysis of the data based on genotype averages and instead we identified interesting candidates from amongst the most differentially expressed probes. We went on to focus on probes that exhibited the strongest differential expression in the hope of capturing hits that may be relevant in at least some of the tumours within a genetic group. One of the most variably expressed genes on our list was *Spp1*, which was upregulated at least 6-fold across ten individual probes in the p110α-null/NIC samples relative to the wildtype NIC samples (Figure 4-17A). The *Spp1* gene encodes for osteopontin (OPN), a secreted ECM-associated protein that is overexpressed in breast cancers and was found to have prognostic significance in patients with metastatic disease [428-431]. This made it a promising candidate for driving the

formation of p110α-deficient/NIC tumours. Upon assessment of *Spp1* mRNA levels by RT-qPCR, it became clear that the increased average expression of transcript on the microarray was originating from three individual $p110\alpha^{flx/flx}$/NIC samples (Figure 4-17B). Interestingly, these same three tumour samples were grouped together on a distant dendrogram branch after unsupervised hierarchical clustering, suggesting that perhaps in addition to OPN they may express other genes in common (Figure 4-16).

Having validated *Spp1* at the transcript level, we were interested in analysing protein expression of OPN in an expanded sample set of NIC tumours that were wildtype or null for p110α. Immunoblotting of tumour lysates with an anti-OPN antibody revealed a band at the predicted molecular weight for the full-length protein (~55 kilodaltons) in five $p110\alpha^{flx/flx}$/NIC tumours; for three of the five the signal was very strong while it was very weak for the other two (Figure 4-18A). OPN was not detected in any of the wildtype NIC tumour lysates. To extend these results to incorporate protein expression of OPN *in situ*, we performed immunohistochemical staining on tumour sections from the same tumours used in the immunoblot analysis. With the exception of one sample, the remaining eleven wildtype NIC tumours were negative for OPN expression although some samples contained a few positive cells (data not shown; Figure 4-18B). Similar to the immunoblot analysis, a subset of p110α-deficient/NIC tumours expressed high levels of OPN in the tumour epithelium, with increasing intensity toward the periphery of the lesions (Figure 4-18B). We also noticed in the $p110\alpha^{flx/flx}$/NIC tumour sections that OPN staining was restricted to late stage lesions and seemed to be excluded from earlier lesions and normal ducts (Figure 4-18B; bottom row). This observation provided some preliminary evidence that OPN is upregulated during early stages of

Figure 4-15: Sample list of p110α-wildtype and -null/NIC tumours for microarray analysis

(**A**) Tumours from $p110\alpha^{wt/wt}$/NIC and $p110\alpha^{flx/flx}$/NIC mice used for microarray analysis were chosen to represent a variety of tumour onsets and lung metastasis status.

(**B**) p110α (*PIK3CA*) transcript expression normalized to *Gapdh* transcript was confirmed using quantitative PCR on cDNA from the tumours shown in (A) (striped bars are averages for each genetic group). Error bars are standard error of mean. The p value was calculated using a two-tailed t-test.

A

ID#	NIC	Tumour onset (days)	# Lung lesions
3214	p110α$^{wt/wt}$	171	0
4647	p110α$^{wt/wt}$	137	10
4713	p110α$^{wt/wt}$	124	10
4729	p110α$^{wt/wt}$	142	23
4890	p110α$^{wt/wt}$	116	3
2324	p110α$^{flx/flx}$	365	1
2386	p110α$^{flx/flx}$	430	0
4006	p110α$^{flx/flx}$	456	0
4650	p110α$^{flx/flx}$	260	0
5178	p110α$^{flx/flx}$	246	2
6969	p110α$^{flx/flx}$	186	0

B

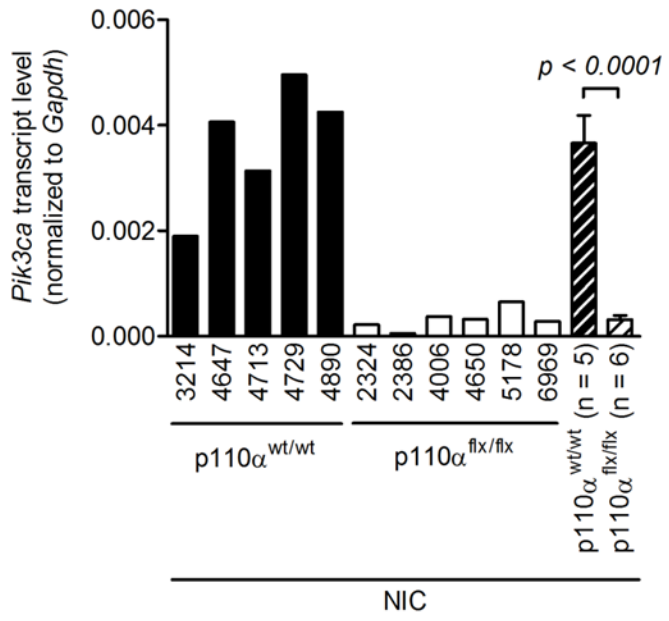

Figure 4-16: Gene expression profiling reveals that p110α-null/NIC tumours form distinct subgroups

Unsupervised hierarchical clustering of samples of the indicated ID numbers/genotypes using the top 500 most variable genes.

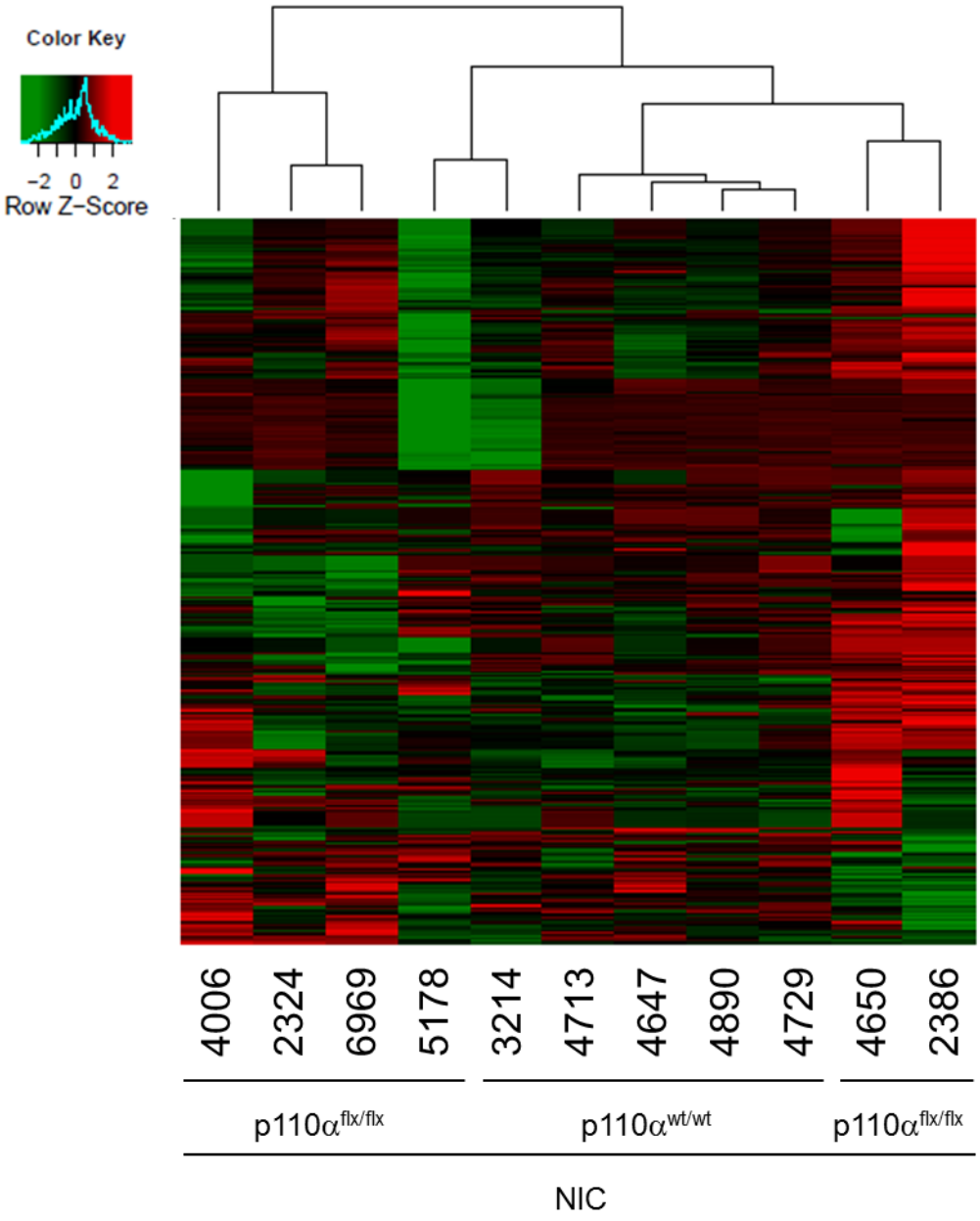
Color Key
−2 0 2
Row Z−Score
4006
2324
6969
5178
3214
4713
4647
4890
4729
4650
2386
p110α^flx/flx
p110α^wt/wt
p110α^flx/flx
NIC

Figure 4-17: OPN transcript is elevated in some p110α-null/NIC tumours

(**A**) Across ten probes on the microarray, the average OPN (*Spp1*) transcript expression was increased at least 6-fold in the average for all p110α-null/NIC tumours as compared to the average for all wildtype NIC group. P values are indicated for each probe.

(**B**) OPN (*Spp1*) transcript levels normalized to *Gapdh* transcript as determined by quantitative PCR in cDNA from the tumours used for the microarray (striped bars are averages for each genetic group). Error bars are standard error of mean. The p value was calculated using a two-tailed t-test.

A

Spp1 probe	Fold change (null vs wildtype)	p value
1	6.9	0.0938
2	6.5	0.108
3	6.4	0.109
4	6.3	0.111
5	6.3	0.109
6	6.3	0.118
7	6.3	0.116
8	6.3	0.117
9	6.2	0.119
10	6.1	0.121

B

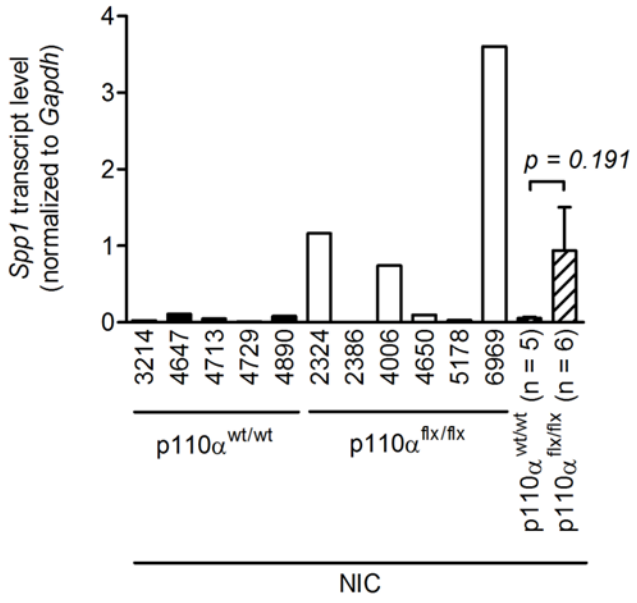

Figure 4-18: A proportion of p110α-null/NIC tumours exhibit upregulation of OPN at the protein level

(**A**) OPN (OPN) immunoblot on tumour lysates of the indicated genotypes. β-actin was used as a loading control. Numbers correspond to the mouse ID for each sample.

(**B**) Immunohistochemical staining of tumours from the indicated genotypes using an antibody against OPN (OPN). The bottom row images are higher magnifications of the top row images. Scale bars are 100 μm (top row) and 50 μm (bottom row).

(**C**) Table listing the percentage of samples with increased OPN expression analyzed by RT-qPCR, immunoblot, and immunohistochemistry. The overall percentages considering all methods (transcript and/or protein) were calculated so that individual samples exhibiting increased levels in multiple analyses were not counted more than once.

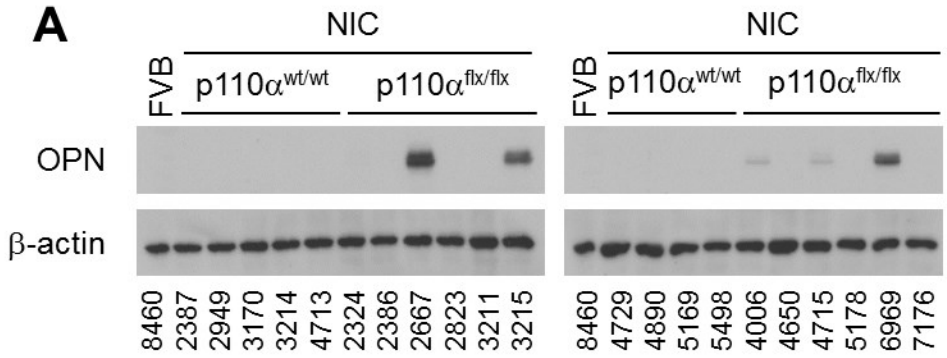

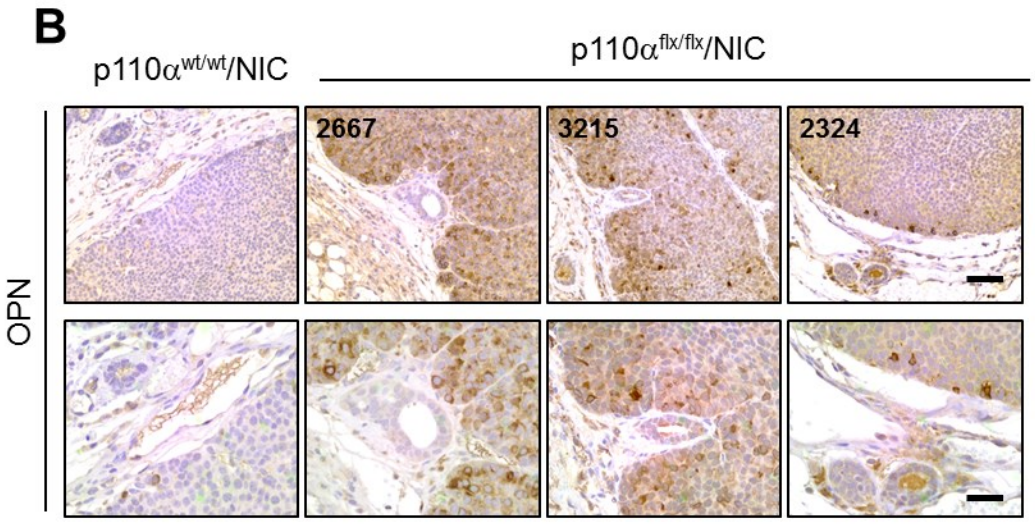

C

Elevated OPN expression	**p110α$^{wt/wt}$/NIC**	**p110α$^{flx/flx}$/NIC**
transcript (qRT-PCR)	0% (0/5)	50% (3/6)
protein (immunoblot)	0% (0/11)	41.7% (5/12)
protein (IHC)	9.1% (1/11)	25% (3/12)
transcript and/or protein	**9.1% (1/11)**	**58.3% (7/12)**

tumour progression in at least some of the p110α-deficient/NIC mice. Considering both mRNA and protein analyses in all samples, we can conclude that 7/12 (58.3%) of the p110α-deficient/NIC tumours analyzed showed elevation of OPN expression in contrast to just 1/11 (9.1%) of p110α-proficient/NIC tumours (individual samples with increased levels in multiple analyses were not counted more than once) (Figure 4-18C).

Secreted OPN binds to cell surface receptors to engage downstream signalling including members of the integrin family. A major integrin receptor that responds to OPN is the αvβ3 heterodimer which can induce many aspects of cell transformation [432]. Tumour lysates were immunoblotted with antibodies against both αv and β3 integrins and revealed decreased signals in the majority of p110α-null/NIC tumours as compared to wildtype counterparts (Figure 4-19A). We revisited our panel of mRNA samples and found that p110α-deficient/NIC tumours had significantly reduced β3 integrin transcript (*Itgb3*) relative to wildtype NIC tumours; αv integrin transcript (*Itgav*) was lower in 2/6 samples (Figure 4-19B). It was now apparent that in addition to enhanced expression of OPN, NIC tumours lacking p110α also had impaired expression of αv and β3 integrin. The latter phenotype seemed to be more universal across all of the samples, whereas the former appeared to be a less common event. This led us to hypothesize that loss of β3 integrin may be a direct or indirect effect of p110α ablation in the mammary epithelium of $p110\alpha^{flx/flx}$/NIC of young mice; consequently, its ligand OPN may be upregulated to compensate for this reduction in expression. Further evidence for this comes from our prior observation that normal ducts and early lesions in NIC tumours were negative for OPN expression (Figure 4-18B).

To test this theory, we isolated mammary epithelial cells from $p110\alpha^{wt/wt}$ and $p110\alpha^{flx/flx}$/NIC mice at an age before tumours normally arise in the NIC model (i.e. 3-5 months of age). mRNA levels of both OPN (*Spp1*) and β3 integrin (*Itgb3*) were assessed in these

premalignant mammary epithelium samples and compared to previously collected tumour expression data (taken from Figures 4-17B and 4-19B). In agreement with our proposed theory, *Spp1* levels were unchanged between wildtype and p110α-deficient/NIC premalignant samples, even trending towards decreased expression in knockouts (Figure 4-20, top). The significant reduction in *Itgb3* expression in p110α-deficient versus -proficient/NIC groups was consistent between premalignant and tumour epithelium (Figure 4-20, bottom). We had previously confirmed loss of p110α expression in these epithelial-enriched samples relative to wildtype NIC and FVB controls (Figure 4-2A).

Loss of Pten is associated with OPN expression in p110α-deficient/NIC tumours

After observing an upregulation of OPN expression in a subset of p110α-deficient/NIC tumours, it followed to investigate potential signalling mechanisms that might be at play in our system. Interestingly, the PI3K pathway has been shown to be involved in inducing OPN transcription either through *in vitro* stimulation of PI3K signalling or through loss of the PTEN tumour suppressor [433-435]. We had initially noted reduced Pten protein levels in some p110α-deficient/NIC tumour lysates and chose to repeat the immunoblot but this time ordered samples with respect to OPN status. Pten expression was accordingly reduced in the three p110α-null/NIC tumours with high OPN expression and in one of the two tumours with intermediate levels of OPN (Figure 4-21A). Since changes in Pten expression can be attributed to several factors, we assayed mRNA using Pten-specific primers. Two of the six $p110\alpha^{flx/flx}$/NIC samples had lower expression of Pten transcript and only one of these correlated with slightly low protein levels (#2386) (Figures 4-10 and 4-21B).

Figure 4-19: p110α-null/NIC tumours exhibit reduced expression of αv and β3 integrins

(**A**) Immunoblot of tumour lysates of the indicated genotypes using antibodies against αv and β3 integrin. β-actin was used as a loading control. Numbers correspond to the mouse ID for each sample.

(**B**) β3 integrin (*Itgb3*) and αv integrin (*Itgav*) transcript expression normalized to *Gapdh* transcript were determined using quantitative PCR on tumour cDNA from the indicated genotypes (striped bars are averages for each genetic group). Error bars are standard error of mean. P values were calculated using a two-tailed t-test.

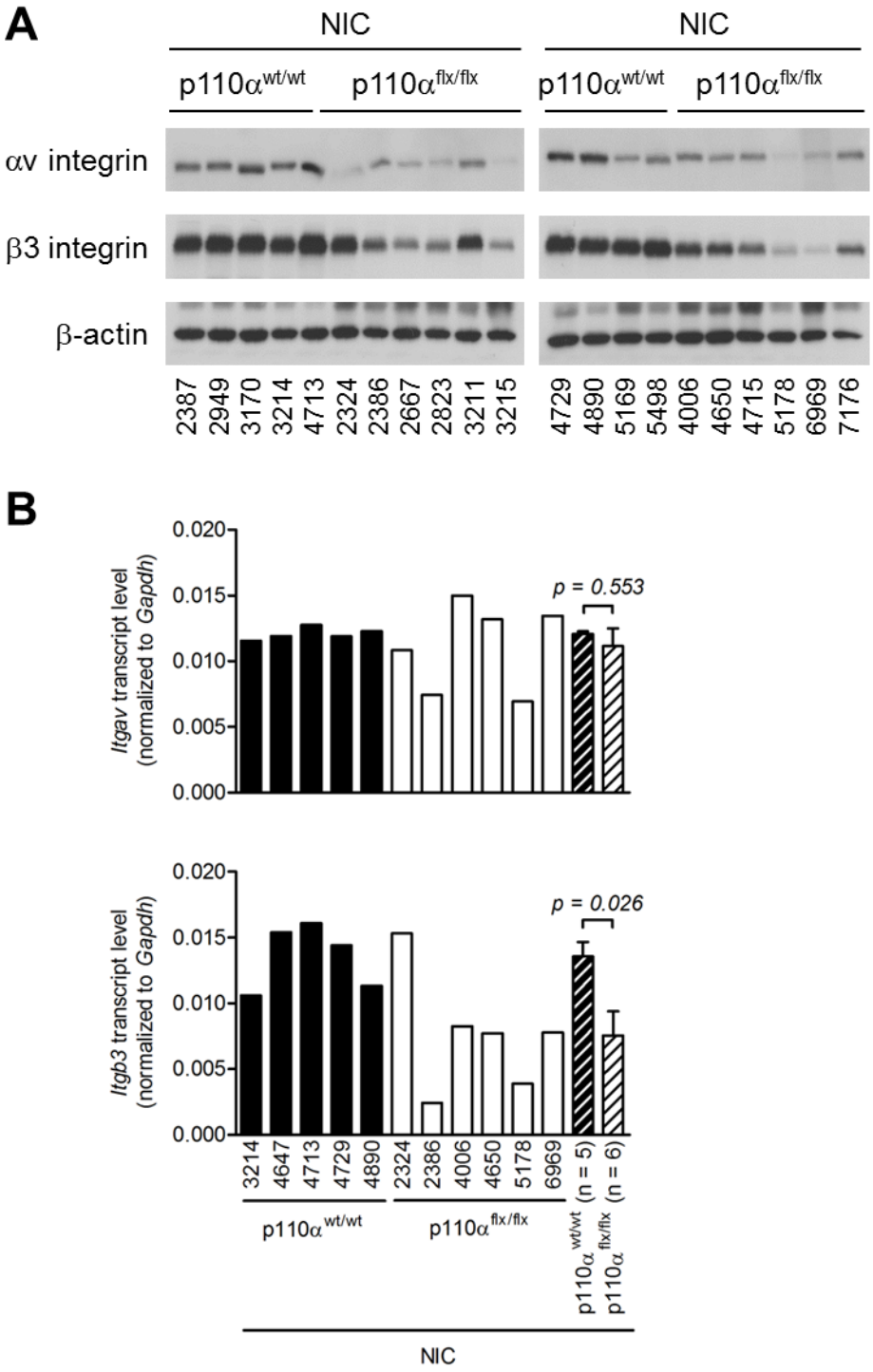
A
NIC
NIC
p110α^wt/wt
p110α^flx/flx
p110α^wt/wt
p110α^flx/flx
αv integrin
β3 integrin
β-actin
2387 2949 3170 3214 4713 2324 2386 2667 2823 3211 3215
4729 4890 5169 5498 4006 4650 4715 5178 6969 7176
B
Itgav transcript level (normalized to Gapdh)
0.020
0.015
0.010
0.005
0.000
p = 0.553
Itgb3 transcript level (normalized to Gapdh)
0.020
0.015
0.010
0.005
0.000
p = 0.026
3214 4647 4713 4729 4890 2324 2386 4006 4650 5178 6969
p110α^wt/wt (n = 5)
p110α^flx/flx (n = 6)
p110α^wt/wt
p110α^flx/flx
NIC

Figure 4-20: In premalignant mammary epithelium, OPN mRNA expression is unchanged while that of β3 integrin is decreased in p110α$^{flx/flx}$/NIC mice relative to wildtype counterparts

OPN (*Spp1*) and β3 integrin (*Itgb3*) transcript (normalized to *Gapdh* transcript) assessed by quantitative PCR on cDNA from pre-malignant and tumour epithelium of the indicated genotypes. Pre-malignant samples were the same as used in Figure 4-2A. Tumour epithelium data is taken from Figures 4-17B and 4-19B and is shown again for comparison.

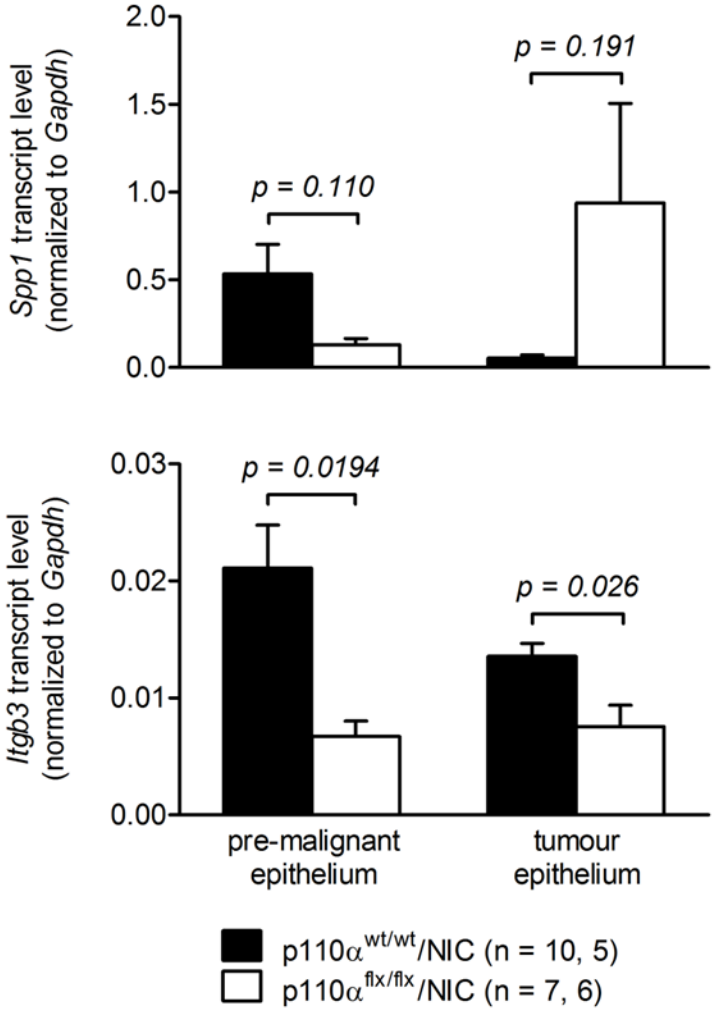
2.0
1.5
1.0
0.5
0.0
Spp1 transcript level (normalized to *Gapdh*)
p = 0.110
p = 0.191
0.03
0.02
0.01
0.00
Itgb3 transcript level (normalized to *Gapdh*)
p = 0.0194
p = 0.026
pre-malignant epithelium
tumour epithelium
p110α$^{wt/wt}$/NIC (n = 10, 5)
p110α$^{flx/flx}$/NIC (n = 7, 6)

Figure 4-21: Upregulation of OPN correlates with downregulation of Pten protein

(**A**) Immunoblot of tumour lysates of the indicated genotypes for OPN (OPN) and Pten. Tumours were grouped according to high (2667, 3215, 6969), medium (4006, 4715), and low/absent (2324, 5178) OPN protein expression. α/β-tubulin was used as a loading control. Numbers correspond to the mouse ID for each sample.

(**B**) Pten (*Pten*) transcript expression normalized to *Gapdh* transcript was determined using quantitative PCR on tumour cDNA from the indicated genotypes (striped bars are averages for each genetic group). Error bars are standard error of mean. The p value was calculated using a two-tailed t-test.

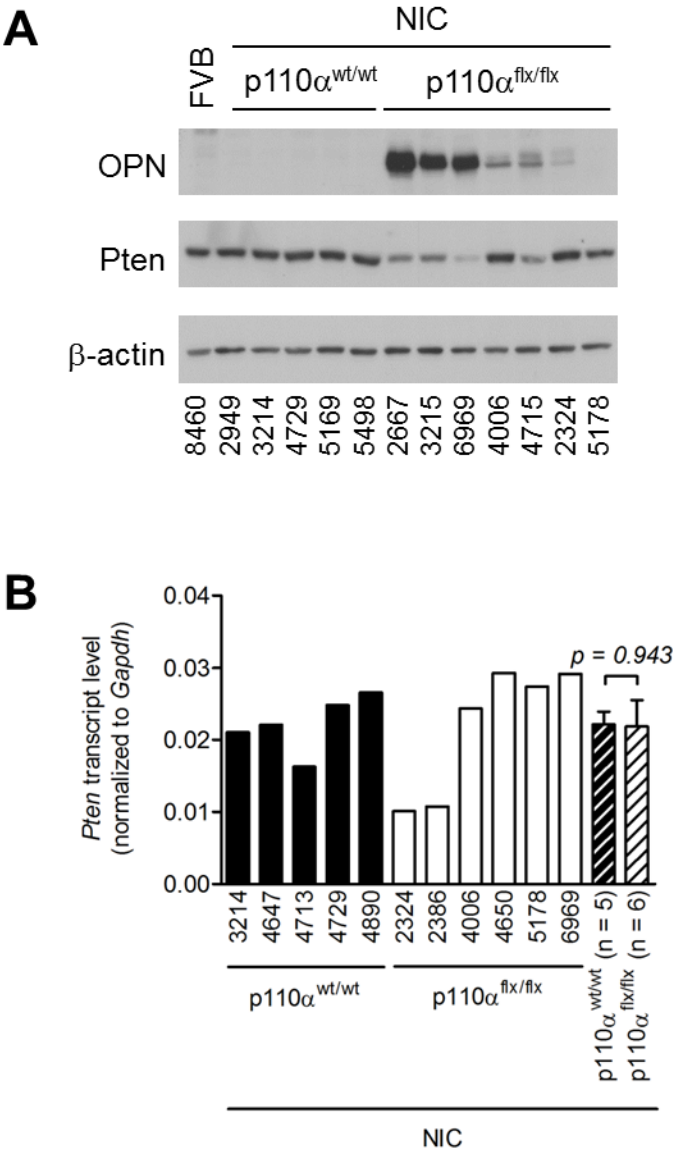
A
NIC
FVB
p110α^wt/wt
p110α^flx/flx
OPN
Pten
β-actin
8460
2949
3214
4729
5169
5498
2667
3215
6969
4006
4715
2324
5178
B
Pten transcript level
(normalized to Gapdh)
0.04
0.03
0.02
0.01
0.00
p = 0.943
3214
4647
4713
4729
4890
2324
2386
4006
4650
5178
6969
p110α^wt/wt (n = 5)
p110α^flx/flx (n = 6)
p110α^wt/wt
p110α^flx/flx
NIC

Activation of the PI3K pathway increases OPN expression in two different mouse models of ErbB2 mammary tumourigenesis

The association between low Pten and high OPN was encouraging however the number of samples exhibiting this phenotype was low. To determine if this correlation was a recurring phenomenon in ErbB2-driven mammary tumours with loss of Pten, we investigated OPN expression in our NIC mouse model driven by Pten deletion (Chapter 3). The majority of Pten-deficient/NIC tumours expressed OPN in contrast to wildtype NIC controls (Figure 4-22A). Notably this was apparent in both homozygous and heterozygous contexts. It was also interesting to see two bands on the immunoblot in contrast to the single band observed in the p110α-deficient/NIC immunoblots.

In addition to loss of PTEN, PI3K pathway activation in cancer can occur through activating mutations in *PIK3CA*/p110α. We recently acquired a mouse strain in which the cancer-associated hotspot mutation H1047R is knocked in to the endogenous *PIK3CA* gene; expression of this activated mutant ($p110\alpha^{HR}$) is dependent on Cre recombinase [64, 65]. By breeding this strain to our $ErbB2^{KI}$ model (NeuNT/Cre), we can achieve physiological levels of both oncogenic mutants in the mammary epithelium since expression is driven by their respective endogenous promoters [62]. Mammary tumours in mice that arise from this cross provide an ideal context for determining if PI3K pathway activation can contribute to OPN expression. Preliminary data from our laboratory demonstrates that co-expression of $p110\alpha^{HR}$ and activated ErbB2 in the mammary epithelium results in tumours that express high levels of OPN protein by immunoblot (Figure 4-22B). By contrast, tumours from $p110\alpha^{HR}$/Cre or NeuNT/Cre animals appear to express lower amounts. The detection of multiple bands was noted in these samples, similar to what was observed in the Pten-deficient/NIC samples (Figure

4-22A). The tumours with the activating mutation in p110α also exhibit increased Akt phosphorylation as compared to NeuNT/Cre samples, which may preclude a necessity for Pten loss (Figure 4-22B).

Figure 4-22: ErbB2-driven mammary tumours with genetic activation of PI3K signalling exhibit increased OPN expression

(**A**) Immunoblots for OPN (OPN), Pten, and α/β-tubulin (loading control) in tumour lysates of the indicated genotypes. Numbers correspond to the mouse ID for each sample; multiple tumours from the same animal are distinguished by ".1" and ".2".

(**B**) Mammary tumour lysates of the indicated genotypes were probed for phosphorylated and total forms of Akt (S473), OPN (OPN), Pten, and α/β-tubulin (loading control) by immunoblot. Numbers correspond to the mouse ID for each sample.

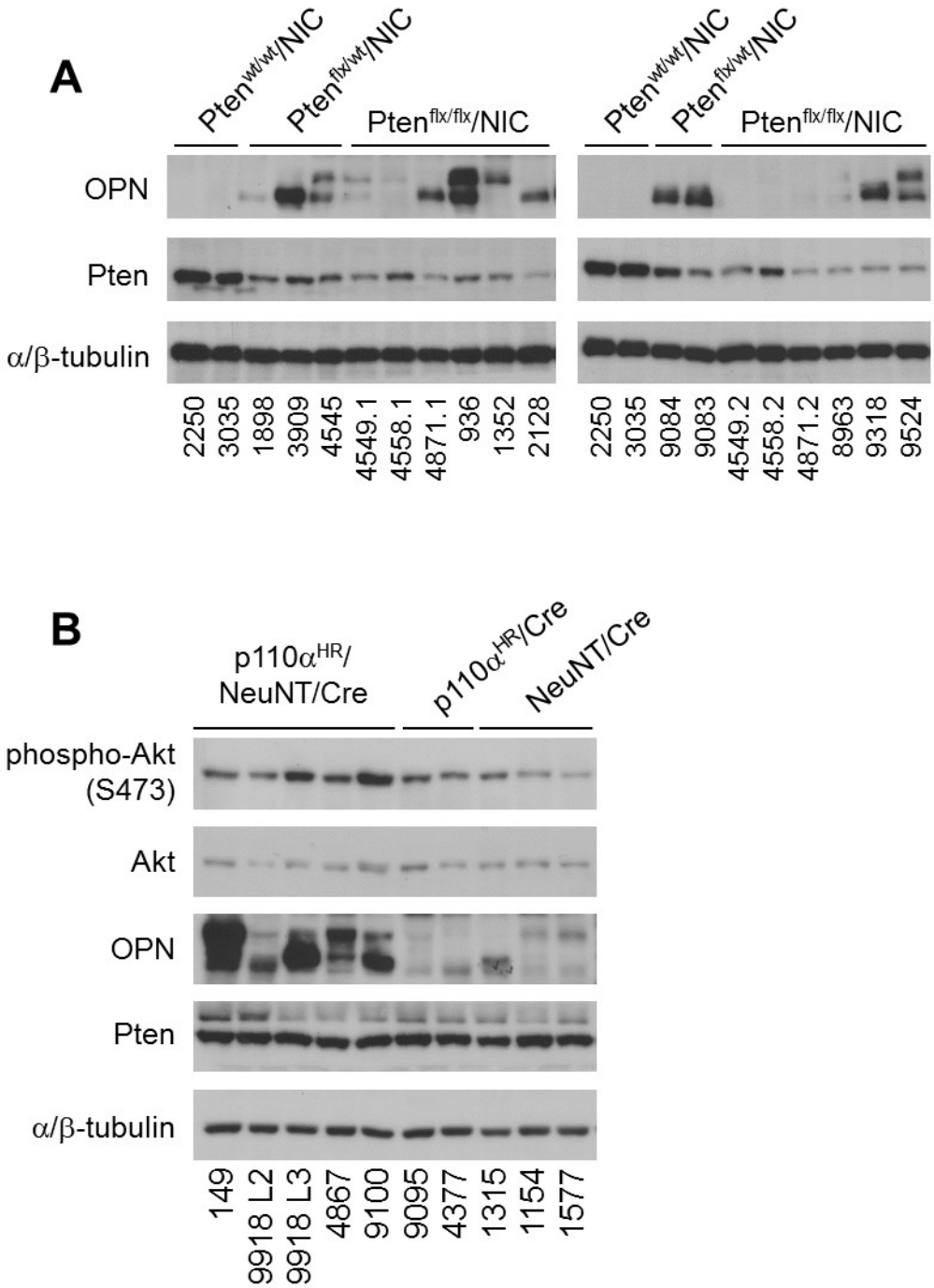
A
Pten^wt/wt/NIC
Pten^flx/wt/NIC
Pten^flx/flx/NIC
Pten^wt/wt/NIC
Pten^flx/wt/NIC
Pten^flx/flx/NIC
OPN
Pten
α/β-tubulin
2250
3035
1898
3909
4545
4549.1
4558.1
4871.1
936
1352
2128
2250
3035
9084
9083
4549.2
4558.2
4871.2
8963
9318
9524
B
p110α^HR/ NeuNT/Cre
p110α^HR/Cre
NeuNT/Cre
phospho-Akt (S473)
Akt
OPN
Pten
α/β-tubulin
149
9918 L2
9918 L3
4867
9100
9095
4377
1315
1154
1577

4.3 Discussion

Loss of p110α impairs ErbB2-mediated tumour initiation and metastasis

The α isoform of p110 has been shown to be important in ErbB2-mediated transformation *in vitro* and so we chose to investigate the *in vivo* consequences of mammary-specific p110α loss in a model driven by activated ErbB2/Neu (MMTV-NIC strain) (Figure 4-1). Our initial observations indicated that mammary-specific ablation of p110α in the NIC model almost completely abrogated tumour initiation [114]. However we continued monitoring animals as they aged and eventually all $p110\alpha^{flx/flx}$/NIC mice developed tumours, albeit with a much longer latency than wildtype and heterozygous cohorts (Figure 4-3). We confirmed that tumours from $p110\alpha^{flx/flx}$/NIC animals were null for p110α transcript and protein and maintained expression of the activated ErbB2 oncogene (Figure 4-4B and 4-15B). These observations indicated that p110α was indeed important for tumour initiation in the NIC model but also that p110α was not absolutely necessary for tumours to ultimately evolve.

Far fewer tumours developed in $p110\alpha^{flx/flx}$/NIC mice as compared to wildtype or heterozygous NIC animals and this focality was evident in tumour volume assessments and analysis of adjacent mammary glands (Figure 4-5A and 4-6). These results collectively indicate that tumour development in $p110\alpha^{flx/flx}$/NIC mice is indeed restricted to one or two glands and that evasion of p110α loss is a relatively rare event in the mammary epithelium of a single animal. Interestingly, these sporadic p110α-deficient/NIC masses were comparable in size to individual tumours in p110α-proficient/NIC mice and exhibited no differences in the expression of proliferative, apoptotic or angiogenic markers (Figure 4-5B and 4-7). We had anticipated differences in tumour vasculature given the p110α-specific role in regulating the embryonic angiogenesis [274]. However, it is likely that in an oncogenic context this may be compensated

for by other signalling events, including pathways downstream of ErbB2 such as the activation of cyclooxygenase-2 or suppression of thrombospondin 1 which promote and inhibit angiogenesis, respectively [436, 437]. Furthermore, orthotopic injection of p110α-wildtype and -null/NIC tumour cells resulted in similar rates of outgrowth (Figure 4-8A). In this experiment, tumours derived from all of the wildtype NIC line exhibited similar latencies post-injection whereas there were differences in the average latency for each of the p110α-deficient/NIC lines. This inconsistency might reflect differences in the ability of each $p110\alpha^{flx/flx}$/NIC tumour line to establish in the fat pad and proliferate. Although this injection experiment does not fully mimic spontaneous tumour development in the transgenic animals because the tumour cells derive from already established tumours, the latencies of tumour outgrowths in injected recipients were reminiscent of the broad range of tumour onsets observed in the transgenic mice (Figure 4-3). Taken together, these results suggest that once p110α-deficient/NIC mammary cells initiate a tumour it grows to the same extent as a wildtype NIC tumour.

Loss of p110α not only impaired tumour initiation in NIC mice, it also hindered metastasis to the lung (Figure 4-9A). Tail vein assays confirmed this impairment of p110α-deficient/NIC tumour cells to colonize the lung, negating any potential influence of differential tumour burden on this phenotype in the transgenic animals (Figure 4-9B and 4-5). Additionally, the results of this experiment may reflect a cell-autonomous defect of p110α-null tumour cells in colonizing the lung microenvironment, since these cells are put directly into the vasculature and therefore bypass the initial stages of metastasis. In support of this idea, the metastatic defect in the transgenic mice did not correlate with differences in blood vessel density in the primary tumours which suggests that diminished angiogenesis was not responsible (Figure 4-7). We did not include $p110\alpha^{flx/wt}$/NIC tumour lines in the tail vein experiments which may have been

informative considering the reduced proportion of p110α$^{flx/wt}$/NIC mice with metastases relative to the wildtype NIC cohort, despite exhibiting similar overall tumour burdens (Figure 4-5A and Figure 4-9A). Furthermore, a haploinsufficient effect of p110α was observed with regard to the incidence but not the number of lung metastases in tumour-bearing mice (Figure 4-9A). This implies that if a p110α$^{flx/wt}$/NIC tumour can metastasize, it appears to do so to the same extent as a wildtype tumour, analogous to the similar growth of p110α-wildtype and -null/NIC tumours after they have initiated. Perhaps complete p110α ablation worsens the defective metastasis of heterozygous tumour cells, impacting on both the decision to metastasize as well as later colonization steps at the secondary site. It would be interesting to address at least some of these issues by assessing the ability of p110α$^{flx/wt}$/NIC tumour cells to colonize the lung when injected directly into the bloodstream. Finally, we noted that lung colonization from transgenic NIC tumours was generally sparse (aside from one wildtype NIC tumour line, #8665) which conflicts with previous studies from our laboratory which utilized cultured primary tumour cells that more readily colonized the lung (Figure 4-9B) [111]. Primary tumour-derived cell lines, as well as orthotopic transplant tumour lines, undergo some degree of selection during serial passages which may confer an advantage over naïve cells from transgenic tumours when adapting to a new microenvironment. In the future we may consider extending the time between tail vein injection and sacrifice to increase the metastatic burden of transgenic tumour cells to more practical levels.

Collectively these results indicate that although p110α is important for ErbB-mediated tumourigenesis, it is not absolutely essential for this process. Focal tumours eventually develop in the absence of this proto-oncogene and they exhibit similar growth to wildtype NIC tumours.

Furthermore, a proportion of p110α-deficient/NIC tumours may even acquire the ability to metastasize to the lung.

Tumours in p110α$^{flx/flx}$/NIC mice are partially dependent on the activity of non-α p110 isoforms

The development of tumours in 100% of the p110α$^{flx/flx}$/NIC cohort indicated that the mammary epithelium of these mice must have experienced additional molecular changes in order to circumvent the lack of p110α and undergo transformation. Despite deficiency of p110α, signalling downstream of PI3K appeared to be unaffected, with similar levels of phospho-Akt and phospho-S6 in p110α-deficient and -proficient/NIC tumours (Figure 4-10; data not shown). We found that non-α p110 isoforms, such as β and gamma, were also comparably expressed and could potentially be responsible for the maintenance of Akt signalling in p110α-null/NIC tumours (Figure 4-11). Furthermore, p85 immunoprecipitates from p110α-deficient/NIC tumour lysates were enriched in p110β and ErbB3 (Figure 4-12). Although this experiment does not prove a direct interaction between the three proteins, it suggests that p85 continues to associate with p110β in the absence of p110α and in doing so p85 may be recruited as a heterodimer to ErbB3 to potentiate PI3K signalling.

Using the pan class I PI3K inhibitor GDC-0941, we went on to show that the *in vivo* growth of NIC tumours lacking p110α depends on the activity of other p110 isoforms (Figure 4-13). In addition, the observed susceptibility of wildtype NIC tumour lines to GDC-0941 was observed previously and provides evidence for a role for class I PI3K signalling in the maintenance of ErbB2 tumours [114]. Interestingly, for all genotypes tumour growth was not

completely impeded nor did masses ever regress with GDC-0941 treatment. Although we confirmed on-target efficacy of the drug at hourly timepoints post-treatment, we found that tumours taken at endpoint (i.e. after up to 6 weeks of ongoing treatment) did not show clear inhibition of Akt phosphorylation relative to matched vehicle controls (Figure 4-13B; data not shown). This is suggestive of compensation mechanisms at work even during the time period of this experiment. Despite this, it will be important to analyze the proliferative and apoptotic status of the drug- and vehicle-treated tumours from this experiment by immunohistochemical staining for Ki67 and TUNEL, respectively. The use of a pan PI3K inhibitor allowed us to identify a partial reliance on the activity of p110 isoforms in general, however in future we can carry out similarly designed experiments using isoform-specific inhibitors to distinguish exactly which isoforms are involved. In light of this, our collaborators found that the p110α-specific inhibitor A66, and not the p110β-specific inhibitor TGX-221, could attenuate growth of tumours driven by a different mutant transgene of ErbB2, NeuNT [114]. In addition, it may be interesting to identify the Akt isoform(s) signalling downstream in this context.

Although these findings demonstrated that PI3K signalling from non-α p110 isoforms is relevant in p110α-null/NIC tumours it is not likely to be the mechanism driving tumour initiation. If non-α p110 isoforms had been sufficient for tumour initiation in our $p110\alpha^{flx/flx}$/NIC transgenic mice we would not have witnessed such a strong delay in onset. Furthermore, these tumours would have exhibited a more pronounced growth inhibition or may have possibly regressed when treated with the pan PI3K inhibitor. This is in contrast to p110β-deficient/NIC mice, where p110α readily substitutes for the lack of p110β to such an extent that tumour initiation occurs earlier than in wildtype NIC animals [114]. These observations collectively suggest that additional mechanisms must have evolved to fully compensate for p110α ablation;

the increased tumour latency in p110α$^{flx/flx}$/NIC animals could theoretically be long enough to accommodate genetic aberrations necessary for tumour initiation in the absence of p110α. In this respect, our collaborators have performed whole exome sequencing on these tumours however the data from this experiment has yet to be analyzed.

Dysregulated expression of OPN and its receptor αvβ3 integrin in p110α-deficient/NIC mammary epithelium

In order to identify molecular changes that may have occurred to allow NIC tumours to evolve without p110α, we performed gene expression profiling. It was immediately apparent from unsupervised hierarchical clustering that the p110α-null/NIC tumours were inherently different from each other (Figure 4-16). This finding corroborated the lack of any overwhelming differences between each genetic cohort when analyzing general oncogenic signalling by immunoblot (Figure 4-10; data not shown). However, from the list of differentially expressed probes we identified *Spp1*/OPN as one of the most highly upregulated genes when comparing the average expression in p110α-null/NIC tumours relative to wildtype counterparts (Figure 4-17A). OPN, originally identified in rat bone, belongs to the small integrin binding ligand N-linked glycoprotein (SIBLING) family of secreted proteins and is subject to extensive post-translational modifications including phosphorylation, glycosylation, and cleavage [438]. A conserved arginine-glycine-aspartic acid (RGD) motif allows OPN to interact with integrin receptors, one of the major ones being αvβ3 heterodimer [432, 439]. Integrin activation can engage several downstream signalling pathways involved in adhesion and migration, as well as proliferative and anti-apoptotic pathways; this is often mediated by PI3K/Akt pathway downstream of OPN [440,

441]. Binding of OPN to αvβ3 specifically allows for the activation of c-Src which can transactivate RTKs such as EGFR and possibly MET, leading to subsequent activation of PI3K and MAPK pathways [442-444]. OPN also induces PI3K signalling by binding to the CD44 receptor [445]. Through these signalling pathways OPN can enhance breast cancer cell migration and invasion *in vitro* [432, 446-450]. OPN can also promote tumour growth, angiogenesis and metastasis of breast cancer cells *in vivo* [432, 450]. Overexpression of OPN has been documented in several human cancers and can be correlated with progression [431, 451-453]. In these studies it was noted that OPN could be detected in tumour epithelium, tumour-associated stromal cells, and in the serum of cancer patients. In breast cancer, increased OPN levels in tumours or in plasma is associated with poor prognosis [428-430, 454, 455]. Some studies have also reported that OPN overexpression may preferentially occur in particular breast cancer subtypes, including the HER2-enriched and basal-like groups [455, 456]. Interestingly, studies in mice have indicated that OPN functions in mammary gland lactation and involution; whether transgenic expression OPN is sufficient for tumourigenesis has not been fully addressed [457-459].

We validated the upregulation of *Spp1*/OPN at the transcript and/or protein level in almost 60% of p110α-deficient/NIC tumours (Figure 4-17B and Figure 4-18). Consistent with other studies assessing OPN expression in tumours by immunohistochemistry, we observed positive staining exclusively in the tumour epithelium (Figure 4-18B) [428, 429]. We also noted stronger OPN staining at the tumour-stroma boundary which has been reported previously as well [451]. This proximity may be necessary to allow secretion to the ECM and subsequent paracrine signalling within the tumour microenvironment. Interestingly, OPN was expressed only in adenocarcinoma and not in early lesions or apparently normal ducts, suggesting that

increasing OPN might correlate with progression in our system (Figure 4-18B). As we collected OPN expression data from the three analyses (RT-qPCR, immunoblot, and immunohistochemistry), it was apparent that transcript and protein levels were not correlated in all cases. For example, #2324 was positive for OPN expression at the mRNA level and by immunohistochemistry, but not by immunoblot (Figure 4-17B, 4-18A-B). Most likely these discrepancies are due to the use of different pieces of tumour for separate analyses. Our immunohistochemical staining, which combines expression and localization data, supports this idea as staining of OPN was not homogenous in tumour sections (Figure 4-18B). Bearing in mind the heterogeneity of our tumours and the being limited by "sampling error", it is possible that a greater proportion of p110α-deficient/NIC tumours are potentially positive for OPN.

In addition to increased expression of OPN, p110α-deficient/NIC tumours also exhibited decreased expression of αv and β3 integrins relative to wildtype NIC samples (Figure 4-19). The αvβ3 integrin heterodimer is considered one of the major receptors for OPN as well as other RGD-containing proteins such as fibronectin and vitronectin [460]. β3 integrin is not expressed in the normal mammary epithelium and so its upregulation is thought to be associated with a tumourigenic state. Many functions of αvβ3 in tumourigenesis are induced by OPN, including the promotion of cell migration, activation of MMPs, and *in vivo* metastasis [432, 446]. In fact, the interaction between OPN and integrins has been shown to be important for tumour cell growth and metastasis in animal models [461, 462]. Interestingly, in premalignant NIC mammary epithelium β3 integrin transcript was also significantly lower in the absence of p110α (Figure 4-20, bottom). The reduced β3 expression in p110α-deficient/NIC mammary epithelium relative to wildtype could mechanistically explain the delay in tumour initiation; its absence in tumour epithelium may also contribute to the metastatic defect we observed. Furthermore, in

these same premalignant samples, there was a trend toward lower OPN expression in the p110α-null/NIC samples as compared to wildtype (Figure 4-20, top). These observations suggest that the sporadic increases in OPN across the panel of samples may be an adaptive response to β3 downregulation in an attempt to restore OPN/αvβ3 signalling in p110α-deficient/NIC epithelium and allow tumours to emerge. In fact, OPN has been shown to increase β3 expression in breast cancer cells, perhaps as a positive feedback mechanism [432]. The ideal internal control for this experiment would have been to use the same animals for both premalignant and tumour epithelium, however this was not possible. Further immunohistochemical analyses of OPN and β3 integrin expression on tissue sections that include histologically "normal" ducts as well as lesions at various stages of tumour progression could be useful.

These findings point to a potential role for p110α in indirectly regulating β3 transcription. This may extend to αv integrin in distinct cases: we noticed that two samples with lower than average levels of αv transcript also exhibited the lowest expression of β3 mRNA. The possibility that these two integrins are transcriptionally co-regulated is supported by a recent study showing that they both can be repressed by c-Myc [463]. We plan on investigating the potential regulation of expression of these integrins by PI3K signalling *in vitro* by treating cell lines derived from ErbB2- and PyV mT-expressing tumours with pan and isoform-specific PI3K inhibitors.

The dysregulation of integrin expression provides a possible explanation for our failed attempts to establish cell lines from $p110\alpha^{flx/flx}$/NIC tumours. The reduced αvβ3 integrin expression in these cells probably impairs attachment and cell-cell contacts. This speculation is substantiated by the fact that p110α-deficient/NIC tumours readily transplant in the mammary fat pad of athymic nude mice, which likely provides a more amenable microenvironment replete

with ECM components to engage the low levels of β3 still detectable in these samples. We plan to investigate cell adhesion on different matrices including fibronectin and vitronectin as well as supplementing with recombinant OPN.

Together, these findings suggest that loss of p110α in the NIC model causes a decrease in β3 integrin expression which may be responsible for the long delay in tumour onset. This eventual development of tumours in p110α$^{flx/flx}$/NIC mice may be due to an upregulation of OPN which can promote proto-oncogenic signalling through the residual levels of αvβ3 integrin. It will be worthwhile to assess the expression of other OPN receptors, including additional integrin heterodimers and CD44. Perhaps in circumstances of low β3 integrin, OPN can shift its actions onto CD44; this potential receptor switching may be further enhanced by the fact that OPN can induce CD44 expression [447].

OPN expression correlates with loss of Pten or activation of p110α in ErbB2-driven mammary tumours

We were curious if p110α$^{flx/flx}$/NIC mice harbouring OPN-positive tumours had other features in common, such as age of onset and positivity for metastasis. However we could not draw any parallels with these phenotypes. It was also difficult to compare the degree of β3 integrin downregulation with OPN upregulation. For example, when comparing the results from immunoblots of the same tumour lysates, there are several samples with low β3 expression that do not exhibit a corresponding increase in signal for OPN (Figures 18A and 19A). This echoes the earlier discussion on tumour heterogeneity and sampling different pieces of tumour for different analyses. Given the reputation of OPN in driving invasiveness and malignancy, it will

be worthwhile to investigate if the rare metastatic lesions originating from p110α-null/NIC tumours express OPN by immunohistochemistry.

We did come across one correlation with OPN and that was the reduced expression of Pten (Figure 4-21A). One p110α-null/NIC sample with low Pten protein also exhibited slightly reduced Pten transcript (#2386) (Figures 4-10 and 4-21B). In this sample, transcription of Pten or the stability of the mRNA may be impaired; this may even reflect mutations or deletions at the genomic level. By contrast, a sample with low Pten protein expression did not exhibit a concurrent reduction in Pten mRNA (#6969); perhaps in this case Pten translation or stability is inhibited. This suggests that the mechanisms leading to downregulation of Pten protein are not common to all samples in this subset. Loss of Pten has been previously correlated with the induction of OPN expression in a mouse model of prostate tumourigenesis as well as in human melanoma cell lines [433, 434]. These phenotypes are likely driven by activation of PI3K signalling. Indeed stimulation of PI3K signalling itself has been shown to induce OPN *in vitro* [435]. In our p110α-deficient/NIC tumours Pten loss may allow for increased PI3K signalling through non-α p110 isoforms leading to upregulation of OPN. Since OPN can activate PI3K signalling through αvβ3 and CD44 signalling, downregulation of Pten likely potentiates this positive feedback loop. Perhaps disruption of this hypothetical pathway is in part responsible for the sensitivity of p110α-null/NIC tumour lines to PI3K inhibition (Figure 4-14A). To test this theory using a genetic approach, we plan to cross in conditional Pten alleles into the $p110\alpha^{flx/flx}$/NIC background to determine if Pten loss can effectively "rescue" the delay in tumour initiation.

The correlation between upregulated OPN and Pten loss was not limited to the p110α-deficient/NIC model. In tumours from NIC mice with conditional loss of Pten (described in

Chapter 3), we confirmed expression of OPN protein in several Pten-deficient/NIC tumours as compared to wildtype NIC samples (Figure 4-22A) [106]. We also saw increased OPN levels in immunoblots of tumours from mice expressing an activated point mutant of p110α (H1047R) with or without activated ErbB2 (NeuNT transgene) [62, 64, 65]. Further study of OPN expression in these transgenic models will be especially important considering that a single band was observed on the immunoblot of p110α-deficient/NIC samples whereas a doublet was observed in both the Pten-deficient/NIC and $p110\alpha^{HR}$/NeuNT/Cre models (Figures 4-18A and 4-22). OPN is known to undergo a variety of post-translational modifications and it will be interesting to attempt to identify the different variants of OPN in our models.

Taken together, the upregulation of OPN in multiple models driven by different mechanisms of PI3K pathway activation demonstrates that this may be a common feature of ErbB2 mammary tumourigenesis.

Future directions

Although these studies clearly define p110α as a critical mediator of mammary tumourigenesis and metastasis downstream of activated ErbB2, our analysis of the p110α-null/NIC tumours that eventually developed have raised several important questions.

Considering our previous conjecture that p110α indirectly drives β3 integrin expression, this raises the possibility that PI3Ks can regulate the expression of different components within the OPN/αvβ3 integrin signalling pathway. Interestingly the mRNA analysis revealed that the three samples with high OPN transcript corresponded to three samples that clustered separately from all of the other tumours in the microarray analysis, suggesting that these tumours may have

other genes in common which may be related to this pathway in addition to integrins. Moreover, these differentially expressed genes may be regulated by a common transcriptional network. Further biochemical validation using a combination of pan and isoform specific inhibitors as well as targeted knockdown strategies in established cell lines will help us to probe into the mechanisms regulating the transcription of both OPN and β3 integrin in our system.

We would like to analyze additional p110α-deficient/NIC tumours for the overexpression of OPN with concomitant downregulation of Pten. In doing so, we hope to expand our sample set for further analysis of these features, including genomic aberrations and the regulation/stability of mRNA and protein. In addition to testing if mammary tumourigenesis in p110α$^{flx/flx/}$NIC mice can be rescued by Pten deletion, future projects can investigate if a similar effect ensues upon transgenic expression of OPN (MMTV-OPN strain) [459]. Conversely, mouse strains with mammary-specific overexpression of Pten or an antisense OPN transgene can be crossed to p110α-deficient/NIC animals in an attempt to completely prevent tumour development [313, 458].

We are also interested in quantifying the levels of circulating OPN in the plasma and serum of tumour-bearing p110α$^{flx/flx}$/NIC mice by mouse-specific enzyme-linked immunosorbent assay (ELISA). The relevance of systemic OPN has been demonstrated by studies in mice showing that tumour-derived OPN can enter the bloodstream to activate stromal precursors in the bone marrow leading to their mobilization and instigation of secondary tumour growth at distant sites [464]. It is possible that these mechanisms might be involved in sustaining growth of the primary tumour in our model as an extended autocrine loop.

Collectively, our studies imply that the treatment of HER2-expressing breast cancers with a p110α-specific inhibitor will most likely lead to acquired resistance in these patients. Perhaps better efficacy can be attained with the use of pan PI3K inhibitors, although our own orthotopic injection experiment indicates that even this approach may eventually fail. The molecular mechanisms that may be relevant in mediating resistance to pan or isoform-specific PI3K inhibitors might be evident in our p110α-deficient tumours. We have identified some potential candidates in our model, including the reactivation of PI3K signalling through non-targeted p110 isoforms and the upregulation of OPN (both of which may be dependent on Pten). However, there may be many other mechanisms involved in the emergence of p110α-deficient/NIC tumours and further molecular analyses will be required to uncover them.

5 Characterization of a novel model of murine mammary tumourigenesis driven by polyomavirus middle T antigen (PyV mT)

5.1 Introduction

The studies in Chapter 4 pointed to an important role for the p110α isoform in tumourigenesis downstream of activated ErbB2. We were interested in seeing if this phenotype could be recapitulated in a second model of mammary tumourigenesis, specifically one driven by polyomavirus middle T antigen (PyV mT). Although heterozygous loss of p110α was shown to impair both tumour initiation and penetrance in an MMTV-PyV mT/MMTV-Cre recombinase background, homozygous loss could not be achieved due to the likely selection of Cre recombinase-negative/p110α-positive mammary epithelial cells [114].

It was clear that a Cre-coupled version of the PyV mT oncogene was needed, analogous to the MMTV-NIC model which was developed to study conditional ablation of genes during Neu-driven tumourigenesis [105]. Hence, the PyV mT transgene was similarly linked to Cre recombinase through an IRES (PyV mT-IRES-Cre or "MIC"). In addition to replicating this coupling strategy for a new PyV mT strain, we sought to expand the applicability of the model to temporal regulation. The recent departure from constitutive or hormone-responsive promoters in transgenic breast cancer mouse models (e.g. MMTV) to a chemically-inducible approach has been made possible by the advent of the MMTV-reverse tetracycline transactivator (rtTA) strain used in combination with the well-established TetON system [424]. The tetracycline-inducible promoter is only turned on in response to the tetracycline derivative, doxycycline, in contrast to the hormone-responsive MMTV promoter that becomes constitutively active at approximately 3 weeks of age. By turning on expression of a tetracycline-responsive transgene in the adult mouse, one can avoid potential complications caused by overexpression of the oncogene or by Cre recombinase-mediated removal of a LoxP-flanked cassette during development; likewise, expression can then be turned off after tumour formation to investigate the possibility of

regression and recurrence. It should be noted that a TetON-PyV mT mouse strain has been reported which is sensitive to inducible mammary tumour progression in the presence of the MMTV-rtTA transgene, however PyV mT is not coupled to Cre recombinase in this case (Table 1-2) [73].

In order to link expression of the PyV mT oncogene with that of Cre recombinase in an inducible manner, we generated a TetOMIC transgenic mouse that, when crossed to the MMTV-rtTA strain and treated with doxycycline, expresses both PyV mT and Cre recombinase from the same bi-cistronic transcript in the mammary epithelium [144]. In the majority of experimental mice, mammary tumours develop within 2 weeks of induction, progress through the typical PyV mT histological stages, and metastasize to the lung. These tumours were susceptible to regression upon doxycycline withdrawal however recurrent tumours ultimately arose in de-induced animals. This chapter details the characterization of this novel inducible model and reflects on its potential use in future studies of PyV mT mammary tumourigenesis.

5.2 Results

Induction of MIC transgene expression in the mammary gland results in rapid tumour onset

PyV mT and Cre recombinase cDNAs were sub-cloned into a pTE vector containing an IRES to produce a TetO-PyV mT-IRES-Cre recombinase (MIC) transgene (Figure 5-1). MIC virgin females were aged to 1 year without issue and the transgene did not disrupt normal breeding in either sex or nursing by females. MIC founder lines were crossed to the MMTV-rtTA strain to drive doxycycline-inducible transgene expression to the mammary epithelium [424]. Tumour

Figure 5-1: Doxycycline-inducible expression of PyV mT and Cre recombinase in the mammary epithelium of rtTA/MIC mice

Experimental and control animals were generated by crossing the MMTV-rtTA strain to the TetO-MIC strain [424]. The MMTV directs expression of the reverse tetracycline transactivator (rtTA) to the mammary epithelium. Administration of doxycycline to the animal allows the rtTA to bind the Tet operon (TetO) and induce co-expression of PyV mT and Cre recombinase due to an internal ribosome entry site (IRES) linking the transgenes.

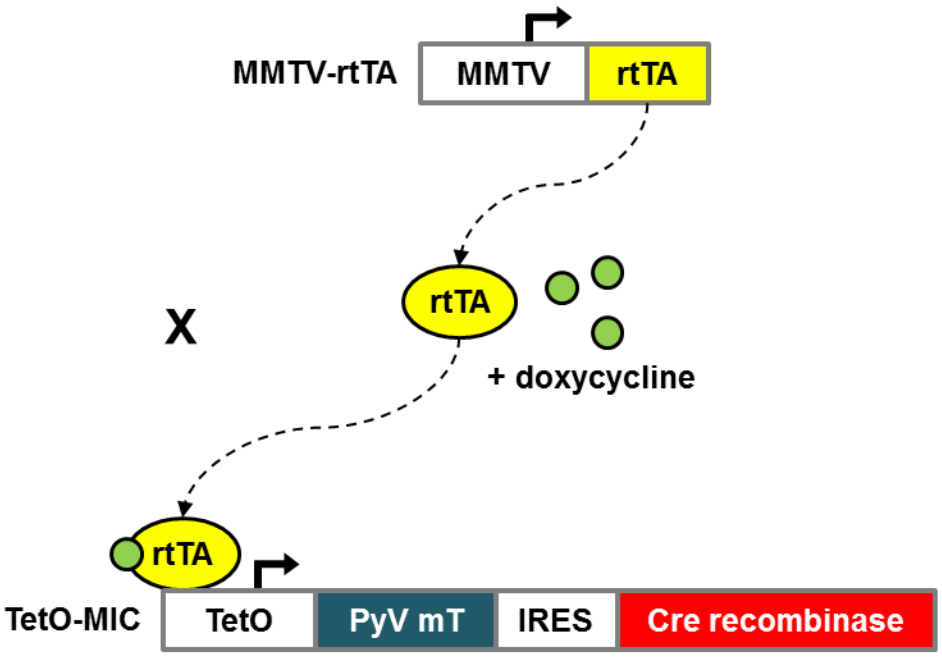
MMTV-rtTA
MMTV
rtTA
rtTA
+ doxycycline
X
rtTA
TetO-MIC
TetO
PyV mT
IRES
Cre recombinase

onset in the original constitutive MMTV-PyV mT model occurs with relatively short onset, with virgin females developing mammary masses with a T_{50} of 40 days of age [109, 141]. To evaluate whether this was also the case for the MIC model, we induced cohorts of rtTA/MIC, rtTA, and MIC virgin female mice between 8 and 16 weeks of age with 2 mg/mL doxycycline which has been previously shown to lead to robust expression of the Tet-inducible transgene in an MMTV-rtTA background [424]. The minimum age of 8 weeks for induction was chosen to ensure that the mammary epithelium would be almost fully developed. Induced animals were initially examined every other day by physical palpation for mammary tumour formation, alongside un-induced controls of the same genotypes. A single founder line in which mammary tumours were detected was chosen for further breeding to generate cohorts that would be more extensively characterized.

Mammary gland masses were detected in rtTA/MIC mice as early as 4 days post-induction, with 74.4% (29/39) of the cohort developing multifocal tumours within 16 days of induction (Figure 5-2). The few animals that did not palpate within this short 16-day window of induction could be subdivided into two groups: those that developed tumours between 17 and 365 days post-induction (12.8%; 5/39) and those that remained tumour-free after 1 year of induction (12.8%; 5/39). Considering the entire rtTA/MIC induction cohort, the average tumour onset was 22.0 ± 7.1 days post-induction while the T_{50} was 7 days of induction, reflecting the very rapid and complete induction observed in the majority of animals. Precise regulation of the MIC transgene was evident based on the concurrent observations that rtTA/MIC mice developed mammary tumours exclusively and that all control animals (both induced and un-induced) remained tumour-free after 1 year post-induction.

Tumour growth in rtTA/MIC mice progressed differently from what has been observed in the MMTV-PyV mT model. In the latter, tumours develop as focal masses in each gland that are easily measurable. At defined time-points, histological analysis of the inguinal mammary glands from MMTV-PyV mT mice shows a gradient of transformation, with the older and more advanced lesions proximal to the nipple, and newer lesions at earlier stages of tumourigenesis towards the terminal end buds of the epithelial network [142]. While distinct masses are initially palpable in an induced rtTA/MIC mouse, the entire gland promptly thickens within days, making it difficult to perform calliper measurements at this stage. Animals sacrificed at onset (approximately 4 days post-induction) or 2 weeks post-induction harboured inguinal mammary glands filled with early lesions (data not shown; Figure 5-3). This difference between the two models could be explained by the fact that constitutive PyV mT-mediated transformation occurs during puberty as the ductal epithelial network progressively penetrates the fat pad, while in the MIC model transformation was initiated in an almost mature gland.

All tumour-bearing rtTA/MIC females were sacrificed at a total tumour volume of approximately 6 cubic centimetres (denoted as "end-stage"). Histological analysis of mammary glands and tumours from these animals revealed the presence of all previously characterized stages of PyV mT tumourigenesis, ranging from hyperplasia, to MIN/adenoma, and finally to early and late carcinoma (Figure 5-4). Adjacent mammary gland whole mounts from tumour-bearing mice were also fully transformed (Figure 5-5A). Mammary gland sections and whole mounts from age-matched control animals were normal (Figure 5-4, 5-5B). It appeared that our novel inducible PyV mT strain was closely recapitulating the histological stepwise tumour progression documented in the MMTV-PyV mT model [143].

Figure 5-2: Rapid induction of mammary tumours in the majority of rtTA/MIC mice in response to doxycycline

Kaplan-Meier tumour onset curve for induced rtTA/MIC mice and controls (un-induced rtTA/MIC; induced or un-induced rtTA or MIC). The table lists the penetrance (the percentage/number of animals that developed tumours), T_{50} (days of induction when 50% of animals have developed tumours), and average tumour onset with standard deviation for each of the curves shown on the graph.

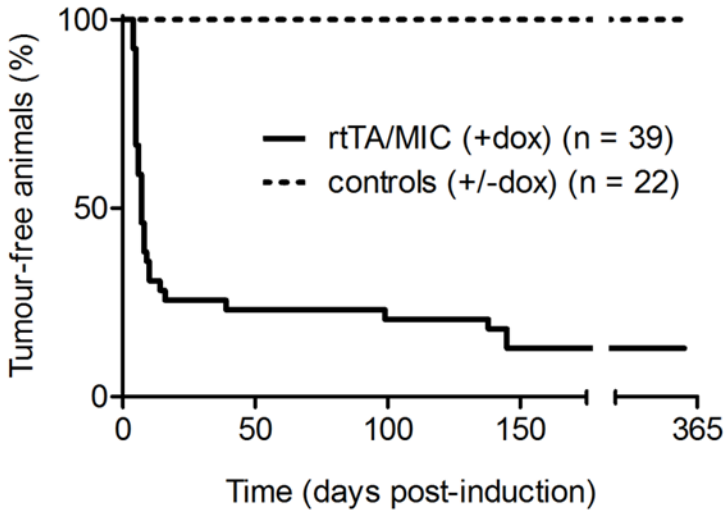

Genotype	Penetrance	T_{50} (days post-induction)	Average onset (days post-induction)
rtTA/MIC (+dox)	87.1% (34/39)	7	22 ± 7.1
controls: rtTA/MIC (-dox) rtTA (+/-dox) MIC (+/-dox)	0% (0/22)	n/a	n/a

Figure 5-3: After 2 weeks of induction, mammary glands from rtTA/MIC mice are transformed

(**A**) An H&E-stained wholemount (left) and corresponding histological section (right) of a typical rtTA/MIC mammary gland after 2 weeks of induction (top row) as compared to a normal mammary gland from an un-induced control (bottom row). High and low magnifications are shown for each set of images. Scale bars from left to right are 5 mm, 0.5 mm, 500 μm, and 100 μm.

(**B**) Quantification of the average percentage of normal, hyperplastic, and filled ducts relative to the total number of ducts in mammary gland sections from rtTA/MIC mice induced for 2 weeks and matched controls (induced or un-induced).

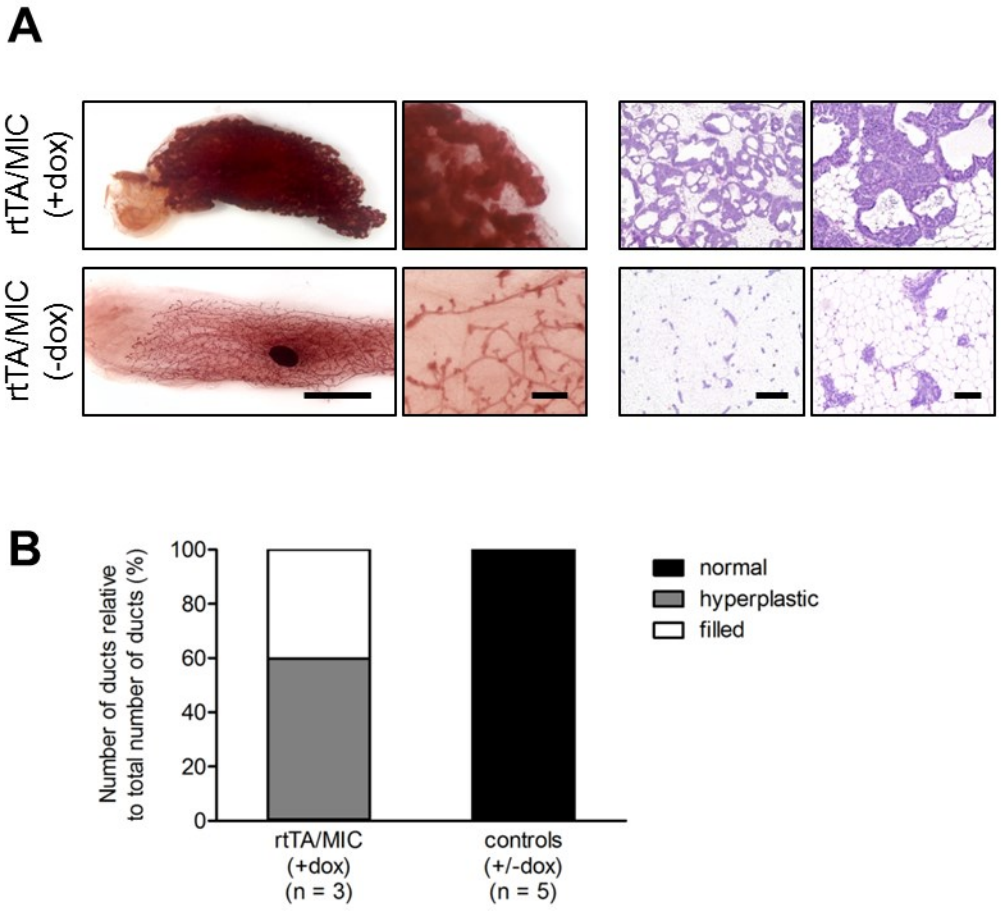
A
rtTA/MIC (+dox)
rtTA/MIC (-dox)
B
Number of ducts relative to total number of ducts (%)
100
80
60
40
20
0
rtTA/MIC (+dox) (n = 3)
controls (+/-dox) (n = 5)
normal
hyperplastic
filled

Figure 5-4: rtTA/MIC animals develop tumours with characteristic histopathological features of PyV mT-driven mammary tumourigenesis

Representative H&E-stained sections of normal ductal structures in a mammary gland from an un-induced control animal followed by typical stages of PyV mT mammary tumour progression (hyperplasia, mammary intraepithelial neoplasia [MIN], and adenocarcinoma) in mammary glands and tumours from rtTA/MIC mice following doxycycline induction. Scale bar is 100 μm.

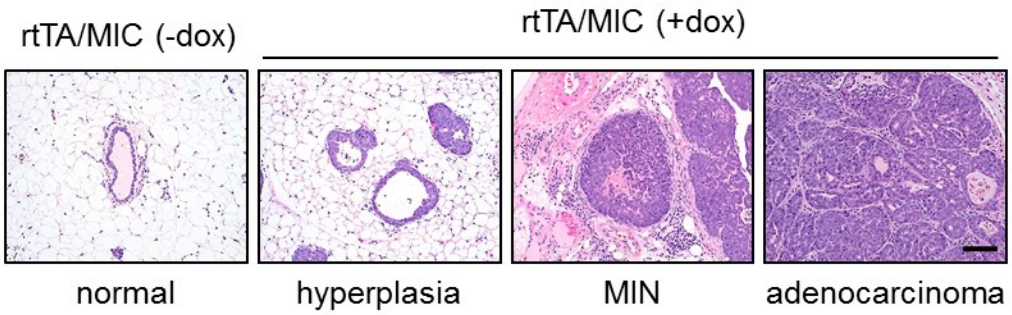
rtTA/MIC (-dox)
rtTA/MIC (+dox)
normal
hyperplasia
MIN
adenocarcinoma

Figure 5-5: End-stage tumour-bearing rtTA/MIC mice have adjacent mammary glands that are extensively transformed in contrast to normal controls

(**A**) Representative H&E-stained wholemount preparations of inguinal adjacent mammary glands from 3 different rtTA/MIC tumour-bearing mice induced with doxycycline for 9 to 11 weeks. Scale bars are 5 mm (left) and 0.5 mm (right).

(**B**) Control mammary gland wholemounts stained with H&E from the indicated genotypes either induced for 9 to 11 weeks or age-matched when un-induced. Scale bars are 5 mm (left) and 0.5 mm (right).

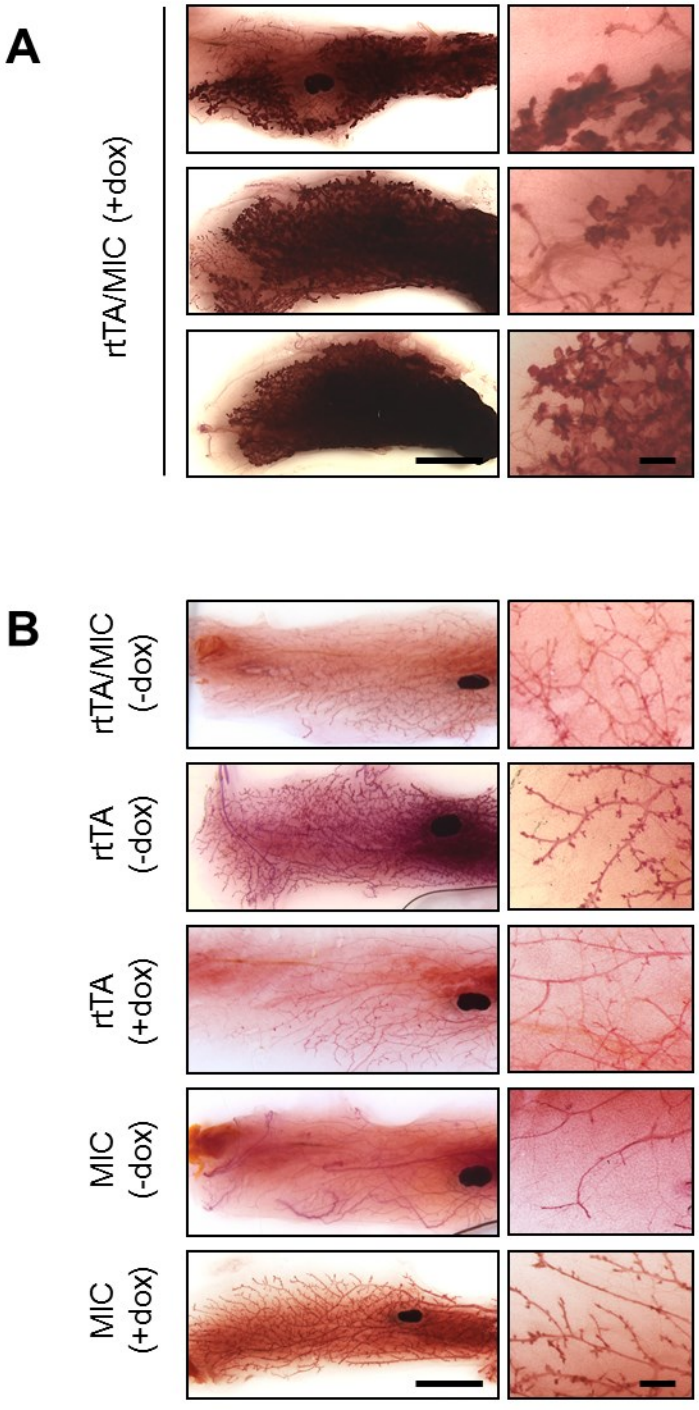
A
rtTA/MIC (+dox)
B
rtTA/MIC (-dox)
rtTA (-dox)
rtTA (+dox)
MIC (-dox)
MIC (+dox)

rtTA/MIC mammary tumours co-express the PyV mT oncogene and a functional Cre recombinase

Having established that mammary tumours were indeed inducible in the rtTA/MIC system, our next step was to verify expression of the MIC transgene by immunohistochemistry. PyV mT and Cre recombinase antibodies stained the membrane and nuclei, respectively, of cells in rtTA/MIC lesions in a mosaic pattern (Figure 5-6A). Notably, normal ductal epithelium in both age-matched controls and wildtype animals did not stain positively for PyV mT or Cre recombinase.

To confirm MIC transgene expression by immunoblot, protein extracts were prepared from mammary glands and tumours from rtTA/MIC mice sacrificed at palpation or at end-stage tumour burden ("late onset" refers to palpation after 16 days of induction). These lysates were positive for PyV mT expression; Cre recombinase was also detected in rtTA/MIC tumours, although it was lowly expressed in mammary gland lysates which likely have relatively less epithelial content as indicated by E-cadherin levels (Figure 5-6B). Induced and un-induced control mammary glands did not express PyV mT or Cre recombinase protein.

In order to use this model for Cre recombinase/LoxP-mediated excision of genes, we needed to confirm that the Cre recombinase produced from the MIC transgene was functionally active. To accomplish this, we utilized a Rosa26-β-galactosidase reporter strain ("GTRosa") in which the lacZ gene is downstream of a LoxP-flanked stop codon (Figure 5-7A) [67]. The presence of Cre recombinase allows for expression of the β-galactosidase enzyme from the lacZ transgene, which can cleave the compound X-gal into an insoluble blue-coloured product. The mammary epithelium of rtTA/MIC/GTRosa tumour sections turned blue upon staining with X-gal, indicating that Cre recombinase had been expressed and active in these cells (Figure 5-7B).

This outcome is comparable to an MMTV-PyV mT/MMTV-Cre recombinase/GTRosa mammary tumour in which there are no conditional alleles present. Collectively, these results demonstrate that the rtTA/MIC mouse model can be used to study Cre recombinase-dependent genetic alterations in conjunction with PyV mT oncogenic activation.

Proliferation and apoptosis in rtTA/MIC lesions

The very quick detection of palpable masses in the rtTA/MIC mammary glands and subtle fluctuations in tumour growth at early stages of induction suggested that there may be a particular balance between proliferation and apoptosis influencing progression in our model. Ki67- and TUNEL-positive nuclei were quantified in mammary tumours from rtTA/MIC mice that had reached tumour burden endpoint (Figure 5-8). The average levels of both Ki67 and TUNEL obtained in our inducible PyV mT mammary tumours were approximately 2-fold higher than these parameters in the constitutive PyV mT model [105]. The rtTA/MIC mammary tumour cells appear to be both actively dividing and dying at the same time. While lesions at both early and later stages of tumourigenesis show morphological evidence of cell death and necrosis, the fact that tumours reach clinical burden endpoint in this model suggests that proliferation ultimately prevails over apoptosis during progression.

Figure 5-6: PyV mT and Cre recombinase are expressed at all stages of tumourigenesis in rtTA/MIC animals

(**A**) Immunohistochemical detection of PyV mT (middle row) and Cre recombinase (bottom row) in ductal structures at the indicated stages of tumour progression in rtTA/MIC mice, contrasted by the absence of these proteins in a normal duct from an un-induced control animal. The corresponding H&E-stained sections are shown for comparison (top row). Scale bar is 50 μm.

(**B**) Immunoblot analysis of protein lysates from rtTA/MIC mammary glands (mg), mammary tumours (tum), and adjacent mammary glands (amg) from animals sacrificed at palpation or at end-stage ("late onset" refers to palpation after 16 days of induction) using antibodies directed to E-cadherin (epithelial content control), PyV mT, Cre recombinase, and α-tubulin (loading control). Controls include (from left to right) mammary glands from two un-induced rtTA/MIC mice, one induced MIC mouse, and one induced rtTA mouse. Positive controls for PyV mT and Cre recombinase expression were tumours from MMTV-PyV mT (PyV mT) and MMTV-NIC (NIC) animals, respectively; arrowheads indicate specific bands for these proteins. Numbers correspond to the mouse ID for each sample.

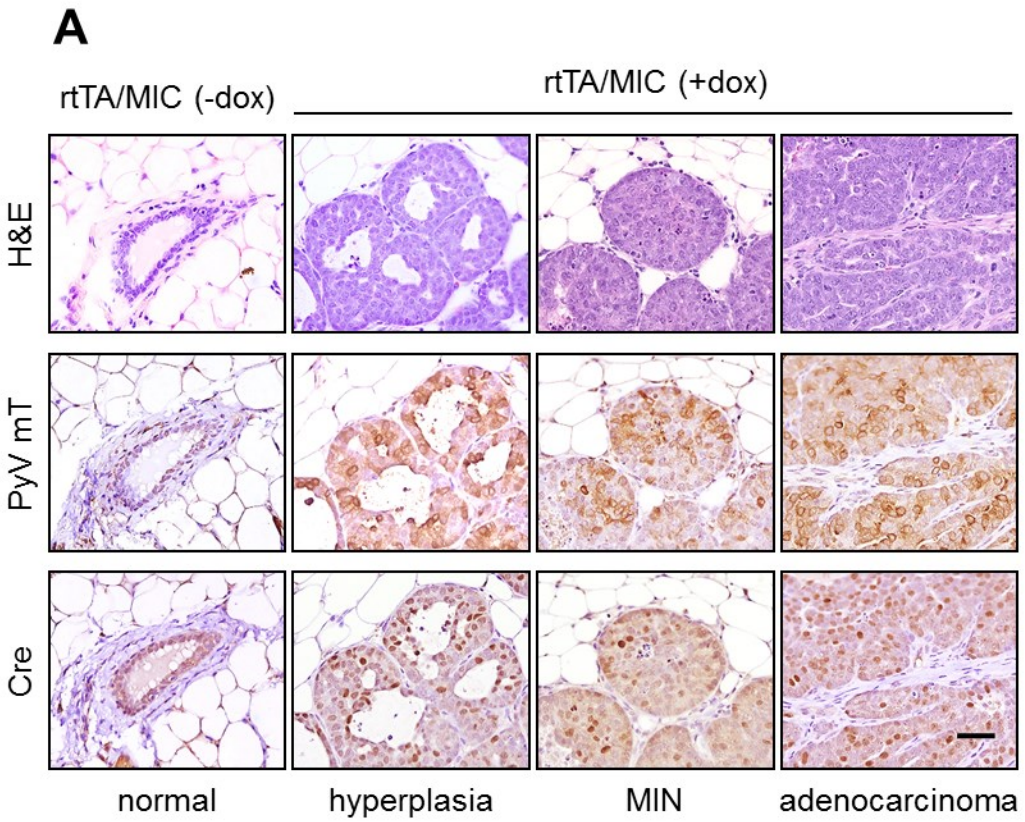
A
rtTA/MIC (-dox)
rtTA/MIC (+dox)
H&E
PyV mT
Cre
normal
hyperplasia
MIN
adenocarcinoma
B
rtTA/MIC (+dox)
controls
(+/-dox)
PyV mT
NIC
E-cadherin
PyV mT
Cre
α-tubulin
1227
1239
1241
9785
207
1334
1352
1550
2090
1334
1550
2391
2958
3040
1336
2098
1877
1474
mg
tum
amg
tum
mg
tum
palpation
end-stage
end-stage
(late onset)

Figure 5-7: Cre recombinase expression and activity are uniform in the epithelium of rtTA/MIC tumours

(**A**) Simplified schematic of the Cre recombinase-activated β-galactosidase reporter strain designated as "GTRosa" (adapted from Friedrich and Soriano, 1999). The presence of Cre recombinase allows for removal of the floxed STOP cassette and expression of the *lacZ* transgene which encodes for the β-galactosidase protein.

(**B**) X-gal staining (blue) of tumour sections from rtTA/MIC animals carrying the GTRosa transgene. Negative controls include MMTV-PyV mT tumours with either GTRosa (PyV mT/GTRosa) or MMTV-Cre recombinase transgenes (PyV mT/Cre). An MMTV-PyV mT tumour with both transgenes (PyV mT/Cre/GTRosa) was used as a positive control. Samples were counterstained with nuclear fast red (pink). Scale bar is 200 μm.

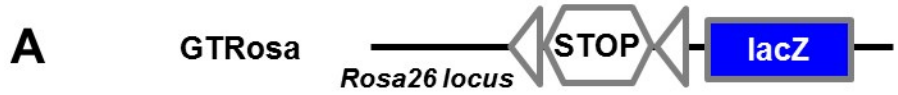
A
GTRosa
Rosa26 locus
STOP
lacZ

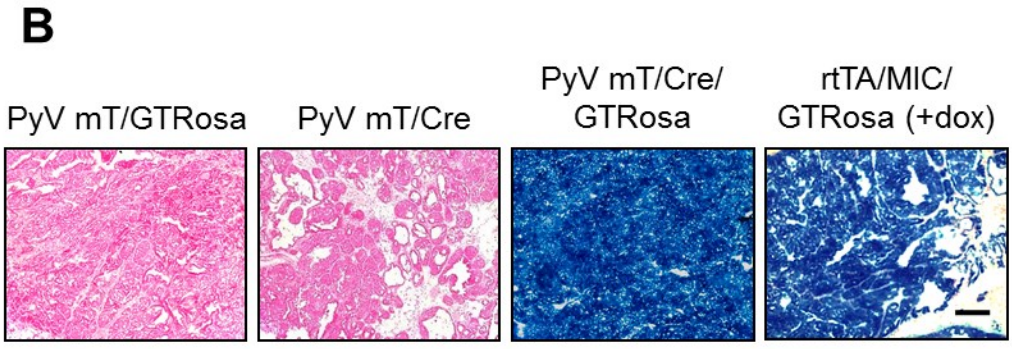
B
PyV mT/GTRosa
PyV mT/Cre
PyV mT/Cre/
GTRosa
rtTA/MIC/
GTRosa (+dox)

Figure 5-8: rtTA/MIC tumours express both proliferative and apoptotic signals

(**A**) Representative images of Ki67 staining (proliferative marker; top row) and TUNEL staining (apoptotic marker; bottom row) in 2 different end-stage rtTA/MIC tumours. Scale bar is 100 μm.

(**B**) Quantification of the staining shown in (A) expressed as the percentage of positive nuclei (Ki67, left axis; TUNEL, right axis). Bars represent averages for each parameter.

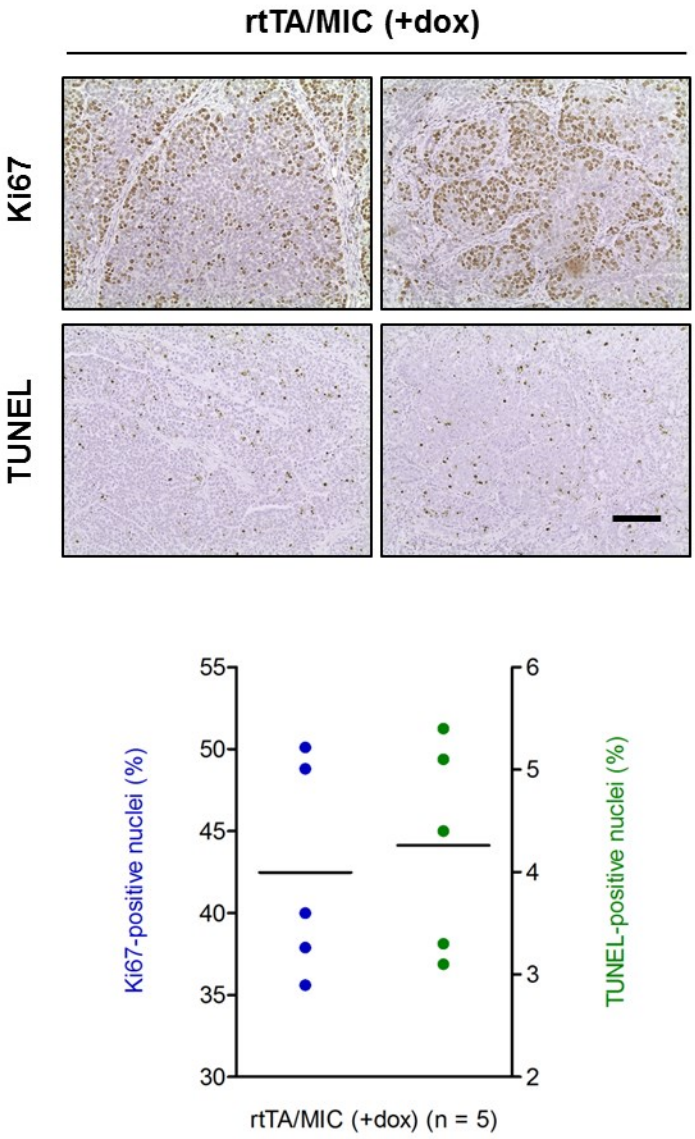
rtTA/MIC (+dox)
Ki67
TUNEL
55
50
45
40
35
30
6
5
4
3
2
Ki67-positive nuclei (%)
TUNEL-positive nuclei (%)
rtTA/MIC (+dox) (n = 5)

The rapid induction of rtTA/MIC lesions is associated with metastatic dissemination of tumour cells to the lung

One of the most useful features of the original constitutive PyV mT model is the ability of the mammary tumours to effectively metastasize to the lungs, an organ that is a common site of distal lesions in the human disease. To determine if rtTA/MIC mammary tumours were capable of forming pulmonary metastases, we examined step sections of the lung lobes from animals that had reached similar end-stage tumour burdens. All tumour-bearing mice presented with lung metastases, albeit to varying degrees, with some lungs harbouring only a few small lesions while others were made up almost entirely of secondary tumour tissue (Figure 5-9A). These lung lesions stained positively for PyV mT, confirming that they derived from the primary rtTA/MIC mammary tumour (Figure 5-9B). Interestingly, there was no correlation between the extent of metastasis and tumour burden, extending the idea that PyV mT tumours are heterogeneous in their transforming capabilities and may thus also be in terms of malignancy (data not shown) [142]. Taken together, these observations demonstrate that this inducible MIC model reproduces many of the pathological features of the original MMTV-PyV mT strain.

De-induction of the MIC transgene results in immediate tumour regression and eventual recurrence of doxycycline-independent masses

Another important feature of inducible systems is the capacity to "turn off" the oncogene by withdrawal of the inducing agent; one can then evaluate whether tumours regress and if they have the potential to recur in the absence of transgene expression. To test this in our model, doxycycline treatment was discontinued for a cohort of rtTA/MIC mice bearing end-stage

mammary tumours. Upon de-induction of PyV mT expression the tumours began to shrink rapidly (Figure 5-10A). By 10 weeks post-de-induction, most of the tumours had regressed to palpable masses that were no longer measurable. Interestingly, all of the de-induced rtTA/MIC mice eventually developed recurrent masses (15-50 weeks post-de-induction) and were sacrificed at burden endpoint. The number of measurable recurrent tumours arising was significantly less than the number of measurable masses the animal had prior to de-induction (Figure 5-10B). This suggests that the emergence of more focal, doxycycline-independent tumours in post-regression mice is a spontaneous event, in contrast to the consistent and complete penetrance of multifocal, doxycycline-dependent tumours driven by the inducible MIC transgene to all mammary glands of a given animal. Analysis of sections from mid-regression tumours and completely regressed mammary glands revealed relatively normal ductal structures surrounded by extensive stromal deposition and occasionally abnormal adipose tissue, which may explain why these glands remained palpable so long after de-induction (Figure 5-10C). Doxycycline-independent tumours arose only in rtTA/MIC mice and not in control animals de-induced at the same time, which remained normal (Figure 5-10D).

The morphology of the recurrent masses exhibited striking intra- and intertumoural heterogeneity, with individual tumours differing between animals and between tumours from the same mouse (Figure 5-11). Some histopathologies resembled pre-regression adenocarcinoma while others were more divergent, such as EMT-like and striated/punctate morphologies. All mice with recurrent tumours had evidence of lung metastases at sacrifice, varying in number, size and stage (data not shown). A single animal sacrificed prior to recurrent tumour development did not present with any metastases which suggests that, at least in this individual

Figure 5-9: rtTA/MIC end-stage tumours exhibit a high capacity for metastatic dissemination to the lungs

(**A**) H&E-stained whole lung sections representative of low, medium, and high levels of metastasis (left). The quantification of the number of metastatic lung lesions (left axis) and the percentage of lung tissue occupied by metastases (right axis) in rtTA/MIC animals at end-stage tumour burden is shown on the right. Bars represent the average value for each parameter.

(**B**) Representative lung lesion from a tumour-bearing rtTA/MIC animal stained with H&E (top row) and PyV mT (bottom row). An MMTV-NIC (NIC) lung lesion is shown as a negative control for PyV mT staining. Scale bar is 500 μm.

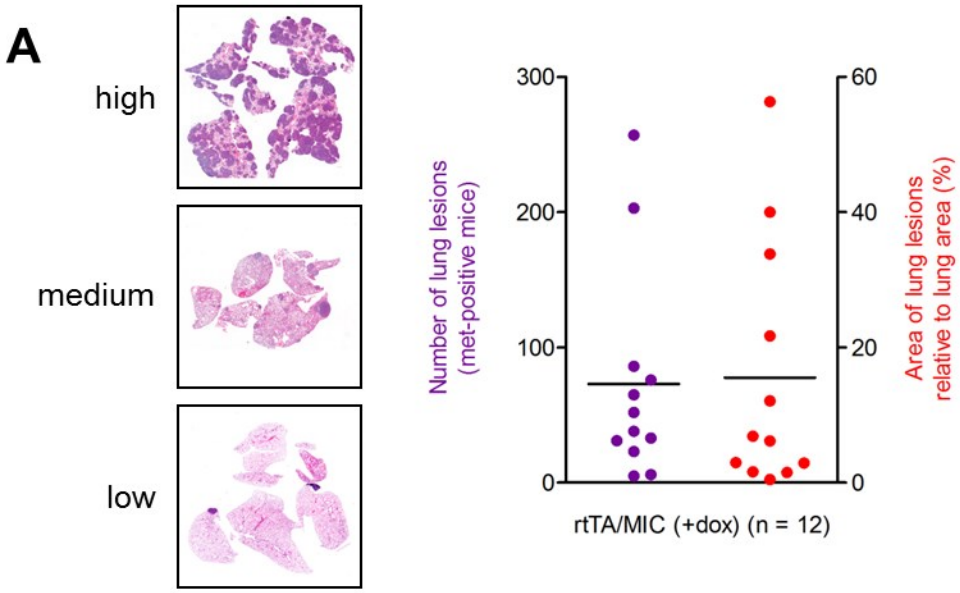
A
high
medium
low
Number of lung lesions (met-positive mice)
Area of lung lesions relative to lung area (%)
300
200
100
0
60
40
20
0
rtTA/MIC (+dox) (n = 12)
B
rtTA/MIC (+dox)
NIC
H&E
PyV mT

Figure 5-10: Doxycycline withdrawal in rtTA/MIC tumours leads to rapid regression and eventual spontaneous recurrence of masses

(**A**) Total tumour burden measured over time in rtTA/MIC mice prior to and following doxycycline withdrawal (indicated by the dotted line at time 0). Tumour-bearing mice were de-induced upon reaching burden endpoint. Each line represents an individual animal labeled by its ID number.

(**B**) Quantification of the number of measurable masses detected pre-regression (pre, +dox), at the point of maximum regression (mid, +dox → -dox), and at sacrifice (recurrent, +dox → -dox). Bars represent the average value at each time-point. The p value was calculated using a two-tailed t-test.

(**C**) H&E-stained sections of resected rtTA/MIC tumours undergoing regression (mid-regression or completely regressed) following doxycycline withdrawal. Scale bar is 100 μm.

(**D**) H&E-stained sections of normal mammary gland controls of the indicated genotypes post-doxycycline withdrawal. Scale bar is 100 μm.

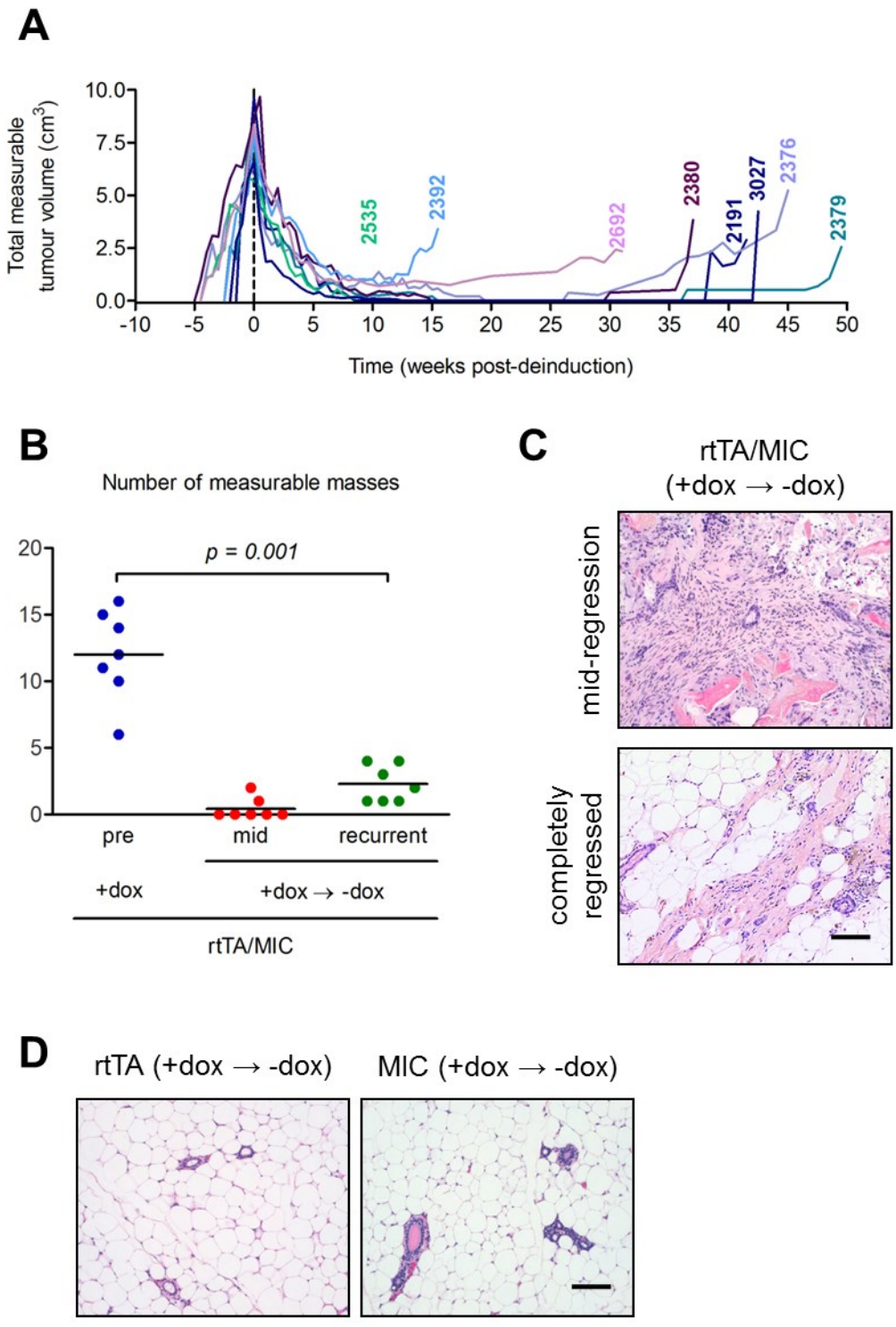
A
Total measurable tumour volume (cm3)
10.0
7.5
5.0
2.5
0.0
-10
-5
0
5
10
15
20
25
30
35
40
45
50
Time (weeks post-deinduction)
2535
2392
2692
2380
2191
3027
2376
2379
B
Number of measurable masses
p = 0.001
20
15
10
5
0
pre
mid
recurrent
+dox
+dox → -dox
rtTA/MIC
C
rtTA/MIC
(+dox → -dox)
mid-regression
completely regressed
D
rtTA (+dox → -dox)
MIC (+dox → -dox)

Figure 5-11: Recurrent masses from de-induced rtTA/MIC mice have variable histopathologies

An H&E panel of the different tumour morphologies observed in recurrent tumours arising in rtTA/MIC mice post-doxycycline withdrawal. The mouse ID number (followed by the tumour location in the case of multiple recurrences, e.g. "R1") and histopathology of the tumour are indicated for each image. A pre-regression rtTA/MIC doxycycline-dependent tumour exhibiting typical end-stage adenocarcinoma is shown for comparison (top left). Scale bar is 100 μm.

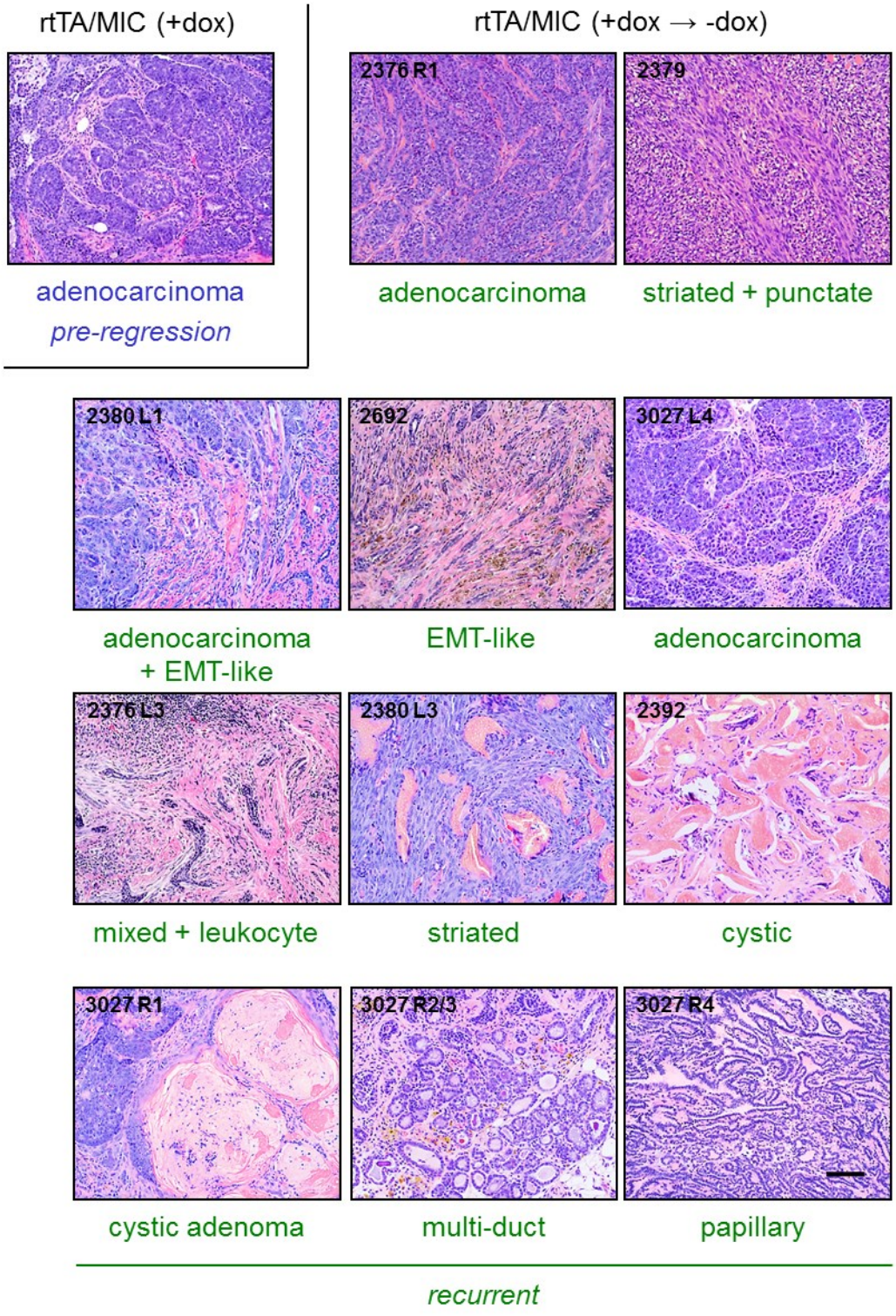
rtTA/MIC (+dox)
rtTA/MIC (+dox → -dox)
2376 R1
2379
adenocarcinoma
pre-regression
adenocarcinoma
striated + punctate
2380 L1
2692
3027 L4
adenocarcinoma
+ EMT-like
EMT-like
adenocarcinoma
2376 L3
2380 L3
2392
mixed + leukocyte
striated
cystic
3027 R1
3027 R2/3
3027 R4
cystic adenoma
multi-duct
papillary
recurrent

case, MIC-induced lung lesions may regress in parallel with the primary tumour upon doxycycline withdrawal.

To determine if the recurrent tumours were no longer dependent on the PyV mT oncogene, we subjected lysates to immunoblot analysis (Figure 5-12A). Two samples clearly showed detectable bands at the expected size for PyV mT (2376 R1 and 3027 L4), while weaker signals were observed in two other samples (2380 L1 and 2692); one sample appeared to be completely negative for PyV mT expression (2379). To achieve a more quantitative assessment of PyV mT levels, RT-qPCR was carried out on these and other recurrent tumours as well as corresponding metastatic lung lesions from two animals. We found that PyV mT transcript levels in the recurrent tumours reflected the protein levels obtained by immunoblotting (Figure 5-12B). For the most part, re-expression of the PyV mT transgene correlated with the incidence of adenocarcinoma in the tumour's corresponding histological section. The lack of complete correlation can be explained by the fact that we must use different pieces of a histologically heterogeneous tumour for different analyses. Interestingly, PyV mT transcript was detected in a metastatic lung lesion in addition to a recurrent tumour from the same animal (2376; Figure 5-12B); PyV mT protein expression in the lung lesions was confirmed by immunohistochemistry (data not shown). On the other hand, in an animal with a PyV mT-expressing recurrent tumour (2380 L1) and a non-expressing recurrent tumour (2380 L3), PyV mT transcript was undetectable in a metastatic lung lesion. This may reflect the presence of separate recurrent lesions that either re-expressed the transgene or arose in the absence of PyV mT transcript. It may additionally indicate the capability of non-PyV mT-expressing, recurrent mammary lesions to metastasize to the lungs, or the PyV mT-independent recurrence of an originally doxycycline-dependent lung metastasis *in situ*. We should note that the lower transcript levels of PyV mT

transgene in the rtTA/MIC tumours relative to that of the MMTV-PyV mT tumour are likely due to the different strengths of the promoters driving the transcription of the oncogene (TetON versus MMTV). This does not impact on overexpression of PyV mT protein in the inducible system, as evidenced by the strong levels detected by immunoblot and ultimately the fact that transformation occurs rapidly in the model (Figure 5-6B).

It appeared that while some recurrent tumours arose by re-expressing the PyV mT transgene, others did so by alternative mechanisms. In an attempt to identify these potential mediators of recurrence, we used an antibody array to analyse phospho-RTK levels in primary and recurrent tumour lysates and focused on candidates with relatively high fluorescence intensities, specifically Egfr, ErbB2, and Pdgfrβ (Figure 5-13). While not all candidates validated by immunoblotting, we did observe phosphorylation of both ErbB2 and Pdgfrβ in at least some of the recurrent tumours suggesting that RTK signalling was actively occurring (Figure 5-14). ErbB2 is known to be upregulated during mammary tumour progression in the MMTV-PyV mT model [143]. While we observed relatively low expression of ErbB2 in our samples as compared to an MMTV-NIC control lysate, the strong levels of phosphorylated ErbB2 in the doxycycline-independent rtTA/MIC recurrences may represent an avenue of recapitulating the signalling associated with PyV mT tumourigenesis in the absence of transgene re-expression. This may be the case for 2379, which also showed overexpression of c-Myc protein; interestingly, amplification of the c-Myc gene has been observed in a model of recurrence after de-induction of the doxycycline-dependent oncogene [367].

We wondered if genomic mutations had contributed to the development of recurrent tumours in our model. Mutations in the three Ras genes (*HRas*, *KRas*, and *NRas*) and in the p53 gene (*Trp53*) have been reported previously as mechanisms of recurrence in other doxycycline-

Figure 5-12: Re-expression of PyV mT correlates with the adenocarcinoma phenotype

(**A**) Immunoblot analysis of protein lysates from rtTA/MIC tumours prior to and following doxycycline withdrawal using antibodies directed to E-cadherin (epithelial content control), PyV mT, Cre recombinase and Hsp90 (loading control); the arrowheads indicate the specific bands for PyV mT and Cre recombinase. Resected tumours were used for pre- and mid-regression time-points ("pre" and "mid", respectively), while recurrent masses were harvested from mice sacrificed at clinical endpoint. Numbers correspond to the mouse ID (and tumour location if applicable) for each sample. The incidence of adenocarcinoma in the corresponding histological section for each sample is indicated below by a "+" symbol.

(**B**) *PyV mT* transcript level as assessed by qPCR on cDNA from primary (+dox; blue bars) and recurrent (+dox → -dox; green bars) rtTA/MIC tumours or lung lesions ("met"). Data were normalized to *Gapdh* transcript. Positive and negative controls were tumour cDNA from MMTV-PyV mT (PyV mT) and MMTV-NIC (NIC) mice, respectively (black bars). Error bars represent technical replicates (n = 3 for each sample). Numbers correspond to the mouse ID (and tumour location if applicable) for each sample. The incidence of adenocarcinoma in the corresponding histological section for each sample is indicated below by a "+" symbol.

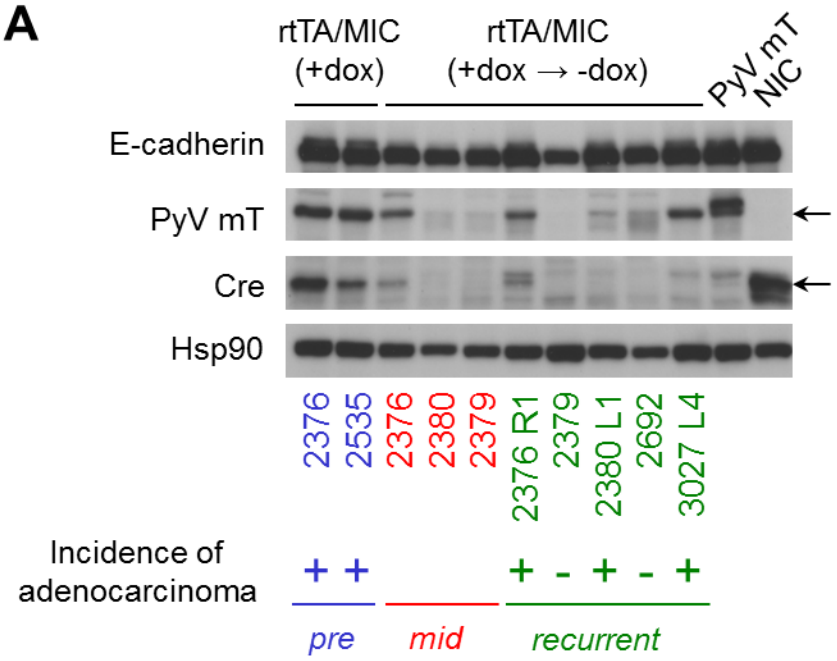
A
rtTA/MIC
(+dox)
rtTA/MIC
(+dox → -dox)
PyV mT
NIC
E-cadherin
PyV mT
Cre
Hsp90
2376
2535
2376
2380
2379
2376 R1
2379
2380 L1
2692
3027 L4
Incidence of
adenocarcinoma
+ +
+ - + - +
pre
mid
recurrent

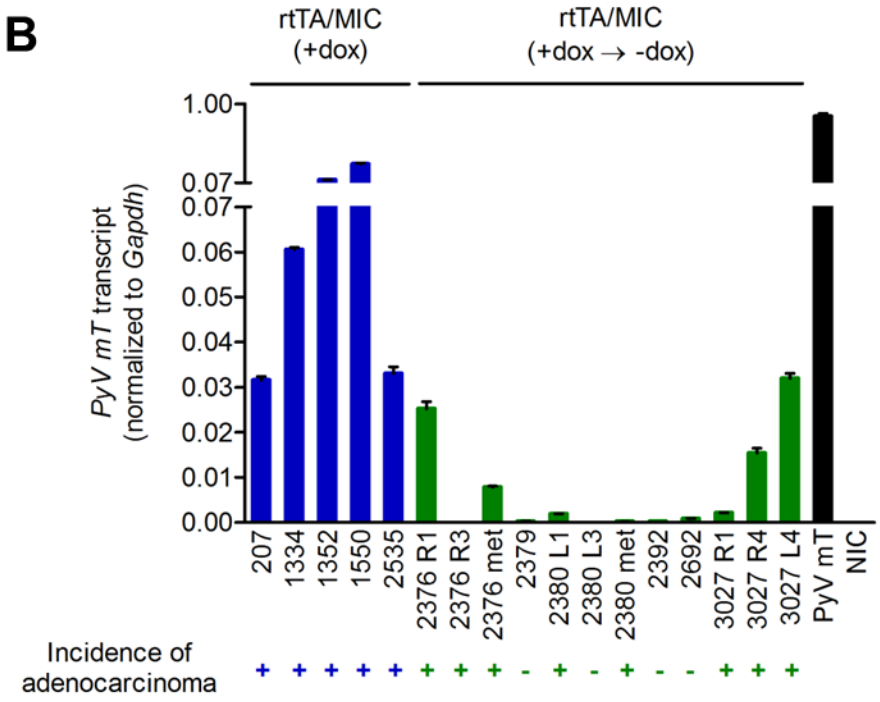
B
rtTA/MIC
(+dox)
rtTA/MIC
(+dox → -dox)
PyV mT transcript
(normalized to Gapdh)
1.00
0.07
0.07
0.06
0.05
0.04
0.03
0.02
0.01
0.00
207
1334
1352
1550
2535
2376 R1
2376 R3
2376 met
2379
2380 L1
2380 L3
2380 met
2392
2692
3027 R1
3027 R4
3027 L4
PyV mT
NIC
Incidence of
adenocarcinoma
+ + + + + + + + - + - + - - + + +

Figure 5-13: Doxycycline-independent masses in rtTA/MIC mice display RTK signalling that may represent mechanisms of recurrence

Levels of phosphorylated Egfr, ErbB2, and Pdgfrβ primary (+dox; blue bars) and recurrent (+dox → -dox; green bars) rtTA/MIC tumours as determined from a phospho-RTK array. Values represent fluorescence intensity of the probe on the array normalized to PBS (negative control probe). An MMTV-PyV mT (PyV mT) tumour was used as a control (black bar). Numbers correspond to the mouse ID (and tumour location if applicable) for each sample.

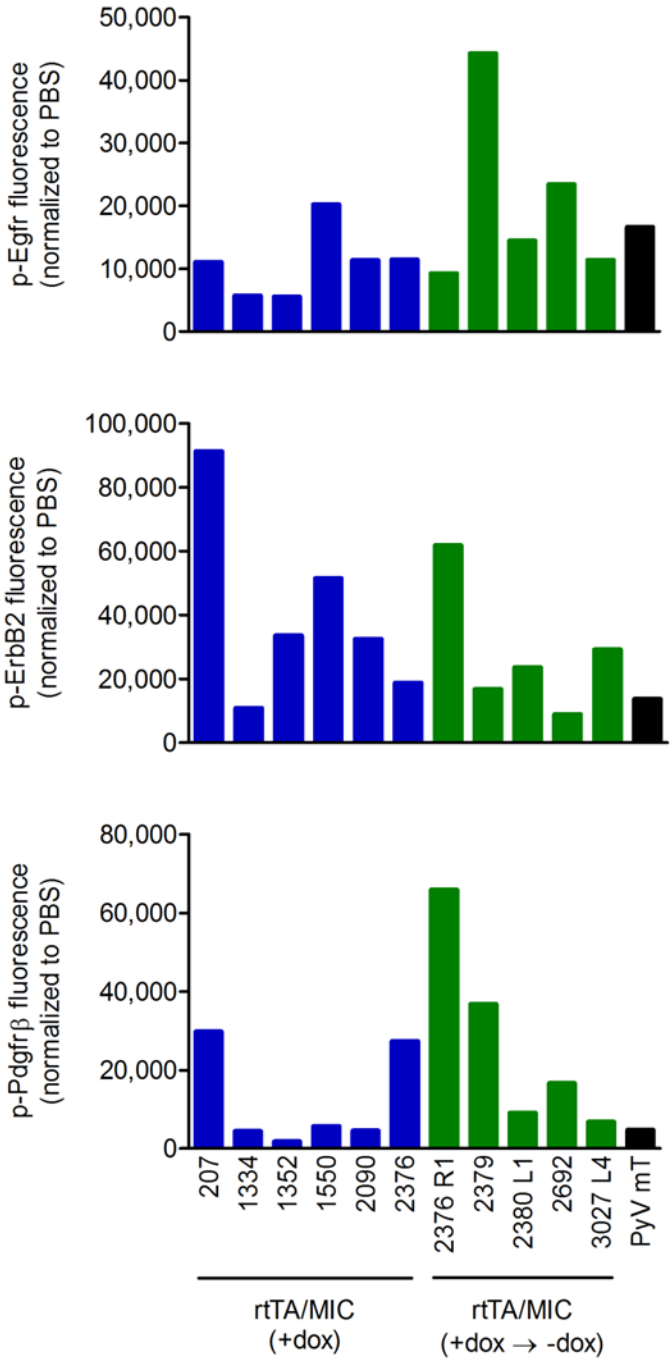
p-Egfr fluorescence (normalized to PBS)
50,000
40,000
30,000
20,000
10,000
0
p-ErbB2 fluorescence (normalized to PBS)
100,000
80,000
60,000
40,000
20,000
0
p-Pdgfrβ fluorescence (normalized to PBS)
80,000
60,000
40,000
20,000
0
207
1334
1352
1550
2090
2376
2376 R1
2379
2380 L1
2692
3027 L4
PyV mT
rtTA/MIC (+dox)
rtTA/MIC (+dox → -dox)

Figure 5-14: Activation of proto-oncogenic proteins in select recurrent rtTA/MIC tumours

Immunoblot analysis of protein lysates from rtTA/MIC tumours prior to and following doxycycline withdrawal using antibodies directed to phospho-ErbB2 (Y1248), ErbB2, phospho-Egfr (Y1068), Egfr, phospho-Pdgfrβ (Y1021), Pdgfrβ, c-Myc and Hsp90 (loading control). Resected tumours were used for pre- and mid-regression time-points ("pre" and "mid", respectively), while recurrent masses were harvested from mice sacrificed at clinical endpoint. Numbers correspond to the mouse ID (and tumour location if applicable) for each sample. The incidence of adenocarcinoma in the corresponding histological section for each sample is indicated by a "+" symbol.

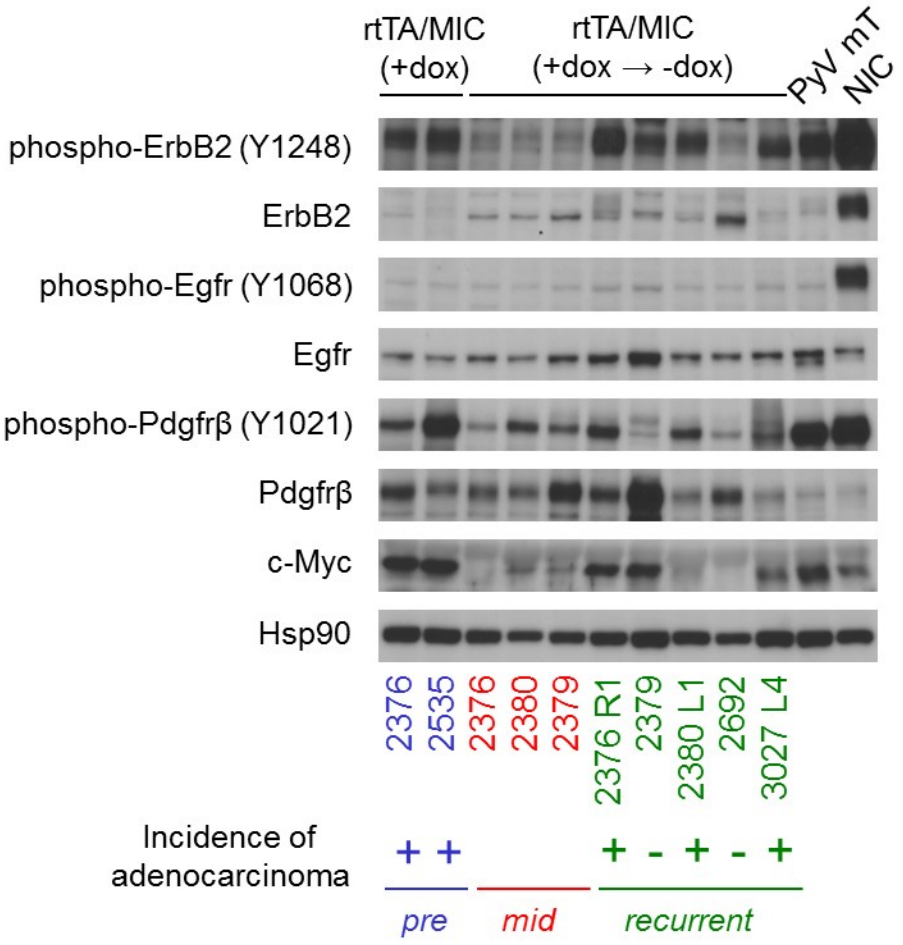
rtTA/MIC
(+dox)
rtTA/MIC
(+dox → -dox)
PyV mT
NIC
phospho-ErbB2 (Y1248)
ErbB2
phospho-Egfr (Y1068)
Egfr
phospho-Pdgfrβ (Y1021)
Pdgfrβ
c-Myc
Hsp90
2376
2535
2376
2380
2379
2376 R1
2379
2380 L1
2692
3027 L4
Incidence of
adenocarcinoma
+ +
+ - + - +
pre
mid
recurrent

inducible mammary tumour models [72, 465]. Sequencing of doxycycline-dependent and -independent rtTA/MIC tumours revealed no mutations in exons 2 and 3 of *Ras* (data not shown). We identified a single recurrent rtTA/MIC tumour harbouring an arginine to cysteine substitution (R245C) in *Trp53* which corresponds to a frequent mutation found in human cancer at residue R248 (data not shown). Despite the low frequency of this mutation in our panel of samples, it demonstrates that mutations in tumour suppressor genes of relevance to human cancer can drive recurrence in the rtTA/MIC model. It is possible that other genetic aberrations might be uncovered with additional sequencing analyses.

Collectively these data illustrate that, while we can demonstrate rapid tumour regression in rtTA/MIC animals by withdrawal of doxycycline, the emergence of doxycycline-independent tumours ultimately transpires. This can be attributed in at least some cases to the reactivation of the PyV mT transgene and corresponds with an adenocarcinoma phenotype. In other cases, tumour recurrence may be associated with activation of RTK signalling. The results of our sequencing analysis demonstrated that other genetic aberrations could be driving recurrence. These molecular alterations may confer the divergence in tumour morphologies that we observed upon recurrence. Of note, the recurrent mass with the p53 mutation (R245C) happened to be an adenocarcinoma with EMT-like features which resembles the spindle morphologies seen in mammary tumour mouse models driven by p53 loss (Figure 5-11) [466].

Table 5-1: Comparison of features between the constitutive MMTV-PyV mT/Cre recombinase model and the inducible rtTA/MIC model

	MMTV-PyV mT/ MMTV-Cre recombinase	**MMTV-rtTA/TetO-MIC (rtTA/MIC [+Dox])**
PyV mT transgene promoter	Mouse mammary tumour virus (MMTV)	Tetracycline operator (TetO)
Inducible transgene expression	No	Yes
Coupling to Cre recombinase	No	Yes
Time when 50% of animals have tumours (T_{50})	40 days of age [109]	7 days of induction
Tumour pathology	Solid adenocarcinoma [141, 143]	Solid adenocarcinoma
Cre recombinase expression and function in PyV mT tumour cells (by β-galactosidase assay)	0% when conditional gene is essential for tumourigenesis [[108-110]	100%
Percentage of tumour-bearing mice with lung metastases	93.3% [109]	100%

5.3 Discussion

The development of inducible transgene systems for *in vivo* studies has made it possible to more accurately model human diseases. The ability to control transgene expression in mice allows the researcher to initiate tissue-specific changes at relevant time-points and, in the case of oncogenic transgenes such as PyV mT, mimic disease initiation (induction) and treatment (de-induction). The TetO-PyV mT-IRES-Cre recombinase (MIC) strain generated in our laboratory not only utilizes inducible expression of the PyV mT oncoprotein, but incorporates Cre recombinase-mediated genetic changes as well, due to the bi-cistronic linking of these transgenes. In this study, we have chosen a mammary epithelial-specific rtTA (MMTV-rtTA) to characterize a new model of mammary tumourigenesis driven by the MIC transgene [424].

Induction of rtTA/MIC mice with doxycycline led to the rapid onset of invasive mammary tumours in the majority of animals. MIC-expressing lesions developed in a stepwise fashion that resembled the progression observed in the constitutive MMTV-driven model of PyV mT tumourigenesis (MMTV-PyV mT). Notably, earlier lesions displayed more uniform staining of PyV mT and Cre recombinase protein and at a higher intensity than carcinoma stages, suggesting a potential dampening of transgene expression once the tumour has progressed (Figure 5-6A). There may be a reduced requirement for strong PyV mT levels in an advanced lesion due to the presence of other genetic aberrations. Despite a rapid tumour onset, it may be possible for cooperating genetic or epigenetic events to occur in this short time period; in fact, constitutive expression of PyV mT was shown to be insufficient for transformation without additional changes in endogenous genes [142]. This hypothesis may be extended to the expression of Cre recombinase. The homogenous staining of rtTA/MIC mammary tumours obtained in the X-gal assay contrasts with the heterogeneous Cre recombinase expression

determined by immunohistochemistry, which may simply be due to inherent differences between the two analyses (Figure 5-6A; Figure 5-7B). We suspect that all of the mammary epithelial cells in these animals expressed Cre recombinase at some point at least once given that 100% of the tumour epithelium is positive for the β-galactosidase reporter, however, as Cre recombinase is only required for the initial recombination event, its expression may have been turned off during tumour progression.

One important difference between the inducible PyV mT model and the conventional MMTV-PyV mT model is that tumour development in our inducible PyV mT model was not 100% penetrant. A proportion of the animals in our cohort either developed masses much later than 16 weeks post-induction or had no palpable masses prior to 1 year post-induction (Figure 5-2). Despite the longer latency, the tumours from the late onset group resembled early onset tumours in terms of progression, metastatic capacity, and MIC transgene expression (data not shown; Figure 5-6B). The delayed onset in some rtTA/MIC mice contrasts with the complete penetrance observed in both the MMTV-PyV mT strain and the previously published inducible PyV mT strain (TetO-PyV mT-IRES-Luciferase) [73, 141]. An initial explanation would be that the discrepancy is due to differences in the number and/or location of transgene integration site(s), especially given that specific loci appear to be more permissible than others. Another possible explanation is that the rtTA is non-responsive in certain transgene carriers. However, this is not likely the case, as demonstrated by the robust induction of hyperplastic lesions in mammary gland wholemounts from 100% (19/19) of animals following 2 weeks of doxycycline administration (Figure 5-3A). Analysis of mammary gland sections at this time-point revealed that the ducts were almost exclusively abnormal (either hyperplastic or filled), in contrast to only normal ducts in a control animal (Figure 5-3). These data argue that the observed incomplete

tumour penetrance is not due to technical issues with the inducible MIC system but rather reflect the natural history of tumour development and progression in this model. An additional theory for the difference in tumour penetrance deals with the fact that PyV mT and Cre recombinase are expressed during adulthood and may be subject to immune rejection, in contrast to the pre-pubescent onset of PyV mT expression in the conventional MMTV-PyV mT model. We may have some evidence to support this hypothesis: unpublished experiments in our laboratory have found that MMTV-NIC mammary tumour cells do not grow in immune-competent mice, while they readily propagate in immune-compromised hosts (e.g. NCr, SCIDbeige) or in a tolerant environment, such as the MMTV-Cre recombinase strain. Moreover, MMTV-NDL mammary tumour cells, which lack Cre recombinase but express the same ErbB2/Neu oncogene used in the MMTV-NIC model, are tolerated in an FVB/N background (unpublished observations; Muller, WJ). Future studies investigating the sustainability of rtTA/MIC mammary epithelial cells in immune-deficient mice should allow this issue to be addressed.

The inducibility of the MIC transgene and mammary tumour progression in our model was found to be reversible upon withdrawal of doxycycline; however tumour recurrence became a reproducible phenomenon in de-induced animals (Figure 5-10). It is possible that the accruement of additional genetic lesions during doxycycline-dependent tumour progression allowed the regressed mammary glands to reinitiate tumourigenesis. Unlike typical end-stage rtTA/MIC mammary tumours, the recurrent masses were often focal and the remarkable array of histopathologies documented was unexpected, particularly considering the homogeneous nature of the initial doxycycline-dependent tumours which all presented as adenocarcinoma at end-stage (Figure 5-11). As revealed by immunoblotting and RT-qPCR analyses of recurrent tumour lysates, reactivation of signalling may be attributable to re-expression of the MIC transgene in

some cases (Figure 5-12). Indeed, reactivation of inducible transgenes as a consequence of mutations in the rtTA has been reported previously and may present a possible explanation for a subset of our recurrent tumours [73]. From a clinical standpoint, the fact that tumours can evolve in the absence of PyV mT reactivation recapitulates the well-established problem of therapeutic resistance in breast cancer. The PyV mT oncogene is widely regarded as an RTK mimic and so the recurrence experiment could be thought of as another way of modelling recurrence of RTK-driven breast cancer upon chronic administration of an RTK inhibitor. Indeed, several of the recurrent tumours (including a non-PyV mT-expressing sample) showed expression and/or activation of known proto-oncogenes (Figures 5-13, 5-14). We also observed a mutation in the *Trp53* tumour suppressor gene in a single recurrent sample. The fact that none of the primary doxycycline-dependent tumours that we analyzed harboured this genetic event suggests that it may be associated with recurrence in this case. In summary, our rtTA/MIC model of de-induction appears to be a valuable system for investigating clinical treatment and relapse.

We have demonstrated that our novel MIC mouse strain in conjunction with the MMTV-rtTA is a suitable model of PyV mT mammary tumourigenesis with the added benefit of temporal regulation. Our rtTA/MIC mice can be induced to develop metastatic tumours in a classical stepwise fashion, closely recapitulating the human disease. A brief comparison of our new model with the original, constitutive MMTV-PyV mT strain emphasizes the greater experimental practicality of the former (Table 5-1). In addition to the inherent improvements to the mouse model design (i.e. inducibility of the oncogene combined with coupling to Cre recombinase), tumour initiation begins just days after induction of the MIC transgene with complete penetrance to all mammary glands. Importantly, the rtTA/MIC model maintains key desirable traits of its predecessor in terms of tumour progression, in particular, the invasive,

metastatic nature of PyV mT mammary tumour cells to distal sites such as the lungs. Perhaps the most useful feature of the MIC strain is that it can be used to study the effect of Cre recombinase-dependent genetic alterations on PyV mT-mediated transformation in any tissue with the appropriate rtTA, making this an important clinical tool for studying many types cancer in the mouse.

6 Genetic ablation of PI3K p110α in a mouse model of PyV mT mammary tumourigenesis

6.1 Introduction

PI3K activity was first discovered in association with the viral oncogene PyV mT (ref!). Indeed, it has been well established that PI3Ks are directly recruited to PyV mT and that this signalling axis is a key mediator of PyV mT-induced mammary tumourigenesis and metastasis in mice [193, 194, 374]. Furthermore, transformation of mammary epithelial cells *in vitro* appears to be specifically dependent on the α isoform of p110 [375]. Previous studies have indicated p110α is likely required for mammary tumourigenesis in conditional p110α mice expressing PyV mT and Cre on separate MMTV-driven transgenes; tumours develop in these animals that have lost Cre expression and thus retain p110α [114]. This system allowed for the study of $p110\alpha^{flx/wt}$/PyV mT/Cre animals which exhibited a profound delay in tumour initiation in only 20% of the cohort as compared to wildtype PyV mT mice.

Having characterized a new Cre recombinase-coupled version of a PyV mT mammary tumour mouse model (MMTV-rtTA/TetOMIC; described in the previous chapter), we could finally address whether complete ablation of p110α could affect PyV mT-driven tumourigenesis *in vivo*. In doing so we also hoped to validate our findings from Chapter 4 where we identified p110α as a critical effector of activated ErbB2/Neu during mammary tumourigenesis. By using a PyV mT-driven mouse model, where mammary tumourigenesis progresses through distinct histopathological stages that are reminiscent of lesions in human breast cancer, we have the opportunity to identify the phase at which p110α is required during progression [143, 144]. This feature is not readily offered by the MMTV-NIC model where it is difficult to capture definitively early stage lesions (Figure 4-6). In addition, PyV mT-induced mammary tumours are highly metastatic to the lung and therefore the rtTA/MIC strain is also useful for confirming the effect of p110α loss on lung metastasis that we observed in the NIC strain (Figures 4-9 and 5-

9) [109, 144]. A final advantage to using an inducible model is that we can avoid potential defects in mammary gland development that may be incurred by loss of p110α, which was encountered in the PyV mT/Cre background [114]. Indeed, we were able to corroborate our results from Chapter 4, demonstrating that p110α is important for mammary tumour initiation and metastasis downstream of both activated ErbB2 and PyV mT oncogenes (unpublished observations, T Rao and WJ Muller).

6.2 Results

PI3K p110α is critical for PyV mT-mediated tumour initiation in the newly characterized rtTA/MIC inducible mouse model

The conditional p110α strain introduced in Chapter 4 was bred to the rtTA/MIC model described in Chapter 5 (Figure 6-1). rtTA/MIC mice were generated that were wildtype, heterozygous or homozygous for the p110α floxed alleles. Experimental animals and additional controls (induced rtTA or MIC; un-induced rtTA/MIC) were induced with doxycycline water (2 mg/mL) between the ages of 8 and 16 weeks. It was immediately apparent from physical palpations that $p110\alpha^{flx/flx}$/rtTA/MIC mammary glands were absolved from the very rapid and complete transformation that was occurring in wildtype cohorts. To confirm this observation at a histological level, mice were sacrificed after 2 weeks of doxycycline induction, a timepoint when all wildtype rtTA/MIC animals should exhibit transformed mammary glands (Figure 5-3). At necropsy, all mammary glands were excised from each mouse and weighed to obtain a rudimentary measurement of transformation. A significant decrease in mammary gland weight normalized to total body weight was calculated for p110α-deficient/rtTA/MIC cohorts as

Figure 6-1: Conditional loss of PI3K p110α in the rtTA/MIC model

Breeding strategy to generate mice with mammary epithelial-specific expression of PyV mT and ablation of PI3K p110α (*PIK3CA*). The conditional p110α strain (Flox- p110α) carries a p110α allele in which exon 1 is flanked by LoxP sites [276]. When crossed with mice that are bigenic for MMTV-rtTA [424]; "rtTA") and TetO-MIC [144]; "MIC"), the conditional p110α allele(s) will undergo Cre-mediated recombination specifically in the mammary epithelium. Single transgene carriers (rtTA or MIC) were generated to serve as doxycycline-induced controls alongside un-induced bigenic controls.

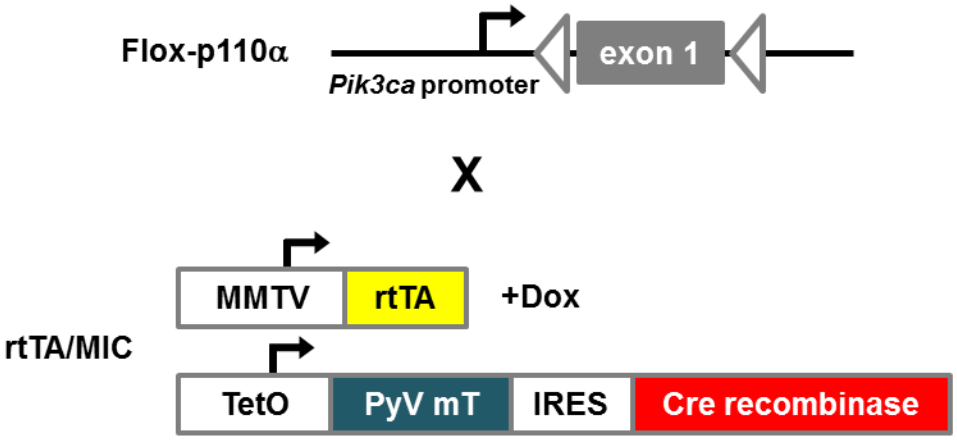
Flox-p110α
exon 1
Pik3ca promoter
X
rtTA/MIC
MMTV
rtTA
+Dox
TetO
PyV mT
IRES
Cre recombinase

compared to wildtype rtTA/MIC mice and relative weights for homozygous animals were similar to that obtained for controls (Figure 6-2A). The inguinal mammary glands were then wholemounted and stained for H&E; a very dramatic impairment in transformation was observed with p110α loss in a dose-dependent manner (Figure 6-2B, top and middle). While mammary glands from wildtype rtTA/MIC animals were fully transformed and devoid of normal ductal structures, $p110\alpha^{flx/wt}$/rtTA/MIC glands exhibited abnormalities to a lesser extent with an overall thickening of the ducts. Perhaps most striking was the completely normal ductal organization in p110α-null/rtTA/MIC glands, resembling the phenotype from an induced control mouse. The inclusion of the Cre recombinase-activated GFP reporter transgene allowed for fluorescence imaging of the mammary ducts in these animals and provided indirect proof of MIC transgene expression (Figure 6-2B, bottom).

We further characterized tumourigenesis at the 2 week induction timepoint by analyzing histological sections of mammary glands, which confirmed the phenotypes we had observed at the anatomical level (Figure 6-3A). Wildtype and heterozygous rtTA/MIC glands were filled with early PyV mT-type lesions, while the homozygous group was comprised solely of normal ducts similar to the control. Since we had observed a haploinsufficient effect of p110α, we were interested to see if the distribution of early lesions was affected when compared to wildtype rtTA/MIC samples. The majority of ducts in both $p110\alpha^{wt/wt}$ and $p110\alpha^{flx/wt}$/rtTA/MIC mammary glands were hyperplastic or filled, with little or no normal ducts counted (Figure 6-3B). By contrast, ducts were exclusively normal in homozygous mice and controls. These findings collectively indicated that p110α plays a role in initiating tumours in this PyV mT model. Cre recombinase-mediated excision of the conditional p110α allele in these animals was verified by PCR amplification in p110α-deficient/rtTA/MIC mammary gland DNA (Figure 6-

4A). It should be noted that GFP reporter expression was detectable in mammary gland wholemounts as early as 3 days post-induction (Figure 6-4B). The wildtype rtTA/MIC sample in this figure exhibits evidence of ductal abnormalities even at this early timepoint, whereas the p110α$^{flx/flx}$/rtTA/MIC gland appears normal.

Eventual mammary tumour development in p110α$^{flx/flx}$/rtTA/MIC mice occurs in less than half of the cohort

To determine if tumours would ultimately arise in rtTA/MIC homozygous for p110α loss, we subjected cohorts to long-term induction (up to 18 months). Consistent with previous tumour onset data, the majority of wildtype rtTA/MIC mice developed tumours within 2 weeks of starting doxycycline treatment and all controls remained tumour-free (Figure 6-5; Figure 5-2). A significant delay in average tumour onset by over 2 months was seen in heterozygous cohorts, although there was no difference in penetrance. Tumours eventually developed in 6 out of 19 (31.6%) p110α$^{flx/flx}$/rtTA/MIC animals after long latencies with the average onset being well over 1 year of induction.

Similar to our observations in the NIC model, p110α-deficiency had an effect on tumour burden in the rtTA/MIC strain. As discussed in Chapter 5, we chose to use a total tumour volume of at least 4 cm^3 as the endpoint in the rtTA/MIC model and attempted to apply this to our p110α studies. The wildtype rtTA/MIC cohort and most of the heterozygous animals surpassed this minimum volume due to the development of multifocal masses. However, tumours were more focal in some p110α$^{flx/wt}$/rtTA/MIC mice as well as the entire homozygous cohort; in these cases, single masses often reached the 2.5 cm^3 limit set by animal care guidelines

Figure 6-2: After 2 weeks of induction, mammary glands from p110α-deficient/rtTA/MIC mice exhibit reduced transformation as compared to wildtype counterparts

(**A**) Mammary gland mass relative to body mass was calculated at sacrifice for each animal of the indicated genotypes and controls (induced rtTA and MIC; un-induced rtTA/MIC). Error bars are standard error of mean. P values were calculated using a two-tailed t-test.

(**B**) Representative H&E-stained mammary gland wholemounts from mice of the indicated genotypes as compared to an induced control mammary gland (top two rows). The middle row images are higher magnifications of the top row images. Fluorescence from a Cre recombinase-activated GFP reporter transgene is shown in the corresponding glands in the bottom row images. Scale bars from top to bottom are 5 mm, 0.5 mm, and 1 mm.

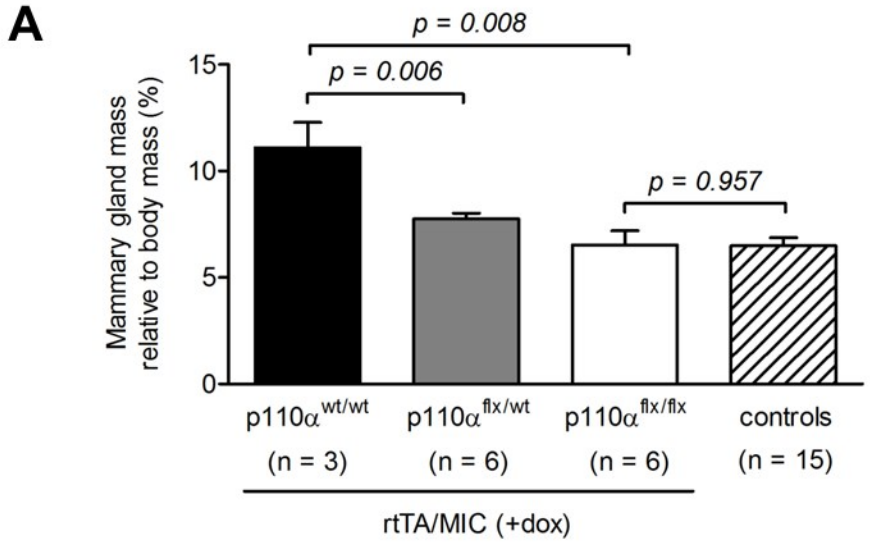
A
p = 0.008
p = 0.006
p = 0.957
Mammary gland mass relative to body mass (%)
15
10
5
0
p110α wt/wt
p110α flx/wt
p110α flx/flx
controls
(n = 3)
(n = 6)
(n = 6)
(n = 15)
rtTA/MIC (+dox)

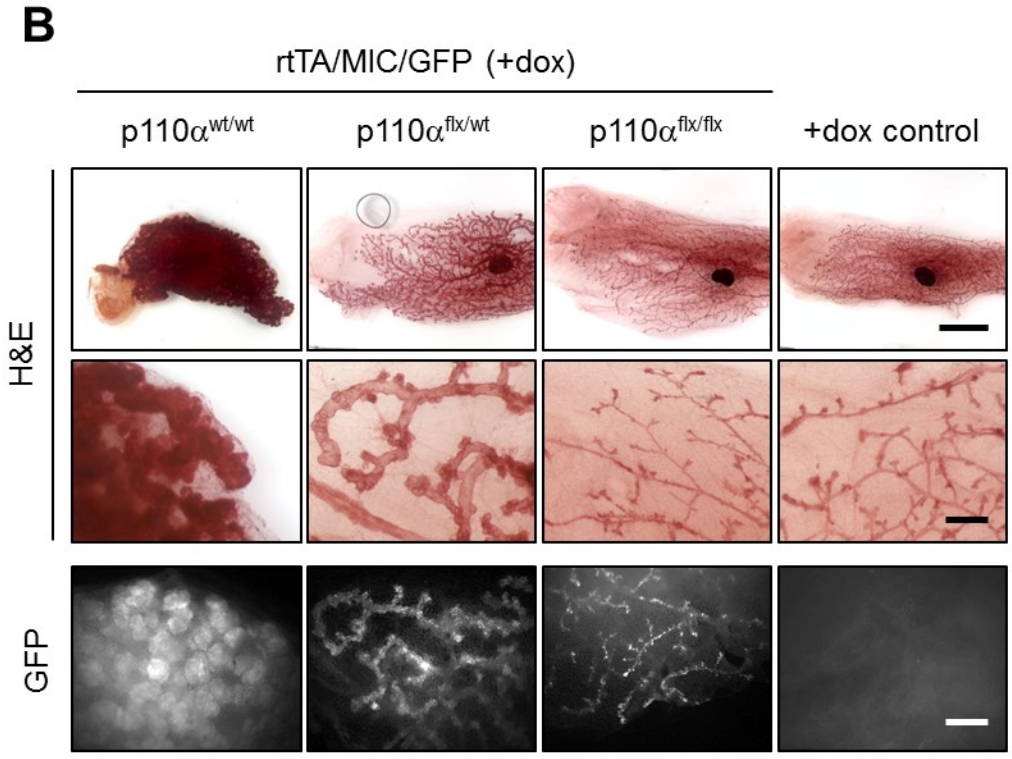
B
rtTA/MIC/GFP (+dox)
p110α wt/wt
p110α flx/wt
p110α flx/flx
+dox control
H&E
GFP

Figure 6-3: p110α-null/rtTA/MIC mice induced for 2 weeks have histologically normal mammary glands in contrast to wildtype and heterozygous groups

(**A**) Representative mammary gland sections stained with H&E from the indicated genotypes and an induced control animal. The bottom images are higher magnifications of the top images. Scale bars are 500 μm (top) and 100 μm (bottom).

(**B**) Quantification of the number of normal, hyperplastic, enlarged, and filled ducts expressed as an average percentage of the total number of ducts for the sections shown in (A).

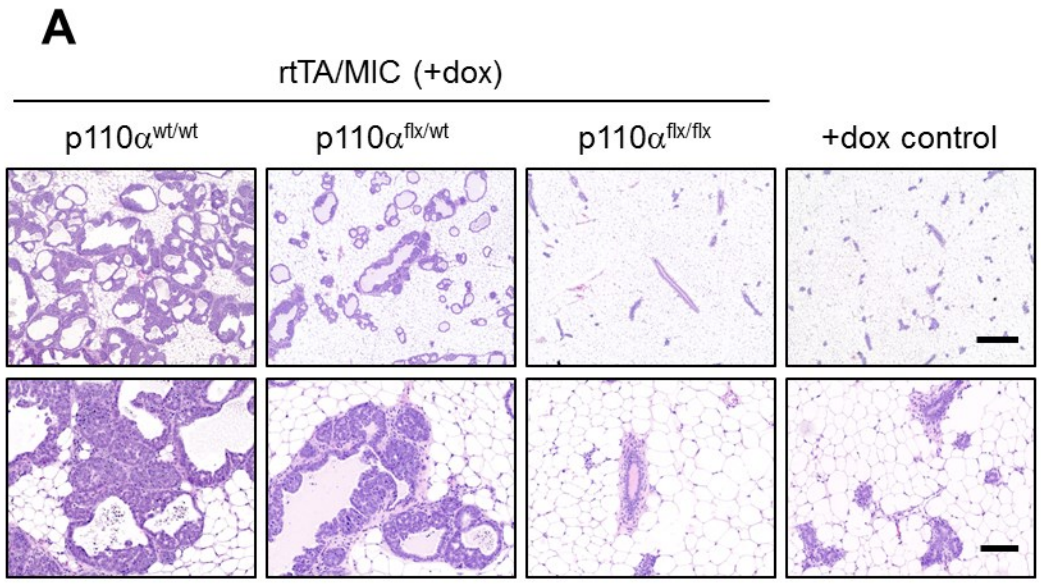
A
rtTA/MIC (+dox)
p110α^wt/wt
p110α^flx/wt
p110α^flx/flx
+dox control

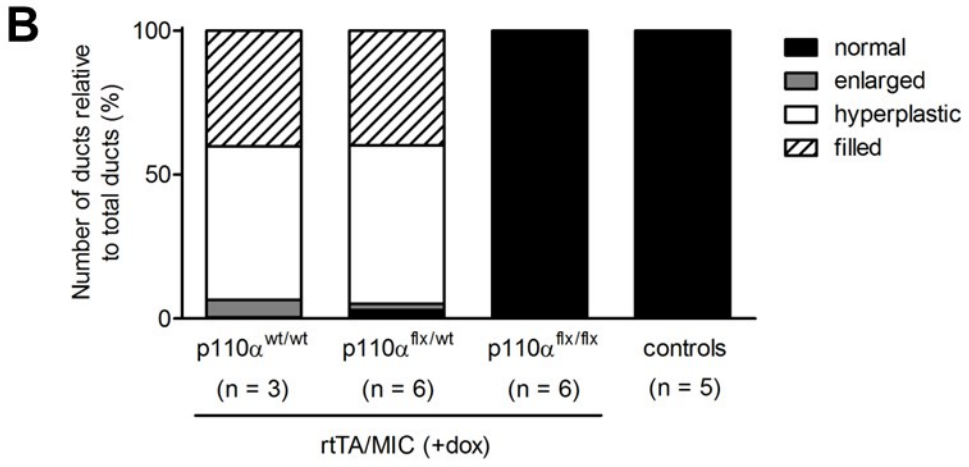
B
Number of ducts relative to total ducts (%)
100
50
0
normal
enlarged
hyperplastic
filled
p110α^wt/wt
(n = 3)
p110α^flx/wt
(n = 6)
p110α^flx/flx
(n = 6)
controls
(n = 5)
rtTA/MIC (+dox)

Figure 6-4: Evidence of excision of the conditional p110α allele in mammary glands of induced p110α$^{flx/flx}$/rtTA/MIC mice

(**A**) The Cre recombinase-excised p110α allele is detectable in mammary gland DNA from rtTA/MIC mice heterozygous and homozygous for the conditional p110α allele. Mice were treated with doxycycline for 2 weeks.

(**B**) Fluorescence from the Cre-inducible GFP reporter is observed 3 days post-induction in mammary gland wholemounts from mice of the indicated genotypes. Scale bar is 1 mm.

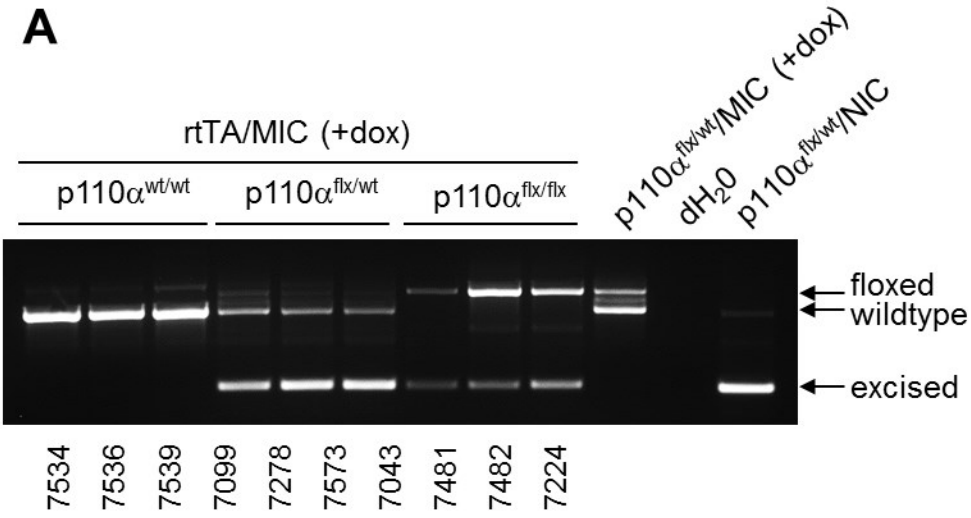
A
rtTA/MIC (+dox)
p110α^wt/wt
p110α^flx/wt
p110α^flx/flx
p110α^flx/wt/MIC (+dox)
dH20
p110α^flx/wt/NIC
floxed
wildtype
excised
7534
7536
7539
7099
7278
7573
7043
7481
7482
7224

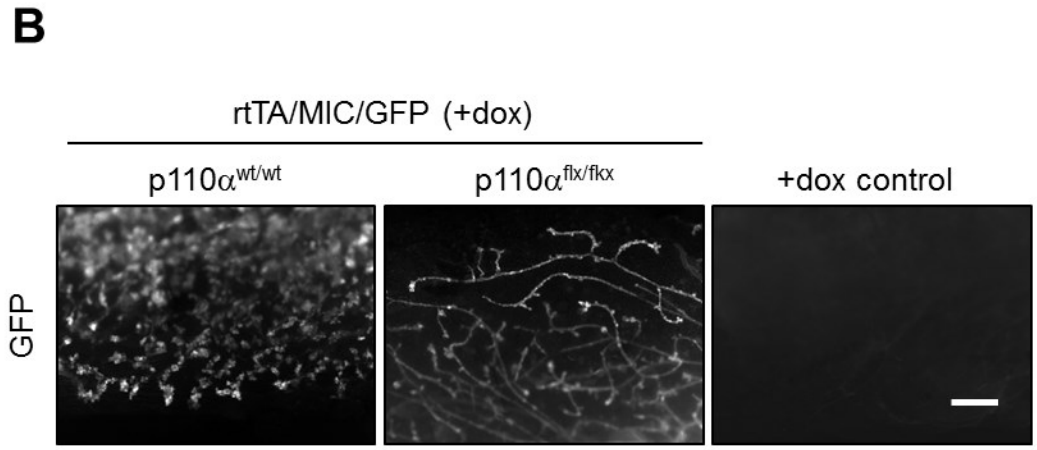
B
rtTA/MIC/GFP (+dox)
p110α^wt/wt
p110α^flx/fkx
+dox control
GFP

Figure 6-5: Homozygous ablation of p110α in the rtTA/MIC model results in ~30% of animals developing tumours and only after a long latency

Kaplan-Meier tumour onset curve for induced rtTA/MIC mice that are wildtype, heterozygous, or homozygous for the p110α conditional allele as compared to controls (un-induced rtTA/MIC; induced or un-induced rtTA or MIC). The table lists the penetrance (the percentage/number of animals that developed tumours), T_{50} (days of induction when 50% of animals have developed tumours), and average tumour onset with standard deviation for each of the curves shown on the graph. P values were calculated using a two-tailed t-test.

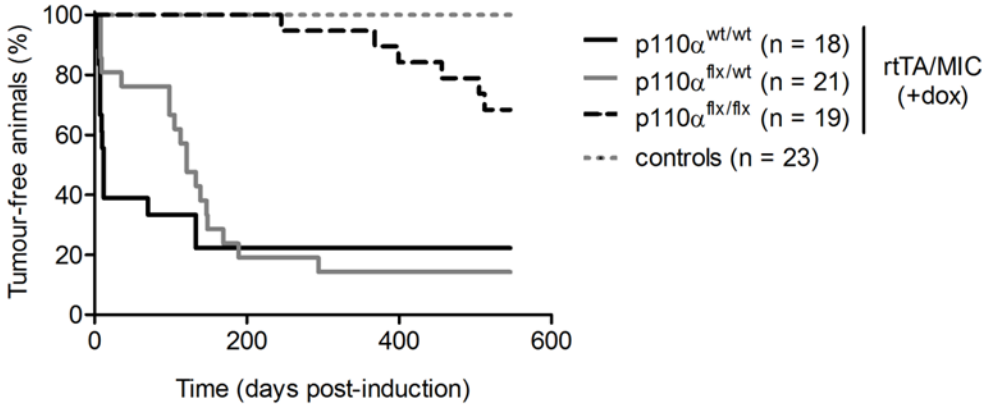

rtTA/MIC (+dox)	Penetrance	T_{50} (days post-induction)	Average onset (days post-induction)
$p110\alpha^{wt/wt}$	77.8% (14/18)	12	31 ± 47.0
$p110\alpha^{flx/wt}$	85.7% (18/21)	121	108 ± 74.9 (*p = 0.0020*)
$p110\alpha^{flx/flx}$	31.6% (6/19)	n/a	414 ± 100.5 (*p < 0.0001*)

and had to be sacrificed prematurely. For this reason, overall tumour burden at endpoint (as measured by volume and number) was significantly reduced in p110α-deficient/rtTA/MIC mice as compared to wildtype counterparts (Figure 6-6).

Histological analysis of heterozygous rtTA/MIC tumours revealed adenocarcinoma morphologies similar to what we have seen previously in wildtype rtTA/MIC tumours (Figure 6-7, top). By contrast, tumours from p110α$^{flx/flx}$/rtTA/MIC mice displayed intratumoural heterogeneity although all samples commonly exhibited areas of adenocarcinoma-like lesions infiltrated by a high degree of stromal cells and ECM deposition (Figure 6-7, bottom). Our inability to detect loss of p110α by immunoblot is likely due to the excessive stromal component in these bulk tumour lysates, precluding interpretation of Akt activation from this analysis as well (Figure 6-8A). Interestingly, expression of E-cadherin was slightly reduced in one p110α$^{flx/flx}$/rtTA/MIC lysate (#7880). We were able to confirm PyV mT expression in all genetic groups and could detect the recombined p110α allele in DNA from p110α-deficient/rtTA/MIC tumours (Figure 6-8A and B, respectively) (see schematic in Figure 4-2 for PCR design).

Heterozygous loss of p110α affects the size but not the number of lung lesions in rtTA/MIC tumour-bearing mice

All rtTA/MIC mice with tumour burdens of at least 4 cm3 developed pulmonary metastases, including those heterozygous for p110α (Figure 6-9A). One tumour-bearing homozygous mouse presented with a lung lesion, however as no animals in the cohort reached the burden limit they cannot be directly compared to the wildtype or heterozygous mice (Figure 6-6, top). Upon quantification of the lung metastases, we saw that there were no significant differences in

the number of lesions between wildtype rtTA/MIC and p110α$^{flx/wt}$/rtTA/MIC lungs in metastasis-positive animals (Figure 6-9B, top right). However the average size of lesions relative to the total lung area was significantly less in the heterozygous mice as compared to the wildtype rtTA/MIC group (Figure 6-9B, bottom right). This suggests that while p110α$^{flx/wt}$/rtTA/MIC tumour cells can probably colonize the lung as well as wildtype counterparts, they are impaired in their ability to grow and establish in this secondary site. This speculation will have to be tested using a lung colonization assay, especially considering the decreased tumour burden in heterozygous mice relative to wildtypes.

OPN is expressed in endstage rtTA/MIC tumours regardless of p110α status

The upregulation of OPN in some of our p110α$^{flx/flx}$/NIC tumours prompted us to investigate this in our rtTA/MIC system. OPN is a known feature of PyV mT-driven mammary tumours and studies using PyV mT mutants uncoupled from PI3K suggest that this pathway may regulate OPN transcription downstream of PyV mT in these tumours [467, 468]. We found OPN to be variably expressed by immunoblot in our rtTA/MIC tumour lysates, and it was also present in lysates deficient for p110α (Figure 6-10A). By immunohistochemistry, staining was more uniform in wildtype rtTA/MIC tumours and occurred sporadically in p110α-null/rtTA/MIC samples (Figure 6-10B). Like what we had observed in the NIC model, OPN expression appeared to be coming from the tumour epithelium, and was not associated with stromal cells. Interestingly, when we analyzed expression of αv and β3 integrins in these same samples they appeared to be increased in some p110α-deficient/rtTA/MIC tumours (Figure 6-10A). Taken

Figure 6-6: p110α-deficiency confers a more focal penetrance to rtTA/MIC tumours

Tumour burden for the indicated genotypes is represented as the total tumour volume (top) and total number of tumours (bottom) at sacrifice. Bars are average values for each genetic group. Animals were sacrificed when total tumour volume was at least 4 cm^3 (indicated by the dotted line) or if an individual mass reached 2.5 cm^3. P values were calculated using a two-tailed t-test.

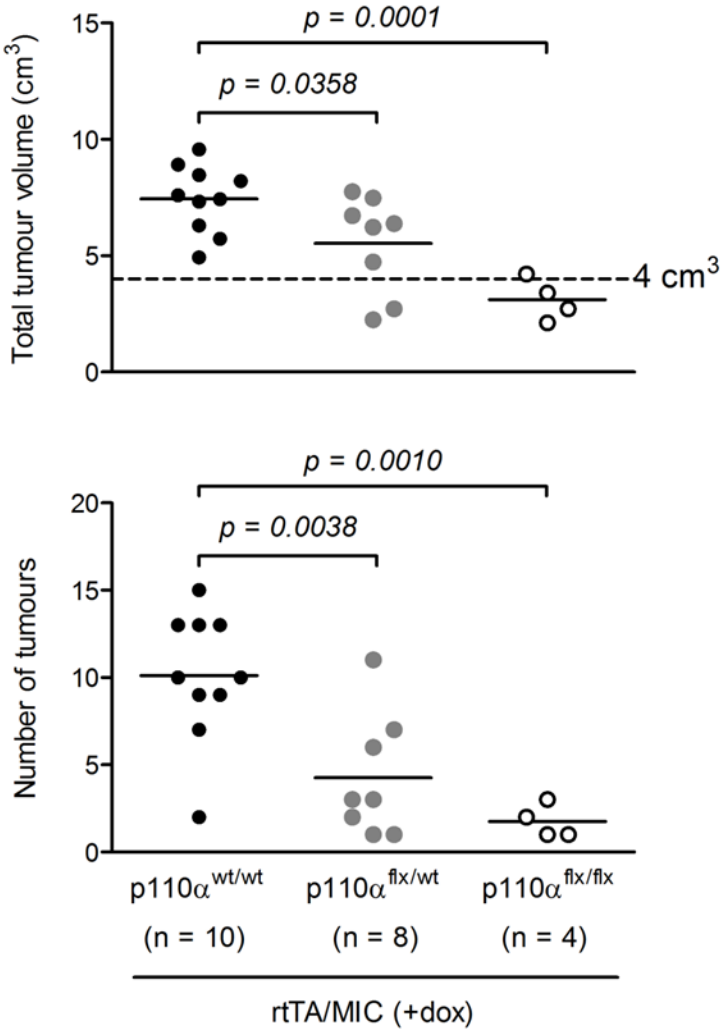
p = 0.0001
p = 0.0358
Total tumour volume (cm3)
15
10
5
0
4 cm3
p = 0.0010
p = 0.0038
Number of tumours
20
15
10
5
0
p110α wt/wt
(n = 10)
p110α flx/wt
(n = 8)
p110α flx/flx
(n = 4)
rtTA/MIC (+dox)

Figure 6-7: p110α-null/rtTA/MIC tumours present with increased stromal deposition as compared to the solid adenocarcinoma phenotype of wildtype and heterozygous tumours

Representative H&E-stained images of tumours from p110α-wildtype and -heterozygous/rtTA/MIC mice (top) as compared to tumours from each of the 6 p110α-null/rtTA/MIC mice that developed masses (bottom). Numbers correspond to the mouse ID for each sample. Scale bar is 100 μm.

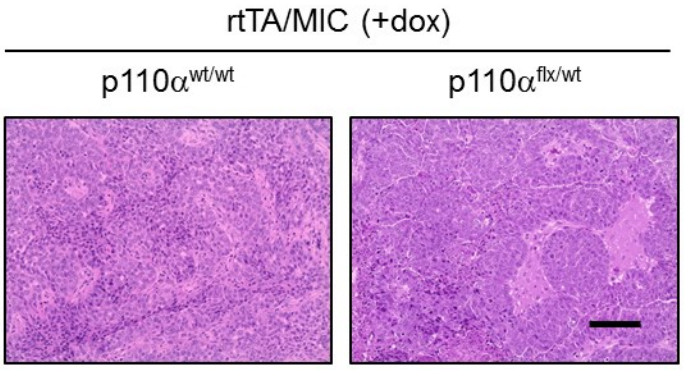
rtTA/MIC (+dox)
p110α^wt/wt
p110α^flx/wt

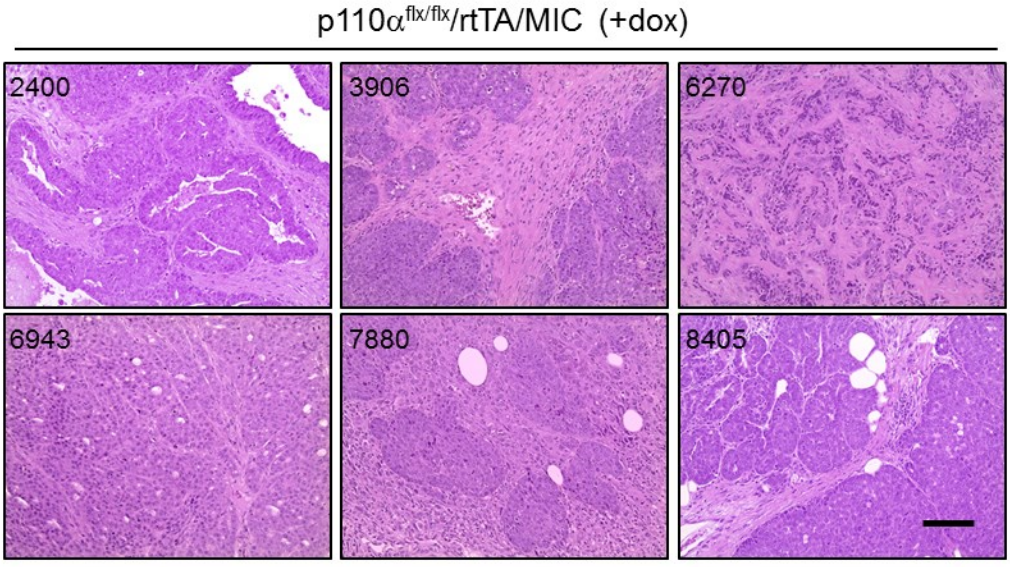
p110α^flx/flx/rtTA/MIC (+dox)
2400
3906
6270
6943
7880
8405

Figure 6-8: p110α protein is retained in p110α-deficient/rtTA/MIC tumour lysates although the conditional allele is excised

(**A**) Immunoblot of tumour lysates of the indicated genotypes for p110α, phospho-Akt (S473), Akt, PyV mT, E-cadherin (epithelial content control), and Hsp90 (loading control). Numbers correspond to the mouse ID for each sample.

(**B**) The Cre recombinase-excised p110α allele is detectable in tumour DNA from rtTA/MIC mice heterozygous and homozygous for the conditional p110α allele.

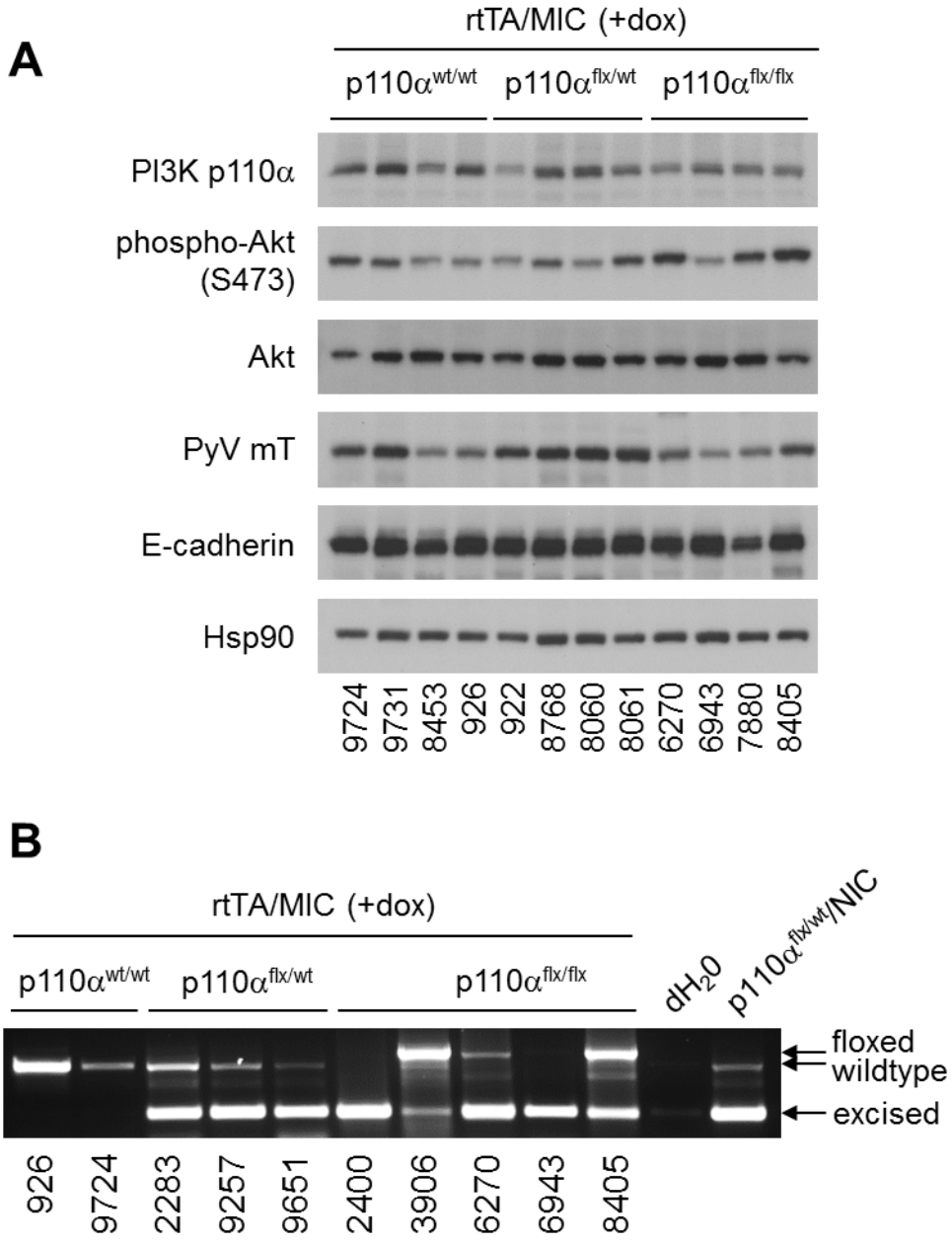
A
rtTA/MIC (+dox)
p110α^wt/wt
p110α^flx/wt
p110α^flx/flx
PI3K p110α
phospho-Akt (S473)
Akt
PyV mT
E-cadherin
Hsp90
9724
9731
8453
926
922
8768
8060
8061
6270
6943
7880
8405
B
rtTA/MIC (+dox)
p110α^wt/wt
p110α^flx/wt
p110α^flx/flx
dH2O
p110α^flx/wt/NIC
floxed
wildtype
excised
926
9724
2283
9257
9651
2400
3906
6270
6943
8405

Figure 6-9: Smaller lung lesions in tumour-bearing rtTA/MIC mice lacking one allele of p110α

(**A**) The percentage of mice with lung metastases for the indicated genotypes. Data for the wildtype and heterozygous groups include only mice with a total tumour volume over 4 cm^3; none of the homozygous animals reached this volume limit and therefore cannot be directly compared to the other two groups.

(**B**) Representative images of H&E-stained lung sections from tumour-bearing mice of the indicated genotypes (left). Scale bar is 500 μm. Quantification is shown for the number of lesions in metastasis-positive mice ("met+") (top right) and the relative size of the lesions (bottom right). Error bars are standard error of mean. P values were calculated using a two-tailed t-test.

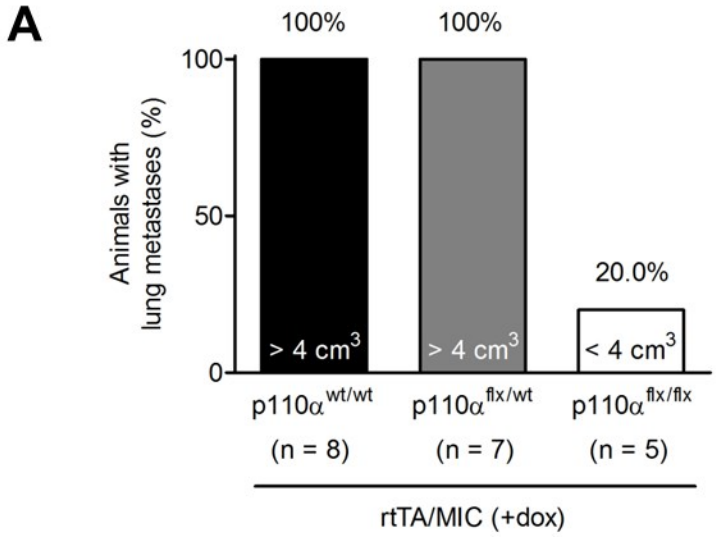
A
100%
100%
20.0%
100
50
0
Animals with lung metastases (%)
> 4 cm3
> 4 cm3
< 4 cm3
p110α wt/wt
p110α flx/wt
p110α flx/flx
(n = 8)
(n = 7)
(n = 5)
rtTA/MIC (+dox)

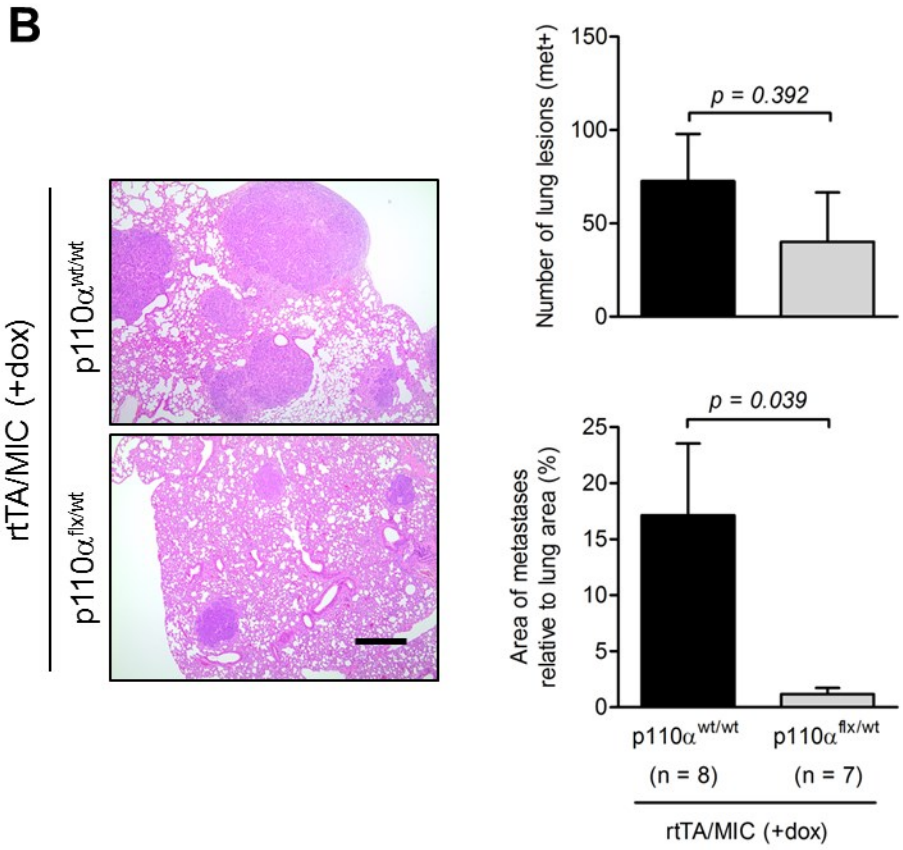
B
rtTA/MIC (+dox)
p110α wt/wt
p110α flx/wt
Number of lung lesions (met+)
150
100
50
0
p = 0.392
Area of metastases relative to lung area (%)
25
20
15
10
5
0
p = 0.039
p110α wt/wt
p110α flx/wt
(n = 8)
(n = 7)
rtTA/MIC (+dox)

Figure 6-10: OPN is expressed to variable extents in rtTA/MIC tumours in the presence and absence of p110α

(**A**) Immunoblot analysis of OPN (OPN) and β3 integrin expression in tumour lysates of the indicated genotypes. α/β-tubulin was used as a loading control. Numbers correspond to the mouse ID for each sample.

(**B**) Representative tumour sections of the indicated genotypes stained with OPN (OPN) by immunohistochemistry. The bottom row images are higher magnifications of the top row images. Scale bars are 100 μm (top row) and 50 μm (bottom row).

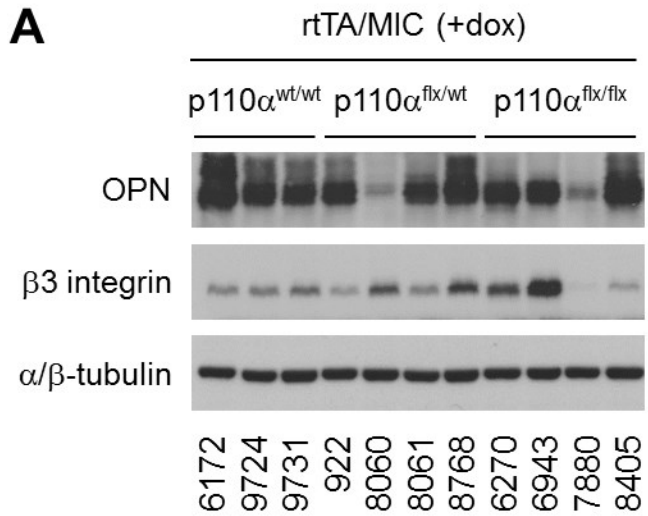
A
rtTA/MIC (+dox)
p110α^wt/wt
p110α^flx/wt
p110α^flx/flx
OPN
β3 integrin
α/β-tubulin
6172
9724
9731
922
8060
8061
8768
6270
6943
7880
8405

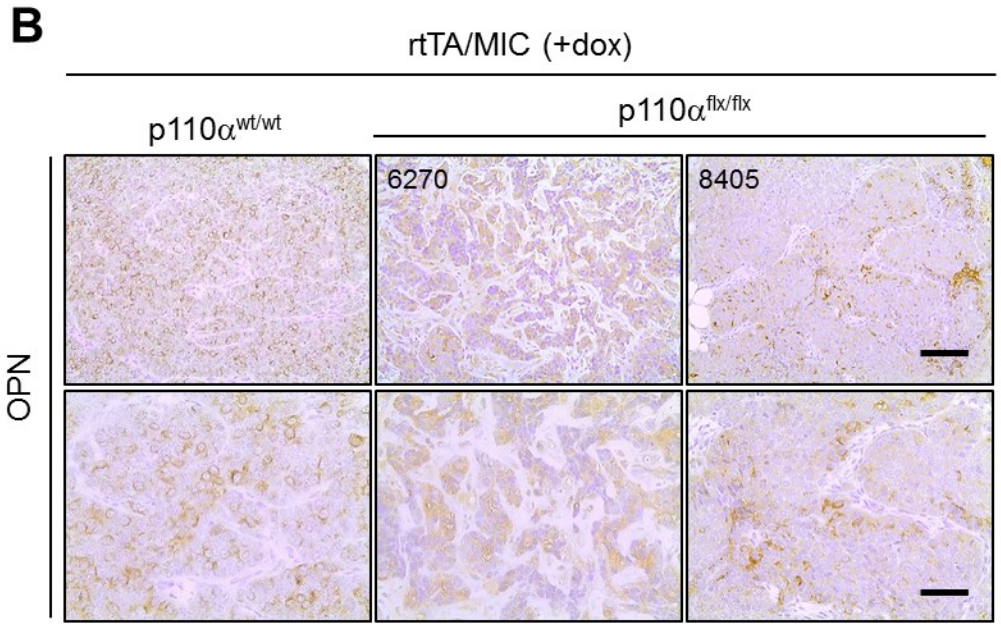
B
rtTA/MIC (+dox)
p110α^wt/wt
p110α^flx/flx
6270
8405
OPN

together, the co-expression of OPN as well as one of its major receptors suggests that this pathway may be important for rtTA/MIC tumours that evolve without p110α.

6.3 Discussion

Progression into early stages of mammary tumourigenesis is impaired in rtTA/MIC deficient for p110α

In Chapter 4 we demonstrated that ablation of p110α had a significant impact on tumour initiation and metastasis in an ErbB2 model of mammary tumourigenesis. To validate our findings from the characterization of p110α-deficient/NIC mice in a second model, we crossed the conditional p110α strain to the inducible rtTA/MIC model just described in Chapter 5 [144, 276]. Use of the rtTA/MIC strain allowed us to investigate early stages of mammary tumour progression, which were severely impaired by loss of p110α after 2 weeks of induction (Figure 6-2, -3 and -4). This effect appeared to be dependent on p110α dosage, as $p110\alpha^{flx/wt}$/rtTA/MIC mice exhibited transformation that was milder than that observed in wildtype rtTA/MIC glands. Despite this, wildtype and heterozygous rtTA/MIC glands contained a similar proportion of hyperplasia and MINs, in contrast to the exclusively normal ducts in homozygous glands and controls.

We believe that the impairment of tumourigenesis is an immediate effect as we observed this phenotype as early as 3 days after induction (Figure 6-4B). The fact that the mammary epithelium of $p110\alpha^{flx/flx}$/rtTA/MIC mice expresses a Cre-inducible GFP reporter suggests that these cells express the MIC transgene and are null for p110α. This would imply that the mammary epithelium is truly defective in transformation in the absence of p110α. Furthermore,

these results indicate that clearance by the immune system is not likely at play here which, as discussed in Chapter 5, contributes to the incomplete penetrance of the wildtype rtTA/MIC cohorts (Figure 5-2). Immunohistochemical staining for PyV mT and Cre recombinase must be carried out on p110α-deficient/rtTA/MIC mammary gland sections to confirm this. Taken together, these results indicate that p110α is important at very early stages of mammary epithelial transformation driven by PyV mT oncogene.

Loss of p110α affects both tumour initiation and metastasis in rtTA/MIC mice

Heterozygous loss of p110α in the rtTA/MIC strain caused a significant delay in tumour onset and a reduced tumour burden as compared to wildtype rtTA/MIC animals (Figure 6-5 and 6-6). This is consistent with increased tumour latency of $p110\alpha^{flx/wt}$/PyV mT/Cre mice, although this study also reported a reduction in penetrance [114]. Furthermore, $p110\alpha^{flx/wt}$/PyV mT/Cre tumours were histologically less transformed than wildtype PyV mT controls, in contrast to the adenocarcinoma histopathologies of tumours from both $p110\alpha^{flx/wt}$ and wildtype rtTA/MIC mice (Figure 6-7, top). It is unclear why heterozygous p110α loss was more potent in the MMTV-driven PyV mT model as compared to our inducible rtTA/MIC model; it is possible that this reflects differences in transgene integration or regulation of transgene expression. Despite these observations, tumours from rtTA/MIC mice heterozygous for p110α could metastasize to the lung however these lesions were significantly smaller relative to wildtype rtTA/MIC lesions (Figure 6-9). This was an interesting result and suggests that $p110\alpha^{flx/wt}$/rtTA/MIC tumour cells are impaired in lung colonization, perhaps due to defective proliferative or survival capabilities at this secondary site. Staining of lung lesions for markers of these processes (e.g. Ki67 and

TUNEL, respectively) as well as tail vein assays will be essential for further investigation of this metastatic phenotype.

Complete p110α deletion had a more profound effect on rtTA/MIC tumourigenesis than loss of one p110α allele. Approximately 30% of $p110\alpha^{flx/flx}$/rtTA/MIC mice developed tumours after a long latency (Figure 6-5). Tumour burden was significantly lower as compared to the wildtype rtTA/MIC cohort and the focality of these tumours prevented the inclusion of metastasis data, although lung lesions were rarely detected (Figure 6-6 and 6-9). Interestingly, tumours from $p110\alpha^{flx/flx}$/rtTA/MIC animals displayed areas of both adenocarcinoma and stromal infiltration, in contrast to the exclusively solid adenocarcinoma of the other genetic cohorts (Figure 6-7). These heterogeneous tumours require more detailed immunohistochemical characterization for various cytokeratins, epithelial and mesenchymal markers (such as E-cadherin and vimentin, respectively), as well as ECM components (such as collagen). Although the increased stromal content obscured molecular analysis of p110α expression by immunoblotting, confirmation of p110α ablation was demonstrated by PCR of the excised conditional alleles (Figure 6-8B). Furthermore, tumours in $p110\alpha^{flx/flx}$/rtTA/MIC mice were positive for PyV mT expression and were therefore not spontaneous masses occurring due to old age (Figure 6-8A). These long-term induction studies show that while ablation of p110α can significantly delay tumour onset in this PyV mT model, this signalling block can be evaded in rare cases.

OPN expression in endstage rtTA/MIC tumours may be a compensatory response in p110α-deficient mammary epithelium

Given our findings that tumour formation in p110α$^{flx/flx}$/NIC mice may be driven by increases in OPN, we were interested to evaluate OPN expression in our p110α-deficient/rtTA/MIC tumours. Indeed, OPN was detected in rtTA/MIC tumours in the presence and absence of p110α (Figure 6-10). The discrepancy between the strong signal on the immunoblot and the irregular immunohistochemical staining might suggest that OPN is being secreted into the extracellular space and which may cause its exclusion from paraffin-embedded tumour sections. This theory can be investigated further by analyzing OPN levels in plasma and serum from tumour-bearing animals. Considering that PyV mT can induce transcription of OPN and this may occur through a PI3K-dependent pathway, it is possible that in p110α$^{flx/flx}$/rtTA/MIC mammary epithelium OPN expression is lost, leading to a delay in tumour initiation, and must be upregulated by alternative mechanisms in order to drive tumour formation [467, 468]. We have initiated experiments to test this hypothesis in a similar manner to our methods in Chapter 4, by comparing differential expression between the genetic groups at early timepoints of induction to that of endstage tumours. Preliminary results indicate that OPN is indeed downregulated in p110α-deficient mammary epithelium relative to both rtTA/MIC and induced controls at 2 weeks of induction (data not shown). Of course we cannot ignore that the heterogeneous histopathology of the p110α-null/rtTA/MIC tumours may present some challenges for these analyses. These findings coincide with our previous results from Chapter 4 and imply that upregulation of OPN may be a universal mechanism for tumour development in the absence of p110α. Furthermore, the αvβ3 integrin receptor is expressed at higher levels in some p110α-deficient/rtTA/MIC tumours (Figure 6-10A). It will of course be necessary to assess β3 integrin

expression in premalignant p110α$^{flx/flx}$/rtTA/MIC epithelium relative to wildtype rtTA/MIC controls considering our observations in the p110α-deficient/NIC model. Perhaps in these instances, OPN/αvβ3 signalling is enhanced at multiple points in the pathway to allow PyV mT tumours to develop in the absence of p110α.

Future directions

The results from our characterization of p110α-deficient/rtTA/MIC transgenic animals suggest that p110α is indeed an important mediator of PyV mT-driven mammary tumour initiation and metastasis. The differential tumour burden between the genetic cohorts establishes an immediate necessity to investigate the relative levels of proliferative and apoptotic markers in primary tumours as well as outgrowth potential using orthotopic injection experiments. In addition, tail vein assays will allow us to directly assess the effect of p110α loss on lung colonization; this was not afforded to us in the transgenic studies given the tendency toward focal tumours in p110α$^{flx/flx}$/rtTA/MIC mice. The rarity of tumours in this cohort will force us to use transplanted tumour material from athymic hosts. However, we must first verify that the histological and molecular integrity of these transplant lines has been somewhat maintained during serial passaging.

We are also very interested in pursuing the potential regulation of OPN transcription by p110α in the rtTA/MIC mammary epithelium as well as the possibility that OPN is re-expressed as a mechanism for the eventual development of tumours in p110α$^{flx/flx}$/rtTA/MIC animals. Additional experiments are needed examining OPN expression in premalignant mammary epithelium. If OPN and/or αvβ3 integrin are indeed upregulated in order for tumours to evolve,

it will be important to identify the mechanisms driving this event. An interesting candidate is the activation of PI3K signalling which may be a result of Pten loss, as we had observed previously in Chapter 4. The recapitulation of several p110α-dependent phenotypes between the ErbB2- and PyV mT-driven tumour models illustrates the versatility of the PyV mT oncogene as an experimental tool in breast cancer research. This is no doubt due to the fact that PyV mT mimics the activity of an RTK and so the studies presented here suggest that p110α may be important in RTK-driven breast cancers in general.

7 General discussion, conclusions, and future directions

7.1 PI3K signalling in RTK-driven mammary tumourigenesis and metastasis

The studies performed in this thesis illustrate the significance of the PI3K pathway in a variety of mouse models of mammary tumourigenesis. We have demonstrated this by two opposing approaches in which we investigated how activation versus impairment of PI3K signalling would affect mammary tumourigenesis driven by oncogenic RTKs. In Chapter 3, we found that loss of the PI3K pathway antagonist Pten or constitutive activation of the p110α proto-oncogene can enhance HER2/ErbB2-mediated tumour initiation and/or metastasis (unpublished observations, T. Rao and W.J. Muller) [106]. Conversely, we observed in Chapters 4 and 6 that genetic ablation of p110α was required for mammary tumourigenesis and malignancy downstream of activated HER2/ErbB2 or the viral oncoprotein PyV mT (unpublished observations, T. Rao and W.J. Muller) [114]. Collectively these findings highlight that PI3K pathway activation can cooperate with other genetic events during transformation of the mammary epithelium, but also suggests that these oncogenes are dependent on PI3K signalling even in the absence of p110α mutation or Pten loss. This dependence becomes relevant for the development of tumours lacking p110α which may lose Pten expression or function in order to maintain PI3K signalling through non-α p110 isoforms.

We were able to demonstrate the importance of p110α in mammary tumourigenesis using two different oncogenic models, one of which represents a physiological oncogene in human breast cancer (activated HER2/ErbB2) while the other induces tumour progression in a clinically relevant fashion (PyV mT). In both systems, p110α deficiency led to delayed tumour onset, fewer tumours, and reduced lung metastasis. However some important differences were apparent when comparing these p110α-deficient models. Firstly, p110α-deficiency appears to have a more dramatic effect on tumour initiation in the PyV mT model than in the activated

HER2/ErbB2 model, with both heterozygous and homozygous p110α loss delaying tumour onset and the latter causing a profound decrease in penetrance. This suggests that PyV mT is more dependent on p110α than activated ErbB2 is; this may be because in the PyV mT model the PyV mT transgene is the predominant oncogene, whereas in the activated ErbB2 model there may be more of a reliance on other concurrent oncogenic events. The impact of p110α loss on tumour initiation in the ErbB2 model was confirmed by the more stepwise model driven by PyV mT. This suggests that p110α-dependent signalling is of prime importance at the onset of transformation. The fact that activating mutations in p110α have been found in early stage breast cancer also supports the idea that PI3K signalling is probably critical at this point [349, 469]. We may be able to address the importance of p110α in very early events during transformation using our new PyV mT model by inducing naïve mammary epithelial cells in *ex vivo* culture. Secondly, the metastatic defect in mice heterozygous for p110α mice was restricted to lung lesion size in the PyV mT model whereas both incidence and number were affected in the activated ErbB2 strain. The results from Chapter 4 suggest that this is likely a cell-autonomous defect; it will be interesting to investigate this in the p110α-deficient PyV mT tumour cells. Thus, in addition to tumour initiation, p110α-dependent signalling may also have relevance during metastatic phases of tumour progression. Taken together, the comparison of p110α-deficiency in ErbB2- versus PyV mT-driven mammary tumour models demonstrates that p110α can have slightly different effects on tumourigenesis depending on the oncogenic context.

Importantly our findings indicate that PI3K inhibitors as single agent treatments will likely be ineffective in HER2-overexpressing cancers. In fact, while we observed sensitivity of ErbB2 tumours to the pan PI3K inhibitor GDC-0941 they did not reach stasis or regress which suggests that inhibiting this pathway will likely not be sufficient to reverse the growth of HER2-

expressing tumours in patients. This is in support of many other studies showing that PI3K inhibitors have better efficacy when combined with therapies targeting HER2 and MEK [206, 368, 377, 394, 396]. The use of PI3K inhibitors in combination with standard HER2-targeted therapies may not only improve initial responses but may also prevent resistance. This is especially relevant for HER2-positive cancers with *PIK3CA* mutation or PTEN loss, but may also be beneficial for patients with "intact" PI3K signalling since this pathway may become activated during tumour progression or following treatment.

7.2 Selectivity of p110 isoforms during mammary tumour progression

Our investigations into the impairment of PI3K signalling focused on conditional ablation of p110α since this isoform is selectively mutated in breast cancers. While mammary tumour initiation appears to strongly depend on p110α, we believe that the eventual development of tumours in a p110α-deficient background may be a result of Pten loss leading to enhanced signalling through non-α p110 isoforms. Considering that p110β loss does not impair ErbB2 tumourigenesis, it appears that p110α is the predominant isoform downstream of this RTK during mammary tumourigenesis in the mouse [114]. It is possible that in the absence of p110α, loss of Pten causes a switch in the dependence of ErbB2 to p110β since in humans PTEN-deficient tumours tend to depend on p110β more than p110α [283, 376-378]. We could revisit Chapter 3 to determine which isoform Pten-deficient ErbB2 tumours are dependent on in this system. Furthermore, it will be interesting to see if Pten loss is also a compensatory pathway for p110α-deficient/PyV mT tumours; if it is, does this change the dependency of PyV mT to p110β (considering that PyV mT models seem to depend on p110α and not p110β) [114, 381]?

Our studies suggest that compensation from non-α p110 isoforms might occur in patients with HER2-positive breast cancer treated with p110α-specific inhibitors. We propose that agents targeting multiple p110 isoforms may be more effective at combatting this potential resistance mechanism. However, as we observed in our orthotopic model, ErbB2-expressing tumours do not regress upon treatment with the pan PI3K inhibitor GDC-0941. Again, this points to the idea that combining PI3K inhibition with HER2-targeted therapies will likely result in synergistic effects.

7.3 Potential regulation of OPN/αvβ3 integrin expression by the PI3K pathway

An interesting observation from our work was the possibility that OPN signalling represents a compensatory mechanism in ErbB2 and PyV mT tumours that arise in the absence of p110α. Our hypothesis that this was due to reactivation of PI3K signalling through non-α p110 isoforms was supported by the fact that PI3K pathway activation in two individual ErbB2-driven mouse models was also associated with overexpression of OPN in mammary tumours. Interestingly, the αvβ3 integrin heterodimer, a key receptor for OPN, appears to be differentially modulated in p110α-deficient mammary epithelium depending on the driving oncogene. A p110α-dependent reduction in β3 integrin levels was seen in the ErbB2 model regardless of the tumourigenic state, suggesting that expression of OPN is a way to reactivate signalling through this pathway. However, in the PyV mT model, β3 integrin is increased in p110α-deficient tumours; perhaps in this context the epithelium must upregulate both the ligand and the receptor in order to transform. It will be important to investigate relative levels of OPN and αvβ3 integrin at premalignant timepoints in the PyV mT system. The possibility that p110α is involved in β3 integrin transcription is a novel idea considering that little is known about the pathways

regulating expression of this protein. Furthermore, if the lack of β3 integrin is directly responsible for the delay in the initiation of p110α-deficient tumours or in their impaired ability to colonize the lung, it may be interesting to investigate the importance of this signalling axis itself during mammary tumourigenesis. Several reagents that can disrupt this pathway impair tumourigenic properties of breast cancer cells *in vitro*, including inhibitors or neutralizing antibodies for integrins as well as RNA interference approaches specific for OPN [446, 470-472]. In addition to analyzing established primary tumour cells lines from our mouse models, future projects can utilize these strains to study the genetic contribution of OPN and β3 integrin to mammary tumourigenesis *in vivo*.

These studies also highlight the potential importance of OPN and αvβ3 integrin in HER2-mediated breast cancer. Indeed, OPN has been reported to be highly expressed in more aggressive breast cancers, including HER2-positive and TNBC/basal-like subtypes [455, 456]. Additionally, in humans there are three splice isoforms of OPN (designated as OPN-a, -b and -c) which show differential expression in breast cancer. The OPN-c isoform specifically is enhanced in advanced stage breast cancers and may be associated with increased risk for recurrence [454, 455]. Given that OPN appears to be regulated in part by PI3K signalling, and considering the data presented here, it would be very interesting to investigate whether OPN overexpression associates with PI3K pathway activation in breast cancer. In addition to the HER2-positive cases, the basal-like subtype may also be of relevance since it has been individually correlated with both of these alterations [4, 455]. If OPN expression is indeed indicative of a hyperactive PI3K pathway in breast cancer, screening for this candidate biomarker in the blood of patients could identify individuals that might be responsive to PI3K inhibitors. Importantly, given our findings that OPN may be compensating for p110α loss in

mouse models of mammary tumourigenesis, pan PI3K inhibitors may be more effective in treating OPN-positive tumours than those targeting an individual p110 isoform.

7.4 Conclusion

In the decades of research centered on PI3K signalling, this proto-oncogenic pathway still offers many complexities that are yet to be fully understood. Although therapies targeting the PI3K pathway have already entered drug trials for cancer treatment, *in vivo* preclinical models have remained an important area of research. The work presented in this thesis has focused on how cancer-associated alterations in PI3K pathway components operate in transgenic mouse models of breast cancer. We have found that activation of PI3K signalling can cooperate with physiological oncogenes, such as HER2/ErbB2, during mammary tumour progression. Conversely, inactivation of PI3K signalling can dramatically impair mammary tumour initiation and metastasis in two different transgenic systems including a newly characterized inducible PyV mT strain. The eventual emergence of p110α-deficient tumours in these studies highlighted that isoform selectivity will be of importance when choosing PI3K inhibitors in the clinic. Importantly, we have identified some molecular consequences of PI3K signalling dysregulation, comprising both well-established and potentially novel mechanisms involving the pro-tumourigenic OPN/αvβ3 pathway. These mechanisms may become relevant in breast cancer patients that develop resistance to PI3K inhibition. Collectively, the work from this thesis clearly implicates PI3K signalling in mammary tumour initiation and progression to malignancy while highlighting the potential of several mouse strains as preclinical models of breast cancer.

8 References

1. *Canadian Cancer Society's Advisory Committee on Cancer Statistics*, in *Canadian Cancer Statistics 2014*2014.
2. Society, A.C., *Breast Cancer Facts & Figures 2013-2014.* Atlanta: American Cancer Society, Inc., 2013.
3. Walsh, T., et al., *Detection of inherited mutations for breast and ovarian cancer using genomic capture and massively parallel sequencing.* Proceedings of the National Academy of Sciences, 2010. **107**(28): p. 12629-12633.
4. Network, C.G.A., *Comprehensive molecular portraits of human breast tumours.* Nature, 2012. **490**(7418): p. 61-70.
5. Hall, J., et al., *Linkage of early-onset familial breast cancer to chromosome 17q21.* Science, 1990. **250**(4988): p. 1684-1689.
6. Friedman, L.S., et al., *Confirmation of BRCA1 by analysis of germline mutations linked to breast and ovarian cancer in ten families.* Nature genetics, 1994. **8**(4): p. 399-404.
7. Malkin, D., et al., *Germ line p53 mutations in a familial syndrome of breast cancer, sarcomas, and other neoplasms.* Science, 1990. **250**(4985): p. 1233-1238.
8. Liaw, D., et al., *Germline mutations of the PTEN gene in Cowden disease, an inherited breast and thyroid cancer syndrome.* Nature genetics, 1997. **16**(1): p. 64-67.
9. Slamon, D., et al., *Human breast cancer: correlation of relapse and survival with amplification of the HER-2/neu oncogene.* Science, 1987. **235**(4785): p. 177-182.
10. Slamon, D., et al., *Studies of the HER-2/neu proto-oncogene in human breast and ovarian cancer.* Science, 1989. **244**(4905): p. 707-712.
11. Kauraniemi, P., et al., *Amplification of a 280-Kilobase Core Region at the ERBB2 Locus Leads to Activation of Two Hypothetical Proteins in Breast Cancer.* The American Journal of Pathology, 2003. **163**(5): p. 1979-1984.
12. Wolff, A.C., et al., *Recommendations for Human Epidermal Growth Factor Receptor 2 Testing in Breast Cancer: American Society of Clinical Oncology/College of American Pathologists Clinical Practice Guideline Update.* Journal of Clinical Oncology, 2013. **31**(31): p. 3997-4013.
13. Cardiff, R.D. and S.R. Wellings, *The comparative pathology of human and mouse mammary glands.* Journal of mammary gland biology and neoplasia, 1999. **4**(1): p. 105-122.
14. Barcellos-Hoff, M.H., et al., *Functional differentiation and alveolar morphogenesis of primary mammary cultures on reconstituted basement membrane.* Development, 1989. **105**(2): p. 223-235.
15. Streuli, C.H. and M.J. Bissell, *Expression of extracellular matrix components is regulated by substratum.* The Journal of Cell Biology, 1990. **110**(4): p. 1405-1415.
16. Neville, M.C., et al., *The mammary fat pad.* Journal of mammary gland biology and neoplasia, 1998. **3**(2): p. 109-116.
17. Talhouk, R.S., M.J. Bissell, and Z. Werb, *Coordinated expression of extracellular matrix-degrading proteinases and their inhibitors regulates mammary epithelial function during involution.* The Journal of Cell Biology, 1992. **118**(5): p. 1271-1282.
18. Richert, M.M., et al., *An atlas of mouse mammary gland development.* Journal of mammary gland biology and neoplasia, 2000. **5**(2): p. 227-241.
19. Russo, I.H. and J. Russo, *Mammary gland neoplasia in long-term rodent studies.* Environmental Health Perspectives, 1996. **104**(9): p. 938.

20. Silberstein, G.B., et al., *Essential role of endogenous estrogen in directly stimulating mammary growth demonstrated by implants containing pure antiestrogens.* Endocrinology, 1994. **134**(1): p. 84-90.
21. Feng, Y., et al., *Estrogen receptor-α expression in the mammary epithelium is required for ductal and alveolar morphogenesis in mice.* Proceedings of the National Academy of Sciences, 2007. **104**(37): p. 14718-14723.
22. Brisken, C., et al., *A paracrine role for the epithelial progesterone receptor in mammary gland development.* Proceedings of the National Academy of Sciences, 1998. **95**(9): p. 5076-5081.
23. Brisken, C., et al., *Prolactin Controls Mammary Gland Development via Direct and Indirect Mechanisms.* Developmental Biology, 1999. **210**(1): p. 96-106.
24. Lee, E.Y., et al., *Interaction of mouse mammary epithelial cells with collagen substrata: regulation of casein gene expression and secretion.* Proceedings of the National Academy of Sciences, 1985. **82**(5): p. 1419-1423.
25. Howlett, A. and M. Bissell, *The influence of tissue microenvironment (stroma and extracellular matrix) on the development and function of mammary epithelium.* Epithelial cell biology, 1993. **2**(2): p. 79.
26. Quarrie, L.H., C.V. Addey, and C.J. Wilde, *Programmed cell death during mammary tissue involution induced by weaning, litter removal, and milk stasis.* Journal of cellular physiology, 1996. **168**(3): p. 559-569.
27. Strange, R., et al., *Programmed cell death during mammary gland involution.* Methods in cell biology, 1995. **46**: p. 355-368.
28. Furth, P.A., *Mammary gland involution and apoptosis of mammary epithelial cells.* Journal of mammary gland biology and neoplasia, 1999. **4**(2): p. 123-127.
29. Li, M., et al., *Mammary-derived signals activate programmed cell death during the first stage of mammary gland involution.* Proceedings of the National Academy of Sciences, 1997. **94**(7): p. 3425-3430.
30. Silberstein, G., et al., *Progesterone receptors in the mouse mammary duct: distribution and developmental regulation.* Cell Growth Differ, 1996. **7**(7): p. 945-952.
31. Hammond, M.E.H., et al., *American Society of Clinical Oncology/College of American Pathologists Guideline Recommendations for Immunohistochemical Testing of Estrogen and Progesterone Receptors in Breast Cancer.* Journal of Clinical Oncology, 2010. **28**(16): p. 2784-2795.
32. Hanahan, D. and Robert A. Weinberg, *Hallmarks of Cancer: The Next Generation.* Cell, 2011. **144**(5): p. 646-674.
33. Goldhirsch, A., et al., *Personalizing the treatment of women with early breast cancer: highlights of the St Gallen International Expert Consensus on the Primary Therapy of Early Breast Cancer 2013.* Annals of Oncology, 2013. **24**(9): p. 2206-2223.
34. Perou, C.M., et al., *Molecular portraits of human breast tumours.* Nature, 2000. **406**(6797): p. 747-752.
35. Sørlie, T., et al., *Gene expression patterns of breast carcinomas distinguish tumor subclasses with clinical implications.* Proceedings of the National Academy of Sciences, 2001. **98**(19): p. 10869-10874.
36. van't Veer, L.J., et al., *Gene expression profiling predicts clinical outcome of breast cancer.* nature, 2002. **415**(6871): p. 530-536.

37. Sørlie, T., et al., *Repeated observation of breast tumor subtypes in independent gene expression data sets.* Proceedings of the National Academy of Sciences, 2003. **100**(14): p. 8418-8423.
38. Paik, S., et al., *A Multigene Assay to Predict Recurrence of Tamoxifen-Treated, Node-Negative Breast Cancer.* New England Journal of Medicine, 2004. **351**(27): p. 2817-2826.
39. Parker, J.S., et al., *Supervised Risk Predictor of Breast Cancer Based on Intrinsic Subtypes.* Journal of Clinical Oncology, 2009. **27**(8): p. 1160-1167.
40. Prat, A., et al., *Phenotypic and molecular characterization of the claudin-low intrinsic subtype of breast cancer.* Breast Cancer Res, 2010. **12**(5): p. R68.
41. Bertucci, F., et al., *Gene Expression Profiling Identifies Molecular Subtypes of Inflammatory Breast Cancer.* Cancer Research, 2005. **65**(6): p. 2170-2178.
42. Finak, G., et al., *Stromal gene expression predicts clinical outcome in breast cancer.* Nature medicine, 2008. **14**(5): p. 518-527.
43. Allinen, M., et al., *Molecular characterization of the tumor microenvironment in breast cancer.* Cancer Cell, 2004. **6**(1): p. 17-32.
44. West, R.B., et al., *Determination of Stromal Signatures in Breast Carcinoma.* PLoS Biol, 2005. **3**(6): p. e187.
45. Chin, K., et al., *Genomic and transcriptional aberrations linked to breast cancer pathophysiologies.* Cancer Cell, 2006. **10**(6): p. 529-541.
46. Bergamaschi, A., et al., *Distinct patterns of DNA copy number alteration are associated with different clinicopathological features and gene-expression subtypes of breast cancer.* Genes, Chromosomes and Cancer, 2006. **45**(11): p. 1033-1040.
47. Hennessy, B.T., et al., *A technical assessment of the utility of reverse phase protein arrays for the study of the functional proteome in non-microdissected human breast cancers.* Clinical proteomics, 2010. **6**(4): p. 129-151.
48. Hennighausen, L.G., et al., *Comparative sequence analysis of the mRNAs coding for mouse and rat whey protein.* Nucleic Acids Research, 1982. **10**(12): p. 3733-3744.
49. Pittius, C.W., et al., *Comparison of the Regulation of the Whey Acidic Protein Gene with that of a Hybrid Gene Containing the Whey Acidic Protein Gene Promoter in Transgenic Mice.* Molecular Endocrinology, 1988. **2**(11): p. 1027-1032.
50. Bittner, J.J., *Some possible effects of nursing on the mammary gland tumour incidence in mice.* Science, 1936. **84**(2172): p. 162.
51. Huang, A.L., et al., *Glucocorticoid regulation of the Ha-MuSV p21 gene conferred by sequences from mouse mammary tumor virus.* Cell, 1981. **27**(2, Part 1): p. 245-255.
52. Lee, F., et al., *Glucocorticoids regulate expression of dihydrofolate reductase cDNA in mouse mammary tumour virus chimaeric plasmids.* Nature, 1981. **294**(5838): p. 228-232.
53. Stewart, T.A., P.K. Pattengale, and P. Leder, *Spontaneous mammary adenocarcinomas in transgenic mice that carry and express MTV/myc fusion genes.* Cell, 1984. **38**(3): p. 627-637.
54. Sinn, E., et al., *Coexpression of MMTV/v-Ha-ras and MMTV/c-myc genes in transgenic mice: Synergistic action of oncogenes in vivo.* Cell, 1987. **49**(4): p. 465-475.
55. Muller, W.J., et al., *Single-step induction of mammary adenocarcinoma in transgenic mice bearing the activated c-neu oncogene.* Cell, 1988. **54**(1): p. 105-115.

56. Hoess, R., K. Abremski, and N. Sternberg, *The Nature of the Interaction of the P1 Recombinase Cre with the Recombining Site loxP.* Cold Spring Harbor Symposia on Quantitative Biology, 1984. **49**: p. 761-768.
57. Wagner, K.-U., et al., *Cre-mediated gene deletion in the mammary gland.* Nucleic Acids Research, 1997. **25**(21): p. 4323-4330.
58. Wagner, K.-U., et al., *Spatial and temporal expression of the Cre gene under the control of the MMTV-LTR in different lines of transgenic mice.* Transgenic Research, 2001. **10**(6): p. 545-553.
59. Xu, X., et al., *Conditional mutation of Brca1 in mammary epithelial cells results in blunted ductal morphogenesis and tumour formation.* Nature genetics, 1999. **22**(1): p. 37-43.
60. Cheung, A.M.Y., et al., *Brca2 Deficiency Does Not Impair Mammary Epithelium Development but Promotes Mammary Adenocarcinoma Formation in p53+/− Mutant Mice.* Cancer Research, 2004. **64**(6): p. 1959-1965.
61. Lakhani, S.R., et al., *The Pathology of Familial Breast Cancer: Predictive Value of Immunohistochemical Markers Estrogen Receptor, Progesterone Receptor, HER-2, and p53 in Patients With Mutations in BRCA1 and BRCA2.* Journal of Clinical Oncology, 2002. **20**(9): p. 2310-2318.
62. Andrechek, E.R., et al., *Amplification of the neu/erbB-2 oncogene in a mouse model of mammary tumorigenesis.* Proceedings of the National Academy of Sciences, 2000. **97**(7): p. 3444-3449.
63. Dankort, D., et al., *A new mouse model to explore the initiation, progression, and therapy of BRAFV600E-induced lung tumors.* Genes & Development, 2007. **21**(4): p. 379-384.
64. Kinross, K.M., et al., *An activating Pik3ca mutation coupled with Pten loss is sufficient to initiate ovarian tumorigenesis in mice.* The Journal of Clinical Investigation, 2012. **122**(2): p. 553-557.
65. Tikoo, A., et al., *Physiological Levels of Pik3ca^{H1047R} Mutation in the Mouse Mammary Gland Results in Ductal Hyperplasia and Formation of ERα-Positive Tumors.* PLoS ONE, 2012. **7**(5): p. e36924.
66. Yuan, W., et al., *Conditional activation of Pik3caH1047R in a knock-in mouse model promotes mammary tumorigenesis and emergence of mutations.* Oncogene, 2012. **32**(3): p. 318-326.
67. Friedrich, G. and P. Soriano, *Promoter traps in embryonic stem cells: a genetic screen to identify and mutate developmental genes in mice.* Genes & Development, 1991. **5**(9): p. 1513-1523.
68. Kawamoto, S., et al., *A novel reporter mouse strain that expresses enhanced green fluorescent protein upon Cre-mediated recombination.* FEBS Letters, 2000. **470**(3): p. 263-268.
69. Furth, P.A., et al., *Temporal control of gene expression in transgenic mice by a tetracycline-responsive promoter.* Proceedings of the National Academy of Sciences, 1994. **91**(20): p. 9302-9306.
70. Kistner, A., et al., *Doxycycline-mediated quantitative and tissue-specific control of gene expression in transgenic mice.* Proceedings of the National Academy of Sciences, 1996. **93**(20): p. 10933-10938.

71. Moody, S.E., et al., *Conditional activation of Neu in the mammary epithelium of transgenic mice results in reversible pulmonary metastasis.* Cancer Cell, 2002. **2**(6): p. 451-461.
72. D'Cruz, C.M., et al., *c-MYC induces mammary tumorigenesis by means of a preferred pathway involving spontaneous Kras2 mutations.* Nature medicine, 2001. **7**(2): p. 235-239.
73. Podsypanina, K., et al., *Seeding and Propagation of Untransformed Mouse Mammary Cells in the Lung.* Science, 2008. **321**(5897): p. 1841-1844.
74. Shih, C., et al., *Transforming genes of carcinomas and neuroblastomas introduced into mouse fibroblasts.* 1981.
75. Schechter, A.L., et al., *The neu oncogene: an erb-B-related gene encoding a 185,000-Mr tumour antigen.* 1984.
76. Schulze, W.X., L. Deng, and M. Mann, *Phosphotyrosine interactome of the ErbB-receptor kinase family.* Molecular systems biology, 2005. **1**(1).
77. Holgado-Madruga, M., et al., *Grb2-associated binder-1 mediates phosphatidylinositol 3-kinase activation and the promotion of cell survival by nerve growth factor.* Proceedings of the National Academy of Sciences, 1997. **94**(23): p. 12419-12424.
78. Garrett, T.P.J., et al., *The Crystal Structure of a Truncated ErbB2 Ectodomain Reveals an Active Conformation, Poised to Interact with Other ErbB Receptors.* Molecular Cell, 2003. **11**(2): p. 495-505.
79. Holbro, T., et al., *The ErbB2/ErbB3 heterodimer functions as an oncogenic unit: ErbB2 requires ErbB3 to drive breast tumor cell proliferation.* Proceedings of the National Academy of Sciences, 2003. **100**(15): p. 8933-8938.
80. Guy, P.M., et al., *Insect cell-expressed p180erbB3 possesses an impaired tyrosine kinase activity.* Proceedings of the National Academy of Sciences, 1994. **91**(17): p. 8132-8136.
81. Schroeder, J. and D. Lee, *Dynamic expression and activation of ERBB receptors in the developing mouse mammary gland.* Cell Growth Differ, 1998. **9**(6): p. 451-464.
82. Luetteke, N.C., et al., *Targeted inactivation of the EGF and amphiregulin genes reveals distinct roles for EGF receptor ligands in mouse mammary gland development.* Development, 1999. **126**(12): p. 2739-2750.
83. Kenney, N., et al., *Induction of ductal morphogenesis and lobular hyperplasia by amphiregulin in the mouse mammary gland.* Cell Growth Differ, 1996. **7**(12): p. 1769-1781.
84. Gassmann, M., et al., *Aberrant neural and cardiac development in mice lacking the ErbB4 neuregulin receptor.* 1995.
85. Lee, K.-F., et al., *Requirement for neuregulin receptor erbB2 in neural and cardiac development.* 1995.
86. Riethmacher, D., et al., *Severe neuropathies in mice with targeted mutations in the ErbB3 receptor.* Nature, 1997. **389**(6652): p. 725-730.
87. Miettinen, P.J., et al., *Epithelial immaturity and multiorgan failure in mice lacking epidermal growth factor receptor.* Nature, 1995. **376**(6538): p. 337-341.
88. Wiesen, J.F., et al., *Signaling through the stromal epidermal growth factor receptor is necessary for mammary ductal development.* Development, 1999. **126**(2): p. 335-344.
89. Sebastian, J., et al., *Activation and function of the epidermal growth factor receptor and erbB-2 during mammary gland morphogenesis.* Cell Growth Differ, 1998. **9**(9): p. 777-785.

90. Xie, W., et al., *Targeted Expression of a Dominant Negative Epidermal Growth Factor Receptor in the Mammary Gland of Transgenic Mice Inhibits Pubertal Mammary Duct Development.* Molecular Endocrinology, 1997. **11**(12): p. 1766-1781.
91. Fowler, K.J., et al., *A mutation in the epidermal growth factor receptor in waved-2 mice has a profound effect on receptor biochemistry that results in impaired lactation.* Proceedings of the National Academy of Sciences, 1995. **92**(5): p. 1465-1469.
92. Andrechek, E.R., D. White, and W.J. Muller, *Targeted disruption of ErbB2/Neu in the mammary epithelium results in impaired ductal outgrowth.* Oncogene, 2004. **24**(5): p. 932-937.
93. Jones, F.E., et al., *Erbb4 Signaling in the Mammary Gland Is Required for Lobuloalveolar Development and Stat5 Activation during Lactation.* The Journal of Cell Biology, 1999. **147**(1): p. 77-88.
94. Long, W., et al., *Impaired differentiation and lactational failure of Erbb4-deficient mammary glands identify ERBB4 as an obligate mediator of STAT5.* Development, 2003. **130**(21): p. 5257-5268.
95. Jackson-Fisher, A., et al., *ErbB3 is required for ductal morphogenesis in the mouse mammary gland.* Breast Cancer Research, 2008. **10**(6): p. 1-12.
96. Lahlou, H., et al., *Uncoupling of PI3K from ErbB3 Impairs Mammary Gland Development but Does Not Impact on ErbB2-Induced Mammary Tumorigenesis.* Cancer Research, 2012. **72**(12): p. 3080-3090.
97. Bouchard, L., et al., *Stochastic appearance of mammary tumors in transgenic mice carrying the MMTV/c-neu oncogene.* Cell, 1989. **57**(6): p. 931-936.
98. Guy, C.T., R.D. Cardiff, and W.J. Muller, *Activated neu Induces Rapid Tumor Progression.* Journal of Biological Chemistry, 1996. **271**(13): p. 7673-7678.
99. Lemoine, N., et al., *Absence of activating transmembrane mutations in the c-erbB-2 proto-oncogene in human breast cancer.* Oncogene, 1990. **5**(2): p. 237-239.
100. Guy, C.T., et al., *Expression of the neu protooncogene in the mammary epithelium of transgenic mice induces metastatic disease.* Proceedings of the National Academy of Sciences, 1992. **89**(22): p. 10578-10582.
101. Siegel, P.M., et al., *Novel activating mutations in the neu proto-oncogene involved in induction of mammary tumors.* Molecular and Cellular Biology, 1994. **14**(11): p. 7068-7077.
102. Siegel, P.M. and W.J. Muller, *Mutations affecting conserved cysteine residues within the extracellular domain of Neu promote receptor dimerization and activation.* Proceedings of the National Academy of Sciences, 1996. **93**(17): p. 8878-8883.
103. Siegel, P.M., et al., *Elevated expression of activated forms of Neu/ErbB-2 and ErbB-3 are involved in the induction of mammary tumors in transgenic mice: implications for human breast cancer*. Vol. 18. 1999. 2149-2164.
104. Kwong, K.Y. and M.-C. Hung, *A novel splice variant of HER2 with increased transformation activity.* Molecular Carcinogenesis, 1998. **23**(2): p. 62-68.
105. Ursini-Siegel, J., et al., *ShcA signalling is essential for tumour progression in mouse models of human breast cancer.* The EMBO journal, 2008. **27**(6): p. 910-920.
106. Schade, B., et al., *PTEN deficiency in a luminal ErbB-2 mouse model results in dramatic acceleration of mammary tumorigenesis and metastasis.* Journal of Biological Chemistry, 2009. **284**(28): p. 19018-19026.

107. Lahlou, H., et al., *Focal adhesion kinase contributes to proliferative potential of ErbB2 mammary tumour cells but is dispensable for ErbB2 mammary tumour induction in vivo.* Breast Cancer Research, 2012. **14**(1): p. 1-14.
108. White, D.E., et al., *Targeted disruption of β1-integrin in a transgenic mouse model of human breast cancer reveals an essential role in mammary tumor induction.* Cancer Cell, 2004. **6**(2): p. 159-170.
109. Lahlou, H., et al., *Mammary epithelial-specific disruption of the focal adhesion kinase blocks mammary tumor progression.* Proceedings of the National Academy of Sciences, 2007. **104**(51): p. 20302-20307.
110. Marcotte, R., et al., *Mammary epithelial-specific disruption of c-Src impairs cell cycle progression and tumorigenesis.* Proceedings of the National Academy of Sciences, 2012. **109**(8): p. 2808-2813.
111. Ranger, J.J., et al., *Identification of a Stat3-dependent transcription regulatory network involved in metastatic progression.* Cancer research, 2009. **69**(17): p. 6823-6830.
112. Huck, L., et al., *β1-integrin is dispensable for the induction of ErbB2 mammary tumors but plays a critical role in the metastatic phase of tumor progression.* Proceedings of the National Academy of Sciences, 2010. **107**(35): p. 15559-15564.
113. Pontier, S., et al., *Integrin-linked kinase has a critical role in ErbB2 mammary tumor progression: implications for human breast cancer.* Oncogene, 2010. **29**(23): p. 3374-3385.
114. Utermark, T., et al., *The p110α and p110β isoforms of PI3K play divergent roles in mammary gland development and tumorigenesis.* Genes & development, 2012. **26**(14): p. 1573-1586.
115. Andrechek, E.R., et al., *Gene expression profiling of neu-induced mammary tumors from transgenic mice reveals genetic and morphological similarities to ErbB2-expressing human breast cancers.* Cancer research, 2003. **63**(16): p. 4920-4926.
116. Montagna, C., et al., *Centrosome abnormalities, recurring deletions of chromosome 4, and genomic amplification of HER2/neu define mouse mammary gland adenocarcinomas induced by mutant HER2/neu.* Oncogene, 2002. **21**(6): p. 890.
117. Hodgson, J.G., et al., *Copy number aberrations in mouse breast tumors reveal loci and genes important in tumorigenic receptor tyrosine kinase signaling.* Cancer research, 2005. **65**(21): p. 9695-9704.
118. Herschkowitz, J.I., et al., *Identification of conserved gene expression features between murine mammary carcinoma models and human breast tumors.* Genome biology, 2007. **8**(5): p. R76.
119. Naidu, R., et al., *Expression of c-erbB3 protein in primary breast carcinomas.* British Journal of Cancer, 1998. **78**(10): p. 1385-1390.
120. Vaught, D.B., et al., *HER3 is required for HER2-induced preneoplastic changes to the breast epithelium and tumor formation.* Cancer research, 2012. **72**(10): p. 2672-2682.
121. Gillgrass, A., et al., *Epidermal growth factor receptor-dependent activation of Gab1 is involved in ErbB-2-mediated mammary tumor progression.* Oncogene, 2003. **22**(57): p. 9151-9155.
122. Jackson-Fisher, A., et al., *Formation of Neu/ErbB2-induced mammary tumors is unaffected by loss of ErbB4.* Oncogene, 2006. **25**(41): p. 5664-5672.

123. Muller, W.J., et al., *Synergistic interaction of the Neu proto-oncogene product and transforming growth factor alpha in the mammary epithelium of transgenic mice.* Molecular and cellular biology, 1996. **16**(10): p. 5726-5736.
124. Gross, L., *A filterable agent, recovered from Ak leukemic extracts, causing salivary gland carcinomas in C3H mice.* Experimental Biology and Medicine, 1953. **83**(2): p. 414-421.
125. Stewart, S.E., et al., *The induction of neoplasms with a substance released from mouse tumors by tissue culture.* Virology, 1957. **3**(2): p. 380-400.
126. Rowe, W.P., *The epidemiology of mouse polyoma virus infection.* Bacteriological reviews, 1961. **25**(1): p. 18.
127. Treisman, R., et al., *The structures of the spliced mRNAs encoding polyoma virus early region proteins.* Journal of molecular and applied genetics, 1981. **1**(2): p. 83.
128. Treisman, R., et al., *Transformation of rat cells by an altered polyoma virus genome expressing only the middle-T protein.* Nature, 1981. **292**(5824): p. 595.
129. Templeton, D. and W. Eckhart, *Mutation causing premature termination of the polyoma virus medium T antigen blocks cell transformation.* Journal of virology, 1982. **41**(3): p. 1014-1024.
130. Carmichael, G.G., et al., *Carboxy terminus of polyoma middle-sized tumor antigen is required for attachment to membranes, associated protein kinase activities, and cell transformation.* Proceedings of the National Academy of Sciences, 1982. **79**(11): p. 3579-3583.
131. Dilworth, S., et al., *Subcellular localisation of the middle and large T-antigens of polyoma virus.* The EMBO journal, 1986. **5**(3): p. 491.
132. Schaffhausen, B.S., et al., *Polyoma virus middle T antigen: relationship to cell membranes and apparent lack of ATP-binding activity.* Molecular and cellular biology, 1982. **2**(10): p. 1187-1198.
133. Courtneidge, S.A. and A.E. Smith, *Polyoma virus transforming protein associates with the product of the c-src cellular gene.* 1983.
134. Campbell, K.S., et al., *Polyoma middle tumor antigen interacts with SHC protein via the NPTY (Asn-Pro-Thr-Tyr) motif in middle tumor antigen.* Proceedings of the National Academy of Sciences, 1994. **91**(14): p. 6344-6348.
135. Dilworth, S.M., et al., *Transformation by polyoma virus middle T-antigen involves the binding and tyrosine phosphorylation of Shc.* 1994.
136. Courtneidge, S. and A. Heber, *An 81 kd protein complexed with middle T antigen and pp60c-src: a possible phosphatidylinositol kinase.* Cell, 1987. **50**(7): p. 1031.
137. Kaplan, D.R., et al., *Common elements in growth factor stimulation and oncogenic transformation: 85 kd phosphoprotein and phosphatidylinositol kinase activity.* Cell, 1987. **50**(7): p. 1021-1029.
138. Freund, R., et al., *Changes in frequency, morphology, and behavior of tumors induced in mice by a polyoma virus mutant with a specifically altered oncogene.* The American journal of pathology, 1992. **141**(6): p. 1409.
139. Kaplan, D.R., et al., *Phosphatidylinositol metabolism and polyoma-mediated transformation.* Proceedings of the National Academy of Sciences, 1986. **83**(11): p. 3624-3628.
140. Cecena, G., et al., *Differential sensitivity of mouse epithelial tissues to the polyomavirus middle T oncogene.* The American journal of pathology, 2006. **168**(1): p. 310-320.

141. Guy, C., R. Cardiff, and W. Muller, *Induction of mammary tumors by expression of polyomavirus middle T oncogene: a transgenic mouse model for metastatic disease.* Molecular and cellular biology, 1992. **12**(3): p. 954-961.
142. Maglione, J.E., et al., *Transgenic Polyoma middle-T mice model premalignant mammary disease.* Cancer research, 2001. **61**(22): p. 8298-8305.
143. Lin, E.Y., et al., *Progression to malignancy in the polyoma middle T oncoprotein mouse breast cancer model provides a reliable model for human diseases.* The American journal of pathology, 2003. **163**(5): p. 2113-2126.
144. Rao, T., et al., *Inducible and coupled expression of the polyomavirus middle T antigen and Cre recombinase in transgenic mice: an in vivo model for synthetic viability in mammary tumour progression.* Breast Cancer Research, 2014. **16**(1): p. R11.
145. Zvelebil, M.J., et al., *Structural and Functional Diversity of Phosphoinositide 3-Kinases [and Discussion]*. Philosophical Transactions: Biological Sciences, 1996. **351**(1336): p. 217-223.
146. Domin, J., et al., *Cloning of a human phosphoinositide 3-kinase with a C2 domain that displays reduced sensitivity to the inhibitor wortmannin.* Biochemical Journal, 1997. **326**(Pt 1): p. 139.
147. Jaber, N., et al., *Class III PI3K Vps34 plays an essential role in autophagy and in heart and liver function.* Proceedings of the National Academy of Sciences, 2012. **109**(6): p. 2003-2008.
148. Hiles, I.D., et al., *Phosphatidylinositol 3-kinase: Structure and expression of the 110 kd catalytic subunit.* Cell, 1992. **70**(3): p. 419-429.
149. Hu, P., et al., *Cloning of a novel, ubiquitously expressed human phosphatidylinositol 3-kinase and identification of its binding site on p85.* Molecular and Cellular Biology, 1993. **13**(12): p. 7677-7688.
150. Vanhaesebroeck, B., et al., *p110δ, a novel phosphoinositide 3-kinase in leukocytes.* Proceedings of the National Academy of Sciences, 1997. **94**(9): p. 4330-4335.
151. Stoyanov, B., et al., *Cloning and characterization of a G protein-activated human phosphoinositide-3 kinase.* Science, 1995. **269**(5224): p. 690-693.
152. Otsu, M., et al., *Characterization of two 85 kd proteins that associate with receptor tyrosine kinases, middle-T/pp60c-src complexes, and PI3-kinase.* Cell, 1991. **65**(1): p. 91-104.
153. Escobedo, J.A., et al., *cDNA cloning of a Novel 85 kd protein that has SH2 domains and regulates binding of PI3-kinase to the PDGF β-receptor.* Cell, 1991. **65**(1): p. 75-82.
154. Sawyer, C., et al., *Regulation of Breast Cancer Cell Chemotaxis by the Phosphoinositide 3-Kinase p110δ.* Cancer Research, 2003. **63**(7): p. 1667-1675.
155. Huang, C.-H., et al., *The Structure of a Human p110{alpha}/p85{alpha} Complex Elucidates the Effects of Oncogenic PI3K{alpha} Mutations.* Science, 2007. **318**(5857): p. 1744-1748.
156. Miled, N., et al., *Mechanism of Two Classes of Cancer Mutations in the Phosphoinositide 3-Kinase Catalytic Subunit.* Science, 2007. **317**(5835): p. 239-242.
157. Mandelker, D., et al., *A frequent kinase domain mutation that changes the interaction between PI3Kα and the membrane.* Proceedings of the National Academy of Sciences, 2009. **106**(40): p. 16996-17001.

158. Yu, J., et al., *Regulation of the p85/p110 Phosphatidylinositol 3'-Kinase: Stabilization and Inhibition of the p110α Catalytic Subunit by the p85 Regulatory Subunit.* Molecular and Cellular Biology, 1998. **18**(3): p. 1379-1387.
159. Yu, J., C. Wjasow, and J.M. Backer, *Regulation of the p85/p110α Phosphatidylinositol 3'-Kinase: Distinct Roles for teh N-terminal and C-terminal SH2 Domains.* Journal of Biological Chemistry, 1998. **273**(46): p. 30199-30203.
160. Zhang, X., et al., *Structure of Lipid Kinase p110β/p85β Elucidates an Unusual SH2-Domain-Mediated Inhibitory Mechanism.* Molecular Cell, 2011. **41**(5): p. 567-578.
161. Burke, John E., et al., *Dynamics of the Phosphoinositide 3-Kinase p110δ Interaction with p85α and Membranes Reveals Aspects of Regulation Distinct from p110α.* Structure, 2011. **19**(8): p. 1127-1137.
162. Zhou, S., et al., *SH2 domains recognize specific phosphopeptide sequences.* Cell, 1993. **72**(5): p. 767-778.
163. Carpenter, C.L., et al., *Phosphoinositide 3-kinase is activated by phosphopeptides that bind to the SH2 domains of the 85-kDa subunit.* Journal of Biological Chemistry, 1993. **268**(13): p. 9478-83.
164. Backer, J.M., et al., *Phosphatidylinositol 3'-kinase is activated by association with IRS-1 during insulin stimulation.* The EMBO Journal, 1992. **11**(9): p. 3469.
165. Coughlin, S., J. Escobedo, and L. Williams, *Role of phosphatidylinositol kinase in PDGF receptor signal transduction.* Science, 1989. **243**(4895): p. 1191-1194.
166. Soltoff, S.P., et al., *ErbB3 is involved in activation of phosphatidylinositol 3-kinase by epidermal growth factor.* Molecular and cellular biology, 1994. **14**(6): p. 3550-3558.
167. Myers, M.G., et al., *IRS-1 activates phosphatidylinositol 3'-kinase by associating with src homology 2 domains of p85.* Proceedings of the National Academy of Sciences, 1992. **89**(21): p. 10350-10354.
168. Holgado-Madruga, M., et al., *A Grb2-associated docking protein in EGF-and insulin-receptor signalling.* 1996.
169. Gu, H., et al., *New Role for Shc in Activation of the Phosphatidylinositol 3-Kinase/Akt Pathway.* Molecular and Cellular Biology, 2000. **20**(19): p. 7109-7120.
170. Rodriguez-Viciana, P., et al., *Phosphatidylinositol-3-OH kinase direct target of Ras.* Nature, 1994. **370**: p. 527-532.
171. Fritsch, R., et al., *RAS and RHO families of GTPases directly regulate distinct phosphoinositide 3-kinase isoforms.* Cell, 2013. **153**(5): p. 1050-1063.
172. Jiménez, C., et al., *The p85 regulatory subunit controls sequential activation of phosphoinositide 3-kinase by Tyr kinases and Ras.* Journal of Biological Chemistry, 2002. **277**(44): p. 41556-41562.
173. Prasad, K., et al., *Src-homology 3 domain of protein kinase p59fyn mediates binding to phosphatidylinositol 3-kinase in T cells.* Proceedings of the National Academy of Sciences, 1993. **90**(15): p. 7366-7370.
174. Kapeller, R., et al., *Identification of two SH3-binding motifs in the regulatory subunit of phosphatidylinositol 3-kinase.* Journal of Biological Chemistry, 1994. **269**(3): p. 1927-1933.
175. Pleiman, C.M., W.M. Hertz, and J.C. Cambier, *Activation of phosphatidylinositol-3'kinase by Src-family kinase SH3 binding to the p85 subunit.* Science, 1994. **263**(5153): p. 1609-1612.

176. Chen, H.-C. and J.-L. Guan, *Association of focal adhesion kinase with its potential substrate phosphatidylinositol 3-kinase.* Proceedings of the National Academy of Sciences, 1994. **91**(21): p. 10148-10152.
177. Stephens, L., et al., *Protein Kinase B Kinases That Mediate Phosphatidylinositol 3,4,5-Trisphosphate-Dependent Activation of Protein Kinase B.* Science, 1998. **279**(5351): p. 710-714.
178. Guillermet-Guibert, J., et al., *The p110β isoform of phosphoinositide 3-kinase signals downstream of G protein-coupled receptors and is functionally redundant with p110γ.* Proceedings of the National Academy of Sciences, 2008. **105**(24): p. 8292-8297.
179. Kurosu, H., et al., *Heterodimeric phosphoinositide 3-kinase consisting of p85 and p110β is synergistically activated by the βγ subunits of G proteins and phosphotyrosyl peptide.* Journal of Biological Chemistry, 1997. **272**(39): p. 24252-24256.
180. Stephens, L.R., et al., *The Gβγ Sensitivity of a PI3K Is Dependent upon a Tightly Associated Adaptor, p101.* Cell, 1997. **89**(1): p. 105-114.
181. Suire, S., et al., *p84, a New Gβγ-Activated Regulatory Subunit of the Type IB Phosphoinositide 3-Kinase p110γ.* Current Biology, 2005. **15**(6): p. 566-570.
182. Voigt, P., M.B. Dorner, and M. Schaefer, *Characterization of p87PIKAP, a Novel Regulatory Subunit of Phosphoinositide 3-Kinase γ That Is Highly Expressed in Heart and Interacts with PDE3B.* Journal of Biological Chemistry, 2006. **281**(15): p. 9977-9986.
183. Pacold, M.E., et al., *Crystal structure and functional analysis of Ras binding to its effector phosphoinositide 3-kinase γ.* Cell, 2000. **103**(6): p. 931-944.
184. Franke, T.F., et al., *Direct Regulation of the Akt Proto-Oncogene Product by Phosphatidylinositol-3,4-bisphosphate.* Science, 1997. **275**(5300): p. 665-668.
185. Klippel, A., et al., *A specific product of phosphatidylinositol 3-kinase directly activates the protein kinase Akt through its pleckstrin homology domain.* Molecular and Cellular Biology, 1997. **17**(1): p. 338-44.
186. Stokoe, D., et al., *Dual Role of Phosphatidylinositol-3,4,5-trisphosphate in the Activation of Protein Kinase B.* Science, 1997. **277**(5325): p. 567-570.
187. Alessi, D.R., et al., *Characterization of a 3-phosphoinositide-dependent protein kinase which phosphorylates and activates protein kinase Bα.* Current Biology, 1997. **7**(4): p. 261-269.
188. Andjelković, M., et al., *Activation and phosphorylation of a pleckstrin homology domain containing protein kinase (RAC-PK/PKB) promoted by serum and protein phosphatase inhibitors.* Proceedings of the National Academy of Sciences, 1996. **93**(12): p. 5699-5704.
189. Bellacosa, A., et al., *Akt activation by growth factors is a multiple-step process: the role of the PH domain.* Oncogene, 1998. **17**(3): p. 313-325.
190. Sarbassov, D.D., et al., *Phosphorylation and Regulation of Akt/PKB by the Rictor-mTOR Complex.* Science, 2005. **307**(5712): p. 1098-1101.
191. Arboleda, M.J., et al., *Overexpression of AKT2/Protein Kinase Bβ Leads to Up-Regulation of β1 Integrins, Increased Invasion, and Metastasis of Human Breast and Ovarian Cancer Cells.* Cancer Research, 2003. **63**(1): p. 196-206.
192. Irie, H.Y., et al., *Distinct roles of Akt1 and Akt2 in regulating cell migration and epithelial–mesenchymal transition.* The Journal of Cell Biology, 2005. **171**(6): p. 1023-1034.

193. Hutchinson, J., et al., *Activation of Akt (Protein Kinase B) in Mammary Epithelium Provides a Critical Cell Survival Signal Required for Tumor Progression.* Molecular and Cellular Biology, 2001. **21**(6): p. 2203-2212.
194. Dillon, R.L., et al., *Akt1 and akt2 play distinct roles in the initiation and metastatic phases of mammary tumor progression.* Cancer research, 2009. **69**(12): p. 5057-5064.
195. Inoki, K., et al., *TSC2 is phosphorylated and inhibited by Akt and suppresses mTOR signalling.* Nature cell biology, 2002. **4**(9): p. 648-657.
196. Manning, B.D., et al., *Identification of the Tuberous Sclerosis Complex-2 Tumor Suppressor Gene Product Tuberin as a Target of the Phosphoinositide 3-Kinase/Akt Pathway.* Molecular Cell, 2002. **10**(1): p. 151-162.
197. Potter, C.J., L.G. Pedraza, and T. Xu, *Akt regulates growth by directly phosphorylating Tsc2.* Nature cell biology, 2002. **4**(9): p. 658-665.
198. Inoki, K., et al., *Rheb GTPase is a direct target of TSC2 GAP activity and regulates mTOR signaling.* Genes & Development, 2003. **17**(15): p. 1829-1834.
199. Garami, A., et al., *Insulin Activation of Rheb, a Mediator of mTOR/S6K/4E-BP Signaling, Is Inhibited by TSC1 and 2.* Molecular Cell, 2003. **11**(6): p. 1457-1466.
200. Tee, A.R., et al., *Tuberous Sclerosis Complex Gene Products, Tuberin and Hamartin, Control mTOR Signaling by Acting as a GTPase-Activating Protein Complex toward Rheb.* Current Biology, 2003. **13**(15): p. 1259-1268.
201. Hara, K., et al., *Regulation of eIF-4E BP1 Phosphorylation by mTOR.* Journal of Biological Chemistry, 1997. **272**(42): p. 26457-26463.
202. Vander Haar, E., et al., *Insulin signalling to mTOR mediated by the Akt/PKB substrate PRAS40.* Nature cell biology, 2007. **9**(3): p. 316-323.
203. Harrington, L.S., et al., *The TSC1-2 tumor suppressor controls insulin–PI3K signaling via regulation of IRS proteins.* The Journal of Cell Biology, 2004. **166**(2): p. 213-223.
204. Manning, B.D., et al., *Feedback inhibition of Akt signaling limits the growth of tumors lacking Tsc2.* Genes & Development, 2005. **19**(15): p. 1773-1778.
205. O'Reilly, K.E., et al., *mTOR Inhibition Induces Upstream Receptor Tyrosine Kinase Signaling and Activates Akt.* Cancer Research, 2006. **66**(3): p. 1500-1508.
206. Carracedo, A., et al., *Inhibition of mTORC1 leads to MAPK pathway activation through a PI3K-dependent feedback loop in human cancer.* The Journal of Clinical Investigation, 2008. **118**(9): p. 3065-3074.
207. Maehama, T. and J.E. Dixon, *The Tumor Suppressor, PTEN/MMAC1, Dephosphorylates the Lipid Second Messenger, Phosphatidylinositol 3,4,5-Trisphosphate.* Journal of Biological Chemistry, 1998. **273**(22): p. 13375-13378.
208. Myers, M.P., et al., *The lipid phosphatase activity of PTEN is critical for its tumor supressor function.* Proceedings of the National Academy of Sciences, 1998. **95**(23): p. 13513-13518.
209. Stambolic, V., et al., *Negative Regulation of PKB/Akt-Dependent Cell Survival by the Tumor Suppressor PTEN.* Cell, 1998. **95**(1): p. 29-39.
210. Pesesse, X., et al., *The SH2 domain containing inositol 5-phosphatase SHIP2 displays phosphatidylinositol 3, 4, 5-trisphosphate and inositol 1, 3, 4, 5-tetrakisphosphate 5-phosphatase activity.* FEBS letters, 1998. **437**(3): p. 301-303.
211. Norris, F.A., R.C. Atkins, and P.W. Majerus, *The cDNA Cloning and Characterization of Inositol Polyphosphate 4-Phosphatase Type II: EVIDENCE FOR CONSERVED*

ALTERNATIVE SPLICING IN THE 4-PHOSPHATASE FAMILY. Journal of Biological Chemistry, 1997. **272**(38): p. 23859-23864.
212. Li, J., et al., *PTEN, a Putative Protein Tyrosine Phosphatase Gene Mutated in Human Brain, Breast, and Prostate Cancer.* Science, 1997. **275**(5308): p. 1943-1947.
213. Steck, P.A., et al., *Identification of a candidate tumour suppressor gene, MMAC1, at chromosome 10q23. 3 that is mutated in multiple advanced cancers.* Nature genetics, 1997. **15**(4): p. 356-362.
214. Wu, X., et al., *The PTEN/MMAC1 tumor suppressor phosphatase functions as a negative regulator of the phosphoinositide 3-kinase/Akt pathway.* Proceedings of the National Academy of Sciences, 1998. **95**(26): p. 15587-15591.
215. Li, D.-M. and H. Sun, *PTEN/MMAC1/TEP1 suppresses the tumorigenicity and induces G1 cell cycle arrest in human glioblastoma cells.* Proceedings of the National Academy of Sciences, 1998. **95**(26): p. 15406-15411.
216. Li, J., et al., *The PTEN/MMAC1 Tumor Suppressor Induces Cell Death That Is Rescued by the AKT/Protein Kinase B Oncogene.* Cancer Research, 1998. **58**(24): p. 5667-5672.
217. Tamura, M., et al., *Inhibition of Cell Migration, Spreading, and Focal Adhesions by Tumor Suppressor PTEN.* Science, 1998. **280**(5369): p. 1614-1617.
218. Dey, N., et al., *The protein phosphatase activity of PTEN regulates SRC family kinases and controls glioma migration.* Cancer research, 2008. **68**(6): p. 1862-1871.
219. Davidson, L., et al., *Suppression of cellular proliferation and invasion by the concerted lipid and protein phosphatase activities of PTEN.* Oncogene, 2009. **29**(5): p. 687-697.
220. Poon, J., R. Eves, and A. Mak, *Both lipid-and protein-phosphatase activities of PTEN contribute to the p53-PTEN anti-invasion pathway.* Cell cycle (Georgetown, Tex.), 2010. **9**(22): p. 4450.
221. Hlobilkova, A., et al., *Cell cycle arrest by the PTEN tumor suppressor is target cell specific and may require protein phosphatase activity.* Experimental cell research, 2000. **256**(2): p. 571-577.
222. Weng, L.-P., J.L. Brown, and C. Eng, *PTEN coordinates G1 arrest by down-regulating cyclin D1 via its protein phosphatase activity and up-regulating p27 via its lipid phosphatase activity in a breast cancer model.* Human molecular genetics, 2001. **10**(6): p. 599-604.
223. Zhang, S., et al., *Combating trastuzumab resistance by targeting SRC, a common node downstream of multiple resistance pathways.* Nature medicine, 2011. **17**(4): p. 461-469.
224. Shen, W.H., et al., *Essential role for nuclear PTEN in maintaining chromosomal integrity.* Cell, 2007. **128**(1): p. 157-170.
225. Trotman, L.C., et al., *Ubiquitination regulates PTEN nuclear import and tumor suppression.* Cell, 2007. **128**(1): p. 141-156.
226. Song, M.S., et al., *Nuclear PTEN regulates the APC-CDH1 tumor-suppressive complex in a phosphatase-independent manner.* Cell, 2011. **144**(2): p. 187-199.
227. Lindsay, Y., et al., *Localization of agonist-sensitive PtdIns (3, 4, 5) P3 reveals a nuclear pool that is insensitive to PTEN expression.* Journal of cell science, 2006. **119**(24): p. 5160-5168.
228. Dudek, H., et al., *Regulation of Neuronal Survival by the Serine-Threonine Protein Kinase Akt.* Science, 1997. **275**(5300): p. 661-665.
229. Datta, S.R., et al., *Akt Phosphorylation of BAD Couples Survival Signals to the Cell-Intrinsic Death Machinery.* Cell, 1997. **91**(2): p. 231-241.

230. del Peso, L., et al., *Interleukin-3-Induced Phosphorylation of BAD Through the Protein Kinase Akt.* Science, 1997. **278**(5338): p. 687-689.
231. Zha, J., et al., *Serine Phosphorylation of Death Agonist BAD in Response to Survival Factor Results in Binding to 14-3-3 Not BCL-XL.* Cell, 1996. **87**(4): p. 619-628.
232. Datta, S.R., et al., *14-3-3 Proteins and Survival Kinases Cooperate to Inactivate BAD by BH3 Domain Phosphorylation.* Molecular Cell, 2000. **6**(1): p. 41-51.
233. Cardone, M.H., et al., *Regulation of Cell Death Protease Caspase-9 by Phosphorylation.* Science, 1998. **282**(5392): p. 1318-1321.
234. Brunet, A., et al., *Akt Promotes Cell Survival by Phosphorylating and Inhibiting a Forkhead Transcription Factor.* Cell, 1999. **96**(6): p. 857-868.
235. Dijkers, P.F., et al., *Expression of the pro-apoptotic Bcl-2 family member Bim is regulated by the forkhead transcription factor FKHR-L1.* Current Biology, 2000. **10**(19): p. 1201-1204.
236. Brunet, A., et al., *Protein Kinase SGK Mediates Survival Signals by Phosphorylating the Forkhead Transcription Factor FKHRL1 (FOXO3a).* Molecular and Cellular Biology, 2001. **21**(3): p. 952-965.
237. Park, J., et al., *Serum and glucocorticoid-inducible kinase (SGK) is a target of the PI 3-kinase-stimulated signaling pathway.* The EMBO Journal, 1999. **18**(11): p. 3024-3033.
238. Mayo, L.D. and D.B. Donner, *A phosphatidylinositol 3-kinase/Akt pathway promotes translocation of Mdm2 from the cytoplasm to the nucleus.* Proceedings of the National Academy of Sciences, 2001. **98**(20): p. 11598-11603.
239. Zhou, B.P., et al., *HER-2/neu induces p53 ubiquitination via Akt-mediated MDM2 phosphorylation.* Nature cell biology, 2001. **3**(11): p. 973-982.
240. Stambolic, V., et al., *Regulation of PTEN Transcription by p53.* Molecular Cell, 2001. **8**(2): p. 317-325.
241. Ghosh, A., et al., *PTEN transcriptionally modulates c-myc gene expression in human breast carcinoma cells and is involved in cell growth regulation.* Gene, 1999. **235**(1-2): p. 85.
242. Lu, Y., et al., *The PTEN/MMAC1/TEP tumor suppressor gene decreases cell growth and induces apoptosis and anoikis in breast cancer cells.* Oncogene, 1999. **18**(50): p. 7034-7045.
243. Romashkova, J.A. and S.S. Makarov, *NF-κB is a target of AKT in anti-apoptotic PDGF signalling.* Nature, 1999. **401**(6748): p. 86-90.
244. Kane, L.P., et al., *Induction of NF-κB by the Akt/PKB kinase.* Current Biology, 1999. **9**(11): p. 601-S1.
245. Bai, D., L. Ueno, and P.K. Vogt, *Akt-mediated regulation of NFκB and the essentialness of NFκB for the oncogenicity of PI3K and Akt.* International Journal of Cancer, 2009. **125**(12): p. 2863-2870.
246. Dijkers, P.F., et al., *Forkhead Transcription Factor FKHR-L1 Modulates Cytokine-Dependent Transcriptional Regulation of p27KIP1.* Molecular and Cellular Biology, 2000. **20**(24): p. 9138-9148.
247. Viglietto, G., et al., *Cytoplasmic relocalization and inhibition of the cyclin-dependent kinase inhibitor p27Kip1 by PKB/Akt-mediated phosphorylation in breast cancer.* Nature medicine, 2002. **8**(10): p. 1136-1144.

248. Shin, I., et al., *PKB/Akt mediates cell-cycle progression by phosphorylation of p27Kip1 at threonine 157 and modulation of its cellular localization.* Nature medicine, 2002. **8**(10): p. 1145-1152.
249. Liang, J., et al., *PKB/Akt phosphorylates p27, impairs nuclear import of p27 and opposes p27-mediated G1 arrest.* Nature medicine, 2002. **8**(10): p. 1153-1160.
250. Graff, J.R., et al., *Increased AKT Activity Contributes to Prostate Cancer Progression by Dramatically Accelerating Prostate Tumor Growth and Diminishing p27Kip1 Expression.* Journal of Biological Chemistry, 2000. **275**(32): p. 24500-24505.
251. Medema, R.H., et al., *AFX-like Forkhead transcription factors mediate cell-cycle regulation by Ras and PKB through p27kip1.* Nature, 2000. **404**(6779): p. 782-787.
252. Zhou, B.P., et al., *Cytoplasmic localization of p21Cip1/WAF1 by Akt-induced phosphorylation in HER-2/neu-overexpressing cells.* Nature cell biology, 2001. **3**(3): p. 245-252.
253. Rössig, L., et al., *Akt-Dependent Phosphorylation of p21Cip1 Regulates PCNA Binding and Proliferation of Endothelial Cells.* Molecular and Cellular Biology, 2001. **21**(16): p. 5644-5657.
254. Xia, W., et al., *Phosphorylation/Cytoplasmic Localization of p21Cip1/WAF1 Is Associated with HER2/neu Overexpression and Provides a Novel Combination Predictor for Poor Prognosis in Breast Cancer Patients.* Clinical Cancer Research, 2004. **10**(11): p. 3815-3824.
255. El-Deiry, W.S., et al., *WAF1, a potential mediator of p53 tumor suppression.* Cell, 1993. **75**(4): p. 817-825.
256. Diehl, J.A., et al., *Glycogen synthase kinase-3β regulates cyclin D1 proteolysis and subcellular localization.* Genes & Development, 1998. **12**(22): p. 3499-3511.
257. Cross, D.A., et al., *Inhibition of glycogen synthase kinase-3 by insulin mediated by protein kinase B.* Nature, 1995. **378**(6559): p. 785-789.
258. Katome, T., et al., *Use of RNA Interference-mediated Gene Silencing and Adenoviral Overexpression to Elucidate the Roles of AKT/Protein Kinase B Isoforms in Insulin Actions.* Journal of Biological Chemistry, 2003. **278**(30): p. 28312-28323.
259. Zhou, Q., et al., *Analysis of insulin signalling by RNAi-based gene silencing.* Biochemical Society Transactions, 2004. **32**(5): p. 817-821.
260. Sano, H., et al., *Insulin-stimulated Phosphorylation of a Rab GTPase-activating Protein Regulates GLUT4 Translocation.* Journal of Biological Chemistry, 2003. **278**(17): p. 14599-14602.
261. Nakae, J., et al., *The forkhead transcription factor Foxo1 (Fkhr) confers insulin sensitivity onto glucose-6-phosphatase expression.* The Journal of Clinical Investigation, 2001. **108**(9): p. 1359-1367.
262. Li, X., et al., *Akt/PKB regulates hepatic metabolism by directly inhibiting PGC-1α transcription coactivator.* Nature, 2007. **447**(7147): p. 1012-1016.
263. Berwick, D.C., et al., *The Identification of ATP-citrate Lyase as a Protein Kinase B (Akt) Substrate in Primary Adipocytes.* Journal of Biological Chemistry, 2002. **277**(37): p. 33895-33900.
264. Fingar, D.C., et al., *Mammalian cell size is controlled by mTOR and its downstream targets S6K1 and 4EBP1/eIF4E.* Genes & Development, 2002. **16**(12): p. 1472-1487.

265. Corradetti, M.N., et al., *Regulation of the TSC pathway by LKB1: evidence of a molecular link between tuberous sclerosis complex and Peutz-Jeghers syndrome.* Genes & Development, 2004. **18**(13): p. 1533-1538.
266. Han, J., et al., *Role of Substrates and Products of PI 3-kinase in Regulating Activation of Rac-Related Guanosine Triphosphatases by Vav.* Science, 1998. **279**(5350): p. 558-560.
267. Welch, H., et al., *Protein Kinase B and Rac Are Activated in Parallel within a Phosphatidylinositide 3OH-kinase-controlled Signaling Pathway.* Journal of Biological Chemistry, 1998. **273**(18): p. 11248-11256.
268. Welch, H.C.E., et al., *P-Rex1, a PtdIns(3,4,5)P3- and Gβγ-Regulated Guanine-Nucleotide Exchange Factor for Rac.* Cell, 2002. **108**(6): p. 809-821.
269. Liliental, J., et al., *Genetic deletion of the Pten tumor suppressor gene promotes cell motility by activation of Rac1 and Cdc42 GTPases.* Current Biology, 2000. **10**(7): p. 401-404.
270. Martin-Belmonte, F., et al., *PTEN-Mediated Apical Segregation of Phosphoinositides Controls Epithelial Morphogenesis through Cdc42.* Cell, 2007. **128**(2): p. 383-397.
271. Krugmann, S., et al., *Identification of ARAP3, a Novel PI3K Effector Regulating Both Arf and Rho GTPases, by Selective Capture on Phosphoinositide Affinity Matrices.* Molecular Cell, 2002. **9**(1): p. 95-108.
272. Bi, L., et al., *Proliferative Defect and Embryonic Lethality in Mice Homozygous for a Deletion in the p110α Subunit of Phosphoinositide 3-Kinase.* Journal of Biological Chemistry, 1999. **274**(16): p. 10963-10968.
273. Foukas, L.C., et al., *Critical role for the p110α phosphoinositide-3-OH kinase in growth and metabolic regulation.* Nature, 2006. **441**(7091): p. 366-370.
274. Graupera, M., et al., *Angiogenesis selectively requires the p110α isoform of PI3K to control endothelial cell migration.* Nature, 2008. **453**(7195): p. 662-666.
275. Gupta, S., et al., *Binding of Ras to Phosphoinositide 3-Kinase p110α Is Required for Ras-Driven Tumorigenesis in Mice.* Cell, 2007. **129**(5): p. 957-968.
276. Zhao, J.J., et al., *The p110α isoform of PI3K is essential for proper growth factor signaling and oncogenic transformation.* Proceedings of the National Academy of Sciences, 2006. **103**(44): p. 16296-16300.
277. Brachmann, S.M., et al., *Phosphoinositide 3-Kinase Catalytic Subunit Deletion and Regulatory Subunit Deletion Have Opposite Effects on Insulin Sensitivity in Mice.* Molecular and Cellular Biology, 2005. **25**(5): p. 1596-1607.
278. Knight, Z.A., et al., *A Pharmacological Map of the PI3-K Family Defines a Role for p110α in Insulin Signaling.* Cell, 2006. **125**(4): p. 733-747.
279. Shioi, T., et al., *The conserved phosphoinositide 3-kinase pathway determines heart size in mice.* The EMBO journal, 2000. **19**(11): p. 2537-2548.
280. Bi, L., et al., *Early embryonic lethality in mice deficient in the p110β catalytic subunit of PI 3-kinase.* Mammalian Genome, 2002. **13**(3): p. 169-172.
281. Bénistant, C., H. Chapuis, and S. Roche, *A specific function for phosphatidylinositol 3-kinase alpha (p85alpha-p110alpha) in cell survival and for phosphatidylinositol 3-kinase bold beta (p85alpha-p110bold beta) in de novo DNA synthesis of human colon carcinoma cells.* Oncogene, 2000. **19**(44): p. 5083-5090.
282. Ciraolo, E., et al., *Phosphoinositide 3-Kinase p110{beta} Activity: Key Role in Metabolism and Mammary Gland Cancer but Not Development.* Sci. Signal., 2008. **1**(36): p. ra3-.

283. Jia, S., et al., *Essential roles of PI(3)K–p110β in cell growth, metabolism and tumorigenesis.* Nature, 2008. **454**(7205): p. 776-779.
284. Okkenhaug, K., et al., *Impaired B and T Cell Antigen Receptor Signaling in p110δ PI 3-Kinase Mutant Mice.* Science, 2002. **297**(5583): p. 1031-1034.
285. Clayton, E., et al., *A Crucial Role for the p110δ Subunit of Phosphatidylinositol 3-Kinase in B Cell Development and Activation.* The Journal of Experimental Medicine, 2002. **196**(6): p. 753-763.
286. Jou, S.-T., et al., *Essential, Nonredundant Role for the Phosphoinositide 3-Kinase p110δ in Signaling by the B-Cell Receptor Complex.* Molecular and Cellular Biology, 2002. **22**(24): p. 8580-8591.
287. Hirsch, E., et al., *Central Role for G Protein-Coupled Phosphoinositide 3-Kinase γ in Inflammation.* Science, 2000. **287**(5455): p. 1049-1053.
288. Sasaki, T., et al., *Function of PI3Kγ in Thymocyte Development, T Cell Activation, and Neutrophil Migration.* Science, 2000. **287**(5455): p. 1040-1046.
289. Fruman, D.A., et al., *Impaired B Cell Development and Proliferation in Absence of Phosphoinositide 3-Kinase p85α.* Science, 1999. **283**(5400): p. 393-397.
290. Ueki, K., et al., *Positive and Negative Roles of p85α and p85β Regulatory Subunits of Phosphoinositide 3-Kinase in Insulin Signaling.* Journal of Biological Chemistry, 2003. **278**(48): p. 48453-48466.
291. MacDonald, P.E., et al., *Impaired Glucose-Stimulated Insulin Secretion, Enhanced Intraperitoneal Insulin Tolerance, and Increased β-Cell Mass in Mice Lacking the p110γ Isoform of Phosphoinositide 3-Kinase.* Endocrinology, 2004. **145**(9): p. 4078-4083.
292. Terauchi, Y., et al., *Increased insulin sensitivity and hypoglycaemia in mice lacking the p85α subunit of phosphoinositide 3–kinase.* Nature genetics, 1999. **21**(2): p. 230-235.
293. Fruman, D.A., et al., *Hypoglycaemia, liver necrosis and perinatal death in mice lacking all isoforms of phosphoinositide 3-kinase p85α.* Nature genetics, 2000. **26**(3): p. 379-382.
294. Ueki, K., et al., *Increased insulin sensitivity in mice lacking p85β subunit of phosphoinositide 3-kinase.* Proceedings of the National Academy of Sciences, 2002. **99**(1): p. 419-424.
295. Chen, D., et al., *p50α/p55α Phosphoinositide 3-Kinase Knockout Mice Exhibit Enhanced Insulin Sensitivity.* Molecular and Cellular Biology, 2004. **24**(1): p. 320-329.
296. Taniguchi, C.M., et al., *Divergent regulation of hepatic glucose and lipid metabolism by phosphoinositide 3-kinase via Akt and PKCλ/ζ.* Cell Metabolism, 2006. **3**(5): p. 343-353.
297. Luo, J., et al., *Loss of class IA PI3K signaling in muscle leads to impaired muscle growth, insulin response, and hyperlipidemia.* Cell Metabolism, 2006. **3**(5): p. 355-366.
298. Luo, J., et al., *Class IA phosphoinositide 3-kinase regulates heart size and physiological cardiac hypertrophy.* Molecular and cellular biology, 2005. **25**(21): p. 9491-9502.
299. Suzuki, A., et al., *High cancer susceptibility and embryonic lethality associated with mutation of the PTEN tumor suppressor gene in mice.* Current Biology, 1998. **8**(21): p. 1169-1178.
300. Di Cristofano, A., et al., *Pten is essential for embryonic development and tumour suppression.* Nature genetics, 1998. **19**(4): p. 348-355.
301. Di Cristofano, A., et al., *Impaired Fas Response and Autoimmunity in Pten+/− Mice.* Science, 1999. **285**(5436): p. 2122-2125.
302. Suzuki, A., et al., *T Cell-Specific Loss of Pten Leads to Defects in Central and Peripheral Tolerance.* Immunity, 2001. **14**(5): p. 523-534.

303. Kurlawalla-Martinez, C., et al., *Insulin hypersensitivity and resistance to streptozotocin-induced diabetes in mice lacking PTEN in adipose tissue.* Molecular and cellular biology, 2005. **25**(6): p. 2498-2510.
304. Chen, S., et al., *VHL and PTEN loss coordinate to promote mouse liver vascular lesions.* Angiogenesis, 2010. **13**(1): p. 59-69.
305. Backman, S.A., et al., *Deletion of Pten in mouse brain causes seizures, ataxia and defects in soma size resembling Lhermitte-Duclos disease.* Nature genetics, 2001. **29**(4): p. 396-403.
306. Groszer, M., et al., *Negative Regulation of Neural Stem/Progenitor Cell Proliferation by the Pten Tumor Suppressor Gene in Vivo.* Science, 2001. **294**(5549): p. 2186-2189.
307. Crackower, M.A., et al., *Regulation of Myocardial Contractility and Cell Size by Distinct PI3K-PTEN Signaling Pathways.* Cell, 2002. **110**(6): p. 737-749.
308. Shen-Li, H., et al., *Reduction of Pten dose leads to neoplastic development in multiple organs of PtenshRNA mice.* Cancer biology & therapy, 2010. **10**(11): p. 1194.
309. Renner, O., et al., *Activation of phosphatidylinositol 3-kinase by membrane localization of p110α predisposes mammary glands to neoplastic transformation.* Cancer research, 2008. **68**(23): p. 9643-9653.
310. Meyer, D.S., et al., *Luminal expression of PIK3CA mutant H1047R in the mammary gland induces heterogeneous tumors.* Cancer research, 2011. **71**(13): p. 4344-4351.
311. Meyer, D., et al., *Expression of PIK3CA mutant E545K in the mammary gland induces heterogeneous tumors but is less potent than mutant H1047R.* Oncogenesis, 2013. **2**(9): p. e74.
312. Ackler, S., et al., *Delayed mammary gland involution in MMTV-AKT1 transgenic mice.* Oncogene, 2002. **21**(2): p. 198-206.
313. Dupont, J., et al., *PTEN overexpression suppresses proliferation and differentiation and enhances apoptosis of the mouse mammary epithelium.* Journal of Clinical Investigation, 2002. **110**(6): p. 815-825.
314. Marsh, D.J., et al., *Mutation spectrum and genotype-phenotype analyses in Cowden disease and Bannayan-Zonana syndrome, two hamartoma syndromes with germline PTEN mutation.* Human Molecular Genetics, 1998. **7**(3): p. 507-515.
315. Singh, B., M.M. Ittmann, and J.J. Krolewski, *Sporadic breast cancers exhibit loss of heterozygosity on chromosome segment 10q23 close to the Cowden disease locus.* Genes, Chromosomes and Cancer, 1998. **21**(2): p. 166-171.
316. García, J.M., et al., *Promoter methylation of the PTEN gene is a common molecular change in breast cancer.* Genes, Chromosomes and Cancer, 2004. **41**(2): p. 117-124.
317. Pérez-Tenorio, G., et al., *PIK3CA mutations and PTEN loss correlate with similar prognostic factors and are not mutually exclusive in breast cancer.* Clinical Cancer Research, 2007. **13**(12): p. 3577-3584.
318. Saal, L.H., et al., *Recurrent gross mutations of the PTEN tumor suppressor gene in breast cancers with deficient DSB repair.* Nature genetics, 2007. **40**(1): p. 102-107.
319. Mendes-Pereira, A.M., et al., *Synthetic lethal targeting of PTEN mutant cells with PARP inhibitors.* EMBO molecular medicine, 2009. **1**(6-7): p. 315-322.
320. Saal, L.H., et al., *PIK3CA Mutations Correlate with Hormone Receptors, Node Metastasis, and ERBB2, and Are Mutually Exclusive with PTEN Loss in Human Breast Carcinoma.* Cancer Research, 2005. **65**(7): p. 2554-2559.

321. Berns, K., et al., *A Functional Genetic Approach Identifies the PI3K Pathway as a Major Determinant of Trastuzumab Resistance in Breast Cancer.* Cancer Cell, 2007. **12**(4): p. 395-402.
322. Tokunaga, E., et al., *Coexistence of the loss of heterozygosity at the PTEN locus and HER2 overexpression enhances the Akt activity thus leading to a negative progesterone receptor expression in breast carcinoma.* Breast Cancer Research and Treatment, 2007. **101**(3): p. 249-257.
323. Podsypanina, K., et al., *Mutation of Pten/Mmac1 in mice causes neoplasia in multiple organ systems.* Proceedings of the National Academy of Sciences, 1999. **96**(4): p. 1563-1568.
324. Stambolic, V., et al., *High Incidence of Breast and Endometrial Neoplasia Resembling Human Cowden Syndrome in pten+/− Mice.* Cancer Research, 2000. **60**(13): p. 3605-3611.
325. Alimonti, A., et al., *Subtle variations in Pten dose determine cancer susceptibility.* Nature genetics, 2010. **42**(5): p. 454-458.
326. Chen, Z., et al., *Crucial role of p53-dependent cellular senescence in suppression of Pten-deficient tumorigenesis.* Nature, 2005. **436**(7051): p. 725-730.
327. Alimonti, A., et al., *A novel type of cellular senescence that can be enhanced in mouse models and human tumor xenografts to suppress prostate tumorigenesis.* The Journal of Clinical Investigation, 2010. **120**(3): p. 681-693.
328. Chen, M.-L., et al., *The deficiency of Akt1 is sufficient to suppress tumor development in Pten+/− mice.* Genes & Development, 2006. **20**(12): p. 1569-1574.
329. Bayascas, J.R., et al., *Hypomorphic Mutation of PDK1 Suppresses Tumorigenesis in PTEN+/− Mice.* Current Biology, 2005. **15**(20): p. 1839-1846.
330. Guertin, D.A., et al., *The mTOR complex 2 is required for the development of prostate cancer induced by Pten loss in mice.* Cancer cell, 2009. **15**(2): p. 148.
331. Li, G., et al., *Conditional loss of PTEN leads to precocious development and neoplasia in the mammary gland.* Development, 2002. **129**(17): p. 4159-4170.
332. Abate-Shen, C., et al., *Nkx3. 1; Pten mutant mice develop invasive prostate adenocarcinoma and lymph node metastases.* Cancer research, 2003. **63**(14): p. 3886-3890.
333. Suzuki, A., et al., *T cell-specific loss of Pten leads to defects in central and peripheral tolerance.* Immunity, 2001. **14**(5): p. 523-534.
334. Dourdin, N., et al., *Phosphatase and tensin homologue deleted on chromosome 10 deficiency accelerates tumor induction in a mouse model of ErbB-2 mammary tumorigenesis.* Cancer research, 2008. **68**(7): p. 2122-2131.
335. Samuels, Y., et al., *High Frequency of Mutations of the PIK3CA Gene in Human Cancers.* Science, 2004. **304**(5670): p. 554.
336. Bachman, K.E., et al., *The PIK3CA gene is mutated with high frequency in human breast cancers.* Cancer Biology & Therapy, 2004. **3**(8): p. 772-775.
337. Campbell, I.G., et al., *Mutation of the PIK3CA Gene in Ovarian and Breast Cancer.* Cancer Research, 2004. **64**(21): p. 7678-7681.
338. Lee, J.W., et al., *PIK3CA gene is frequently mutated in breast carcinomas and hepatocellular carcinomas.* Oncogene, 2005. **24**(8): p. 1477-1480.
339. Levine, D.A., et al., *Frequent Mutation of the PIK3CA Gene in Ovarian and Breast Cancers.* Clinical Cancer Research, 2005. **11**(8): p. 2875-2878.

340. Boyault, S., et al., *Mutational characterization of individual breast tumors: TP53 and PI3K pathway genes are frequently and distinctively mutated in different subtypes.* Breast Cancer Research and Treatment, 2012. **132**(1): p. 29-39.
341. Kalinsky, K., et al., *PIK3CA mutation associates with improved outcome in breast cancer.* Clinical Cancer Research, 2009. **15**(16): p. 5049-5059.
342. Loi, S., et al., *PIK3CA mutations associated with gene signature of low mTORC1 signaling and better outcomes in estrogen receptor–positive breast cancer.* Proceedings of the National Academy of Sciences, 2010. **107**(22): p. 10208-10213.
343. Cizkova, M., et al., *PIK3CA mutation impact on survival in breast cancer patients and in ERα, PR and ERBB2-based subgroups.* Breast Cancer Research, 2012. **14**(1): p. 1-9.
344. Ellis, M.J., et al., *Phosphatidyl-inositol-3-kinase alpha catalytic subunit mutation and response to neoadjuvant endocrine therapy for estrogen receptor positive breast cancer.* Breast cancer research and treatment, 2010. **119**(2): p. 379-390.
345. Li, S.Y., et al., *PIK3CA mutations in breast cancer are associated with poor outcome.* Breast cancer research and treatment, 2006. **96**(1): p. 91-95.
346. Mangone, F.R., et al., *PIK3CA exon 20 mutations are associated with poor prognosis in breast cancer patients.* Clinics, 2012. **67**(11): p. 1285-1290.
347. Campbell, I.G., et al., *Mutation of the PIK3CA gene in ovarian and breast cancer.* Cancer research, 2004. **64**(21): p. 7678-7681.
348. Dunlap, J., et al., *Phosphatidylinositol-3-kinase and AKT1 mutations occur early in breast carcinoma.* Breast Cancer Research and Treatment, 2010. **120**(2): p. 409-418.
349. Li, H., et al., *PIK3CA mutations mostly begin to develop in ductal carcinoma of the breast.* Experimental and molecular pathology, 2010. **88**(1): p. 150.
350. Miron, A., et al., *PIK3CA Mutations in In situ and Invasive Breast Carcinomas.* Cancer Research, 2010. **70**(14): p. 5674-5678.
351. Stemke-Hale, K., et al., *An Integrative Genomic and Proteomic Analysis of PIK3CA, PTEN, and AKT Mutations in Breast Cancer.* Cancer Research, 2008. **68**(15): p. 6084-6091.
352. Wang, L., et al., *PI3K pathway activation results in low efficacy of both trastuzumab and lapatinib.* BMC cancer, 2011. **11**(1): p. 248.
353. Vasudevan, K.M., et al., *AKT-Independent Signaling Downstream of Oncogenic PIK3CA Mutations in Human Cancer.* Cancer Cell, 2009. **16**(1): p. 21-32.
354. Chang, H.W., et al., *Transformation of Chicken Cells by the Gene Encoding the Catalytic Subunit of PI 3-Kinase.* Science, 1997. **276**(5320): p. 1848-1850.
355. Aoki, M., et al., *The catalytic subunit of phosphoinositide 3-kinase: requirements for oncogenicity.* Journal of Biological Chemistry, 2000. **275**(9): p. 6267-6275.
356. Jiang, B.-H., et al., *Phosphatidylinositol 3-kinase signaling mediates angiogenesis and expression of vascular endothelial growth factor in endothelial cells.* Proceedings of the National Academy of Sciences, 2000. **97**(4): p. 1749-1753.
357. Kang, S., A.G. Bader, and P.K. Vogt, *Phosphatidylinositol 3-kinase mutations identified in human cancer are oncogenic.* Proceedings of the National Academy of Sciences of the United States of America, 2005. **102**(3): p. 802-807.
358. Bader, A.G., S. Kang, and P.K. Vogt, *Cancer-specific mutations in PIK3CA are oncogenic in vivo.* Proceedings of the National Academy of Sciences of the United States of America, 2006. **103**(5): p. 1475-1479.

359. Samuels, Y., et al., *Mutant PIK3CA promotes cell growth and invasion of human cancer cells.* Cancer Cell, 2005. **7**(6): p. 561-573.
360. Isakoff, S.J., et al., *Breast Cancer–Associated PIK3CA Mutations Are Oncogenic in Mammary Epithelial Cells.* Cancer Research, 2005. **65**(23): p. 10992-11000.
361. Zhao, J.J., et al., *The oncogenic properties of mutant p110α and p110β phosphatidylinositol 3-kinases in human mammary epithelial cells.* Proceedings of the National Academy of Sciences of the United States of America, 2005. **102**(51): p. 18443-18448.
362. Zhang, H., et al., *Comprehensive analysis of oncogenic effects of PIK3CA mutations in human mammary epithelial cells.* Breast Cancer Research and Treatment, 2008. **112**(2): p. 217-227.
363. Zhao, L. and P.K. Vogt, *Helical domain and kinase domain mutations in p110α of phosphatidylinositol 3-kinase induce gain of function by different mechanisms.* Proceedings of the National Academy of Sciences, 2008. **105**(7): p. 2652-2657.
364. Pang, H., et al., *Differential enhancement of breast cancer cell motility and metastasis by helical and kinase domain mutations of class IA phosphoinositide 3-kinase.* Cancer research, 2009. **69**(23): p. 8868-8876.
365. Hao, Y., et al., *Gain of interaction with IRS1 by p110α-helical domain mutants is crucial for their oncogenic functions.* Cancer cell, 2013. **23**(5): p. 583-593.
366. Adams, J.R., et al., *Cooperation between Pik3ca and p53 mutations in mouse mammary tumor formation.* Cancer research, 2011. **71**(7): p. 2706-2717.
367. Liu, P., et al., *Oncogenic PIK3CA-driven mammary tumors frequently recur via PI3K pathway-dependent and PI3K pathway-independent mechanisms.* Nature medicine, 2011. **17**(9): p. 1116-1120.
368. Engelman, J.A., et al., *Effective use of PI3K and MEK inhibitors to treat mutant Kras G12D and PIK3CA H1047R murine lung cancers.* Nature medicine, 2008. **14**(12): p. 1351-1356.
369. Hanker, A.B., et al., *Mutant PIK3CA accelerates HER2-driven transgenic mammary tumors and induces resistance to combinations of anti-HER2 therapies.* Proceedings of the National Academy of Sciences, 2013. **110**(35): p. 14372-14377.
370. Shekar, S.C., et al., *Mechanism of Constitutive Phosphoinositide 3-Kinase Activation by Oncogenic Mutants of the p85 Regulatory Subunit.* Journal of Biological Chemistry, 2005. **280**(30): p. 27850-27855.
371. Jaiswal, B.S., et al., *Somatic mutations in p85α promote tumorigenesis through class IA PI3K activation.* Cancer cell, 2009. **16**(6): p. 463-474.
372. Castellano, E., et al., *Requirement for Interaction of PI3-Kinase p110α with RAS in Lung Tumor Maintenance.* Cancer cell, 2013. **24**(5): p. 617-630.
373. Beeton, C., et al., *Comparison of the kinetic properties of the lipid-and protein-kinase activities of the p110α and p110β catalytic subunits of class-Ia phosphoinositide 3-kinases.* Biochem. J, 2000. **350**: p. 353-359.
374. Webster, M.A., et al., *Requirement for both Shc and phosphatidylinositol 3' kinase signaling pathways in polyomavirus middle T-mediated mammary tumorigenesis.* Molecular and cellular biology, 1998. **18**(4): p. 2344-2359.
375. Utermark, T., et al., *The p110α Isoform of Phosphatidylinositol 3-Kinase Is Essential for Polyomavirus Middle T Antigen-Mediated Transformation.* Journal of Virology, 2007. **81**(13): p. 7069-7076.

376. Wee, S., et al., *PTEN-deficient cancers depend on PIK3CB.* Proceedings of the National Academy of Sciences, 2008. **105**(35): p. 13057-13062.
377. Torbett, N., et al., *A chemical screen in diverse breast cancer cell lines reveals genetic enhancers and suppressors of sensitivity to PI3K isoform-selective inhibition.* Biochem. J, 2008. **415**: p. 97-110.
378. Berenjeno, I.M., et al., *Both p110alpha and p110beta isoforms of PI3K can modulate the impact of loss-of-function of the PTEN tumour suppressor.* Biochemical Journal, 2012. **442**(1): p. 151-159.
379. Wang, Q., et al., *Spatially distinct roles of class Ia PI3K isoforms in the development and maintenance of PTEN hamartoma tumor syndrome.* Genes & development, 2013. **27**(14): p. 1568-1580.
380. Schmit, F., et al., *PI3K isoform dependence of PTEN-deficient tumors can be altered by the genetic context.* Proceedings of the National Academy of Sciences, 2014. **111**(17): p. 6395-6400.
381. Utermark, T., et al., *The PI3K isoform dependence of tumor formation is determined by the genetic mode of PI3K pathway activation rather than by tissue type.* Journal of Virology, 2014.
382. Powis, G., et al., *Wortmannin, a Potent and Selective Inhibitor of Phosphatidylinositol-3-kinase.* Cancer Research, 1994. **54**(9): p. 2419-2423.
383. Vlahos, C.J., et al., *A specific inhibitor of phosphatidylinositol 3-kinase, 2-(4-morpholinyl)-8-phenyl-4H-1-benzopyran-4-one (LY294002).* Journal of Biological Chemistry, 1994. **269**(7): p. 5241-5248.
384. Franke, T.F., et al., *The protein kinase encoded by the Akt proto-oncogene is a target of the PDGF-activated phosphatidylinositol 3-kinase.* Cell, 1995. **81**(5): p. 727-736.
385. Taylor, V., et al., *5′ Phospholipid Phosphatase SHIP-2 Causes Protein Kinase B Inactivation and Cell Cycle Arrest in Glioblastoma Cells.* Molecular and Cellular Biology, 2000. **20**(18): p. 6860-6871.
386. Folkes, A.J., et al., *The identification of 2-(1 H-Indazol-4-yl)-6-(4-methanesulfonyl-piperazin-1-ylmethyl)-4-morpholin-4-yl-thieno [3, 2-d] pyrimidine (GDC-0941) as a potent, selective, orally bioavailable inhibitor of class I PI3 kinase for the treatment of cancer†.* Journal of medicinal chemistry, 2008. **51**(18): p. 5522-5532.
387. Stephen, J., et al., *A drug targeting only p110alpha can block phosphoinositide 3-kinase signalling and tumour growth in certain cell types.* Biochemical Journal, 2011. **438**(1): p. 53-62.
388. Neshat, M.S., et al., *Enhanced sensitivity of PTEN-deficient tumors to inhibition of FRAP/mTOR.* Proceedings of the National Academy of Sciences, 2001. **98**(18): p. 10314-10319.
389. Podsypanina, K., et al., *An inhibitor of mTOR reduces neoplasia and normalizes p70/S6 kinase activity in Pten+/− mice.* Proceedings of the National Academy of Sciences, 2001. **98**(18): p. 10320-10325.
390. Milam, M.R., et al., *Reduced progression of endometrial hyperplasia with oral mTOR inhibition in the< i> Pten</i> heterozygote murine model.* American journal of obstetrics and gynecology, 2007. **196**(3): p. 247. e1-247. e5.
391. Blando, J., et al., *PTEN deficiency is fully penetrant for prostate adenocarcinoma in C57BL/6 mice via mTOR-dependent growth.* The American journal of pathology, 2009. **174**(5): p. 1869-1879.

392. Elkabets, M., et al., *mTORC1 inhibition is required for sensitivity to PI3K p110α inhibitors in PIK3CA-mutant breast cancer.* Science translational medicine, 2013. **5**(196): p. 196ra99-196ra99.
393. Chakrabarty, A., et al., *Feedback upregulation of HER3 (ErbB3) expression and activity attenuates antitumor effect of PI3K inhibitors.* Proceedings of the National Academy of Sciences, 2012. **109**(8): p. 2718-2723.
394. Serra, V., et al., *PI3K inhibition results in enhanced HER signaling and acquired ERK dependency in HER2-overexpressing breast cancer.* Oncogene, 2011. **30**(22): p. 2547-2557.
395. Ihle, N.T., et al., *Mutations in the phosphatidylinositol-3-kinase pathway predict for antitumor activity of the inhibitor PX-866 whereas oncogenic Ras is a dominant predictor for resistance.* Cancer Research, 2009. **69**(1): p. 143-150.
396. Sos, M.L., et al., *Identifying genotype-dependent efficacy of single and combined PI3K- and MAPK-pathway inhibition in cancer.* Proceedings of the National Academy of Sciences, 2009. **106**(43): p. 18351-18356.
397. Shimizu, T., et al., *The clinical effect of the dual-targeting strategy involving PI3K/AKT/mTOR and RAS/MEK/ERK pathways in patients with advanced cancer.* Clinical Cancer Research, 2012. **18**(8): p. 2316-2325.
398. Ilic, N., et al., *PI3K-targeted therapy can be evaded by gene amplification along the MYC-eukaryotic translation initiation factor 4E (eIF4E) axis.* Proceedings of the National Academy of Sciences, 2011. **108**(37): p. E699-E708.
399. Muellner, M.K., et al., *A chemical-genetic screen reveals a mechanism of resistance to PI3K inhibitors in cancer.* Nature chemical biology, 2011. **7**(11): p. 787-793.
400. Frogne, T., et al., *Activation of ErbB3, EGFR and Erk is essential for growth of human breast cancer cell lines with acquired resistance to fulvestrant.* Breast cancer research and treatment, 2009. **114**(2): p. 263-275.
401. deGraffenried, L.A., et al., *Inhibition of mTOR Activity Restores Tamoxifen Response in Breast Cancer Cells with Aberrant Akt Activity.* Clinical Cancer Research, 2004. **10**(23): p. 8059-8067.
402. Ghayad, S.E., et al., *mTOR inhibition reverses acquired endocrine therapy resistance of breast cancer cells at the cell proliferation and gene-expression levels.* Cancer science, 2008. **99**(10): p. 1992-2003.
403. Shoman, N., et al., *Reduced PTEN expression predicts relapse in patients with breast carcinoma treated by tamoxifen.* Modern pathology, 2004. **18**(2): p. 250-259.
404. Miller, T.W., et al., *Hyperactivation of phosphatidylinositol-3 kinase promotes escape from hormone dependence in estrogen receptor–positive human breast cancer.* The Journal of clinical investigation, 2010. **120**(7): p. 2406-2413.
405. Baselga, J., et al., *Everolimus in postmenopausal hormone-receptor–positive advanced breast cancer.* New England Journal of Medicine, 2012. **366**(6): p. 520-529.
406. Bachelot, T., et al., *Randomized phase II trial of everolimus in combination with tamoxifen in patients with hormone receptor–positive, human epidermal growth factor receptor 2–negative metastatic breast cancer with prior exposure to aromatase inhibitors: A GINECO study.* Journal of Clinical Oncology, 2012. **30**(22): p. 2718-2724.
407. Baselga, J., et al., *Phase III randomized study of the oral pan-PI3K inhibitor BKM120 with fulvestrant in postmenopausal women with HR+/HER2–locally advanced or*

metastatic breast cancer resistant to aromatase inhibitor–BELLE-2. Cancer Research, 2012. **72**(24 Supplement 3).
408. Serra, V., et al., *NVP-BEZ235, a Dual PI3K/mTOR Inhibitor, Prevents PI3K Signaling and Inhibits the Growth of Cancer Cells with Activating PI3K Mutations.* Cancer Research, 2008. **68**(19): p. 8022-8030.
409. Nagata, Y., et al., *PTEN activation contributes to tumor inhibition by trastuzumab, and loss of PTEN predicts trastuzumab resistance in patients.* Cancer Cell, 2004. **6**(2): p. 117-127.
410. Kataoka, Y., et al., *Association between gain-of-function mutations in PIK3CA and resistance to HER2-targeted agents in HER2-amplified breast cancer cell lines.* Annals of Oncology, 2010. **21**(2): p. 255-262.
411. Eichhorn, P.J.A., et al., *Phosphatidylinositol 3-Kinase Hyperactivation Results in Lapatinib Resistance that Is Reversed by the mTOR/Phosphatidylinositol 3-Kinase Inhibitor NVP-BEZ235.* Cancer Research, 2008. **68**(22): p. 9221-9230.
412. Esteva, F.J., et al., *PTEN, PIK3CA, p-AKT, and p-p70S6K status: association with trastuzumab response and survival in patients with HER2-positive metastatic breast cancer.* The American journal of pathology, 2010. **177**(4): p. 1647-1656.
413. Chandarlapaty, S., et al., *Frequent mutational activation of the PI3K-AKT pathway in trastuzumab-resistant breast cancer.* Clinical Cancer Research, 2012. **18**(24): p. 6784-6791.
414. Razis, E., et al., *Evaluation of the association of PIK3CA mutations and PTEN loss with efficacy of trastuzumab therapy in metastatic breast cancer.* Breast cancer research and treatment, 2011. **128**(2): p. 447-456.
415. Dave, B., et al., *Loss of phosphatase and tensin homolog or phosphoinositol-3 kinase activation and response to trastuzumab or lapatinib in human epidermal growth factor receptor 2–overexpressing locally advanced breast cancers.* Journal of Clinical Oncology, 2011. **29**(2): p. 166-173.
416. Loi, S., et al., *Somatic mutation profiling and associations with prognosis and trastuzumab benefit in early breast cancer.* Journal of the National Cancer Institute, 2013: p. djt121.
417. Garrett, J.T., et al., *Transcriptional and posttranslational up-regulation of HER3 (ErbB3) compensates for inhibition of the HER2 tyrosine kinase.* Proceedings of the National Academy of Sciences, 2011. **108**(12): p. 5021-5026.
418. She, Q.-B., et al., *Breast Tumor Cells with PI3K Mutation or HER2 Amplification Are Selectively Addicted to Akt Signaling.* PLoS ONE, 2008. **3**(8): p. e3065.
419. Junttila, T.T., et al., *Ligand-independent HER2/HER3/PI3K complex is disrupted by trastuzumab and is effectively inhibited by the PI3K inhibitor GDC-0941.* Cancer cell, 2009. **15**(5): p. 429-440.
420. Miller, T.W., et al., *Inhibition of mammalian target of rapamycin is required for optimal antitumor effect of HER2 inhibitors against HER2-overexpressing cancer cells.* Clinical Cancer Research, 2009. **15**(23): p. 7266-7276.
421. Jerusalem, G., et al., *Phase I trial of oral mTOR inhibitor everolimus in combination with trastuzumab and vinorelbine in pre-treated patients with HER2-overexpressing metastatic breast cancer.* Breast cancer research and treatment, 2011. **125**(2): p. 447-455.

422. Andre, F., et al., *Phase I study of everolimus plus weekly paclitaxel and trastuzumab in patients with metastatic breast cancer pretreated with trastuzumab.* Journal of Clinical Oncology, 2010: p. JCO. 2009.27. 8549.
423. Lesche, R., et al., *Cre/loxP-mediated inactivation of the murine Pten tumor suppressor gene.* Genesis, 2002. **32**(2): p. 148-149.
424. Gunther, E., et al., *A novel doxycycline-inducible system for the transgenic analysis of mammary gland biology.* FASEB journal: official publication of the Federation of American Societies for Experimental Biology, 2002. **16**(3): p. 283.
425. Trimboli, A.J., et al., *Pten in stromal fibroblasts suppresses mammary epithelial tumours.* Nature, 2009. **461**(7267): p. 1084-1091.
426. Bronisz, A., et al., *Reprogramming of the tumour microenvironment by stromal PTEN-regulated miR-320.* Nature cell biology, 2012. **14**(2): p. 159-167.
427. Kim, J.-S., et al., *Activation of p53-dependent growth suppression in human cells by mutations in PTEN or PIK3CA.* Molecular and cellular biology, 2007. **27**(2): p. 662-677.
428. Tuck, A.B., et al., *Osteopontin expression in a group of lymph node negative breast cancer patients.* International journal of cancer, 1998. **79**(5): p. 502-508.
429. Rudland, P.S., et al., *Prognostic significance of the metastasis-associated protein osteopontin in human breast cancer.* Cancer research, 2002. **62**(12): p. 3417-3427.
430. Bramwell, V.H., et al., *Serial plasma osteopontin levels have prognostic value in metastatic breast cancer.* Clinical Cancer Research, 2006. **12**(11): p. 3337-3343.
431. Fedarko, N.S., et al., *Elevated serum bone sialoprotein and osteopontin in colon, breast, prostate, and lung cancer.* Clinical Cancer Research, 2001. **7**(12): p. 4060-4066.
432. Furger, K.A., et al., *β3 Integrin Expression Increases Breast Carcinoma Cell Responsiveness to the Malignancy-Enhancing Effects of Osteopontin.* Molecular cancer research, 2003. **1**(11): p. 810-819.
433. Wang, S., et al., *Prostate-specific deletion of the murine Pten tumor suppressor gene leads to metastatic prostate cancer.* Cancer Cell, 2003. **4**(3): p. 209-221.
434. Packer, L., et al., *Osteopontin is a downstream effector of the PI3-kinase pathway in melanomas that is inversely correlated with functional PTEN.* Carcinogenesis, 2006. **27**(9): p. 1778-1786.
435. Kim, M.-S., et al., *Hyaluronic acid induces osteopontin via the phosphatidylinositol 3-kinase/Akt pathway to enhance the motility of human glioma cells.* Cancer research, 2005. **65**(3): p. 686-691.
436. Howe, L.R., et al., *HER2/neu-induced mammary tumorigenesis and angiogenesis are reduced in cyclooxygenase-2 knockout mice.* Cancer research, 2005. **65**(21): p. 10113-10119.
437. Rodríguez-Manzaneque, J.C., et al., *Thrombospondin-1 suppresses spontaneous tumor growth and inhibits activation of matrix metalloproteinase-9 and mobilization of vascular endothelial growth factor.* Proceedings of the National Academy of Sciences, 2001. **98**(22): p. 12485-12490.
438. Prince, C.W., et al., *Isolation, characterization, and biosynthesis of a phosphorylated glycoprotein from rat bone.* Journal of Biological Chemistry, 1987. **262**(6): p. 2900-2907.
439. Oldberg, A., A. Franzén, and D. Heinegård, *Cloning and sequence analysis of rat bone sialoprotein (osteopontin) cDNA reveals an Arg-Gly-Asp cell-binding sequence.* Proceedings of the National Academy of Sciences, 1986. **83**(23): p. 8819-8823.

440. Das, R., G.H. Mahabeleshwar, and G.C. Kundu, *Osteopontin stimulates cell motility and nuclear factor κB-mediated secretion of urokinase type plasminogen activator through phosphatidylinositol 3-kinase/Akt signaling pathways in breast cancer cells.* Journal of Biological Chemistry, 2003. **278**(31): p. 28593-28606.
441. Zheng, D.-Q., et al., *Substrate Specificity of αvβ3Integrin-mediated Cell Migration and Phosphatidylinositol 3-Kinase/AKT Pathway Activation.* Journal of Biological Chemistry, 2000. **275**(32): p. 24565-24574.
442. Tuck, A.B., et al., *Osteopontin-induced migration of human mammary epithelial cells involves activation of EGF receptor and multiple signal transduction pathways.* Oncogene, 2003. **22**(8): p. 1198-1205.
443. Das, R., G.H. Mahabeleshwar, and G.C. Kundu, *Osteopontin induces AP-1-mediated secretion of urokinase-type plasminogen activator through c-Src-dependent epidermal growth factor receptor transactivation in breast cancer cells.* Journal of Biological Chemistry, 2004. **279**(12): p. 11051-11064.
444. Tuck, A.B., et al., *Osteopontin-induced, integrin-dependent migration of human mammary epithelial cells involves activation of the hepatocyte growth factor receptor (Met).* Journal of cellular biochemistry, 2000. **78**(3): p. 465-475.
445. Lin, Y.-H. and H.-F. Yang-Yen, *The osteopontin-CD44 survival signal involves activation of the phosphatidylinositol 3-kinase/Akt signaling pathway.* Journal of Biological Chemistry, 2001. **276**(49): p. 46024-46030.
446. Mi, Z., et al., *Integrin-linked kinase regulates osteopontin-dependent MMP-2 and uPA expression to convey metastatic function in murine mammary epithelial cancer cells.* Carcinogenesis, 2006. **27**(6): p. 1134-1145.
447. Khan, S.A., et al., *Enhanced cell surface CD44 variant (v6, v9) expression by osteopontin in breast cancer epithelial cells facilitates tumor cell migration: novel post-transcriptional, post-translational regulation.* Clinical & experimental metastasis, 2005. **22**(8): p. 663-673.
448. Raja, R., et al., *Hypoxia-driven osteopontin contributes to breast tumor growth through modulation of HIF1α-mediated VEGF-dependent angiogenesis.* Oncogene, 2014. **33**(16): p. 2053-2064.
449. Mutrie, J., A. Chambers, and A. Tuck, *Osteopontin increases breast cancer cell sensitivity to specific signaling pathway inhibitors in preclinical models.* Cancer biology & therapy, 2011. **12**(8): p. 680.
450. Chakraborty, G., S. Jain, and G.C. Kundu, *Osteopontin promotes vascular endothelial growth factor–dependent breast tumor growth and angiogenesis via autocrine and paracrine mechanisms.* Cancer Research, 2008. **68**(1): p. 152-161.
451. Brown, L.F., et al., *Osteopontin expression and distribution in human carcinomas.* The American journal of pathology, 1994. **145**(3): p. 610.
452. Coppola, D., et al., *Correlation of osteopontin protein expression and pathological stage across a wide variety of tumor histologies.* Clinical cancer research, 2004. **10**(1): p. 184-190.
453. Bellahcene, A. and V. Castronovo, *Increased expression of osteonectin and osteopontin, two bone matrix proteins, in human breast cancer.* The American journal of pathology, 1995. **146**(1): p. 95.
454. Mirza, M., et al., *Osteopontin-c is a selective marker of breast cancer.* International journal of cancer, 2008. **122**(4): p. 889-897.

455. Ortiz-Martínez, F., et al., *Association of increased osteopontin and splice variant-c mRNA expression with HER2 and triple-negative/basal-like breast carcinomas subtypes and recurrence.* Human pathology, 2014. **45**(3): p. 504-512.
456. Thorat, D., et al., *Association of osteopontin and cyclooxygenase-2 expression with breast cancer subtypes and their use as potential biomarkers.* Oncology letters, 2013. **6**(6): p. 1559-1564.
457. Rittling, S. and K. Novick, *Osteopontin expression in mammary gland development and tumorigenesis.* Cell growth & differentiation: the molecular biology journal of the American Association for Cancer Research, 1997. **8**(10): p. 1061.
458. Nemir, M., et al., *Targeted inhibition of osteopontin expression in the mammary gland causes abnormal morphogenesis and lactation deficiency.* Journal of Biological Chemistry, 2000. **275**(2): p. 969-976.
459. Hubbard, N.E., et al., *Transgenic Mammary Epithelial Osteopontin (Spp1) Expression Induces Proliferation and Alveologenesis.* Genes & cancer, 2013. **4**(5-6): p. 201-212.
460. Helfrich, M.H., et al., *Rat osteoclasts adhere to a wide range of rgd (arg-gly-asp) peptide-containing proteins, including the bone sialoproteins and fibronectin, via a β3 integrin.* Journal of Bone and Mineral Research, 1992. **7**(3): p. 335-343.
461. Cui, R., et al., *Abrogation of the interaction between osteopontin and αvβ3 integrin reduces tumor growth of human lung cancer cells in mice.* Lung Cancer, 2007. **57**(3): p. 302-310.
462. Allan, A.L., et al., *Role of the integrin-binding protein osteopontin in lymphatic metastasis of breast cancer.* The American journal of pathology, 2006. **169**(1): p. 233-246.
463. Liu, H., et al., *MYC suppresses cancer metastasis by direct transcriptional silencing of [alpha] v and [beta] 3 integrin subunits.* Nature cell biology, 2012. **14**(6): p. 567-574.
464. McAllister, S.S., et al., *Systemic endocrine instigation of indolent tumor growth requires osteopontin.* Cell, 2008. **133**(6): p. 994-1005.
465. Gunther, E.J., et al., *Impact of p53 loss on reversal and recurrence of conditional Wnt-induced tumorigenesis.* Genes & development, 2003. **17**(4): p. 488-501.
466. Cardiff, R.D., *The pathology of EMT in mouse mammary tumorigenesis.* Journal of mammary gland biology and neoplasia, 2010. **15**(2): p. 225-233.
467. Jessen, K.A., et al., *Molecular analysis of metastasis in a polyomavirus middle T mouse model: the role of osteopontin.* Breast Cancer Research, 2004. **6**(3): p. R157.
468. Whalen, K.A., et al., *Polyomavirus middle T antigen induces the transcription of osteopontin, a gene important for the migration of transformed cells.* Journal of virology, 2008. **82**(10): p. 4946-4954.
469. Dupont Jensen, J., et al., *PIK3CA Mutations May Be Discordant between Primary and Corresponding Metastatic Disease in Breast Cancer.* Clinical Cancer Research, 2011. **17**(4): p. 667-677.
470. Ahmed, M. and G.C. Kundu, *Osteopontin selectively regulates p70S6K/mTOR phosphorylation leading to NF-κB dependent AP-1-mediated ICAM-1 expression in breast cancer cells.* Molecular Cancer, 2010. **9**(1): p. 101.
471. Talbot, L.J., et al., *Pharmacokinetic characterization of an RNA aptamer against osteopontin and demonstration of in vivo efficacy in reversing growth of human breast cancer cells.* Surgery, 2011. **150**(2): p. 224-230.

472. Mi, Z., et al., *RNA aptamer blockade of osteopontin inhibits growth and metastasis of MDA-MB231 breast cancer cells.* Molecular Therapy, 2008. **17**(1): p. 153-161.